DEVELOPMENT, CHARACTERIZATION AND APPLICATION OF A NOVEL MOUSE LINE HUMANIZED FOR THE INTESTINAL PEPTIDE TRANSPORTER PEPT1

by

Yongjun Hu

A dissertation submitted in partial fulfillment
of the requirements for the degree of
Doctor of Philosophy
(Pharmaceutical Sciences)
in The University of Michigan
2015

Doctoral Committee:

Professor David E. Smith, Chair
Professor Gordon L. Amidon
Professor Richard F. Keep
Professor Duxin Sun

DEDICATION

TO

My Beloved Wife: Xia Jiang

Daughter: Vivian Yuanyuan Hu

Son: Jason Yuanheng Hu

and

My Dearest Parents: Ertong Hu and Ruizhen Deng

ACKNOWLEDGMENTS

First of all, I would like to thank my advisor, Professor David E. Smith, for his comprehensive support during the entire course of my Ph.D. program. As a mentor, he inspired me to recognize the spirit of science and rigorous scholarship; as a friend, he has done many favors to help me stand up when I was in difficult situations of daily life; as a colleague, he taught me numerous strategies to tackle the hardships of my professional career. Without Dr. Smith's interminable encouragement and substantial support, it would be impossible for me to achieve the success in my Ph.D. program and scientific career.

I also want to thank the other committee members of my Ph.D. program, Professor Gordon L. Amidon, Professor Richard F. Keep and Professor Duxin Sun, for their service on my committee and for their helpful advice on my research project. Their thoughtful comments and insightful suggestions were extremely valuable for the successful completion of my doctoral degree.

I would like to thank all my past and current colleagues: Scott M. Hynes, Hong Shen, Jianming Xiang, Zeng Lu, Jun Chen, Jie Shen, Huidi Jiang, Mohamed A. Kamal, Ke Ma, Dilara Jappar, Shupei Wu, Naoki Nishio, Bei Yang, Maria M. Posada, Yeamin Huh, Yehua Xie, Yuqing Wang, Xiaomei Chen, Xiaoxing Wang and Daniel Epling for

their whole-hearted support and assistance in my studies. I truly enjoyed working with them and appreciate their collaboration.

I also would like to acknowledge the Department of Pharmaceutical Sciences, College of Pharmacy and the University of Michigan for their generous financial aid, great facilities and wonderful faculty and staff whose supports make it feasible for me to pursue my Ph.D. degree. I am indebted to the National Institutes of Health (GM035498) for supporting my research project.

Most importantly, no words can completely express my gratitude to my beloved family and my dearest parents, brothers and sisters. Their sacrifice and limitless encouragement always motivated me to realize my dream. In particular, I want to say sorry and thanks to my wife, Xia, for her patience and for standing by me (shoulder to shoulder) during the past years, especially during difficult times. I also want to say thanks to my daughter Vivian and my son Jason. I am so proud of you both for your endeavors and achievements at your age. My life is filled fully with enjoyment, happiness and hope because of all of you. I have to acknowledge I have owed my family and parents too much in my lifetime. Whatever I have is yours … yesterday, today and tomorrow.

Last but not least, I also want to thank all of the friends and relatives in my life. I wish everyone a wonderful time, every day.

May God Bless!

TABLE OF CONTENTS

LIST OF TABLES

LIST OF FIGURES

LIST OF APPENICES

Development, Characterization And Application Of A Novel Mouse Line Humanized For The Intestinal Peptide Transporter PepT1

ABSTRACT

The proton-coupled oligopeptide transporter PepT1 is abundantly expressed on the apical side of small intestinal enterocytes and has major responsibility for the intestinal absorption of nutritional nitrogen, peptides and peptide-like drugs. However, there is growing evidence that a significant species difference exists in the affinity and capacity of substrates for PepT1. Therefore, a humanized PepT1 mouse model (huPepT1) was established by introducing hPepT1 genomic DNA into animals previously nulled for mouse PepT1. The mRNA and protein expression profiles indicated that huPepT1 mice had substantial but lower levels than wildtype animals in their expression of PepT1 in small intestine. However, colonic expression of PepT1 was greater in huPepT1 mice than wildtype mice, where the expression of PepT1 was quite low. *In situ* intestinal perfusion studies revealed that the permeability of glycylsarcosine (GlySar) and cefadroxil were similar, but lower, in the small intestine of huPepT1 mice as compared to wildtype animals. However, in colon, the permeability was greater in huPepT1 mice. Specificity studies, performed in the presence of potential inhibitors,

demonstrated that GlySar and cefadroxil permeability was largely, if not solely, dependent upon PepT1 function in wildtype and humanized mice. However, a species difference was observed in the jejunal flux kinetics of GlySar and cefadroxil, where their K_m values for PepT1 were 2-fold lower in humanized than wildtype mice. The *in vivo* studies indicated that the functional activity of intestinal PepT1 was fully restored for GlySar since nearly identical plasma concentration-time profiles and pharmacokinetic parameters were found following oral doses of GlySar in humanized and wildtype mice. After intravenous bolus doses of cefadroxil, virtually superimposable plasma concentration-time profiles were observed between wildtype and huPepT1 mice, and no differences were noted in clearance (CL), volume of distribution steady-state (V_{ss}), and terminal half-life ($T_{1/2}$) between these two genotypes. However, the C_{max}, T_{max} and AUC of humanized mice were 2-fold smaller than wildtype animals following oral dose escalation; $T_{1/2}$ was unchanged. The slopes of partial cumulative AUC vs. time plots demonstrated that the absorption rate of cefadroxil was 2-fold greater in wildtype mice, and the AUC was dose-proportional in these animals. In contrast, a less than proportional increase was observed in AUC with increasing oral doses of cefadroxil in humanized mice. Finally, the $AUC_{0\text{-}120}$ or C_{max} of cefadroxil vs. dose profiles showed that humanized huPepT1 mice and humans (results obtained from the literature) were more similar visually than that of wildtype mice and humans. In concluding, this dissertation presents for the first time the generation and characterization of a mouse model humanized for the intestinal peptide transporter huPepT1. This animal model should provide a valuable tool in probing the role, relevance and regulation of PepT1,

and in predicting the transport kinetics in humans. huPepT1 mice should also prove useful during the drug discovery process.

CHAPTER I

RESEARCH OBJECTIVES

Understanding the mechanisms of drug absorption, distribution, metabolism, excretion and transport (ADMET) is essential for improving the safety and efficacy of new chemical entities and therapeutic agents currently on the market. Using molecular biology techniques to clarify the role of proteins, particularly enzymes and transporters, in drug absorption and disposition is a priority of the pharmaceutical sciences. The first observation for active transport of the dipeptide glycylsarcosine (GlySar) in hamster jejunum *(in vitro)* lead to a new era of investigation for the cloning and functional characterization of transporters, and their relevance in drug kinetics and dynamics.

Among these well-defined transport proteins, peptide transporter 1 (PepT1), an integral membrane protein with 12 transmembrane domains, was brought to the forefront as a tempting delivery target for oral drugs and prodrugs. PepT1 transporter (SLC15A1) is one of four mammalian members in the solute carrier family 15 (SLC15). PepT1 protein is predominantly expressed on the

apical side of microvilli cells in small intestine, along with potential expression in colon (more controversial). The PepT1 transporter is well studied and responsible for facilitating the uptake of di-/tri-peptides and peptide-like drugs across the cell membrane from intestinal lumen.

Following the cloning of PepT1 from a rabbit intestinal cDNA library, orthologues of this transporter were soon identified, cloned and then evaluated from different species, including human, mouse and rat. Numerous studies have indicated that these cross-species PepT1 transporters shared broad-spectrum biological properties, such as low affinity and high capacity, ion dependence and proton coupling in transporting substrates across cellular membranes. However, one group recently reported that PepT1 transporters showed a species difference in yeast cells expressing the human, rat and mouse cDNA in which GlySar exhibited a saturable uptake in all three species, with 3- to 5-fold differences in the K_m values of mouse (0.30 mM), rat (0.16 mM) and human (0.86 mM). Furthermore, other studies reported a species difference for the PepT1 transporter using mPepT1 knockout and wildtype mice, as compared to human subjects. In particular, while investigating the PepT1-mediated intestinal absorption and pharmacokinetics of cefadroxil and valacyclovir after oral dose escalation, the AUC vs. Dose was linear in mice, as opposed to non-proportional increases in AUC vs. Dose being observed in humans.

In order to investigate *in vivo* species differences in the PepT1-mediated transport of peptides and peptide-like drugs, and to clarify the role and relevance of PepT1 in drug absorption and disposition in humans, a humanized huPepT1

mouse line was proposed as one of the best approaches to address pharmacokinetic discrepancies across species. Humanized huPepT1 mice would be generated using transgenic methodology, where the entire genomic hPepT1 DNA would be introduced into mPepT1 knockout mice. It was hypothesized that the humanized huPepT1 mice would restore the functional activities of PepT1 protein in these knockout mice to the level of wildtype animals. The humanized huPepT1 mouse line would be of special value because the human PepT1 gene would be controlled and regulated by its own regulatory elements, given that other mammalian systemic elements were conserved. Therefore, the protein expression levels, post-translational modifications, tissue distribution and PepT1 functional activity in humanized mice might be similar to that in human subjects.

With this in mind, the following specific aims were addressed in my dissertation:

Aim 1: To develop and validate a humanized huPepT1 mouse model, and characterize the mRNA and protein expression of hPepT1 in small and large intestines, and kidney as compared to that of wildtype mice

Aim 2: To define the *in situ* permeability of peptides (i.e., GlySar) or peptide-like drugs (i.e., cefadroxil) in humanized huPepT1 mice, and compare the results to wildtype and mPepT1 knockout mice

Aim 3: To investigate the *in vivo* oral absorption kinetics of peptides (i.e., GlySar) or peptide-like drugs (i.e., cefadroxil) in humanized huPepT1 mice, and compare the results to wildtype mice and human subjects

To achieve the proposed aims, various techniques in molecular biology, cell biology, animal sciences, pharmacology and pharmacokinetic-computational skills were applied during *in vitro, in situ, in vivo* and *in silico* studies. The derivative data from these studies in humanized huPepT1 and wildtype mice may provide valuable insight into understanding species differences in PepT1-mediated absorption and disposition kinetics of relevant substrates. Collectively, these humanized huPepT1 mice may offer a novel animal model to prospectively translate the pharmacokinetics of peptides/mimetics and peptide-like drugs from mice to humans during drug development.

CHAPTER II

BACKGROUND

2.1 Biological Structure Of Small Intestine

The small intestine in an adult human is approximately 3.5 meters in length (Gondolesi et al., 2012), along with a mean value of 2.5-3.0 centimeter in diameter. It is the longest part of the gastrointestinal tract and the principle site of absorption for any ingested compound and most oral medicines. Normally, the small intestine is divided into three segments differing at the microscopic structures: the duodenum, jejunum and ileum that comprise 5%, 50% and 45% of the length, respectively. The surface of the small intestine wall commonly contains: 1) circular folds that have a crescent shape, 2) small projections called villi, 3) tiny projections called microvilli. Villi are microscopic structures that have a hair-like shape and measures around 0.5-1.6 mm in height depending on the intestinal segment (Smith et al., 2010). Consequently, villi increase the internal surface area of the intestinal walls, which is useful for absorption of nutrients and drugs. Each villus contains a capillary network and a lymph vessel so that the

circulating blood can carry these nutrients away. Microvilli are microscopic cellular membrane protrusions on the apical (luminal) side of the intestinal epithelial cells, also called enterocytes, where highly differentiated microvilli of these cells increase its surface area substantially and are involved in a wide variety of functions, including absorption, secretion, cellular adhesion and mechanic transduction (Figure 2.1). Therefore, the inner surface of the small intestine is extremely scaled-up by villi and microvilli, and it is claimed that the average surface area of the small intestinal mucosa in an adult human is 30 square meters (Helander et al., 2014), which tremendously enhances the efficiency of absorption.

Under normal conditions, most of the absorption of electrolytes, nutrients, water and drugs occurs in the proximal segment of the small intestine, which is facilitated by its vast surface area. In the small intestine, absorption can be divided into two major categories, paracellular permeation and transcellular transport (Pade et al., 1997). Paracellular permeation occurs between the cells and is only possible for small molecules (Figure 2.2). Still, absorption through paracellular permeation is very low since the tight junctions restrict the passive transepithelial movement. Transcellular transport occurs across the cells and includes passive diffusion, endocytosis and carrier-mediated transport. Transcellular transport from lumen to blood requires uptake across the apical membrane, followed by movement through the cytosol, and then exit across the basolateral membrane and into the blood circulation (Figure 2.2). Carrier-mediated transport is facilitated or active for the influx and efflux of hydrophilic

drugs, toxins and metabolites. Numerous transporters have been extensively described in intestinal tissues, and most of them belong to two major transporter super-families, the ATP-binding cassette (ABC) and solute carrier (SLC) family (Oostendorp et al., 2009). Drug absorption relevant SLC families in the small intestine commonly locate on the apical side of epithelial cells, and includes the organic anion-transporting polypeptide (OATP) sub-family, the organic cation transporter (OCT) sub-family, and the proton-coupled oligopeptide transporter (POT; gene SLC15A) sub-family (Englund et al., 2006).

2.2 Proton-Coupled Oligopeptide Transporters (POTs)

Proton-coupled oligopeptide transporters (POTs), also known as peptide transporters (PTRs), are members of the solute carrier membrane proteins (SLC15A subfamilies) that mediate the cellular uptake of di-/tri-peptides in addition to a variety of peptide-like drugs. The mechanism by which peptide transport occurs across cellular membranes is an important topic in membrane carrier research, along with their impact on drug absorption, disposition, pharmacologic response and pathophysiology such as inflammatory bowel disease (Charrier et al., 2006, Merlin et al., 2001, Shi et al., 2006, Teuscher et al., 2004, Vavricka et al., 2006, Zucchelli et al., 2009). In mammals, four transporter members in SLC15 family have been identified with similar topology. They are denoted peptide transporter 1 (PepT1, SLC15A1), peptide transporter 2 (PepT2, SLC15A2), peptide/histidine transporter 1 (PhT1, SLC15A4) and peptide/histidine transporter 2 (PhT2, SLC15A3). In 1994, Hediger and

coworkers (Fei et al., 1994) first isolated the SLC15A1 gene encoding the PepT1 transporter from a rabbit intestinal cDNA library and evaluated its function. Using a similar approach (i.e., expression cloning), the same SCL15A1 gene and functional characteristics of rabbit PepT1 were subsequently confirmed by Boll and coworkers (Boll et al., 1994). In 1995, another peptide transporter PepT2 was cloned from human kidney (Liu et al., 1995). Three years later, the PhT1 transporter was cloned from rat brain and its functional activity characterized (Yamashita et al., 1997). Four years later, the PhT2 transporter was identified (Sakata et al., 2001). At present, the high-capacity low-affinity transporter PepT1 and the low-capacity high-affinity transporter PepT2 have been extensively studied, including their structure, localization, function, substrate specificity and regulation (Wang et al., 2010). However, much less is known about the cellular localization, function and regulation of the PhT1 and PhT2 transporters even though they have been discovered for more than 15 years. Still, it is known that PhT1 and PhT2 can translocate histidine in addition to some di/tri-peptides (Rubio-Aliaga et al., 2008). Recently, PhT1 was shown to have abundant expression in adult, but not neonatal, mouse brain in which expression levels steadily increased with age in rats, a finding believed to impact histamine homeostasis in the brain (Hu et al., 2014a). Furthermore, PhT1 protein was localized in cellular endosomes to regulate toll-like receptors, such as TLR9 and NOD1, thereby affecting the innate immune system and promoting colitis in mice (Baccala et al., 2013, Blasius et al., 2010, Blasius et al., 2012, Dosenovic et al., 2015, Nakamura et al., 2014, Sasawatari et al., 2011). However, the functional

role of PhT2 is still unclear although it is believed to be involved in inflammatory regulation (Wang et al., 2014). A comprehensive description of the four POT transporters is summarized in Table 2.1.

2.2.1 Structure And Function Of PepT1

The PepT1 gene is located on different chromosomes depending on species, where human PepT1 is on chromosome 13 (Liang et al., 1995, Ramamoorthy et al., 1995) and mouse PepT1 is on chromosome 14 (Rubio-Aliaga et al., 2000). Mouse PepT1 protein is composed of 709 amino acid residues, human PepT1 708 amino acid residues, and rat PepT1 710 amino acid resides. PepT1 transporter is an integral membrane protein, with a predicted molecular weight of 78 kDa and a high degree of glycosylation (Herrera-Ruiz et al., 2003, Wuensch et al., 2013a). Based on hydropathic analysis of amino acid sequences, PepT1 transporter has twelve putative transmembrane domains (TMDs) with a large extracellular loop between the 9^{th} and 10^{th} TMDs, and both the N-terminus and C-terminus being oriented toward the cytoplasmic side (Knutter et al., 2004) (Figure 2.3). Since 1990's, various approaches have been used to investigate the membrane topology of human PepT1 and the relationship between functional domains and its corresponding function. Studies with several constructed chimeras, consisting of different regions of PepT1 and PepT2, have shown that TMDs 1-4 and 7-9 are composed of protein domains that determine, or at least contribute, to substrate binding affinity (Doring et al., 1996). Several investigators have reported that TMDs 7-9 (Fei et al., 1998) and TMDs 1-6 determines the functional characteristics (Terada et al., 2000) of PepT1, and that

even small regions of N-terminal PepT1 is very important for affinity and function (Doring et al., 2002). Recently, the first high-resolution crystal structure of a prokaryotic POT transporter, PepTso (From bacterial *Shewanella oniedensis*), provided new insight in our structural understanding of peptide transport within a proton-coupled oligopeptide transporter (Newstead et al., 2011). The structure of PepTso revealed a novel asymmetrical occluded conformation, suggesting that while the N-terminal helix bundle should be less dynamic and more involved in peptide binding, the C-terminal helix bundle contains mobile gates, possibly driven by proton gradient. Furthermore, the 3.3Å resolution crystal structure of PepTst (From Bacterial *Streptococcus thermophilus*) confirmed that H1-H6 forming the N-terminal bundle connects to H7-H12 forming the C-terminal bundle (Solcan et al., 2012) by two additional semi-helices, HA and HB, to form a "V-shaped" structure that defines two hydrophilic cavities with a functional role. Based on the crystal structure of $PepT_{So}$, a possible mechanism of peptide transport was proposed, in which translocation occurred via the transitions among three states: 1) outward-facing, 2) occluded, and 3) inward-facing (Newstead, et al. 2011). A similar model was also proposed by Doki et al (Doki et al., 2013) using X-ray crystallography to assay the GkPOT protein (Figure 2.5). However, many questions remain unsolved regarding the mechanism of coupling, substrate recognition and structural transition. Further efforts are still needed to identify the structure of mammalian peptide transporters and to better understand its structural requirements and transport mechanism.

2.2.2 Substrate Specificity Of PepT1

The proton-coupled oligopeptide transporter PepT1 has a broad substrate spectrum, covering di/tri-peptides and a variety of peptide analogs and drugs. With a few exceptions, peptide transporters are able to recognize and transport up to 400 di-peptides and 8000 tri-peptides formed from 20 standard amino acids, plus numerous β-lactam antibiotics, selected angiotensin-converting enzyme (ACE) inhibitors, and other peptidomimetics (Brandsch et al., 2008, Rubio-Aliaga et al., 2002). Peptides consisting of L-amino acids are preferred over those containing individual D-amino acid residues, while those consisting solely of D-stereoisomers are not transported (Daniel et al., 1992). Most substrate specificity studies are based on the relationship between substrate transport and corresponding inhibition on substrate transporter activity. For example, the minimal structural requirements for a PepT1 substrate is that two opposite charged groups (NH_2 and COOH for di-peptide) be separated by an intra-molecular distance of 500-630 nm (Doring et al., 1998). Common essential structural features of PepT1 substrates are considered the following: a) with respect to stereospecificity, L-amino acids are preferred; b) a *trans*-conformation of the peptide bond, however, it can be replaced by a ketomethylene or thioxo group; c) hydrophobic side chains are preferred for high-affinity interactions, especially a positively charged N-terminus; d) for tripeptides, neutral amino acids are preferred as the third residue; e) a second peptide bond is not essential, and can be modified as well as methylated; f) a carboxylic group is not required at the C-terminus, but should contain a high electrogenic density region, such as an

aryl or phosphoric group; and g) a weakly basic group in the α-position of the N-terminus (Figure 2.7) (Brandsch, et al. 2008, Daniel et al., 2004, Rubio-Aliaga, et al. 2002, Rubio-Aliaga, et al. 2008, Zhang et al., 2013).

2.2.3 Mechanism For Di-/Tri-Peptide Transport

POT members are symporters that use a downhill proton gradient to co-transport di-/tri-peptides from the luminal side (pH≈5.5-6.0) into cells (pH≈7.0-7.2), against the peptide/drug concentration gradient (Kurtin et al., 1984, Lucas et al., 1975). Many PepT1 transport studies using cell cultures, Xenopus laevis oocytes, and yeast *Pichia pastoris* expression systems have confirmed that substrate uptake strongly depends on extracellular pH and membrane potential (Amasheh et al., 1997, Doring et al., 1997, Ganapathy et al., 1983, Margheritis et al., 2013, Zhu et al., 2000). It is generally believed that the proton gradient is generated and maintained by the activity of a Na^+/H^+ exchanger located on the apical side of the enterocyte (Thwaites et al., 1999). A typical model proposed for tertiary-active peptide uptake at the intestinal epithelial cells is illustrated in Figure 2.4. Dipeptides, tripeptides, β-lactams, ACE inhibitors, and prodrugs are transported by PepT1 into cells against a concentration gradient, where these activities are coupled to the movement of protons down an electrochemical proton gradient. The Na^+/H^+ exchanger (NHE) creates and maintains this proton gradient by pumping H^+ out of cells and Na^+ into cells. The intracellular Na^+ is then removed by Na^+-K^+-ATPase at the basolateral membrane. Once naturally occurring di-/tri-peptides enter the cell, they are hydrolyzed rapidly to their constituent amino acids and then enter the blood compartment through a large

group of basolateral-located amino acid transporters. In contrast, non-hydrolysable peptides and peptide-like drugs are transported by basolateral peptide transporter(s) into blood. The nature of this transport process is unclear at present since the responsible protein has not been cloned and characterized.

The dynamic mechanism by which PepT1 translocates di-/tri-peptides and peptide-like drugs was unclear until Doki and coworkers (Doki, et al. 2013) proposed a model to reveal the symport mechanism of proton-coupled oligopeptide transport (Figure 2.5). To understand the molecular mechanism of H^+-driven oligopeptide symport by POTs, a crystal structure of full length GkPOT, which is similar PepTso and PepTst, was defined. In this model, Arg43 and Glu310 played pivotal roles in substrate/H^+ coupling. Glu310 is first protonated and substrates bind to Arg43 and Glu310. The de-protonation of Glu310 and salt bridge formation between Arg43 and Glu310 then induces a structural transition between the inward-open and occluded states, and the subsequent release of peptide to the intracellular side. It should be appreciated that the structural transition cannot take place when o`nly proton is bound to transporter because the weak interaction between protonated Glu310 and Arg43 is of insufficient driving force to bring the N-terminal and C-terminal bundles close together. Likewise, the peptide substrate cannot bind to the peptide-binding pocket in the Glu310-deprotonated form because of the electrostatic repulsion observed between the carboxylate group of the peptide and the negative charge on the deprotonated Glu310 in the binding site.

The above mechanism is similar to the coupling model proposed for a fungal high-affinity phosphate transporter (Pedersen et al., 2013). However, although this model may explain the half-cycle of symport for PepT1, it does not explain the transition mechanism between the outward-facing and occluded forms. Notwithstanding this uncertainty, the authors (Doki, et al. 2013) hypothesized that the highly conserved Glu32 on helix H1 may play a role in the transition between outward-open and occluded states since the mutation of Glu32 to Gln32 abolished both the substrate uptake and counterflow activities. Even though great progress has been made from recent 3D structural studies of the POT membrane proteins, many aspects of transporter structural biology remain enigmatic.

2.2.4 Localization-Expression And Regulation Of PepT1

The expression levels and functional activities of peptide transporters are affected by various factors, such as developmental stage, physiological status, pathological conditions, hormones, and drugs (Rubio-Aliaga, et al. 2008), especially in regard to intestine, kidney and brain. In the small intestine, PepT1 protein is predominantly expressed at the apical membrane of enterocytes in mouse, rat and human duodenum, jejunum and ileum. For example, it was reported that PepT1 protein occupied 50% of the total amount of major membrane transporters present in the human jejunum (Drozdzik et al., 2014). It was also reported that along with species differences in protein density (Jappar et al., 2010, Tanaka et al., 1998), the expression of PepT1 protein in colon is still

controversial (Drozdzik, et al. 2014, Hu et al., 2014b, Jappar, et al. 2010, Wuensch et al., 2013b).

The expression of PepT1 is variable and a function of development and age. After birth, the expression level of PepT1 was found to increase markedly over 3-5 days to a maximal level in the small intestine. It then declined rapidly, reaching steady-state levels, close to that of adult, after 28 days. In the kidney, PepT1 expression levels were low in the adult rat (Hu, et al. 2014a, Shen et al., 1999).

Numerous studies have shown that diet can have a significant effect on the expression and activity of PepT1 in intestine. During a high protein diet, an increase in PepT1 mRNA was observed along with an increase in the intestinal transport of a model dipeptide in rats (Erickson et al., 1995, Shiraga et al., 1999). However, an increase was also observed in PepT1 expression in the small intestine of fasted rats (Ogihara et al., 1999) and mice (Ma et al., 2012). In addition, a diurnal rhythm was observed for PepT1 expression in rat small intestine, which was later speculated to be the result of diurnal food intake (Pan et al., 2004).

The expression of peptide transporters may be affected by some pathological conditions. PepT1 in the small intestine will be upregulated during inflammation, which also elicits an aberrant expression in colon where normally no PepT1 is expressed in healthy adult rats. A similar observation of colonic PepT1 upregulation was confirmed in patients with inflammatory bowel disease, including both ulcerative colitis and Crohn's disease (Coon et al., 2015, Merlin, et

al. 2001, Merlin et al., 1998). Contrary to these findings, PepT1 down regulation was observed by Wuensch et al (Wuensch et al., 2014).

Some hormones such as thyroid hormone, leptin, insulin and EGF, and drugs such as pentazocine, 5-fluorouracil, Ca^{2+}-channel blockers and cyclosporine A have been reported to affect the expression of peptide transporters (Daniel et al., 2003, Rubio-Aliaga, et al. 2008). For example, calcium channel blockers can indirectly stimulate the sodium-proton antiporter in intestine, thereby increasing the proton electromotive force and PepT1 activity (Wenzel et al., 2002).

2.2.5 Single Nucleotide Polymorphisms Of PepT1

Single nucleotide polymorphisms (SNPs) are defined as single base pair positions in genomic DNA that differ from normal alleles in the population with a frequency of 1% or greater (Brookes 1999). However, the term SNP is typically used more loosely, and may refer to single base variants in genomic DNA. Consequently, SNPs data-sets also contain SNP variants of less than 1% allele frequency.

Modern genetic techniques, particularly the advance of high-throughput DNA sequencing, provide powerful tools to screen for the abundance of SNPs that are present in enzymes and transporters during pharmacogenomic and pharmacogenetic studies. Genetic variants of peptide transporters could not only have an impact on nutritional absorption but could also contribute to the variable absorption and disposition of peptide-like drugs. An overview on the SNPs of transporter proteins was summarized by Gerloff (Gerloff 2004). Several studies

have reported the SNPs of POT transporters, especially for human PepT1 and PepT2 (Sobin et al., 2009, Zhang et al., 2004b).

Regarding the SNPs of human PepT1, Leabman and coworkers (Leabman et al., 2003) were the first to report the existence of several genetic variants, however, they did not offer corresponding functional data. Subsequently, Zhang et al (Zhang, et al. 2004b) found nine non-synonymous hPepT1 SNPs from a panel of 44 ethnically diverse individuals. The authors observed that only a Pro586Leu variant demonstrated a significantly reduced uptake of GlySar in transfected HELA cells, a result that might be explained by a post-translational reduction in protein expression. In a study reported by Anderle et al (Anderle et al., 2006), a low frequency PepT1-Phe28Tyr variant displayed a significantly reduced uptake of GlySar in HEK293 cells, an increased k_m for cephalexin in CHO and Cos7 cells, and a change in pH dependency. Other variants included Val2Ile in exon 1, Ser117Asn and Ser122Met in exon 5, Gly419Argin exon 16, Val450Ile, Thr451Asn and Arg459Cys in exon 17, Pro537Ser and many synonymous SNPs that did not show any significant change of peptide uptake (Anderle, et al. 2006, Zhang, et al. 2004b). One interesting “flip-flop” function of hPepT1-SNPs was observed by Zucchelli et al (Zucchelli, et al. 2009) when investigating a functional hPepT1-SNP. They reported a correlation of Ser117Asn with Crohn’s disease susceptibility in two cohorts of Swedish and Finnish patients, where the hPepT1-SNP showed a protective role in Finnish but increasing risk in Swedish subjects.

There is little information regarding the clinical relevance of genetic polymorphisms on oral drug bioavailability. Valacyclovir, a substrate of PepT1, was used to investigate the impact of hPepT1 polymorphisms on a pharmacokinetic study in 16 healthy volunteers (Phan et al., 2003). The authors reported that inter-individual differences in bioavailability were not related to genetic differences, suggesting that hPepT1 variants were, unlikely so far, to have clinical impact on drug absorption.

2.2.6 Homology Of PepT1 In Mammalian Species

Encoded by SLC15A1 genes, the human PepT1 protein has 708 residues, whereas mouse PepT1 has 709 amino acids and rat PepT1 has 710 amino acids. Cross-species protein sequence alignment using the Cluster W 2.1 program has shown that the amino acid identity is about 85.0%, 83.6% and 93.4% between hPepT1-mPepT1, hPepT1-rPepT1 and mPepT1-rPepT1, respectively (Figure 2.6). All important residues were conserved between species, including the Tyr12, His57, Tyr64, Tyr167, Trp294, Phe297 and Glu595 residues, which are crucial for forming the peptide-binding cavity of transporters and are important for peptide uptake. These residues are located within highly conserved transmembrane domains H1, H2, H5, H7 and H10, which match well with the findings from site-directed mutagenesis studies described in section 2.2.5. This is not surprising because, in general, residue mutations within a critical transmembrane domain might be fatal and, therefore, have less evolutionary pressure to change. On the other hand, mutations in non-critical

regions, such as the large extracellular loop between H9 and H10, may have more mutations since their impact is less drastic.

2.2.7 Prodrug Design Targeting Intestinal PepT1

Since the PepT1 transporter was predominantly expressed on the apical side of enterocytes, and assumes major responsibility for the uptake of di-/tri-peptide and mimetics from intestinal lumen, this transport protein has become an important target for enhancing the bioavailability of some poorly absorbed drugs. The PepT1-targeted approach for oral drug design has several advantages. First, PepT1 has a wide spectrum of substrate specificity including 400 dipeptides and 8000 tripeptides, and many peptide-like drugs such as bestatin, β-lactam antibiotics, angiotensin-converting enzyme (ACE) inhibitors and the prodrug valacyclovir (Meredith 2009, Yang et al., 2013a, Yang et al., 2013b). Second, PepT1 is a low-affinity (i.e., K_m ranges from 0.3-10 mM) and high-capacity transporter, therefore, it is not easily saturated following the typical doses of orally administered drugs (Hu et al., 2012). It is also possible that innovative design changes in chemical structure of a drug or prodrug might improve its chemical/metabolic stability in the intestines, as well as attenuates or nullifies the influence of efflux transporters. In particular, targeting of the intestinal transporter PepT1 is emerging as a promising strategy to improve the permeability-limited absorption of oral drugs, particularly those in the BCS III and IV categories.

According to the structure-transport requirements of PepT1, summarized in Figure 2.7 (Bailey et al., 2000, Daniel, et al. 2004, Meredith et al., 2000, Zhang, et al. 2013), rational prodrug design might include modifying parent drug

by adding amino acid or dipeptide-like moieties, or by adding an intermediate linker if necessary. As a result of covalent conjugation, prodrugs can be recognized as PepT1 substrates and, consequently, be effectively transported across cell membrane. However, inadequate bioconversion of prodrug (once absorbed) to the pharmacologically active species could impair its expected efficacy by remaining in the inactive prodrug form with potentially fatal side effects not usually observed in patients.

Successful synthetic approaches in designing prodrugs include the following categories (Zhang, et al. 2013): 1) amide-type prodrug – developed by attaching a carboxyl group of the pro-moiety (i.e., amino acid or small dipeptide) directly onto a free amino group of the parent drug, thus forming an amide bond, generally results in a prodrug with moderate affinity for PepT1. Typical prodrugs in this group include the anti-cancer drugs Pro-Phe-pamidronate and Pro-Phe-alendronate which have 3.8x higher bioavailability than their parent drug (Ezra et al., 2000), the prodrug LY544344 (developed for the anti-anxiety BCS III parent drug LY354740) which has a 10x higher intestinal permeability (Eriksson et al., 2010, Varma et al., 2009), and the hypotension drug midodrine (a derivative of 1-(2,5-dimethoxyphenyl)-2-aminoethanol) which has an improvement in bioavailability of 50% to 93% (Mackenzie et al., 1996, Tsuda et al., 2006); 2) ester-type prodrug - developed by conjugating an amino acid ester or dipeptide ester to the hydroxyl group of parent drug. The best example in this group is valacyclovir, the prodrug of active parent drug acyclovir, which belongs to BCS III and possesses activity against human herpes viruses, but with limited

bioavailability of 10-20%. In contrast, the prodrug valacyclovir has been reported to increase the oral bioavailability of acyclovir by 3- to 5-fold in humans (Weller et al., 1993). Another prodrug successfully approved by the FDA was Val-Val-saquinavir, a human immune-virus-1 (HIV-1) protease inhibitor which was modified from saquinavir in order to target both the PepT1 transporter as well as escape P-gp-mediated efflux to enhance oral bioavailability (Jain et al., 2007); 3) prodrug with intermediate linkers - developed by conjugating ketone-containing drugs with an appropriate intermediate linker, such as PEG. A typical prodrug, nabumeton (Foley et al., 2009), was reported to be a thio-dipeptide carrier prodrug and substrate of PepT1, which improved its transmembrane transport with enhanced resistance to hydrolysis.

Oral dosing is the preferred route of drug administration due to its convenience and patient compliance, and the trending importance of developing more hydrophilic compounds in the pharmaceutical industry. Thus, PepT1-targeted prodrug strategies have become an essential method to enhance the oral bioavailability of BCS III and IV class drugs.

2.3 Humanized Mouse Model

2.3.1 Rationale For Development Of Humanized Mouse Model

Animal models have become a valuable tool in understanding the absorption and disposition of drugs during normal physiology and during disease. Mouse models are especially useful since these animals have a well-known genetic background, are easy to breed, and have low maintenance costs. During

the past few decades, scientists have produced many genetically modified mouse strains in which a specific gene was removed or replaced by transgenic engineering technologies. These transgenic mouse models have proven to be powerful tools for identifying and validating target genes of interest, and in understanding their molecular mechanisms of activity. These engineered mouse models can generally be divided into three categories: additive transgenic, knockout and knock-in (Devoy et al., 2012).

Most humanized mouse models have focused on changing the coding region of the genome before recent progress in genomic analyses have identified the importance of non-coding regions of the genome (both transcribed and non-transcribed). Typically, a humanized mouse model can be generated by pronuclear injection or by gene targeting in embryonic stem cells, thus, creating gene knock-in mice. Since a protein encoded by human DNA can have different biochemical properties from their mouse orthologues, transgenic mice have often been made with human cDNAs encoding human protein, or by substituting the mouse loci with the entire human genomic loci (including coding and non-coding regions) into the mouse genome. The latter method is achieved by the addition of human genomic sequences or by replacing regions of the mouse genome with equivalent human genomic sequences contained in yeast artificial chromosomes (YACs) or bacterial artificial chromosomes (BACs) (Devoy, et al. 2012).

Why does one want to create a humanized mouse model? First, few proteins are conserved 100% between humans and mice (Gregory et al., 2002, Mouse Genome Sequencing et al., 2002), and differences in orthologous

sequences can lead to functional differences. For example, mouse serum amyloid P (SAP) binds to amyloid fibrils with only ~3% of the avidity of the human protein, even though mouse and human SAP are ~70% conserved (Hawkins et al., 1988). Second, a small number (<200) of human protein-coding genes do not have orthologues in mice (Stahl et al., 2009) and, as a result, it is necessary to introduce these human genes into mice for biological assessments. Third, the importance of non-coding regions would make it necessary to generate “genomic” humanized mice in order to investigate species-specific splicing patterns or to determine the function of “non-sense” sequences. For example, a long non-coding RNA of HOTAIR demonstrated different effects in humans as compared to its orthologue in mice, indicating that this RNA has a function in humans not easily determined from non-genomic humanized mice (Schorderet et al., 2011). Therefore, the non-coding genome must also be taken into account in studying gene function and genomic humanization will be essential to create an optimal set of models for human genes.

A key question about transgenic humanized mice concerns the extent to which a human DNA sequence is correctly and efficiently read by mouse transcriptional machinery. Little information is available in this area and it is generally assumed that the mammalian system is conserved between humans and mice.

2.3.2 Application Of Humanized Mouse Model In Drug Studies

As the time, cost and regulatory hurdles for testing new drug candidates in human subjects have increased, a greater emphasis has been placed in

developing preclinical models that can provide more predictive information about drug pharmacokinetic and pharmacodynamic profiles. The results obtained from *in vitro* systems and from *in vivo* animal testing have not always accurately predicted human-specific drug metabolic pathways (Anderson et al., 2009, Walker et al., 2009). Genetic modification of mouse models has proven one of the best ways in drug discovery to overcome potential species differences in the efficacy, pharmacokinetics and toxicological properties of compounds. Species differences in drug discovery were proposed by Caldwell et al (Caldwell 1981) by studying the species' inability to carry out a specific metabolism reaction (e.g., N-hydroxylation of aliphatic amines in rats). It was recognized that rodents metabolize xenobiotics differently from humans due to differences in the expression and catalytic activities of the P450s. For example, the murine Cyp2d genes do not have the same enzymatic activity as that in humans (Bogaards et al., 2000). To overcome species difference in P450s, and xenobiotic receptor expression and regulation machinery between rodents and humans, transgenic humanized mouse models were developed and these P450 humanized mice were evaluated for human toxicity risk and safety in drug discovery. In another example, humanized hCYP1A2 mice were shown to express CYP1A2 protein in a similar manner to that in humans. Compared with wild-type mice, a preferential N^2-hydroxylation of PhiP was demonstrated in humanized hCYP1A2 mice, a pathway for PhiP metabolism that in vitro studies revealed was predominant with the human orthologue (Cheung et al., 2008). Currently available humanized mouse models containing drug-metabolizing enzymes and xenobiotic receptors

were summarized by Scheer et al (Scheer et al., 2013) and Jiang et al (Jiang et al., 2011).

Recently, several organic anion-transporting polypeptide transporters (OATPs) were humanized in mice (van de Steeg et al., 2013) in which humanized OATP1B1, OATP1B3, and OATP1A2 transgenic mice showed partial or complete rescue of transporter function as compared to wildtype and knockout mice. A humanized multidrug resistance associated protein 2 (MRP2) mouse model versus mMRP2 null mice also demonstrated expression of the human transporter in the organs and cell types where MRP2 is normally expressed (Scheer et al., 2012). Still, further research is needed to address their species differences in drug pharmacokinetic studies.

2.3.4 Strategy In Generating A Humanized Mouse Model

Humanized mouse models can be generated with several technologies including additive transgenic and knock-in, as summarized by Devoy et al (Devoy, et al. 2012). The additive strategy for making humanized mouse models has often used human cDNAs, (e.g., MRP2 humanized mouse model (Scheer, et al. 2012) or bacterial artificial chromosome (BAC) DNA containing the complete human gene (e.g., CYP2D6 humanized mouse model by (Corchero et al., 2001)). Commonly, the cDNA construct comprises only the coding region, while the BAC construct consists of all the exons, introns, and 5’ and 3’-regulatory elements that are critical for genetic and epigenetic regulation of the transgene under physiological or pharmacological conditions. The construct is microinjected into fertilized zygotes followed by implantation of the eggs into pseudo-pregnant

females. Founders that carry the human gene can be crossed with a null background mouse to abolish endogenous gene effects, such that the humanized locus is only version expressed for the gene of interest (Figure 2.8). The advantage of this strategy is that the construct is easily prepared, the transgene has high expression of protein, and the humanized mouse model can be generated within a short period of time (<6 months). However, other endogenous genes can sometimes be interrupted, resulting in a loss of function because of random integration of the transgene. As a result, it is recommended that the transgenic mice be maintained as hemizygous rather than homozygous animals. In addition, it is impossible to regulate exactly how many copies of the transgene will be introduced and how many genes will join in a row by head to end as a concatemer (Bishop et al., 1989).

The second common strategy for making humanized mouse models is to integrate the transgene at specific and ubiquitously expressed chromosomal loci by homologous recombination or by site-specific recombination in embryonic stem cells (ESCs) (Figure 2.9) (Heaney et al., 2004, Prosser et al., 2008). The human gene is targeted and accurately integrated into an equivalent region of the mouse genome in ESCs, thus enabling a single copy of the human gene to residue at its natural site for expression while simultaneously replacing the gene at its corresponding mouse locus. This approach avoids the problems of deletion and concatemerization that may occur during random integration by non-homologous recombination. However, in contrast to the pronuclear microinjection, this approach requires a skilled manipulation of gene construct

and cell cultures, and is time consuming (~2 years). Still, it can achieve a more representative expression profile for the gene of interest and avoid the impact of complicating endogenous genes.

2.3.5 Bacterial Artificial Chromosomes

Bacterial artificial chromosomes (BACs) are circular plasmid DNA molecules that are hosted in *E.coli*. BACs, derived from the F factor of *E. coli,* can accommodate genomic inserts of DNA up to 300 kb (Shizuya et al., 1992). BAC vectors, such as pBeloBAC11, carry all the sequences needed for autonomous replication, copy-number control and partitioning of the plasmid (Hunter et al., 1999). BACs are maintained as low-copy replicons and correspondingly yield lower quantities of DNA, but propagate large DNA inserts with high stability and a low frequency (<5%) of chimeras (Monaco et al., 1994).

The use of BACs in transgenic experiments was first reported in 1997 (Yang et al., 1997). Since then, BACs have been applied widely for studies including molecular complementation of mutations, *in vivo* studies of gene function, analysis of gene dosage, and identification and analysis of regulatory sequences (Giraldo et al., 2001). BACs have been microinjected in three different forms: circular supercoiled plasmid, linearized DNA and purified insert. BAC transgenic mice mostly carry a limited number of integrated transgene copies (<5) but up to 13 copies (Nielsen et al., 1997). However, there are not many studies addressing copy number-related expression of BAC transgenic mice.

2.4 Predicting Pharmacokinetic Parameters

2.4.1 Species Differences

Accurately and efficiently predicting the pharmacokinetic profiles of drugs in humans from preclinical data remains a problem in drug development. In general, the approach for predicting drug pharmacokinetics in humans can be broadly divided into two categories: physiologically-based pharmacokinetic modeling and allometric scaling. The application of allometric scaling in humans is widely accepted because of its simplicity (Obach et al., 1997). Predictions of human pharmacokinetics using interspecies allometric scaling was summarized by Kang et al (Kang et al., 2011).

Interspecies allometric scaling methods are highly empirical and may be unreliable in predicting ADME because of differential expression patterns and functional characteristics of the proteins involved in differing animal species. For example, Takahashi et al. (Takahashi et al., 2009) concluded that the low bioavailability of several drugs (e.g., verapamil, methotrexate) in cynomolgus monkeys could be attributed not only to hepatic first-class metabolism but to intestinal absorption differences caused by divergent P450 enzyme activities between humans and monkeys. One impressive case involved a comparison of the permeability coefficients of 10 compounds between rat and human jejunum, as reported by Fagerholm et al (Fagerholm et al., 1996). The P_{eff} coefficients were investigated with *in situ* single-pass perfusions of rat jejunum and compared to corresponding human values in vivo. The results indicated that, for passively absorbed drugs, P_{eff} values were 3.6 times higher in human than rat and

significant deviations from linearity occurred for compounds that were actively transported. In 2006, Cao et al. compared the oral bioavailability of rats and humans for a variety of compounds with different absorption mechanisms, including passive diffusion and active transport. No correlation was found in oral drug bioavailability between these two species (r^2=0.29), a finding agreed to by a previous report (Chiou et al., 2002), even though some transcripts shared similarly high expression levels of mRNA in the small intestine (r^2>0.56). Furthermore, conflicting results were obtained by another group (Kim et al., 2007), who compared mRNA expression profiles of intestinal transporters in mice, rats and humans. In analyzing a total of 86 transporter genes in mice, 50 transporter genes in rats and 61 transporter genes in humans, they found the PepT1 gene to exhibit significant differences between species (i.e. about 2-fold between mice and humans, and about 6-fold between rats and humans). Overall, the results indicated that rodents and humans exhibit disparate levels of transcriptional proteins.

A tragedy during the first Phase I clinical trial of TGN1412 made a good point of illustrating the difficulty of prediction from animal models to humans (Suntharalingam et al., 2006). It was observed that all six healthy subjects suffered an unexpected severe cytokine storm that resulted in multiple organ failure shortly after TGN1412 administration, even though preclinical animal models, including mice and monkeys, had shown that this monoclonal antibody was safe. Recent data suggested that the CD28 receptor for binding TGN1412 was not expressed in the $CD4^+$ effecter memory T cells of preclinical animals that

were used for safety testing (Eastwood et al., 2010). The unexpected 'cytokine storm' occurred in humans even though the amino acid sequences of receptor CD28 were identical between species as was the affinity for binding with TGN1412.

With the increasing number of species differences being discovered in drug development, further effort is necessary to improve the reliability in translating animal pharmacokinetics, response and toxicity to humans.

2.4.2 Glycylsarcosine (GlySar)

Peptide transporters (POTs) predominantly absorb di-/tri-peptides and peptide-like drugs from the intestinal lumen via uptake across the apical membrane. Glycylsarcosine (GlySar, MW=146) is currently used as a model dipeptide substrate for evaluating the functional activity of peptide transporters (Figure 2.10 top) because it is resistant to hydrolysis by peptidases, not metabolized, and commercially available in radioactive form (Hu, et al. 2012, Jappar, et al. 2010, Ocheltree et al., 2005). Since GlySar is a synthetic chemical, with no medical indications in human patients, there are no any data available from clinical studies.

However, when GlySar was compared in wildtype and PepT1 knockout mice, its partial AUC was proportional to dose in both genotypes, along with a 60% reduction in GlySar absorption in PepT1 knockout mice compared with wildtype animals (Jappar et al., 2011). Furthermore, our group recently reported that PepT1 transporters showed a species difference in yeast cells expressing the human, rat and mouse PepT1 cDNA, in which GlySar uptake exhibited

saturable kinetics in all three species, with 3- to 5-fold differences in Km values for mouse (0.30 mM), rat (0.16 mM) and human (0.86 mM) (Table 2.2).

2.4.3 Cefadroxil (CEF)

Cefadroxil (Figure 2.10 bottom), the para-hydroxy derivative of cephalexin, belongs to the first generation of β-lactam antibiotics that are usually administrated orally to patients for the treatment of mild to moderate susceptible infections, such as pneumonia caused by *Streprococcus pyogenes* and urinary tract infections caused by *E. coli* and *P.mirabilis* (Tanrisever et al., 1986). Among the aminocephalosporin drugs, cefadroxil has broad-spectrum activity, is more effective agent than either cephalexin or cephradine because of its slow rate of excretion into urine and slightly slower rate of absorption from the gastrointestinal tract. This drug is also a good oral candidate to substitute for penicillins because of concerns over allergic reactions to penicillins during outpatient therapy (Campagna et al., 2012).

Cefadroxil (6R,7R)-7-[D-2-amino-2-(4-hydroxyphenyl) acetyl]amino]-3-methyl-8-oxo-5-thia-l-anabicyclo[4.2.0]oct-2-ene-2-carboxylic acid, has a zwitter-ionic structure with an α-amino group in the side chain at position 7 and a free carboxylate group at position 4, in which the free α-amino group is generally believed to be essential for affinity to the peptide transporters (Tamai et al., 1995). However, recent studies indicated that beta-lactam antibiotics without an α-amino group are transported by a carrier-mediated mechanism that is common

to dipeptides (Muranushi et al., 1989, Tsuji et al., 1987a, Tsuji et al., 1993, Tsuji et al., 1987b, Yoshikawa et al., 1989).

Cefadroxil is believed to be a substrate for proton-coupled oligopeptide transporters (POT) because of the presence of an α-amino group, carboxylic group and peptide bond (Taylor et al., 1995), which are similar to physiological occurring peptides. Soon after cloning the PepT1 gene, which is predominantly expressed on the apical side of enterocytes, cefadroxil was confirmed as a substrate of PepT1 (Boll, et al. 1994). In addition, the intestinal transport of cefadroxil was saturable and shown to follow Michaelis-Menten kinetics (Garcia-Carbonell et al., 1993, Garrigues et al., 1991, Sanchez-Pico et al., 1989, Sinko et al., 1988, Wenzel et al., 1996). Still, other transporters have been found to transport cefadroxil. For example, the PepT2 transporter, which is located on the apical side of epithelial cells in choroid plexus and renal proximal tubule cells, is responsible for cefadroxil uptake from CSF and reabsorbed from urine (Ocheltree et al., 2004, Shen et al., 2005, Shen et al., 2007). However, it is still unclear how cefadroxil crosses the basolateral membrane of renal epithelial cells to reach the blood. However, transporters (active and facilitative) present at the basolateral membrane of epithelial cells in small intestine and kidney tubule cells are thought to be responsible for the cellular efflux of negatively charged endogenous and exogenous compounds, including cefadroxil. Transport experiments with plasma membrane vesicles indicated that cefadroxil was transported, in part, by ABCC3 (MRP3) and ABCC4 (MRP4), which localize on the basolateral membrane of small intestine (de Waart et al., 2012). In the kidney, vectorial secretion of

cefadroxil is achieved via cellular uptake at the renal basolateral membrane by OAT1 (SLC22A6) and OAT3 (SLC22A8), coupled to cellular efflux at the renal apical membrane by ABCC4 (MRP4) (Granero et al., 1994, Khamdang et al., 2003, Russel et al., 2008). In addition, the OATP2 transporter was shown to transport cefadroxil using a *Xenopus laevis* oocyte expressing system (Nakakariya et al., 2008a, Nakakariya et al., 2008b).

In metabolism and pharmacokinetic studies, cefadroxil is stable both *in vitro* and *in vivo*. It is neither hydrolyzed in the acidic environment of the stomach nor degraded by intra-/extra-cellular enzymes. As a substrate of PepT1, cefadroxil has a high bioavailability despite its anionic charge in the intestine and poor lipophilicity (Ginsburg et al., 1980, Oliveira et al., 2000, Otoom et al., 2004, Santella et al., 1982). The oral bioavailability of cefadroxil is not influenced by food and >90% of the drug is excreted unchanged in the urine within 24 hours because of free glomerular filtration, due to low serum binding of less than 20% (Bergan 1984), and active tubular secretion (Bins et al., 1988). Cefadroxil is also a substrate of PepT2 and, because of extensive renal reabsorption, the drug has a relatively longer half-life (~1.5 hrs.) than cephalexin, which is prolonged in patients with renal impairment (Brisson et al., 1982, Hampel et al., 1982, La Rosa et al., 1982, Marino et al., 1982, Olin 1980, Pfeffer et al., 1977, Prenna et al., 1980, Santella, et al. 1982, Tanrisever, et al. 1986). To complicate matters, cefadroxil has been reported to have non-linear oral absorption and disposition kinetics within the usual dosage range of 250 - 2000 mg in healthy subjects, presumably because of capacity-limited PepT1 intestinal absorption, OAT renal

secretion, and PepT2 renal reabsorption (Arvidsson et al., 1979, Garcia-Carbonell, et al. 1993, Garrigues, et al. 1991, La Rosa, et al. 1982). However, cefadroxil was found to have linear absorption and disposition kinetics in wildtype mice during oral escalation studies, where its partial $AUC_{0\text{-}120}$ and C_{max} was proportionally increased with increasing dose (Posada et al., 2013).

Overall, PepT1, located at the apical membrane of small intestine, is a high-capacity low-affinity POT family member that is solely responsible for the uptake of nutrient di/tri-peptides and peptide-like drugs from the intestinal lumen. However, cross-species differences in pharmacokinetics make it difficult to translate animal studies in mice to that in humans. Therefore, the development and validation of a humanized huPepT1 mouse model might provide a valuable approach for clarifying the mechanism of species difference in drug absorption, and further aid drug design and discovery in a more rational way.

Table 2.1 Molecular and functional features of POT transporters

Feature	PepT1	PepT2	PhT1	PhT2
Human Gene Name	SLC15A1	SLC15A2	SLC15A4	SLC15A3
Mammalian Species	Rat, rabbit, human, mouse	Rat, rabbit, human, mouse	Rat	Rat
Amino Acids	707-710	729	572	582
Human Gene Locus	13q33-q34	3q13.3-q21	12q24.32	11q12.1
Sequence Accession ID	NM-005073	NM-021082	NM-145648	NM-016582
Splice Variants	hPEPT1-RF		A, A', B and hPTR4	Multiple
Transmembrane Domains	12	12	12	12
Protein Kinase A Sites	0-1	0-3	0	2
Protein Kinase C Sites	1-2	2-5	11	4
Glycosylation Sites	4-7	2-5	4	3
Amino Acid Identity	~80-90% (species)	~80-90% (species) ~50% (PEPT1)	< 20% (PEPT1/2)	<20% (PEPT1/2) ~50% (PHT1)
Transport Type/Coupling	Cotransporter/H^+	Cotransporter/H^+	Cotransporter/H^+	Cotransporter/H^+
Amino Acids in Substrate	2-3	2-3	2-3	2
L-Histidine Transport	No	No	Yes	Yes
Stereoselectivity	L>D	L>D	---	---
Substrate Affinity	Low	High	High	---
K_m Values	mM	uM	uM	---
Stoichiometry	1:1 (proton:substrate)	2:1 (proton:substrate)	---	---

Information was obtained Hong Shen's Dissertation(Hong 2006).

Table 2.2 Species-dependent affinity of glycylsarcosine for PepT1 (Hu, et al. 2012)

Animal Species	GlySar Km (mM)	Experimental Conditions for Uptake	Reference
Rabbit	1.9	cRNA-injected XLO, pH5.5	(Fei, et al. 1994)
Human	0.29	cDNA-transfected HeLa Cells, ph6.0	(Liang, et al. 1995)
Rat	0.24	cRNA-injected XLO, pH6.0	(Zhu, et al. 2000)
Mouse	0.75	cRNA-injected XLO, pH5.5	(Fei et al., 2000)
Sheep	0.61	cRNA-injected XLO, pH5.5	(Pan et al., 2001)
Chicken	0.47	cRNA-injected XLO, pH6.0	(Chen et al., 2002)
	2.6	cDNA-transfected CHO Cells, ph6.0	
Monkey	0.35	cDNA-transfected HeLa Cells, ph6.0	(Zhang et al., 2004a)
Pig	0.94	cDNA-transfected CHO Cells, ph6.0	(Klang et al., 2005)
Salmon	0.5	cRNA-injected XLO, pH6.5	(Ronnestad et al., 2010)
Rat	0.16	cDNA-Yeast Cells, pH 6.5	(Hu, et al. 2012)
Mouse	0.30	cDNA-Yeast Cells, pH 6.5	(Hu, et al. 2012)
Human	0.86	cDNA-Yeast Cells, pH 6.5	(Hu, et al. 2012)

* XLO: Xenopus lavis oocytes

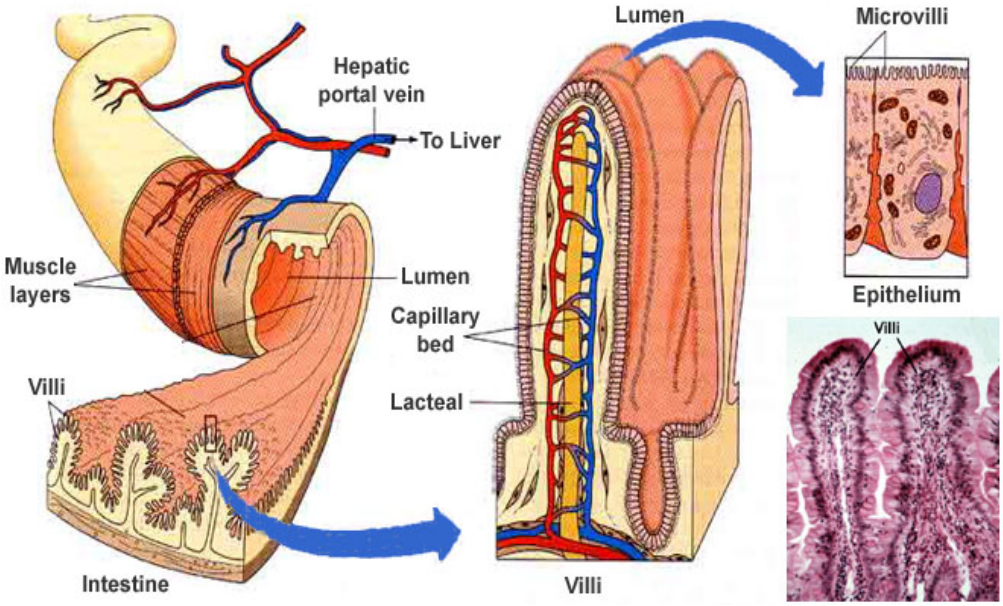

Figure 2.1. Biological structure of the small intestine and its microscopic architecture, including the structure of villi, microvilli and epithelial cells. (Adopted from http://medicalterms.info/anatomy/Small-Intestine/)

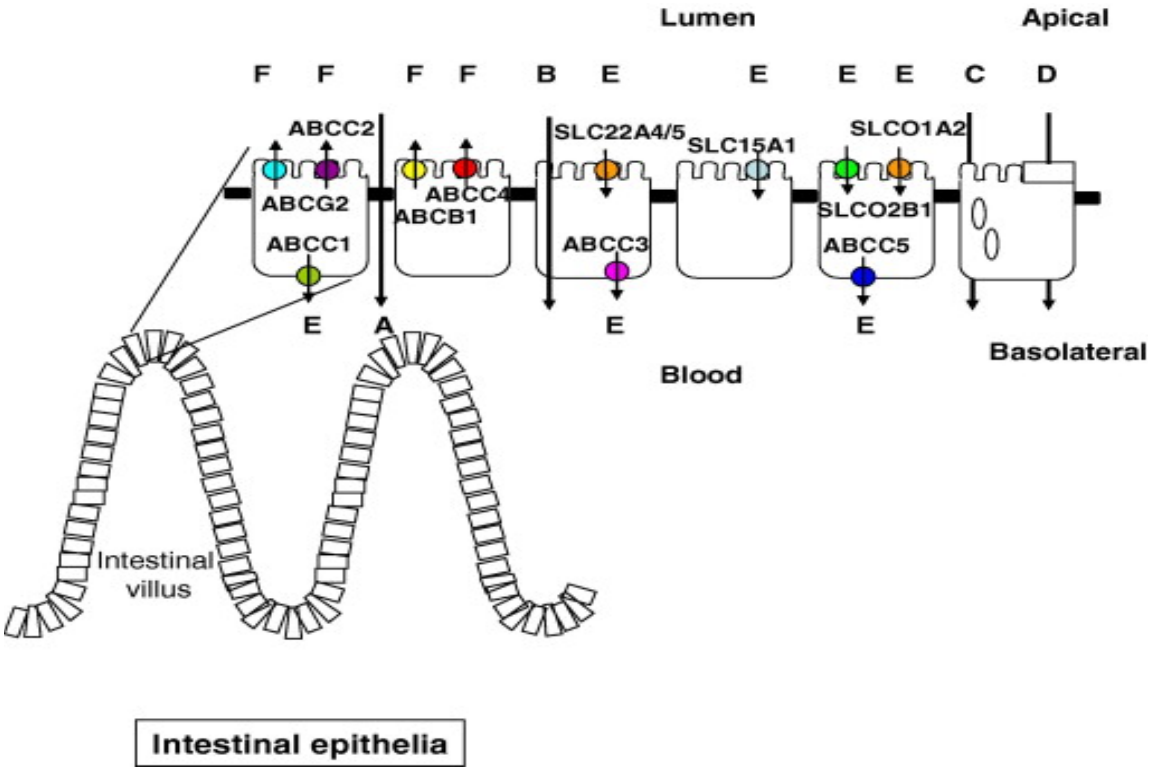

Figure 2.2. Mechanisms of transport through the intestinal epithelium. (A) Paracellular transport; (B) Passive diffusion; (C) Endocytosis; (D) Carrier-mediated transport; (E) Carrier-mediated uptake; (F) Carrier-mediated efflux (Oostendorp, et al. 2009)

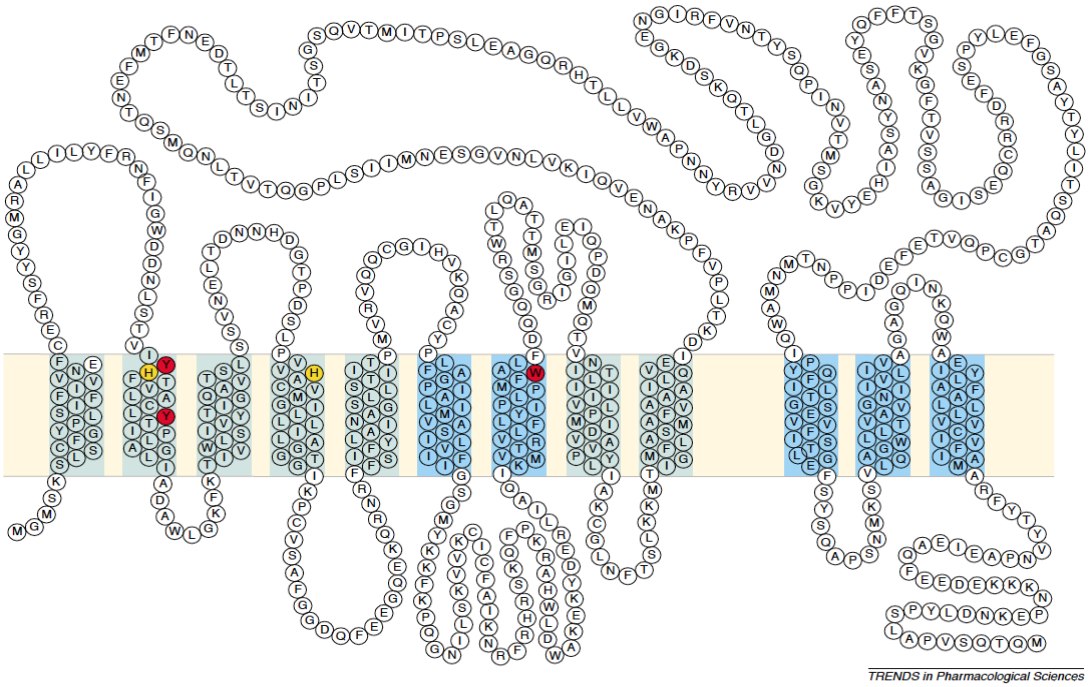

Figure 2.3. Membrane topology of peptide transporter 1 (PepT1). The protein contains 12 transmembrane domains (TMDs), with N-terminal and C-terminal ends in the cytoplasm (Rubio-Aliaga, et al. 2002).

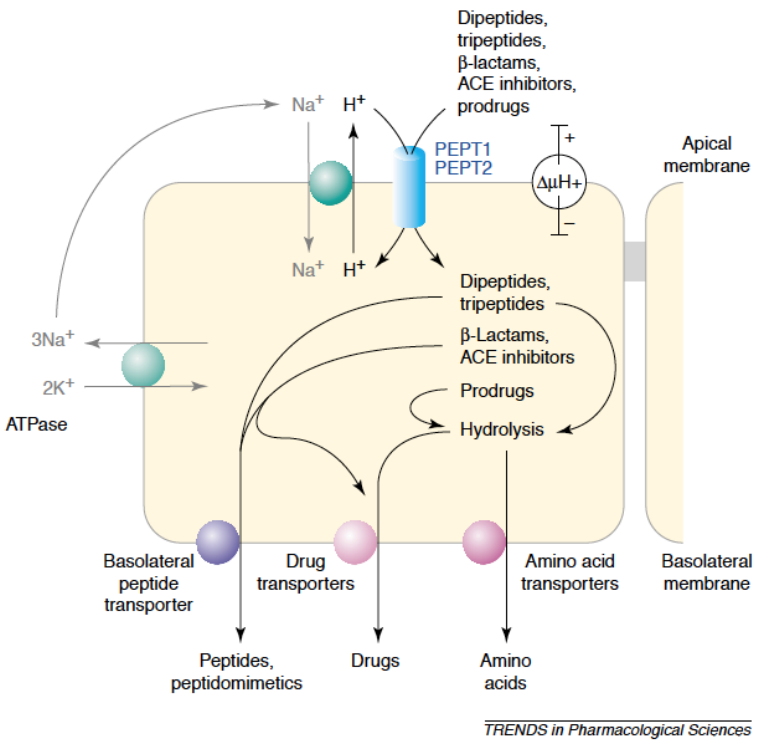

Figure 2.4 Model of peptide transport in epithelial cells. Di-/tri-peptides digested from ingested protein, were transported by the proton-coupled transporter PepT1 from intestinal lumen into epithelial cells, then hydrolyzed in the cytosol and effluxed into blood through various transporters located at the basolateral membrane. The driving force for uptake is dependent upon an electrochemical proton gradient across the membrane, partly produced by the apical Na^+-H^+ exchanger, in which the Na^+ gradient was established by Na^+/K^+ ATPase. (Rubio-Aliaga, et al. 2002)

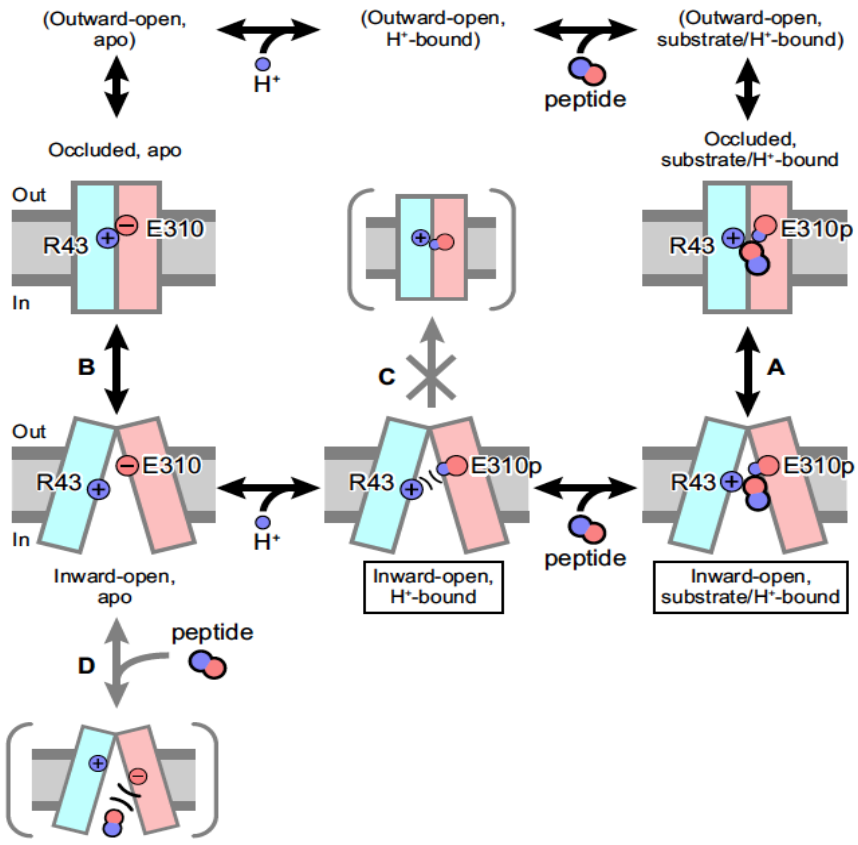

Figure 2.5. Model of the substrate/proton-coupled structural transition between the inward-open and partially occluded states for GsPOT transporter. The symport cycle was illustrated as half of transition including the inward-open and occluded forms. Black arrows represent the physiological symport cycle, and gray arrows represent other transitions (Doki, et al. 2013).

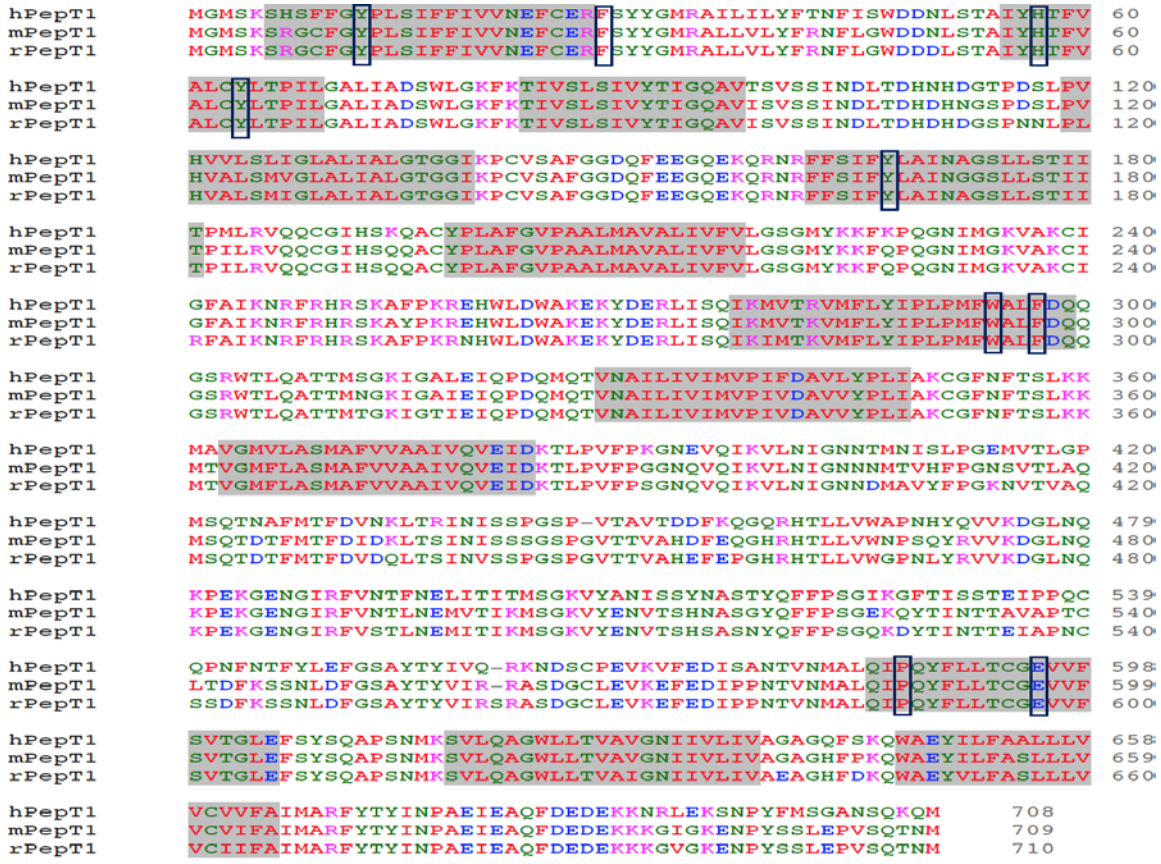

Figure 2.6. Cross-species protein sequence alignment between human, mouse and rat PepT1 transporters using the Cluster W 2.1 program. The transmembrane domains are colored in grey, and conserved amino acid residues are highlighted in the blue box.

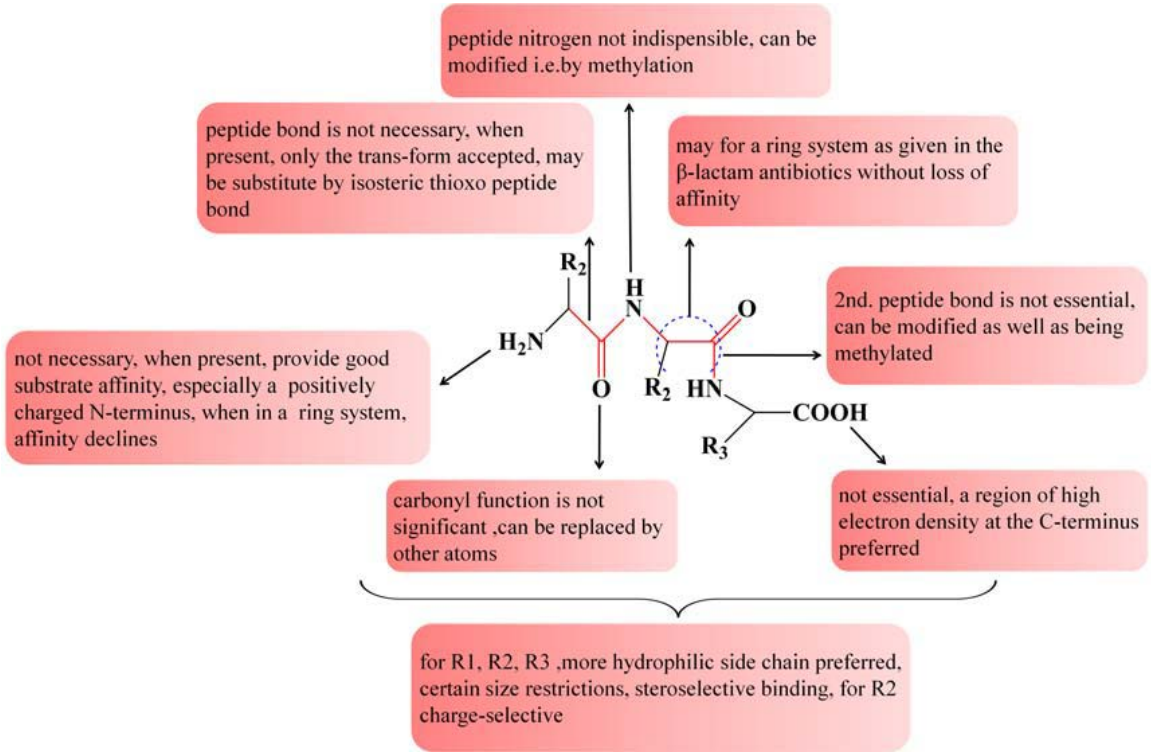

Figure 2.7 Key molecular structural features in compounds determining recognition as a substrate of PepT1. Critical structural properties that are essential for affinity are presented on the backbone of a tripeptide model (Zhang, et al. 2013).

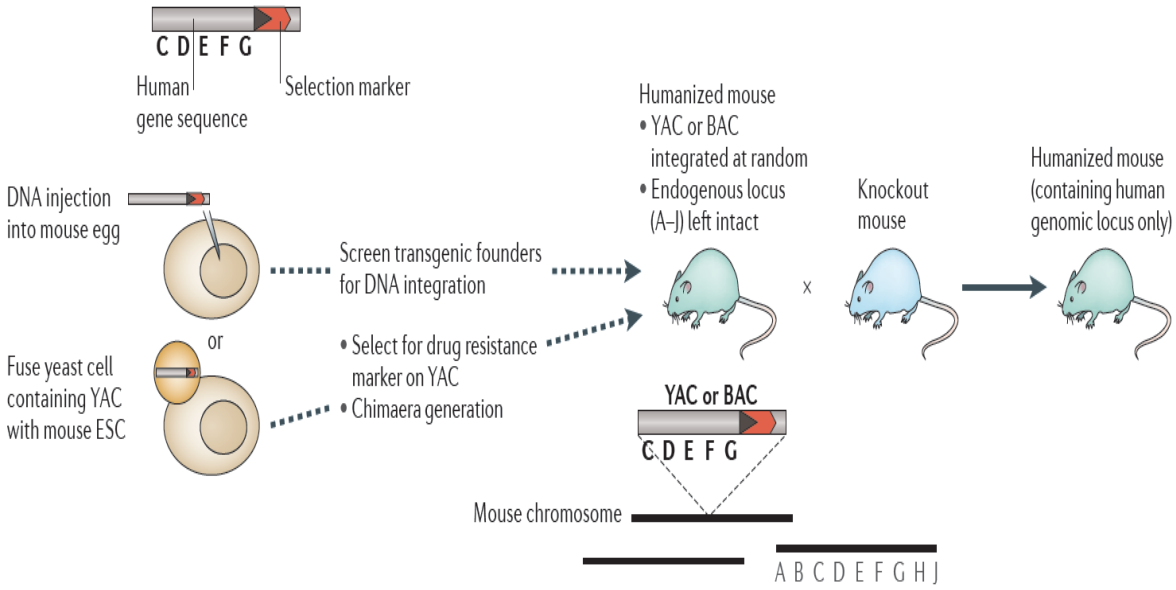

Figure 2.8. Humanized mouse model by additive transgenesis. The targeted human gene, either cDNA or genomic DNA, was injected into a fertilized mouse egg, and the egg was then transferred to a pseudopregnant foster mother for development. After the pups were delivered, genotyping PCR was applied to screen out the positive founders, which were then cross-mated with knockout mice to produce the desired humanized mice (Devoy, et al. 2012).

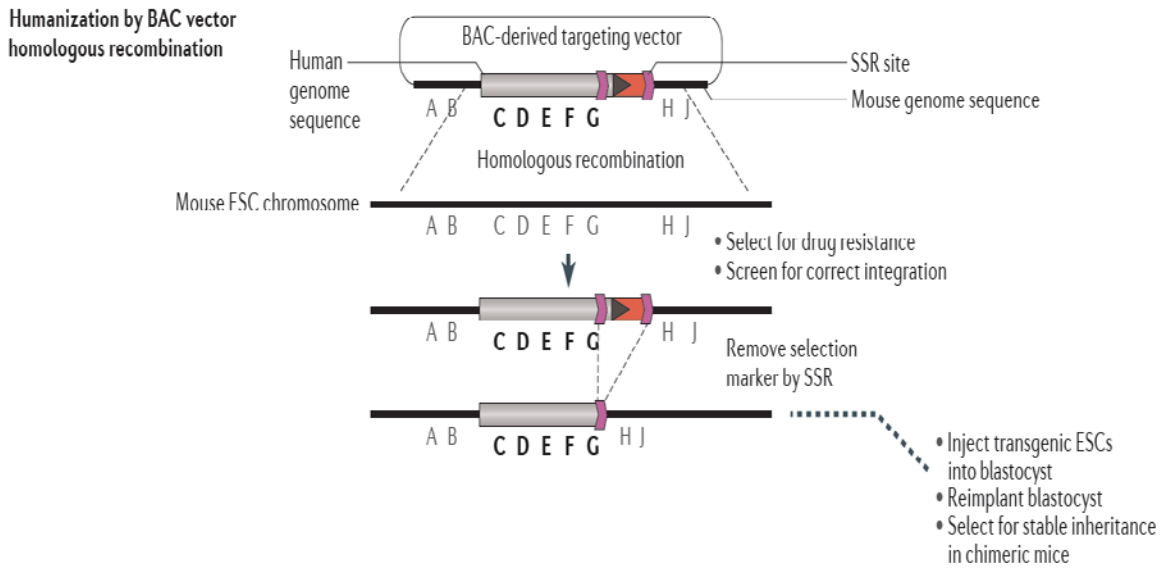

Figure 2.9. Humanized mouse model by specific knock-in strategy. The mouse endogenous genome locus was replaced by a human genome BAC vector through homologous recombination in ESCs (Embryonic Stem Cells), such that the endogenous mouse locus was replaced by an equivalent human sequence. After positive colonies were screen out, the selection marker was removed by SSR (Site Specific Recombinase). Then transgenic ESCs were injected into blastocysts for producing humanized mice that can inherit the human gene by germline transmission (Ahn et al., 2010, Devoy, et al. 2012).

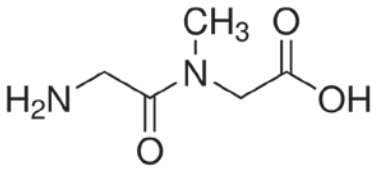

GlySar

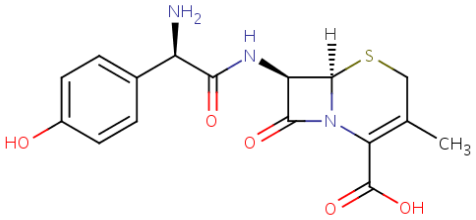

Cefadroxil

Figure 2.10. The molecular structures of GlySar (top) and cefadroxil (bottom). Both compounds are substrates of PepT1 and PepT2.

REFERENCE

Ahn SW, Kim SH, Kim JH, Choi S, Yeum CH, Wie HW, Sun JM, So I and Jun JY (2010) Phentolamine inhibits the pacemaker activity of mouse interstitial cells of Cajal by activating ATP-sensitive K+ channels. *Archives of pharmacal research*. **33:** 479-489.

Amasheh S, Wenzel U, Boll M, Dorn D, Weber W, Clauss W and Daniel H (1997) Transport of charged dipeptides by the intestinal H+/peptide symporter PepT1 expressed in Xenopus laevis oocytes. *J Membr Biol*. **155:** 247-256.

Anderle P, Nielsen CU, Pinsonneault J, Krog PL, Brodin B and Sadee W (2006) Genetic variants of the human dipeptide transporter PEPT1. *J Pharmacol Exp Ther*. **316:** 636-646.

Anderson S, Luffer-Atlas D and Knadler MP (2009) Predicting circulating human metabolites: how good are we? *Chem Res Toxicol*. **22:** 243-256.

Arvidsson A, Borga O and Alvan G (1979) Renal excretion of cephapirin and cephaloridine: evidence for saturable tubular reabsorption. *Clinical pharmacology and therapeutics*. **25:** 870-876.

Baccala R, Gonzalez-Quintial R, Blasius AL, Rimann I, Ozato K, Kono DH, Beutler B and Theofilopoulos AN (2013) Essential requirement for IRF8 and SLC15A4 implicates plasmacytoid dendritic cells in the pathogenesis of lupus. *Proc Natl Acad Sci U S A*. **110:** 2940-2945.

Bailey PD, Boyd CA, Bronk JR, Collier ID, Meredith D, Morgan KM and Temple CS (2000) How to Make Drugs Orally Active: A Substrate Template for Peptide Transporter PepT1. *Angew Chem Int Ed Engl*. **39:** 505-508.

Bergan T (1984) Pharmacokinetics of beta-lactam antibiotics. *Scandinavian journal of infectious diseases. Supplementum*. **42:** 83-98.

Bins JW and Mattie H (1988) Saturation of the tubular excretion of beta-lactam antibiotics. *British journal of clinical pharmacology*. **25:** 41-50.

Bishop JO and Smith P (1989) Mechanism of chromosomal integration of microinjected DNA. *Mol Biol Med*. **6:** 283-298.

Blasius AL, Arnold CN, Georgel P, Rutschmann S, Xia Y, Lin P, Ross C, Li X, Smart NG and Beutler B (2010) Slc15a4, AP-3, and Hermansky-Pudlak syndrome proteins are required for Toll-like receptor signaling in plasmacytoid dendritic cells. *Proc Natl Acad Sci U S A*. **107:** 19973-19978.

Blasius AL, Krebs P, Sullivan BM, Oldstone MB and Popkin DL (2012) Slc15a4, a gene required for pDC sensing of TLR ligands, is required to control persistent viral infection. *PLoS Pathog*. **8:** e1002915.

Bogaards JJ, Bertrand M, Jackson P, Oudshoorn MJ, Weaver RJ, van Bladeren PJ and Walther B (2000) Determining the best animal model for human cytochrome P450 activities: a comparison of mouse, rat, rabbit, dog, micropig, monkey and man. *Xenobiotica*. **30:** 1131-1152.

Boll M, Markovich D, Weber WM, Korte H, Daniel H and Murer H (1994) Expression cloning of a cDNA from rabbit small intestine related to proton-coupled transport

of peptides, beta-lactam antibiotics and ACE-inhibitors. *Pflugers Archiv : European journal of physiology*. **429:** 146-149.

Brandsch M, Knutter I and Bosse-Doenecke E (2008) Pharmaceutical and pharmacological importance of peptide transporters. *The Journal of pharmacy and pharmacology*. **60:** 543-585.

Brisson AM and Fourtillan JB (1982) Pharmacokinetic study of cefadroxil following single and repeated doses. *The Journal of antimicrobial chemotherapy*. **10 Suppl B:** 11-15.

Brookes AJ (1999) The essence of SNPs. *Gene*. **234:** 177-186.

Caldwell J (1981) The current status of attempts to predict species differences in drug metabolism. *Drug Metab Rev*. **12:** 221-237.

Campagna JD, Bond MC, Schabelman E and Hayes BD (2012) The use of cephalosporins in penicillin-allergic patients: a literature review. *The Journal of emergency medicine*. **42:** 612-620.

Charrier L and Merlin D (2006) The oligopeptide transporter hPepT1: gateway to the innate immune response. *Lab Invest*. **86:** 538-546.

Chen H, Pan Y, Wong EA, Bloomquist JR and Webb KE, Jr. (2002) Molecular cloning and functional expression of a chicken intestinal peptide transporter (cPepT1) in Xenopus oocytes and Chinese hamster ovary cells. *J Nutr*. **132:** 387-393.

Cheung C and Gonzalez FJ (2008) Humanized mouse lines and their application for prediction of human drug metabolism and toxicological risk assessment. *The Journal of pharmacology and experimental therapeutics*. **327:** 288-299.

Chiou WL and Buehler PW (2002) Comparison of oral absorption and bioavailablity of drugs between monkey and human. *Pharm Res*. **19:** 868-874.

Coon SD, Rajendran VM, Schwartz JH and Singh SK (2015) Glucose-dependent insulinotropic polypeptide-mediated signaling pathways enhance apical PepT1 expression in intestinal epithelial cells. *American journal of physiology. Gastrointestinal and liver physiology*. **308:** G56-62.

Corchero J, Granvil CP, Akiyama TE, Hayhurst GP, Pimprale S, Feigenbaum L, Idle JR and Gonzalez FJ (2001) The CYP2D6 humanized mouse: effect of the human CYP2D6 transgene and HNF4alpha on the disposition of debrisoquine in the mouse. *Mol Pharmacol*. **60:** 1260-1267.

Daniel H and Kottra G (2004) The proton oligopeptide cotransporter family SLC15 in physiology and pharmacology. *Pflugers Arch*. **447:** 610-618.

Daniel H, Morse EL and Adibi SA (1992) Determinants of substrate affinity for the oligopeptide/H+ symporter in the renal brush border membrane. *J Biol Chem*. **267:** 9565-9573.

Daniel H and Rubio-Aliaga I (2003) An update on renal peptide transporters. *Am J Physiol Renal Physiol*. **284:** F885-892.

de Waart DR, van de Wetering K, Kunne C, Duijst S, Paulusma CC and Oude Elferink RP (2012) Oral availability of cefadroxil depends on ABCC3 and ABCC4. *Drug metabolism and disposition: the biological fate of chemicals*. **40:** 515-521.

Devoy A, Bunton-Stasyshyn RK, Tybulewicz VL, Smith AJ and Fisher EM (2012) Genomically humanized mice: technologies and promises. *Nat Rev Genet*. **13:** 14-20.

Doki S, Kato HE, Solcan N, Iwaki M, Koyama M, Hattori M, Iwase N, Tsukazaki T, Sugita Y, Kandori H, Newstead S, Ishitani R and Nureki O (2013) Structural basis for dynamic mechanism of proton-coupled symport by the peptide transporter POT. *Proc Natl Acad Sci U S A*. **110:** 11343-11348.

Doring F, Dorn D, Bachfischer U, Amasheh S, Herget M and Daniel H (1996) Functional analysis of a chimeric mammalian peptide transporter derived from the intestinal and renal isoforms. *J Physiol*. **497 (Pt 3):** 773-779.

Doring F, Martini C, Walter J and Daniel H (2002) Importance of a small N-terminal region in mammalian peptide transporters for substrate affinity and function. *J Membr Biol*. **186:** 55-62.

Doring F, Theis S and Daniel H (1997) Expression and functional characterization of the mammalian intestinal peptide transporter PepT1 in the methylotropic yeast Pichia pastoris. *Biochemical and biophysical research communications*. **232:** 656-662.

Doring F, Will J, Amasheh S, Clauss W, Ahlbrecht H and Daniel H (1998) Minimal molecular determinants of substrates for recognition by the intestinal peptide transporter. *J Biol Chem*. **273:** 23211-23218.

Dosenovic P, Adori M, Adams WC, Pedersen GK, Soldemo M, Beutler B and Karlsson Hedestam GB (2015) Slc15a4 function is required for intact class switch recombination to IgG2c in response to TLR9 stimulation. *Immunology and cell biology*. **93:** 136-146.

Drozdzik M, Groer C, Penski J, Lapczuk J, Ostrowski M, Lai Y, Prasad B, Unadkat JD, Siegmund W and Oswald S (2014) Protein abundance of clinically relevant

multidrug transporters along the entire length of the human intestine. *Molecular pharmaceutics*. **11:** 3547-3555.

Eastwood D, Findlay L, Poole S, Bird C, Wadhwa M, Moore M, Burns C, Thorpe R and Stebbings R (2010) Monoclonal antibody TGN1412 trial failure explained by species differences in CD28 expression on CD4+ effector memory T-cells. *Br J Pharmacol*. **161:** 512-526.

Englund G, Rorsman F, Ronnblom A, Karlbom U, Lazorova L, Grasjo J, Kindmark A and Artursson P (2006) Regional levels of drug transporters along the human intestinal tract: co-expression of ABC and SLC transporters and comparison with Caco-2 cells. *Eur J Pharm Sci*. **29:** 269-277.

Erickson RH, Gum JR, Jr., Lindstrom MM, McKean D and Kim YS (1995) Regional expression and dietary regulation of rat small intestinal peptide and amino acid transporter mRNAs. *Biochem Biophys Res Commun*. **216:** 249-257.

Eriksson AH, Varma MV, Perkins EJ and Zimmerman CL (2010) The intestinal absorption of a prodrug of the mGlu2/3 receptor agonist LY354740 is mediated by PEPT1: in situ rat intestinal perfusion studies. *Journal of pharmaceutical sciences*. **99:** 1574-1581.

Ezra A, Hoffman A, Breuer E, Alferiev IS, Monkkonen J, El Hanany-Rozen N, Weiss G, Stepensky D, Gati I, Cohen H, Tormalehto S, Amidon GL and Golomb G (2000) A peptide prodrug approach for improving bisphosphonate oral absorption. *Journal of medicinal chemistry*. **43:** 3641-3652.

Fagerholm U, Johansson M and Lennernas H (1996) Comparison between permeability coefficients in rat and human jejunum. *Pharm Res*. **13:** 1336-1342.

Fei YJ, Kanai Y, Nussberger S, Ganapathy V, Leibach FH, Romero MF, Singh SK, Boron WF and Hediger MA (1994) Expression cloning of a mammalian proton-coupled oligopeptide transporter. *Nature*. **368:** 563-566.

Fei YJ, Liu JC, Fujita T, Liang R, Ganapathy V and Leibach FH (1998) Identification of a potential substrate binding domain in the mammalian peptide transporters PEPT1 and PEPT2 using PEPT1-PEPT2 and PEPT2-PEPT1 chimeras. *Biochem Biophys Res Commun*. **246:** 39-44.

Fei YJ, Sugawara M, Liu JC, Li HW, Ganapathy V, Ganapathy ME and Leibach FH (2000) cDNA structure, genomic organization, and promoter analysis of the mouse intestinal peptide transporter PEPT1. *Biochim Biophys Acta*. **1492:** 145-154.

Foley D, Bailey P, Pieri M and Meredith D (2009) Targeting ketone drugs towards transport by the intestinal peptide transporter, PepT1. *Organic & biomolecular chemistry*. **7:** 1064-1067.

Ganapathy V and Leibach FH (1983) Role of pH gradient and membrane potential in dipeptide transport in intestinal and renal brush-border membrane vesicles from the rabbit. Studies with L-carnosine and glycyl-L-proline. *J Biol Chem*. **258:** 14189-14192.

Garcia-Carbonell MC, Granero L, Torres-Molina F, Aristorena JC, Chesa-Jimenez J, Pla-Delfina JM and Peris-Ribera JE (1993) Nonlinear pharmacokinetics of cefadroxil in the rat. *Drug Metab Dispos*. **21:** 215-217.

Garrigues TM, Martin U, Peris-Ribera JE and Prescott LF (1991) Dose-dependent absorption and elimination of cefadroxil in man. *Eur J Clin Pharmacol*. **41:** 179-183.

Gerloff T (2004) Impact of genetic polymorphisms in transmembrane carrier-systems on drug and xenobiotic distribution. *Naunyn Schmiedebergs Arch Pharmacol*. **369:** 69-77.

Ginsburg CM and McCracken GH, Jr. (1980) Bioavailability of cefadroxil capsules and suspension in pediatric patients. *The Journal of international medical research*. **8:** 9-14.

Giraldo P and Montoliu L (2001) Size matters: use of YACs, BACs and PACs in transgenic animals. *Transgenic Res*. **10:** 83-103.

Gondolesi G, Ramisch D, Padin J, Almau H, Sandi M, Schelotto PB, Fernandez A, Rumbo C and Solar H (2012) What is the normal small bowel length in humans? first donor-based cohort analysis. *American journal of transplantation : official journal of the American Society of Transplantation and the American Society of Transplant Surgeons*. **12 Suppl 4:** S49-54.

Granero L, Gimeno MJ, Torres-Molina F, Chesa-Jimenez J and Peris JE (1994) Studies on the renal excretion mechanisms of cefadroxil. *Drug metabolism and disposition: the biological fate of chemicals*. **22:** 447-450.

Gregory SG, Sekhon M, Schein J, Zhao S, Osoegawa K, Scott CE, Evans RS, Burridge PW, Cox TV, Fox CA, Hutton RD, Mullenger IR, Phillips KJ, Smith J, Stalker J, Threadgold GJ, Birney E, Wylie K, Chinwalla A, Wallis J, Hillier L, Carter J, Gaige T, Jaeger S, Kremitzki C, Layman D, Maas J, McGrane R, Mead K,

Walker R, Jones S, Smith M, Asano J, Bosdet I, Chan S, Chittaranjan S, Chiu R, Fjell C, Fuhrmann D, Girn N, Gray C, Guin R, Hsiao L, Krzywinski M, Kutsche R, Lee SS, Mathewson C, McLeavy C, Messervier S, Ness S, Pandoh P, Prabhu AL, Saeedi P, Smailus D, Spence L, Stott J, Taylor S, Terpstra W, Tsai M, Vardy J, Wye N, Yang G, Shatsman S, Ayodeji B, Geer K, Tsegaye G, Shvartsbeyn A, Gebregeorgis E, Krol M, Russell D, Overton L, Malek JA, Holmes M, Heaney M, Shetty J, Feldblyum T, Nierman WC, Catanese JJ, Hubbard T, Waterston RH, Rogers J, de Jong PJ, Fraser CM, Marra M, McPherson JD and Bentley DR (2002) A physical map of the mouse genome. *Nature*. **418:** 743-750.

Hampel B, Lode H, Wagner J and Koeppe P (1982) Pharmacokinetics of cefadroxil and cefaclor during an eight-day dosage period. *Antimicrobial agents and chemotherapy*. **22:** 1061-1063.

Hawkins PN, Myers MJ, Epenetos AA, Caspi D and Pepys MB (1988) Specific localization and imaging of amyloid deposits in vivo using 123I-labeled serum amyloid P component. *J Exp Med*. **167:** 903-913.

Heaney JD, Rettew AN and Bronson SK (2004) Tissue-specific expression of a BAC transgene targeted to the Hprt locus in mouse embryonic stem cells. *Genomics*. **83:** 1072-1082.

Helander HF and Fandriks L (2014) Surface area of the digestive tract - revisited. *Scandinavian journal of gastroenterology*. **49:** 681-689.

Herrera-Ruiz D and Knipp GT (2003) Current perspectives on established and putative mammalian oligopeptide transporters. *Journal of pharmaceutical sciences*. **92:** 691-714.

Hong S (2006) PEPT2 Immunolocalization and its Role in Cefadroxil Renal Tubular Reabsorption and Brain Penetration *the University of Michigan* University of Michigan 9780542790829

Hu Y, Chen X and Smith DE (2012) Species-dependent uptake of glycylsarcosine but not oseltamivir in Pichia pastoris expressing the rat, mouse, and human intestinal peptide transporter PEPT1. *Drug Metab Dispos*. **40:** 1328-1335.

Hu Y, Xie Y, Keep RF and Smith DE (2014a) Divergent developmental expression and function of the proton-coupled oligopeptide transporters PepT2 and PhT1 in regional brain slices of mouse and rat. *J Neurochem*. **129:** 955-965.

Hu Y, Xie Y, Wang Y, Chen X and Smith DE (2014b) Development and characterization of a novel mouse line humanized for the intestinal peptide transporter PEPT1. *Mol Pharm*. **11:** 3737-3746.

Hunter K, Greenwood J, Yang YL, Cunningham JM, Birren B and Housman D (1999) An integrated somatic cell hybrid, YAC, and BAC map of the Rmc1 region of mouse chromosome 1. *Genomics*. **58:** 318-322.

Jain R, Duvvuri S, Kansara V, Mandava NK and Mitra AK (2007) Intestinal absorption of novel-dipeptide prodrugs of saquinavir in rats. *International journal of pharmaceutics*. **336:** 233-240.

Jappar D, Hu Y and Smith DE (2011) Effect of dose escalation on the in vivo oral absorption and disposition of glycylsarcosine in wild-type and Pept1 knockout mice. *Drug Metab Dispos*. **39:** 2250-2257.

Jappar D, Wu SP, Hu Y and Smith DE (2010) Significance and regional dependency of peptide transporter (PEPT) 1 in the intestinal permeability of glycylsarcosine: in

situ single-pass perfusion studies in wild-type and Pept1 knockout mice. *Drug Metab Dispos*. **38:** 1740-1746.

Jiang XL, Gonzalez FJ and Yu AM (2011) Drug-metabolizing enzyme, transporter, and nuclear receptor genetically modified mouse models. *Drug Metab Rev*. **43:** 27-40.

Kang HE and Lee MG (2011) Approaches for predicting human pharmacokinetics using interspecies pharmacokinetic scaling. *Arch Pharm Res*. **34:** 1779-1788.

Khamdang S, Takeda M, Babu E, Noshiro R, Onozato ML, Tojo A, Enomoto A, Huang XL, Narikawa S, Anzai N, Piyachaturawat P and Endou H (2003) Interaction of human and rat organic anion transporter 2 with various cephalosporin antibiotics. *European journal of pharmacology*. **465:** 1-7.

Kim HR, Park SW, Cho HJ, Chae KA, Sung JM, Kim JS, Landowski CP, Sun D, Abd El-Aty AM, Amidon GL and Shin HC (2007) Comparative gene expression profiles of intestinal transporters in mice, rats and humans. *Pharmacol Res*. **56:** 224-236.

Klang JE, Burnworth LA, Pan YX, Webb KE, Jr. and Wong EA (2005) Functional characterization of a cloned pig intestinal peptide transporter (pPepT1). *J Anim Sci*. **83:** 172-181.

Knutter I, Hartrodt B, Theis S, Foltz M, Rastetter M, Daniel H, Neubert K and Brandsch M (2004) Analysis of the transport properties of side chain modified dipeptides at the mammalian peptide transporter PEPT1. *European journal of pharmaceutical sciences : official journal of the European Federation for Pharmaceutical Sciences*. **21:** 61-67.

Kurtin P and Charney AN (1984) Intestinal ion transport and intracellular pH during acute respiratory alkalosis and acidosis. *Am J Physiol*. **247:** G24-31.

La Rosa F, Ripa S, Prenna M, Ghezzi A and Pfeffer M (1982) Pharmacokinetics of cefadroxil after oral administration in humans. *Antimicrobial agents and chemotherapy*. **21:** 320-322.

Leabman MK, Huang CC, DeYoung J, Carlson EJ, Taylor TR, de la Cruz M, Johns SJ, Stryke D, Kawamoto M, Urban TJ, Kroetz DL, Ferrin TE, Clark AG, Risch N, Herskowitz I, Giacomini KM and Pharmacogenetics Of Membrane Transporters I (2003) Natural variation in human membrane transporter genes reveals evolutionary and functional constraints. *Proc Natl Acad Sci U S A.* **100:** 5896-5901.

Liang R, Fei YJ, Prasad PD, Ramamoorthy S, Han H, Yang-Feng TL, Hediger MA, Ganapathy V and Leibach FH (1995) Human intestinal H+/peptide cotransporter. Cloning, functional expression, and chromosomal localization. *J Biol Chem*. **270:** 6456-6463.

Liu W, Liang R, Ramamoorthy S, Fei YJ, Ganapathy ME, Hediger MA, Ganapathy V and Leibach FH (1995) Molecular cloning of PEPT 2, a new member of the H+/peptide cotransporter family, from human kidney. *Biochimica et biophysica acta*. **1235:** 461-466.

Lucas ML, Schneider W, Haberich FJ and Blair JA (1975) Direct measurement by pH-microelectrode of the pH microclimate in rat proximal jejunum. *Proc R Soc Lond B Biol Sci*. **192:** 39-48.

Ma K, Hu Y and Smith DE (2012) Influence of fed-fasted state on intestinal PEPT1 expression and in vivo pharmacokinetics of glycylsarcosine in wild-type and Pept1 knockout mice. *Pharm Res*. **29:** 535-545.

Mackenzie B, Fei YJ, Ganapathy V and Leibach FH (1996) The human intestinal H+/oligopeptide cotransporter hPEPT1 transports differently-charged dipeptides with identical electrogenic properties. *Biochimica et biophysica acta*. **1284:** 125-128.

Margheritis E, Terova G, Oyadeyi AS, Renna MD, Cinquetti R, Peres A and Bossi E (2013) Characterization of the transport of lysine-containing dipeptides by PepT1 orthologs expressed in Xenopus laevis oocytes. *Comp Biochem Physiol A Mol Integr Physiol*. **164:** 520-528.

Marino EL, Dominguez-Gil A and Muriel C (1982) Influence of dosage form and administration route on the pharmacokinetic parameters of cefadroxil. *International journal of clinical pharmacology, therapy, and toxicology*. **20:** 73-77.

Meredith D (2009) Review. The mammalian proton-coupled peptide cotransporter PepT1: sitting on the transporter-channel fence? *Philosophical transactions of the Royal Society of London. Series B, Biological sciences*. **364:** 203-207.

Meredith D, Temple CS, Guha N, Sword CJ, Boyd CA, Collier ID, Morgan KM and Bailey PD (2000) Modified amino acids and peptides as substrates for the intestinal peptide transporter PepT1. *Eur J Biochem*. **267:** 3723-3728.

Merlin D, Si-Tahar M, Sitaraman SV, Eastburn K, Williams I, Liu X, Hediger MA and Madara JL (2001) Colonic epithelial hPepT1 expression occurs in inflammatory bowel disease: transport of bacterial peptides influences expression of MHC class 1 molecules. *Gastroenterology*. **120:** 1666-1679.

Merlin D, Steel A, Gewirtz AT, Si-Tahar M, Hediger MA and Madara JL (1998) hPepT1-mediated epithelial transport of bacteria-derived chemotactic peptides enhances neutrophil-epithelial interactions. *The Journal of clinical investigation*. **102:** 2011-2018.

Monaco AP and Larin Z (1994) YACs, BACs, PACs and MACs: artificial chromosomes as research tools. *Trends Biotechnol*. **12:** 280-286.

Mouse Genome Sequencing C, Waterston RH, Lindblad-Toh K, Birney E, Rogers J, Abril JF, Agarwal P, Agarwala R, Ainscough R, Alexandersson M, An P, Antonarakis SE, Attwood J, Baertsch R, Bailey J, Barlow K, Beck S, Berry E, Birren B, Bloom T, Bork P, Botcherby M, Bray N, Brent MR, Brown DG, Brown SD, Bult C, Burton J, Butler J, Campbell RD, Carninci P, Cawley S, Chiaromonte F, Chinwalla AT, Church DM, Clamp M, Clee C, Collins FS, Cook LL, Copley RR, Coulson A, Couronne O, Cuff J, Curwen V, Cutts T, Daly M, David R, Davies J, Delehaunty KD, Deri J, Dermitzakis ET, Dewey C, Dickens NJ, Diekhans M, Dodge S, Dubchak I, Dunn DM, Eddy SR, Elnitski L, Emes RD, Eswara P, Eyras E, Felsenfeld A, Fewell GA, Flicek P, Foley K, Frankel WN, Fulton LA, Fulton RS, Furey TS, Gage D, Gibbs RA, Glusman G, Gnerre S, Goldman N, Goodstadt L, Grafham D, Graves TA, Green ED, Gregory S, Guigo R, Guyer M, Hardison RC, Haussler D, Hayashizaki Y, Hillier LW, Hinrichs A, Hlavina W, Holzer T, Hsu F, Hua A, Hubbard T, Hunt A, Jackson I, Jaffe DB, Johnson LS, Jones M, Jones TA, Joy A, Kamal M, Karlsson EK, Karolchik D, Kasprzyk A, Kawai J, Keibler E, Kells C, Kent WJ, Kirby A, Kolbe DL, Korf I, Kucherlapati RS, Kulbokas EJ, Kulp D, Landers T, Leger JP, Leonard S, Letunic

I, Levine R, Li J, Li M, Lloyd C, Lucas S, Ma B, Maglott DR, Mardis ER, Matthews L, Mauceli E, Mayer JH, McCarthy M, McCombie WR, McLaren S, McLay K, McPherson JD, Meldrim J, Meredith B, Mesirov JP, Miller W, Miner TL, Mongin E, Montgomery KT, Morgan M, Mott R, Mullikin JC, Muzny DM, Nash WE, Nelson JO, Nhan MN, Nicol R, Ning Z, Nusbaum C, O'Connor MJ, Okazaki Y, Oliver K, Overton-Larty E, Pachter L, Parra G, Pepin KH, Peterson J, Pevzner P, Plumb R, Pohl CS, Poliakov A, Ponce TC, Ponting CP, Potter S, Quail M, Reymond A, Roe BA, Roskin KM, Rubin EM, Rust AG, Santos R, Sapojnikov V, Schultz B, Schultz J, Schwartz MS, Schwartz S, Scott C, Seaman S, Searle S, Sharpe T, Sheridan A, Shownkeen R, Sims S, Singer JB, Slater G, Smit A, Smith DR, Spencer B, Stabenau A, Stange-Thomann N, Sugnet C, Suyama M, Tesler G, Thompson J, Torrents D, Trevaskis E, Tromp J, Ucla C, Ureta-Vidal A, Vinson JP, Von Niederhausern AC, Wade CM, Wall M, Weber RJ, Weiss RB, Wendl MC, West AP, Wetterstrand K, Wheeler R, Whelan S, Wierzbowski J, Willey D, Williams S, Wilson RK, Winter E, Worley KC, Wyman D, Yang S, Yang SP, Zdobnov EM, Zody MC and Lander ES (2002) Initial sequencing and comparative analysis of the mouse genome. *Nature*. **420:** 520-562.

Muranushi N, Yoshikawa T, Yoshida M, Oguma T, Hirano K and Yamada H (1989) Transport characteristics of ceftibuten, a new oral cephem, in rat intestinal brush-border membrane vesicles: relationship to oligopeptide and amino beta-lactam transport. *Pharmaceutical research*. **6:** 308-312.

Nakakariya M, Shimada T, Irokawa M, Koibuchi H, Iwanaga T, Yabuuchi H, Maeda T and Tamai I (2008a) Predominant contribution of rat organic anion transporting polypeptide-2 (Oatp2) to hepatic uptake of beta-lactam antibiotics. *Pharmaceutical research*. **25:** 578-585.

Nakakariya M, Shimada T, Irokawa M, Maeda T and Tamai I (2008b) Identification and species similarity of OATP transporters responsible for hepatic uptake of beta-lactam antibiotics. *Drug metabolism and pharmacokinetics*. **23:** 347-355.

Nakamura N, Lill JR, Phung Q, Jiang Z, Bakalarski C, de Maziere A, Klumperman J, Schlatter M, Delamarre L and Mellman I (2014) Endosomes are specialized platforms for bacterial sensing and NOD2 signalling. *Nature*. **509:** 240-244.

Newstead S, Drew D, Cameron AD, Postis VL, Xia X, Fowler PW, Ingram JC, Carpenter EP, Sansom MS, McPherson MJ, Baldwin SA and Iwata S (2011) Crystal structure of a prokaryotic homologue of the mammalian oligopeptide-proton symporters, PepT1 and PepT2. *The EMBO journal*. **30:** 417-426.

Nielsen LB, McCormick SP, Pierotti V, Tam C, Gunn MD, Shizuya H and Young SG (1997) Human apolipoprotein B transgenic mice generated with 207- and 145-kilobase pair bacterial artificial chromosomes. Evidence that a distant 5'-element confers appropriate transgene expression in the intestine. *J Biol Chem*. **272:** 29752-29758.

Obach RS, Baxter JG, Liston TE, Silber BM, Jones BC, MacIntyre F, Rance DJ and Wastall P (1997) The prediction of human pharmacokinetic parameters from preclinical and in vitro metabolism data. *J Pharmacol Exp Ther*. **283:** 46-58.

Ocheltree SM, Shen H, Hu Y, Keep RF and Smith DE (2005) Role and relevance of peptide transporter 2 (PEPT2) in the kidney and choroid plexus: in vivo studies with glycylsarcosine in wild-type and PEPT2 knockout mice. *J Pharmacol Exp Ther*. **315:** 240-247.

Ocheltree SM, Shen H, Hu Y, Xiang J, Keep RF and Smith DE (2004) Mechanisms of cefadroxil uptake in the choroid plexus: studies in wild-type and PEPT2 knockout mice. *The Journal of pharmacology and experimental therapeutics*. **308:** 462-467.

Ogihara H, Suzuki T, Nagamachi Y, Inui K and Takata K (1999) Peptide transporter in the rat small intestine: ultrastructural localization and the effect of starvation and administration of amino acids. *Histochem J*. **31:** 169-174.

Olin BR (1980) Cefadroxil: a new oral cephalosporin. *The Journal of the Louisiana State Medical Society : official organ of the Louisiana State Medical Society*. **132:** 86-88.

Oliveira CH, Salmon J, Sucupira M, Ilha J and De Nucci G (2000) Comparative bioavailability of two cefadroxil formulations in healthy human volunteers after a single-dose administration. *Biopharm Drug Dispos*. **21:** 243-247.

Oostendorp RL, Beijnen JH and Schellens JH (2009) The biological and clinical role of drug transporters at the intestinal barrier. *Cancer Treat Rev*. **35:** 137-147.

Otoom S, Hasan M and Najib N (2004) Comparative bioavailability of two cefadroxil products using serum and urine data in healthy human volunteers. *Clin Exp Pharmacol Physiol*. **31:** 433-437.

Pade V and Stavchansky S (1997) Estimation of the relative contribution of the transcellular and paracellular pathway to the transport of passively absorbed drugs in the Caco-2 cell culture model. *Pharm Res*. **14:** 1210-1215.

Pan X, Terada T, Okuda M and Inui K (2004) The diurnal rhythm of the intestinal transporters SGLT1 and PEPT1 is regulated by the feeding conditions in rats. *J Nutr*. **134:** 2211-2215.

Pan Y, Wong EA, Bloomquist JR and Webb KE, Jr. (2001) Expression of a cloned ovine gastrointestinal peptide transporter (oPepT1) in Xenopus oocytes induces uptake of oligopeptides in vitro. *J Nutr*. **131:** 1264-1270.

Pedersen BP, Kumar H, Waight AB, Risenmay AJ, Roe-Zurz Z, Chau BH, Schlessinger A, Bonomi M, Harries W, Sali A, Johri AK and Stroud RM (2013) Crystal structure of a eukaryotic phosphate transporter. *Nature*. **496:** 533-536.

Pfeffer M, Jackson A, Ximenes J and de Menezes JP (1977) Comparative human oral clinical pharmacology of cefadroxil, cephalexin, and cephradine. *Antimicrob Agents Chemother*. **11:** 331-338.

Phan DD, Chin-Hong P, Lin ET, Anderle P, Sadee W and Guglielmo BJ (2003) Intra- and interindividual variabilities of valacyclovir oral bioavailability and effect of coadministration of an hPEPT1 inhibitor. *Antimicrob Agents Chemother*. **47:** 2351-2353.

Posada MM and Smith DE (2013) In vivo absorption and disposition of cefadroxil after escalating oral doses in wild-type and PepT1 knockout mice. *Pharm Res*. **30:** 2931-2939.

Prenna M and Ripa S (1980) Serum levels and urinary excretion in humans of BL-S 578 (cefadroxil), a new semisynthetic cephalosporin. *Chemotherapy*. **26:** 98-102.

Prosser HM, Rzadzinska AK, Steel KP and Bradley A (2008) Mosaic complementation demonstrates a regulatory role for myosin VIIa in actin dynamics of stereocilia. *Mol Cell Biol*. **28:** 1702-1712.

Ramamoorthy S, Liu W, Ma YY, Yang-Feng TL, Ganapathy V and Leibach FH (1995) Proton/peptide cotransporter (PEPT 2) from human kidney: functional characterization and chromosomal localization. *Biochim Biophys Acta*. **1240:** 1-4.

Ronnestad I, Murashita K, Kottra G, Jordal AE, Narawane S, Jolly C, Daniel H and Verri T (2010) Molecular cloning and functional expression of atlantic salmon peptide transporter 1 in Xenopus oocytes reveals efficient intestinal uptake of lysine-containing and other bioactive di- and tripeptides in teleost fish. *J Nutr*. **140:** 893-900.

Rubio-Aliaga I, Boll M and Daniel H (2000) Cloning and characterization of the gene encoding the mouse peptide transporter PEPT2. *Biochem Biophys Res Commun*. **276:** 734-741.

Rubio-Aliaga I and Daniel H (2002) Mammalian peptide transporters as targets for drug delivery. *Trends in pharmacological sciences*. **23:** 434-440.

Rubio-Aliaga I and Daniel H (2008) Peptide transporters and their roles in physiological processes and drug disposition. *Xenobiotica; the fate of foreign compounds in biological systems*. **38:** 1022-1042.

Russel FG, Koenderink JB and Masereeuw R (2008) Multidrug resistance protein 4 (MRP4/ABCC4): a versatile efflux transporter for drugs and signalling molecules. *Trends in pharmacological sciences*. **29:** 200-207.

Sakata K, Yamashita T, Maeda M, Moriyama Y, Shimada S and Tohyama M (2001) Cloning of a lymphatic peptide/histidine transporter. *The Biochemical journal*. **356:** 53-60.

Sanchez-Pico A, Peris-Ribera JE, Toledano C, Torres-Molina F, Casabo VG, Martin-Villodre A and Pla-Delfina JM (1989) Non-linear intestinal absorption kinetics of cefadroxil in the rat. *J Pharm Pharmacol*. **41:** 179-185.

Santella PJ and Henness D (1982) A review of the bioavailability of cefadroxil. *The Journal of antimicrobial chemotherapy*. **10 Suppl B:** 17-25.

Sasawatari S, Okamura T, Kasumi E, Tanaka-Furuyama K, Yanobu-Takanashi R, Shirasawa S, Kato N and Toyama-Sorimachi N (2011) The solute carrier family 15A4 regulates TLR9 and NOD1 functions in the innate immune system and promotes colitis in mice. *Gastroenterology*. **140:** 1513-1525.

Scheer N, Balimane P, Hayward MD, Buechel S, Kauselmann G and Wolf CR (2012) Generation and characterization of a novel multidrug resistance protein 2 humanized mouse line. *Drug metabolism and disposition: the biological fate of chemicals*. **40:** 2212-2218.

Scheer N and Roland Wolf C (2013) Xenobiotic receptor humanized mice and their utility. *Drug Metab Rev*. **45:** 110-121.

Schorderet P and Duboule D (2011) Structural and functional differences in the long non-coding RNA hotair in mouse and human. *PLoS Genet*. **7:** e1002071.

Shen H, Keep RF, Hu Y and Smith DE (2005) PEPT2 (Slc15a2)-mediated unidirectional transport of cefadroxil from cerebrospinal fluid into choroid plexus. *The Journal of pharmacology and experimental therapeutics*. **315:** 1101-1108.

Shen H, Ocheltree SM, Hu Y, Keep RF and Smith DE (2007) Impact of genetic knockout of PEPT2 on cefadroxil pharmacokinetics, renal tubular reabsorption, and brain penetration in mice. *Drug metabolism and disposition: the biological fate of chemicals*. **35:** 1209-1216.

Shen H, Smith DE, Yang T, Huang YG, Schnermann JB and Brosius FC, 3rd (1999) Localization of PEPT1 and PEPT2 proton-coupled oligopeptide transporter mRNA and protein in rat kidney. *Am J Physiol*. **276:** F658-665.

Shi B, Song D, Xue H, Li J and Li N (2006) Abnormal expression of the peptide transporter PepT1 in the colon of massive bowel resection rat: a potential route for colonic mucosa damage by transport of fMLP. *Dig Dis Sci*. **51:** 2087-2093.

Shiraga T, Miyamoto K, Tanaka H, Yamamoto H, Taketani Y, Morita K, Tamai I, Tsuji A and Takeda E (1999) Cellular and molecular mechanisms of dietary regulation on rat intestinal H+/Peptide transporter PepT1. *Gastroenterology*. **116:** 354-362.

Shizuya H, Birren B, Kim UJ, Mancino V, Slepak T, Tachiiri Y and Simon M (1992) Cloning and stable maintenance of 300-kilobase-pair fragments of human DNA in Escherichia coli using an F-factor-based vector. *Proc Natl Acad Sci U S A*. **89:** 8794-8797.

Sinko PJ and Amidon GL (1988) Characterization of the oral absorption of beta-lactam antibiotics. I. Cephalosporins: determination of intrinsic membrane absorption parameters in the rat intestine in situ. *Pharmaceutical research*. **5:** 645-650.

Smith ME and Morton DG (2010) The Digestive System *Churchill Livingstone* New York 0702033677

Sobin C, Gutierrez M and Alterio H (2009) Polymorphisms of delta-aminolevulinic acid dehydratase (ALAD) and peptide transporter 2 (PEPT2) genes in children with low-level lead exposure. *Neurotoxicology*. **30:** 881-887.

Solcan N, Kwok J, Fowler PW, Cameron AD, Drew D, Iwata S and Newstead S (2012) Alternating access mechanism in the POT family of oligopeptide transporters. *EMBO J*. **31:** 3411-3421.

Stahl PD and Wainszelbaum MJ (2009) Human-specific genes may offer a unique window into human cell signaling. *Sci Signal*. **2:** pe59.

Suntharalingam G, Perry MR, Ward S, Brett SJ, Castello-Cortes A, Brunner MD and Panoskaltsis N (2006) Cytokine storm in a phase 1 trial of the anti-CD28 monoclonal antibody TGN1412. *N Engl J Med*. **355:** 1018-1028.

Takahashi M, Washio T, Suzuki N, Igeta K and Yamashita S (2009) The species differences of intestinal drug absorption and first-pass metabolism between cynomolgus monkeys and humans. *J Pharm Sci*. **98:** 4343-4353.

Tamai I, Tomizawa N, Takeuchi T, Nakayama K, Higashida H and Tsuji A (1995) Functional expression of transporter for beta-lactam antibiotics and dipeptides in Xenopus laevis oocytes injected with messenger RNA from human, rat and rabbit small intestines. *The Journal of pharmacology and experimental therapeutics*. **273:** 26-31.

Tanaka H, Miyamoto KI, Morita K, Haga H, Segawa H, Shiraga T, Fujioka A, Kouda T, Taketani Y, Hisano S, Fukui Y, Kitagawa K and Takeda E (1998) Regulation of

the PepT1 peptide transporter in the rat small intestine in response to 5-fluorouracil-induced injury. *Gastroenterology*. **114:** 714-723.

Tanrisever B and Santella PJ (1986) Cefadroxil. A review of its antibacterial, pharmacokinetic and therapeutic properties in comparison with cephalexin and cephradine. *Drugs*. **32 Suppl 3:** 1-16.

Taylor MD and Amidon GL (1995) Peptide-based drug design: controlling transport and metabolism *American Chemical Society* Washington, DC 0841230587

Terada T, Saito H, Sawada K, Hashimoto Y and Inui K (2000) N-terminal halves of rat H+/peptide transporters are responsible for their substrate recognition. *Pharm Res*. **17:** 15-20.

Teuscher NS, Shen H, Shu C, Xiang J, Keep RF and Smith DE (2004) Carnosine uptake in rat choroid plexus primary cell cultures and choroid plexus whole tissue from PEPT2 null mice. *J Neurochem*. **89:** 375-382.

Thwaites DT, Ford D, Glanville M and Simmons NL (1999) H(+)/solute-induced intracellular acidification leads to selective activation of apical Na(+)/H(+) exchange in human intestinal epithelial cells. *J Clin Invest*. **104:** 629-635.

Tsuda M, Terada T, Irie M, Katsura T, Niida A, Tomita K, Fujii N and Inui K (2006) Transport characteristics of a novel peptide transporter 1 substrate, antihypotensive drug midodrine, and its amino acid derivatives. *The Journal of pharmacology and experimental therapeutics*. **318:** 455-460.

Tsuji A, Hirooka H, Terasaki T, Tamai I and Nakashima E (1987a) Saturable uptake of cefixime, a new oral cephalosporin without an alpha-amino group, by the rat intestine. *The Journal of pharmacy and pharmacology*. **39:** 272-277.

Tsuji A, Tamai I, Nakanishi M, Terasaki T and Hamano S (1993) Intestinal brush-border transport of the oral cephalosporin antibiotic, cefdinir, mediated by dipeptide and monocarboxylic acid transport systems in rabbits. *The Journal of pharmacy and pharmacology*. **45:** 996-998.

Tsuji A, Terasaki T, Tamai I and Hirooka H (1987b) H+ gradient-dependent and carrier-mediated transport of cefixime, a new cephalosporin antibiotic, across brush-border membrane vesicles from rat small intestine. *The Journal of pharmacology and experimental therapeutics*. **241:** 594-601.

van de Steeg E, van Esch A, Wagenaar E, Kenworthy KE and Schinkel AH (2013) Influence of human OATP1B1, OATP1B3, and OATP1A2 on the pharmacokinetics of methotrexate and paclitaxel in humanized transgenic mice. *Clinical cancer research : an official journal of the American Association for Cancer Research*. **19:** 821-832.

Varma MV, Eriksson AH, Sawada G, Pak YA, Perkins EJ and Zimmerman CL (2009) Transepithelial transport of the group II metabotropic glutamate 2/3 receptor agonist (1S,2S,5R,6S)-2-aminobicyclo[3.1.0]hexane-2,6-dicarboxylate (LY354740) and its prodrug (1S,2S,5R,6S)-2-[(2'S)-(2'-amino)propionyl]aminobicyclo[3.1.0]hexane-2,6-dicarbox ylate (LY544344). *Drug metabolism and disposition: the biological fate of chemicals*. **37:** 211-220.

Vavricka SR, Musch MW, Fujiya M, Kles K, Chang L, Eloranta JJ, Kullak-Ublick GA, Drabik K, Merlin D and Chang EB (2006) Tumor necrosis factor-alpha and interferon-gamma increase PepT1 expression and activity in the human colon carcinoma cell line Caco-2/bbe and in mouse intestine. *Pflugers Arch*. **452:** 71-80.

Walker D, Brady J, Dalvie D, Davis J, Dowty M, Duncan JN, Nedderman A, Obach RS and Wright P (2009) A holistic strategy for characterizing the safety of metabolites through drug discovery and development. *Chem Res Toxicol*. **22:** 1653-1662.

Wang M, Zhang X, Zhao H, Wang Q and Pan Y (2010) Comparative analysis of vertebrate PEPT1 and PEPT2 genes. *Genetica*. **138:** 587-599.

Wang Y, Sun D, Song F, Hu Y, Smith DE and Jiang H (2014) Expression and regulation of the proton-coupled oligopeptide transporter PhT2 by LPS in macrophages and mouse spleen. *Mol Pharm*. **11:** 1880-1888.

Weller S, Blum MR, Doucette M, Burnette T, Cederberg DM, de Miranda P and Smiley ML (1993) Pharmacokinetics of the acyclovir pro-drug valaciclovir after escalating single- and multiple-dose administration to normal volunteers. *Clin Pharmacol Ther*. **54:** 595-605.

Wenzel U, Gebert I, Weintraut H, Weber WM, Clauss W and Daniel H (1996) Transport characteristics of differently charged cephalosporin antibiotics in oocytes expressing the cloned intestinal peptide transporter PepT1 and in human intestinal Caco-2 cells. *The Journal of pharmacology and experimental therapeutics*. **277:** 831-839.

Wenzel U, Kuntz S, Diestel S and Daniel H (2002) PEPT1-mediated cefixime uptake into human intestinal epithelial cells is increased by Ca2+ channel blockers. *Antimicrob Agents Chemother*. **46:** 1375-1380.

Wuensch T, Schulz S, Ullrich S, Lill N, Stelzl T, Rubio-Aliaga I, Loh G, Chamaillard M, Haller D and Daniel H (2013a) The peptide transporter PEPT1 is expressed in

distal colon in rodents and humans and contributes to water absorption. *Am J Physiol Gastrointest Liver Physiol*. ajpgi.00491.2012 [pii]

10.1152/ajpgi.00491.2012

Wuensch T, Schulz S, Ullrich S, Lill N, Stelzl T, Rubio-Aliaga I, Loh G, Chamaillard M, Haller D and Daniel H (2013b) The peptide transporter PEPT1 is expressed in distal colon in rodents and humans and contributes to water absorption. *Am J Physiol Gastrointest Liver Physiol*. **305:** G66-73.

Wuensch T, Ullrich S, Schulz S, Chamaillard M, Schaltenberg N, Rath E, Goebel U, Sartor RB, Prager M, Buning C, Bugert P, Witt H, Haller D and Daniel H (2014) Colonic expression of the peptide transporter PEPT1 is downregulated during intestinal inflammation and is not required for NOD2-dependent immune activation. *Inflamm Bowel Dis*. **20:** 671-684.

Yamashita T, Shimada S, Guo W, Sato K, Kohmura E, Hayakawa T, Takagi T and Tohyama M (1997) Cloning and functional expression of a brain peptide/histidine transporter. *J Biol Chem*. **272:** 10205-10211.

Yang B, Hu Y and Smith DE (2013a) Impact of peptide transporter 1 on the intestinal absorption and pharmacokinetics of valacyclovir after oral dose escalation in wild-type and PepT1 knockout mice. *Drug Metab Dispos*. **41:** 1867-1874.

Yang B and Smith DE (2013b) Significance of peptide transporter 1 in the intestinal permeability of valacyclovir in wild-type and PepT1 knockout mice. *Drug Metab Dispos*. **41:** 608-614.

Yang XW, Model P and Heintz N (1997) Homologous recombination based modification in Escherichia coli and germline transmission in transgenic mice of a bacterial artificial chromosome. *Nat Biotechnol*. **15:** 859-865.

Yoshikawa T, Muranushi N, Yoshida M, Oguma T, Hirano K and Yamada H (1989) Transport characteristics of ceftibuten (7432-S), a new oral cephem, in rat intestinal brush-border membrane vesicles: proton-coupled and stereoselective transport of ceftibuten. *Pharmaceutical research*. **6:** 302-307.

Zhang EY, Emerick RM, Pak YA, Wrighton SA and Hillgren KM (2004a) Comparison of human and monkey peptide transporters: PEPT1 and PEPT2. *Mol Pharm*. **1:** 201-210.

Zhang EY, Fu DJ, Pak YA, Stewart T, Mukhopadhyay N, Wrighton SA and Hillgren KM (2004b) Genetic polymorphisms in human proton-dependent dipeptide transporter PEPT1: implications for the functional role of Pro586. *J Pharmacol Exp Ther*. **310:** 437-445.

Zhang Y, Sun J, Sun Y, Wang Y and He Z (2013) Prodrug design targeting intestinal PepT1 for improved oral absorption: design and performance. *Curr Drug Metab*. **14:** 675-687.

Zhu T, Chen XZ, Steel A, Hediger MA and Smith DE (2000) Differential recognition of ACE inhibitors in Xenopus laevis oocytes expressing rat PEPT1 and PEPT2. *Pharmaceutical research*. **17:** 526-532.

Zucchelli M, Torkvist L, Bresso F, Halfvarson J, Hellquist A, Anedda F, Assadi G, Lindgren GB, Svanfeldt M, Janson M, Noble CL, Pettersson S, Lappalainen M, Paavola-Sakki P, Halme L, Farkkila M, Turunen U, Satsangi J, Kontula K,

Lofberg R, Kere J and D'Amato M (2009) PepT1 oligopeptide transporter (SLC15A1) gene polymorphism in inflammatory bowel disease. *Inflamm Bowel Dis*. **15:** 1562-1569.

CHAPTER III

DEVELOPMENT AND CHARACTERIZATION OF HUMANIZED huPEPT1 MOUSE MODEL USING MICROINJECTION TRANSGENIC METHOLOGY

ABSTRACT

Purpose

The proton-coupled oligopeptide transporter PepT1 is predominantly expressed in small intestine and mediates the uptake of protein-digested di-/tri-peptides and peptide-like drugs from the intestinal lumen. However, species differences in PepT1 protein function have been observed in yeast expressing the rat, mouse and human gene. The purpose of this study was to generate a novel humanized mouse line for hPepT1 (using the microinjection transgenic method) in order to examine the physiological, pharmacological and pathological roles and relevance of the hPepT1 protein in humanized mice as compared to wildtype mice.

Methods

A new humanized mouse line for hPepT1 were successfully generated using the

microinjection technique with a BAC construct containing the entire human hPepT1 genomic DNA. The gene copy number, transcripts and protein expression of human PepT1 were assessed using real-time quantitative PCR (qPCR) and immunoblotting, and location of the PepT1 protein was determined using histological fluorescence chemistry hybridization. Moreover, other relevant genes were evaluated for mRNA expression using real-time qPCR.

Results

No obvious behavioral abnormalities were observed in humanized mice. The humanized mice were viable, fertile, grew to normal size and weight, and had no significant differences in clinical serum chemistries as compared to wildtype and mPepT1 knockout mice. Real-time qPCR and immunoblot analyses demonstrated that humanized mice had only one copy of human PepT1 gene integration. They also had abundant hPepT1 protein expression in small intestine, similar to that of mPepT1 in wildtype mice, and a measurable but low protein expression in colon. In addition, other select relevant genes were not aberrantly expressed in the intestine and kidney of humanized mice, although minor changes in gene expressions were observed in these tissues. Moreover, as determined by immunohistochemistry, PepT1 protein was localized at the apical side of epithelial cells in small intestine.

Conclusion

These findings demonstrated that the hPepT1 gene had only one copy of integration in the mouse chromosome. Consequently, the hPepT1 transporter had a comparable expression profile in humanized mice as compared to that of

mPepT1 in wildtype mice. Still, there was a significant, but small, upregulation of mRNA and protein expression in the colon of humanized mice. The human hPepT1 protein was localized at the apical side of epithelial cells in small intestine. These humanized huPepT1 mice might provide a valuable research tool to study the physiological, pharmacological and pathological characteristics of the human hPepT1 transporter, and to compare differences in the pharmacokinetics and pharmacodynamics of PepT1 transporters across species.

INTRODUCTION

Membrane protein PepT1 (SLC15A1), along with PepT2 (SLC15A2), PhT1 (SLC15A4) and PhT2 (SLC15A3), are members of the solute carrier subfamily 15 that mediate the cellular uptake of dipeptides and tripeptides, in addition to a variety of peptide-like drugs. Following the cloning of rabbit PepT1 (Fei et al., 1994), the human hPepT1 and mouse mPepT1 were cloned, where they shared 85% homology to each other (Fei et al., 2000, Liang et al., 1995). The human hPepT1 transporter had 708 amino acid residues whereas the mouse mPepT1 transporter had 709 amino acid residues. All peptide transporters were reported to have 12 transmembrane domains, the C-terminal and N-terminal facing inside the cytoplasm, and important residues including Tyr12, His57, Tyr64, Trp294, Phe297 and Glu595 being located within the highly conserved transmembrane domains H1, H2, H5, H7 and H10 (Smith et al., 2013).

In contrast to PepT2 (SLC15A2), which has a high-affinity low-capacity role in renal drug reabsorption (Ocheltree et al., 2005), the PepT1 transporter is a low-affinity high-capacity transporter responsible for nutritional intake. In this role, PepT1 absorbs digested proteins in the diet, available as di-/tri-peptides, from the intestinal lumen. PepT1 protein also has an important role in absorbing peptide-

like drugs, including β-lactam antibiotics and antiviral nucleoside prodrugs such as valacyclovir (Yang et al., 2013a). Previous PCR and immunoblot results demonstrated that the PepT1 (SLC15A1) protein was predominantly expressed at the apical membrane of enterocytes, especially along the small intestine (Shen et al., 2001). The expression of PepT1 protein in colon is controversial. Notwithstanding this uncertainty, it is unlikely that colonic PepT1 has much of an effect on nutrient absorption, which would be completed in the small intestine.

Species differences in the expression pattern and functional activity of PepT1 have been observed between rodents and humans (Jappar et al., 2010, Wuensch et al., 2013). Our laboratory was the first to evaluate the role and relevance of PepT1 in peptide/mimetic drug absorption and disposition using a mPepT1$^{-/-}$ KO mouse model (Posada et al., 2013a, Yang, et al. 2013a). In particular, we demonstrated that both cefadroxil and valacyclovir exhibited dose-proportional absorption in mice after *in vivo* oral dose escalation, results that were contrary to the nonlinear intestinal absorption kinetics reported in rats and humans for cefadroxil (Garrigues et al., 1991, Sanchez-Pico et al., 1989) and valacyclovir (Weller et al., 1993). More recently, species difference in the substrate affinity of human, rat and mouse PepT1 was confirmed by the uptake of GlySar using a yeast expressing system (Hu et al., 2012). These findings supported the tenet that a species difference existed between human, mouse and rat in the pharmacokinetics of PepT1 for drug absorption and possible disposition. However, these results in animal and yeast expression studies may not truly reflect what happens in humans when physiological conditions are

altered. To resolve potential species differences in transporter protein functionality during drug discovery, a potential solution is to develop a humanized mouse model.

Humanized mice have been proposed as useful animal model to address the issue of species differences in gene functional activities and subsequent relevant events during the past decades. Typically, a humanized mouse model can be generated by pronuclear injection or by gene targeting in embryonic stem cells to insert or replace the entire human genomic loci into the mouse genome, in which YAC or BAC construction was a useful vector to manipulate human genomic targeted DNA (Devoy et al., 2012).

In the present study, the development of an hPepT1 humanized mouse model was achieved by hPepT1 genomic DNA injection into mPepT1$^{-/-}$ knockout mouse. Our findings demonstrated that humanized hPepT1$^{+/-}$ mice (huPepT1) have a different protein expression level and tissue distribution of hPepT1 protein, compared to mPepT1 expression patterns in wildtype mice.

MATERIALS AND METHODS

Chemicals

Rabbit anti-human hPepT1 antiserum was a generous gift of Dr. Hannelore Daniel (Technische Univeristy Muchen, Germany). Alex Fluor488 and Prolong Diamond Antifade Mounting reagent with DAPI was purchased from Thermo Fisher Scientific Inc. (Walthan, MA). Proteinase inhibitor cocktail was

purchased from Roche (Seattle, WA). Power SYBR-green PCR Matrix was purchased from Applied Biosystems (Foster City, CA). All other chemicals were acquired from standard sources.

Animals

In-house breeding of gender- and weight-matched mice, 8 to 10 weeks old, included mPepT1$^{+/+}$ (wildtype; WT), mPepT1$^{-/-}$ (mPepT1 knockout; KO) and humanized mPepT1$^{-/-}$/hPepT1$^{+/-}$ mice (hPepT1 humanized; huPepT1; HU). All mouse strains were congenic on a C57BL/6 background, in which KO and HU mice were identified by genotyping and culled from the same breeding litters. The mice were housed in a temperature-controlled environment with 12-hour light and 12-hour dark cycles, and received a standard diet and water ad libitum (Unit for Laboratory Animal Medicine, University of Michigan, Ann Arbor, MI). All mouse studies were performed in accordance with the Guide for the Care and Use of Laboratory Animals as adopted and promulgated by the U.S. National Institutes of Health (Institute of Laboratory Animal Sources, 1996).

The Sensitivity of Genotyping PCR

The specificity and sensitivity of PCR genotyping for one copy of the human PepT1 gene within the mouse genome was necessary for achieving success in the development of humanized huPepT1 mice, as well as for avoiding interference from the mouse mPepT1 gene. Two pairs of primers were designed to test the sensitivity of PCR genotyping using a series of human hPepT1 genes from 0.001, 0.01, 0.1, 1 to 10 copies in 200 ng of mouse genomic DNA. The first

pair of primers were forward 5'-ATCTTCTTCATCGTGGTCAATG-3' and reverse 5'-CCCAGCTGATGAAATTTGTGAA-3' (product size of 200 bp). The second pair of primers were forward 5'-CCAATCTGCTCACACAGGATAGAGAGGGCAGG-3' and reverse 5'-CCTTGAGGCTGTCCAAGTGATTCAGGCCATCG-3' (product size of 524 bp). The PCR conditions were: 94^{o}C initiated for 2 min, followed by 94^{o}C x 30 sec, 60^{o}C x 45 sec, 72^{o}C x 60 sec for 35 cycles, 72^{o}C x 10 min, then hold at 4^{o}C.

Generation of hPepT1 humanized mouse line and initial characterization

The approach used to generate a humanized mouse line for hPepT1 was described previously (Van Keuren et al., 2009), with help from the Transgenic Core at the University of Michigan. In brief, fertilized eggs donated by female mPepT1 KO mice (Hu et al., 2008), 20-24 days old, which were mated with mPepT1 KO males, were injected with purified BAC DNA, RP11-782G13 (~179kb[chr13: 98,091,462 - 98,270,723], Empire Genomics, Buffalo, New York). The BAC clone contained the entire human hPepT1 genomic DNA (~70kb), including the 5'-terminal regulatory elements, coding area, and 3'-terminal regulatory elements. Only intact microinjected eggs were transferred to pseudopregnant recipients for generating transgenic founder offspring.

The transgenic hPepT1 alleles were detected in offspring by PCR using the genomic DNA isolated from tail biopsies. The lack of an endogenous mPepT1 gene was also confirmed by PCR, as described previously (Hu, et al. 2008). After genotyping, the humanized huPepT1 mice were maintained and subsequently bred to hemizygosity by mating with mPepT1$^{-/-}$ mice (Figure 3.1).

The humanized mice were evaluated for viability and serum chemistry, as described previously for mPepT1 KO mice (Hu, et al. 2008).

Gene Copy Measurement of Human hPepT1 in Humanized Mice

The integration copy number of human hPepT1 gene in the mouse genome was measured using real-time PCR. The procedure was reported before but slightly modified (Huang et al., 2013, Mancini et al., 2011). Briefly, the absolute quantitation of human hPepT1 gene in humanized mice was performed using the 7300 real-time PCR system (Applied Biosystems, Foster City, CA). Mouse endogenous gene β-globin was set as the control amount of mouse genomic DNA because it was identified as a single copy gene (Konkel et al., 1978). Primers and standards for the DNA of mouse β-globin and the human hPepT1 gene (Table 3.3) was designed with Primer 3.0 (Applied Biosystems, Foster City, CA) and synthesized by IDT (Coraville, IA). The real-time qPCR conditions were 1 cycle at 50^{o}C for 2 min, 1 cycle at 95^{o}C for 10 min, 40 cycles at 95^{o}C for 15 sec and 60^{o}C for 60 sec. Relative amounts of the β -globin and human hPepT1 genes were calculated based on the standard curve, and the absolute copy number of human hPepT1 gene was calculated by the ratio of human hPepT1 to β -globin.

Real-time PCR and Immunoblot Analyses

Quantitation of hPepT1, mPepT1, mPepT2, mPhT1, mPhT2 and select relevant genes in the small intestine, colon and kidney from wildtype, mPepT1 knockout and humanized huPepT1 mice was performed using the 7300 Real-time PCR system (Applied Biosystems, Foster City, CA) as described previously

(Hu et al., 2014). In brief, 2.0 μg of total RNA, which was isolated using the RNeasy Plus mini Kit (Qiagen, Valencia, CA), was reversely transcribed into cDNA using Omniscript RT kit (Qiagen, Valencia, CA) with 16-mer random primers. The mouse mGapdh gene was used as an internal standard for cDNA quality and quantity. The primers in Table 3.2 were designed with Primer 3.0 (Applied Biosystems, Foster City, CA) and synthesized by Integrated DNA Technologies (Coraville, IA). The real-time PCR thermal conditions were 1 cycle at 50^{o}C for 2 min, 1 cycle at 95^{o}C for 10 min, 40 cycles at 95^{o}C for 15 sec and 60^{o}C for 60 sec. The ΔCT method was used to calculate the relative gene transcript levels in mice, where the ratio of target gene to mGapdh gene was equal to $2^{-\Delta CT}$, ΔCT=CT(gene)-CT(GAPDH)

Immunoblot analyses were performed using a standard, as described previously (Jappar, et al. 2010), Protein samples were prepared from different segments of the small intestine, colon and kidney of wildtype, mPepT1 knockout and humanized huPepT1 mice using 2.0 ml of Nonidet P40-lysis buffer (50 mM Tris-HCl, 150mM NaCl, 1% Nonidet P40, proteinase inhibitor cocktail, pH 8.0). The homogenates then were sonicated for 10 pulses, on ice at half strength of power, and then centrifuged for 15 min at 15,000g, 4^{o}C. The final concentration of proteins was measured using the BCA Protein Assay Kit (Pierce, Rockford, IL). Proteins were denatured at 40^{o}C for 45 min and resolved by 10% SDS-PAGE gel electrophoresis, transferred to a PVDF membrane (Millipore, Billerica, MA), and then blotted with specific polyclonal anti-hPepT1 antiserum (raised

against the COOH-terminal region, NRLEKSNPYFMSGANSQKQM, amino acids 689-708) (1:3000 diluted).

Cryosectioning and *In Situ* Fluorescence Immunoblot Analyses

After being euthanized with CO_2, the small intestine and colon were removed from the animals, trimmed of contaminating tissue, and then cut into fragments no more than 5 mm thick. The tissues were then placed into Optimal Cutting Temperature (O.C.T)-prefilled base molds, without air bubbles, and set at the bottom of the mold. The base molds containing tissues were quickly placed into a beaker of cold 2-methylbutane, precooled in liquid nitrogen, until the tissue matrix completely solidified, at which time it was stored at -80^{o}C until ready for sectioning.

Before sectioning, the tissue matrix block was equilibrated to that of the cryostat temperature of -25^{o}C, mounted on a cryostat specimen disk with O.C.T (Optimal Cutting Temperature) (Sakura Finetek USA, Torrance, CA), and then adjusted to align with the knife blade. The desired section thickness was set at 5 to 10 μM (usually 7 μM). The cut section was adhered to a Superfrost Plus slide (Thermo Fisher Scientific Inc. Walthan, MA), the slide fixed by immersion in cold fresh acetone (-20^{o}C or ice-cold) for 2 x 10 minutes, and then air dried and processed for staining.

The fixed slides were washed three times with PBS, 2 min each, and then aspirated around the tissue until the slide was dry. The slides were then placed in a humid chamber, prepared by putting one wet paper towel on the bottom of

chamber with a couple of sticks over it. After blocking with 5% goat serum in PBS containing 0.05% Triton X-100 for one hour at room temperature, the slides were then incubated with 150 μL of 2% goat PBS, containing 0.2 μL of anti-human hPepT1 antiserum, for one hour at room temperature in a humidified chamber, then followed by rinsing the slides with PBS five times, 2 min each time. The secondary antibody (Alex Fluor488), diluted 1:300 with 2% goat PBS containing 0.05% Triton X-100, was added to the slides and then incubated in the humidified chamber for one hour at room temperature. After that, the slides were washed twice with PBS/tritonx-100 buffer, 2 min each, followed by three washes with PBS, 2 min each. After the slides were dry, 2 drops of Prolong Diamond Antifade Mounting reagent was added with DAPI to each section, a cover slip placed over the section, and the slides then remaining overnight, at room temperature, protected from the light. Once the slides were completely dry, the edges of the cover slip were sealed with clear nail polish. Fluorescence staining of the slides was checked by microscopy.

H&E Staining for Frozen Tissue Sections

After being air-dried for several minutes to remove moisture, tissue sections were stained with filtered 0.1% Mayers Hematoxylin (Sigma; MHS-16) for 10 min in a 50 mL conical tube. The sections were then placed in a Coplin jar and rinsed with cool running ddH_2O for 5 min. After being dipped in 0.5% Eosin (1.5g dissolved in 300mL of 95% ethanol) 12 times, the sections were washed in distilled water until the eosin stopped streaking. They were then dipped in 50% and then 70% ethanol, 10 times each, and equilibrated in 95% and 100% ethanol

for 30 and 60 sec, respectively. Finally, the sections were dipped in Xylene several times, the excess liquid aspirated away, the slides cleaned with a paper tower, and then mounted by a coverslip with Cytoseal XYL (Thermo Fisher Scientific Inc. Waltham, MA).

Data analysis

Data were reported as mean ± SE, unless otherwise noted. Statistical differences between two groups were determined using an unpaired t-test. Multiple treatment groups were compared using one-way analysis of variance (ANOVA), followed by either a Tukey's or Dunnett's post hoc test (GraphPad Prism 5.0; GraphPad software, Inc., La Jolla, CA). A p value ≤ 0.05 was considered significant.

RESULTS

The Sensitivity of Genotyping PCR

In order to screen founder mice for positive colonies of human hPepT1 genomic DNA contained in the chromosome, PCR genotyping was necessary because of its sensitivity to probe at least one copy of integration in the entire mouse genome. As shown in Figure 3.2, a serial dilution of human hPepT1 gene (BAC DNA: RP11-782G13) was added to the PCR reaction system using two different pairs of primers. Both primer pairs could be used to specifically amplify the target gene of human hPepT1 from samples containing even less than one

copy in 200 ng genomic of DNA (the estimated amount in one mouse genome), up to 0.01 copy per 200 ng genomic DNA for primer #1. Moreover, no band was found in the negative control containing only mouse genomic DNA. Therefore, this genotyping PCR method was sensitive enough to screen for positive colonies of humanized huPepT1 mice.

Identification of Humanized Transgenic Mice

Humanized huPepT1mice were generated on the background of C57BL/6 mPepT1 knockout mice using a traditional microinjection transgenic strategy with BAC DNA (Van Keuren, et al. 2009). In this way, the whole genomic DNA of hPepT1, comprising all regulatory elements and coding regions, can be integrated into the mouse chromosome for inheritance. As shown in Figure 3.3, hPepT1 genomic DNA appeared only in humanized huPepT1 mice and the BAC RP11-782G13, which was set as the positive control. In contrast, hPepT1 genomic DNA was not found in mPepT1$^{-/-}$/hPepT1$^{-/-}$, mPepT1$^{+/+}$ and mPepT1$^{-/-}$ mice, the latter being used as the negative control. In addition, mouse mPepT1 genomic DNA was not detected in mPepT1$^{-/-}$/hPepT1$^{+/-}$, mPepT1$^{-/-}$/hPepT1$^{-/-}$ and mPepT1$^{-/-}$, but was detected in mPepT1$^{+/+}$/hPepT1$^{-/-}$ and wildtype mice using wildtype primers. Since mPepT1 KO primers were targeted for the *Neo* gene, which was designed to replace endogenous mPepT1 genomic DNA when creating the mPepT1 knockout mouse model, the observed band during the PCR reaction with mPepT1 KO primers means that mouse mPepT1 genomic DNA was abolished in mPepT1$^{-/-}$/hPepT1$^{+/-}$, mPepT1$^{-/-}$/hPepT1$^{-/-}$and mPepT1$^{-/-}$ mice, but not mPepT1$^{+/+}$/hPepT1$^{-/-}$ mice.

Six founder mice were identified as containing the BAC RP11-782G13 DNA. However, only five of the mice succeeded in germline transmission of this DNA, and only three mice showed hPepT1 mRNA expression (Figure 3.4). The humanized huPepT1 mouse (HU #4) showed the highest level of mRNA expression and, as a result, was selected for further breeding and studies.

The integration copy number of transferred BAC RP11-782G13 DNA was measured using real-time PCR. Two humanized mouse lines (HU#4 and HU#5) were found to have one copy of hPepT1 genomic DNA in their genome, as shown in Figure 3.5.

Initial Phenotypic and Physiological-Chemical Analysis

Hemizygous humanized huPepT1 mice appeared normal with no obvious behavioral phenotype. They cannot be distinguished from wildtype or mPepT1 knockout mice based on appearance alone. The humanized huPepT1 mice had normal survival rates, fertility, litter size, gender distribution and body weight (Table 3.1) as compared to wildtype and mPepT1 KO mice. Moreover, as shown in Table 3.1, there were no significant differences in serum clinical chemistry between the three genotypes, including electrolytes, protein, glucose and enzymes. Histologic evaluation, by hematoxylin and eosin staining, also demonstrated normal morphology of the small intestine (duodenum, jejunum and ileum) (Figure 3.6), cecum/colon (Figure 3.7) and kidney (Figure 3.8).

Stable Expression of hPepT1 Transporter in Intestine of Humanized Mice

qPCR was carried out to demonstrate that human, but not mouse, PepT1 transcripts were expressed in humanized mice. In this regard, hPepT1 mRNA was abundantly found in small intestine and to a lesser extent in colon of huPepT1, but not wildtype and mPepT1 KO mice (Figure 3.9A). In contrast, mouse mPepT1 was expressed in wildtype, but not in PepT1 KO and humanized huPepT1 mice (Figure 3.9B). Of note, whereas hPepT1 expression was clearly observed in the proximal and distal colon of humanized mice (Figure 3.9A), mouse mPepT1 mRNA levels were only found in distal and not proximal colon of wildtype mice (Figure 3.9B).

Immunoblot analyses of intestinal and kidney tissue were performed to assess whether the expression levels of hPepT1 mRNA matched that of hPepT1 protein. Regional segments of small intestine and colon were probed using specific anti-human hPepT1 antiserum. hPepT1 protein was detected at high levels in humanized mouse duodenum, jejunum and ileum, and at low levels in proximal and distal colon; no hPepT1 protein was observed in kidney (Figure 3.10A). Specificity of the antibody was confirmed by the absence of signal in samples taken from wildtype and mPepT1 mouse jejunum, and by the presence of a strong signal in Caco-2 cells (Figure 3.10A). As expected, there was no mouse mPepT1 protein in the humanized mice, as determined using a specific anti-mouse mPepT1 antibody (Hu, et al. 2008). In agreement with real-time qPCR results, mouse mPepT1 protein was expressed in the jejunum of wildtype mice, but not in the jejunum of mPepT1 knockout and humanized huPepT1 mice (Figure 3.10B).

Tissue Expression Profile of Selected Relevant Transporters

Tissue expression levels of select relevant genes, as assessed by real-time qPCR, are shown in Figures 3.11 (C-E). In these analyses, the three other mouse POT genes (i.e., mPepT2, mPhT1 and mPhT2) had very low expression levels of transcript in both the small and large intestines of wildtype, mPepT1 KO and humanized huPepT1 mice; mPepT2, however, had high expression levels of transcript in kidney for all three genotypes. Even though statistically significant changes were observed for some genes, given their very low expression levels, it highly unlikely that mPepT2 in the intestines and mPhT1/2 in the intestines and kidney will have meaningful protein expression. We also searched for potential changes in mRNA expression of genes involved in amino acid and/or drug transport, as shown in Figure 3.12 (A-C). Thus, mPAT1 expression was increased about 2-fold in the small intestine of humanized huPepT1 mice as compared to wildtype and mPepT1 KO mice. In kidney, mOAT1 transcripts increased about 2-fold in mPepT1 KO mice, however, no change was observed in this transcript between humanized and wildtype mice. Other statistically significant differences were viewed as minor (with little impact) given their very low expression levels.

Localization of hPepT1 Transporters in Humanized Mouse Small Intestine

The correct localization of transport proteins is essential for their correct functional activity. Normally, the PepT1 transporter is localized to the apical side

of epithelial cells in small intestine. As shown in Figure 3.13, fluorescence immunoblotting demonstrated that human hPepT1 protein is also localized to the apical side of enterocytes in humanized mouse jejunum, which is in agreement with that in wildtype mice (Wuensch, et al. 2013).

DISCUSSION

Membrane transporters play an important role in drug absorption, distribution and elimination, along with drug safety and efficacy (International Transporter et al., 2010, Keogh 2012). For example, the peptide transporter PepT1 (a proton-coupled oligopeptide transporter family member), which is located at the apical side of epithelial enterocytes, is responsible for the absorption of protein-digested di-/tri-peptides and peptide-like drugs from the lumen of small intestine. Pharmacologically, intestinal PepT1 was used as a target in drug discovery for increasing the oral bioavailability of drugs/prodrugs (Zhang et al., 2013). For example, by adding a L-valyl ester group to acyclovir, the intestinal absorption of valacyclovir, mediated by PepT1, was substantially improved along with the systemic availability of its parent drug acyclovir (Yang, et al. 2013a, Yang et al., 2013b). However, whereas a dose-proportional increase in the AUC of valacyclovir was observed in wildtype mice, a nonlinear increase in the AUC of valacyclovir, as a function of increasing dose, was observed in human subjects (Weller, et al. 1993, Yang, et al. 2013a). Furthermore, our laboratory reported that the K_m of GlySar for human hPepT1, using yeast

transformants, was three-fold higher than that for mouse mPepT1 (0.86mM vs. 0.30mM) (Hu, et al. 2012). It should be appreciated that species differences in membrane transporters can also be defined by their tissue distribution, expression levels and prevailing isoforms. For example, a single P-gp protein (MDR1) has been observed in humans, but two isoforms (MDR1a and MDR1b) were observed in rodents (Shirasaka et al., 2011).

Humanized mouse models, produced by transgenic methods, are widely used to investigate if differences exist in the gene activity of human transporters, enzymes and receptors as compared to animals. In the past several years, the generation and characterization of humanized mice has lead to substantial progress in the drug discovery arena. For instance, transgenic mouse models containing human CYP450, conjugation enzymes and nuclear receptors were developed to study drug metabolism, degradation and transport (Gonzalez et al., 2006, Gossen et al., 1994, Jiang et al., 2011, Raybon et al., 2011, Scheer et al., 2013, Xie et al., 2000). However, with the exception of several organic anion-transporting polypeptide transporters (OATPS) (van de Steeg et al., 2012, van de Steeg et al., 2009, van de Steeg et al., 2013) and multidrug resistance-associated protein (MRP2) humanized mouse models (Scheer et al., 2012), no other plasma membrane transporters have been humanized so far. Thus, the ability to generate a huPepT1 mouse model containing the entire human genome offers an unparalleled opportunity to more reliably study the *in vivo* performance of human PepT1-mediated processes such as drug transport, intestinal absorption, pharmacologic response, disease and regulation.

In the present studies, a novel mouse line was established and initially characterized for the humanized hPepT1 transporter. In doing so, we made the following observations: 1) humanized huPepT1 mice had no obvious behavioral or pathological phenotype; 2) only one copy of the hPepT1 gene was integrated into the mouse genome; 3) mRNA and protein profiles indicated that huPepT1 mice had substantial hPepT1 expression in all regions of the small intestine (i.e. duodenum, jejunum and Ileum); 4) a low but measurable expression of hPepT1 mRNA and protein was observed in both proximal and distal segments of the colon in humanized mice; 5) *in situ* fluorescence immunoblotting indicated that the hPepT1 protein was correctly localized to the apical side of small intestinal enterocytes.

Previous transgenic mouse models of human hPepT1 were reported, where human hPepT1 cDNA was introduced into wildtype mice and the hPepT1 protein ubiquitously expressed under the control of the β-actin or villin promoter, for investigating hPepT1's potential role in inflammatory bowel disease (IBD) (Dalmasso et al., 2011). However, these transgenic mouse models did not rule out the impact of endogenous mPepT1, even though the human hPepT1 protein was abundantly detected in normal mouse colon and slightly up-regulated in IBD. In contrast, our humanized huPepT1 mouse model was generated by injection of purified BAC DNA, which contained the entire hPepT1 genomic DNA, into eggs from mPepT1 knockout mice. Thus, our humanized mouse model abolished the potential influence of endogenous mPepT1 protein and avoided the interruption of other endogenous genes by maintaining the humanized mice in a hemizygous

state. Another advantage of using genomic DNA is that the transcripts of hPepT1 gene can be regulated by their own regulatory elements given that the mammalian translation mechanism should be conserved among species.

It was difficult to directly compare the protein expression of PepT1 between wildtype and humanized mice because of species-specific antibodies. However, the mRNA levels of hPepT1 in the small intestine of our humanized mice (Colony HU#4 in Figure 3.4) were comparable to that of PepT1 in humans (Ziegler et al., 2002) and wildtype mice (Jappar, et al. 2010). Since the humanized mice have only one copy of hPepT1 genomic DNA, the expression of hPepT1 transcripts in select tissues of humanized mice are somewhat lower than wildtype mice, as are the relatively lower levels of hPepT1 protein (Figure 3.9). Still, there is general agreement among species (e.g., rat, mouse, human) regarding the abundant protein expression of PepT1 in duodenal, jejunal and ileal segments of small intestine, and its apical localization (Ford et al., 2003, Groneberg et al., 2001, Jappar, et al. 2010, Merlin et al., 2001, Ogihara et al., 1996, Shen, et al. 2001, Walker et al., 1998, Wuensch, et al. 2013, Ziegler, et al. 2002).

The colonic expression of PepT1 is controversial and may be the result of species differences, the specificity of antibody being used, regionality of tissue expression, and the methods used by different laboratories in preparing the sample. Whereas some studies have reported the expression of PepT1 protein in normal mouse, rat and human colon (Ford, et al. 2003, Wuensch, et al. 2013, Ziegler, et al. 2002), other studies have been unable to detect PepT1 in normal

human, rat and mouse colon (Groneberg, et al. 2001, Jappar, et al. 2010, Merlin, et al. 2001, Ogihara, et al. 1996, Shen, et al. 2001). In particular, Wuensch et al. (2013) found a distinct spatial distribution of colonic PepT1 in mice, rats and humans, in which immunostaining was not observed in proximal colon but significant staining was observed in the distal colon. In our hands, we have consistently detected abundant expression of PepT1 protein in all regions of mouse and rat small intestine, but not in the colon of rodents past 7 days of age (Jappar, et al. 2010, Shen, et al. 2001). In addition, the functional activity of mouse PepT1 was consistent with these expression levels, as determined by the permeability of GlySar (Jappar, et al. 2010), cefadroxil (Posada et al., 2013b) and valacyclovir (Yang, et al. 2013b) in wildtype compared to mPepT1 knockout mice.

With respect to pathological conditions, PepT1 has been implicated by some investigators, but not others, as having a role in the further development of inflammatory bowel disease (Ayyadurai et al., 2013, Buyse et al., 2001, Buyse et al., 2002, Dalmasso et al., 2008, Dalmasso et al., 2010, Dalmasso, et al. 2011, Ingersoll et al., 2012, Kovacs-Nolan et al., 2012, Nguyen et al., 2009, Wang et al., 2013, Wuensch et al., 2014). Our humanized huPepT1 mice may provide another model to study how PepT1 impacts the development of IBD, since hPepT1 was expressed in the colon in a similar manner to that of PepT1 colonic expression in humans. The humanized huPepT1 mice may also prove useful in studying hPepT1 gene expression and regulation.

In concluding, the present study reports, for the first time, the development and initial characterization of humanized huPepT1 mice. These mice are unique in that they contain a copy of the entire human genome in mice previously nulled for mPepT1, and appear to have comparable protein expression and tissue distribution to that of humans.

Table 3.1 Serum clinical chemistry of wildtype (WT), mPepT1 knockout (KO) and humanized huPepT1 (HU) mice[a]

		WT	KO	HU
Body Weight:				
Male (7-8 wks.)	(g)	21.5±0.6 (12)	21.3±0.6 (12)	22.1±0.5 (12)
Female (7-8 wks.)	(g)	17.9±0.3 (12)	17.7±0.4 (12)	18.0±0.3 (12)
Serum:				
Sodium	(mmol/L)	145±0.87 (6)	147±1.31 (6)	146.±1.40 (6)
Potassium	(mmol/L)	7.28±0.48 (6)	7.35±0.29 (6)	7.72±0.53 (6)
Chloride	(mmol/L)	113±0.91 (6)	113±1.05 (6)	113±1.21 (6)
Calcium	(mg/dL)	9.68±0.47 (6)	9.47±0.14 (6)	9.77±0.20 (6)
Albumin	(g/dL)	3.40±0.058 (6)	3.47±0.021 (6)	3.55±0.067 (6)
Protein	(g/dL)	6.40±0.084 (6)	6.38±0.14 (5)	6.32±0.13 (4)
Creatinine	(mg/dL)	0.24±0.026 (6)	0.25±0.0030 (6)	0.28±0.05 (6)
Bilirubin	(mg/dL)	0.16±0.051 (5)	0.08±0.020 (5)	0.14±0.024 (5)
Glucose	(mg/dL)	131±22.38 (5)	163±17.55 (6)	188±5.86 (4)
Urea Nitrogen	(mg/dL)	29.5±2.35 (6)	27.5±1.50 (6)	33.3±2.11 (6)
Alanine Transaminase	(U/L)	95.2±16.02 (6)	78.0±4.79 (6)	101±5.57 (6)
Alkaline Phosphatase	(U/L)	186±28.54 (6)	94.2±11.71 (6)	149±15.35 (6)
Aspartate Aminotransferase	(U/L)	124±17.51 (6)	124±16.20 (6)	104±9.86 (6)

* WT= mPepT1$^{+/+}$ wildtype mice; KO= mPepT1$^{-/-}$/hPepT1$^{-/-}$ KO mice; HU=mPepT1$^{-/-}$/hPepT1$^{+/-}$ humanized mice

**No statistical significances were observed, as determined using ANOVA followed by a Dunnett's post hoc test where the control group was WT.

Table 3.2 Primers used in quantitative real time PCR of select genes

Gene[a]	Forward primer	Reverse primer
mGapdh (EC=1.2.1.12)	5'-GAGACAGCCGCATCTTCTTGT-3'	5'-CACACCGACCTTCACCATTTT-3'
hPepT1 (SLC15A1)	5'-TGACCTCACAGACCACAACCA-3'	5'-GCCAGGCCGATCAAGGA-3'
mPepT1 (Slc15a1)	5'-CCACGGCCATTTACCATACG-3'	5'-TGCGATCAGAGCTCCAAGAA-3'
mPepT2 (Slc15a2)	5'-TGCAGAGGCACGGACTAGATAC-3'	5'-GGGTGTGATGAACGTAGAAATCAA-3'
mPHT1 (Slc15a4)	5'-GCTGCCACCTGCATTACTACTTC-3'	5'-CGTACTTCACAGACACAATGAGGAA-3'
mPHT2 (Slc15a3)	5'-GCTGAAGCTTGCGTTCCAA-3'	5'-AACAGGTGGGCACTTTCAGAGT-3'
mBPHL (EC=3.1.-.-)	5'-GCCAAGGTGGCTGTGAATG-3'	5'-GATCGCATGTTCCCCTTCTC-3'
$mB^{0,+}$ (Alc6a14)	5'-TCAGGATTTGACTTGGCATTCA-3'	5'-CAAGGCCCAATGTTAAAAGCA-3'
mOat1 (Sl22a6)	5'-CCACCTGCTAATGCCAACCT-3'	5'-GATTCGGGTCGTCCTTGCT-3'
mOat2 (Slc22a7)	5'-TGTCGCAAAGACCCTCGTACT-3'	5'-ACATCATCATGCAGCACAGTGA-3'
mOat3 (Slc22a8)	5'-GCCCCAGCCTCACTGTCTATAT-3'	5'-ACATTCAAGATAATGGTGCTCAGAGA-3'
mOct1 (Slc22a1)	5'-TGGTGTTCAGGCTGATGGAA-3'	5'-GCCCAAAACCCCAAACAAA-3'
mMate1 (Slc47a1)	5'-TTCTGCTTGTGACACGCTCAT-3'	5'-AGTGTCCCCCTTTGCAGGAT-3'
mMate2 (Slc47a2)	5'-GACATCATTTCCCTTGTGAGTCAA-3'	5'-GCCCGCAAGTGCATCAA-3'
mPat1 (Slc36a1)	5'-TCTGCTGTGTCTACTTCGTGTTTCT-3'	5'-GGATCACGGTCACATTGTTGTT-3'

[a]Shown as gene name (solute carrier group or enzyme commission number) for human (h) and mouse (m) transporters or enzymes

Table 3.3 Primers used in quantitative real time PCR of gene copy number

Gene[a]	Sequence
mbeta-globin Primers	Forward: 5'- CTGAGAACTTCAGGGTGAGTCTGA -3' Reverse: 5'- CCCTAGAATCGCTTCCCCTTT -3'
Standard Oligo DNA	5'-CTGAGAACTTCAGGGTGAGTCTGATGGGCACCTCCTGGGTTTCCTTC CCCTGGCTATTCTGCTCAACCTTCCTATCAGAAAAAAAGGGGAAGCGATT CTAGGG -3'
hPepT1 (SLC15a1) Primers	Forward: 5'- TGACCTCACAGACCACAACCA -3' Reverse: 5'- CGAAGACTTAAGGCATCAAATGC -3'
Standard Oligo DNA	5'-TGACCTCACAGACCACAACCATGATGGCACCCCCGACAGCCTTCCTGT GCACGTGTGAGTTGGTGCTCACTGCTGCCCCCATCACCCTCCCACCTTGTG CGCATTTGATGCCTTAAGTCTTCG -3'

[a]Shown as gene name (solute carrier group or enzyme commission number) for human (h) and mouse (m) transporters or enzymes

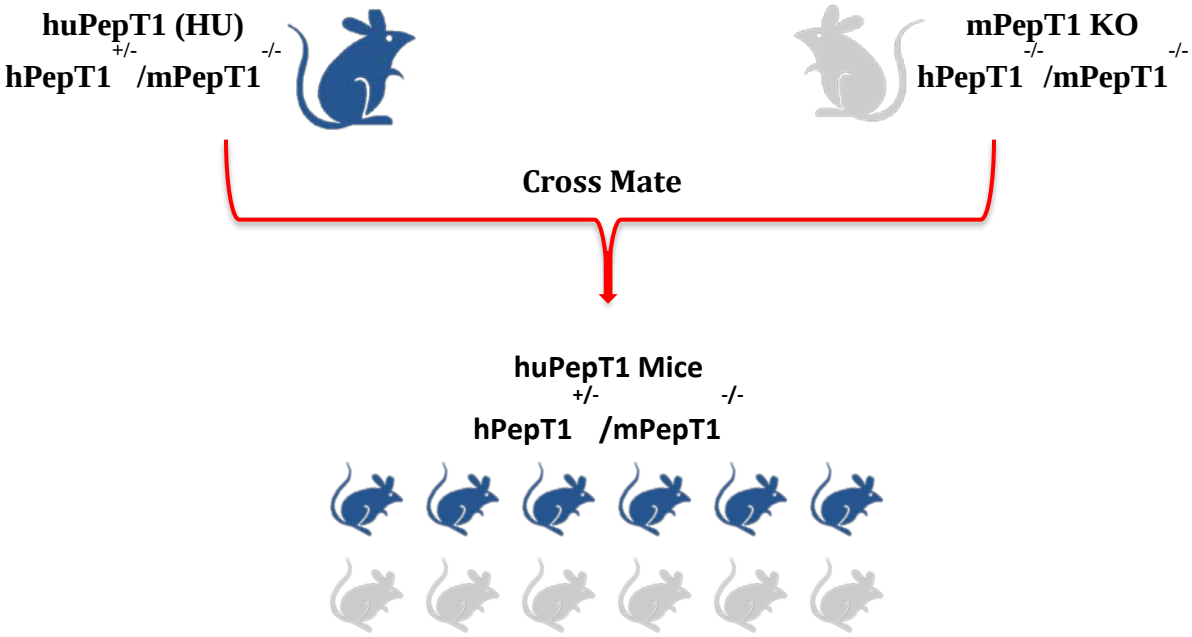

Figure 3.1 Schematic of breeding strategy to maintain the colony of humanized mice. Humanized mice ($hPepT1^{+/-}/mPepT1^{-/-}$) were cross-mated with mPepT1 knockout mice ($hPepT1^{-/-}/mPepT1^{-/-}$) to produce hemizygous humanized mice ($hPepT1^{+/-}/mPepT1^{-/-}$), which were then used for subsequent experiments.

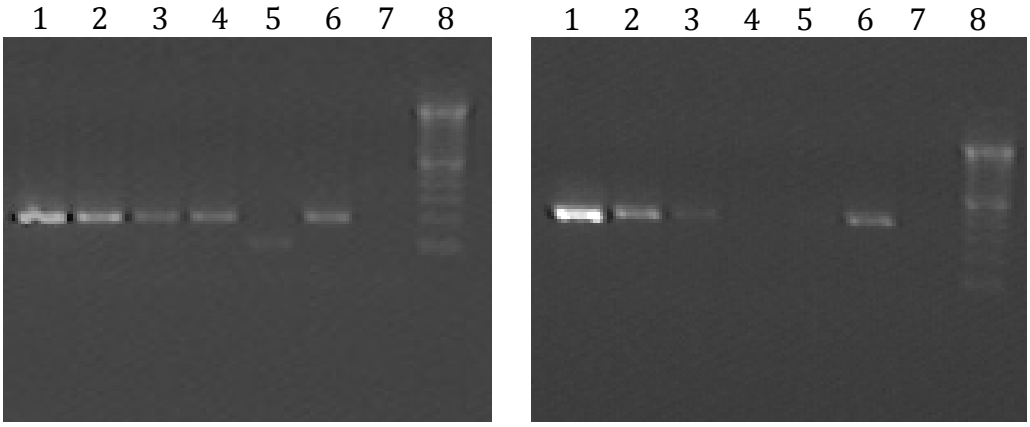

A: Primer #1 for hPepT1 gene

B: Primer #2 for hPepT1 gene

Figure 3.2 Sensitivity of genotyping PCR for identifying the hPepT1 gene. Two pairs of primers were designed and showed similarly high confidence in screening the one copy of gene integrated into the entire mouse genome. Lane 1: 10 copies/200 ng DNA; Lane 2: 1 copy/200 ng DNA; Lane 3: 0.1 copy/200 ng DNA; Lane 4: 0.01 copy/200 ng DNA; Lane 5: 0.001 copy/200 ng DNA; Lane 6: positive control for BAC; Lane 7: Negative control for blank; Lane 8: 100 bp ladder DNA marker.

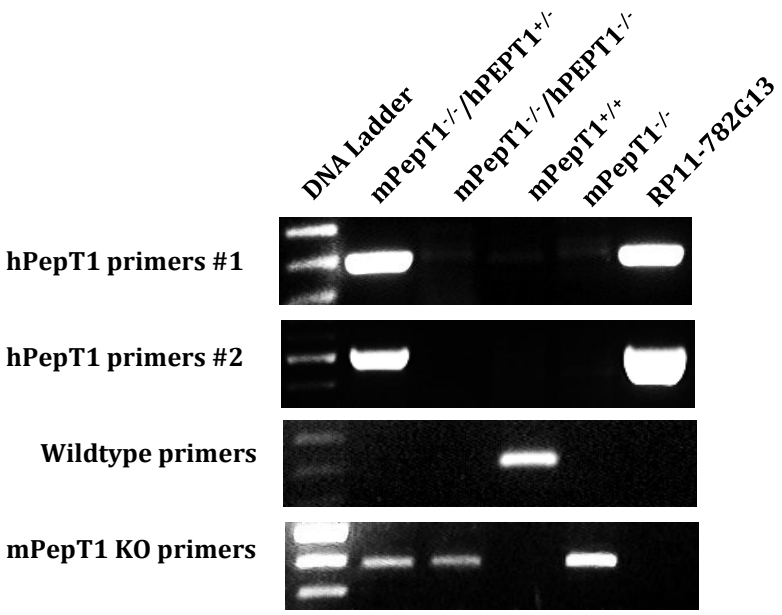

Figure 3.3 Genotyping results for the identification of humanized huPepT1 mice. Genomic DNA was extracted from mouse tail biopsies and genotyped by PCR using specific primers, as described in the text. The DNA ladder, consisting of 100 bp repeats, was used to determine the size of PCR products. $mPepT1^{-/-}/hPepT1^{+/-}$ represents the positive screen for humanized PepT1 (huPepT1) mice, $mPepT1^{-/-}/hPepT1^{-/-}$ the negative screen for humanized PepT1 mice, $mPepT1^{+/+}$ the wildtype mice, $mPepT1^{-/-}$ the PepT1 knockout mice, and RP11-782G13 the purified BAC DNA (used to inject fertilized eggs in generating huPepT1), which served as a positive control.

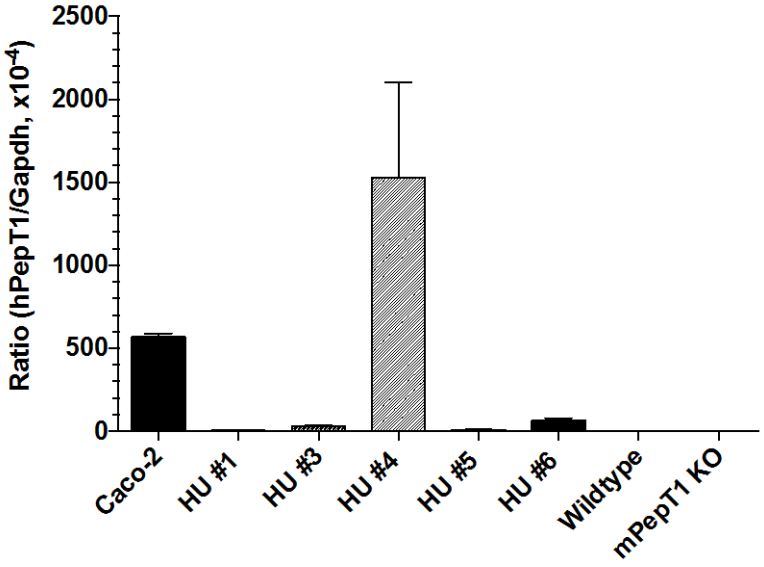

Figure 3.4 Expression of hPepT1 transcripts in humanized mouse founder lines (n=2), as determined by real-time qPCR. Total RNA was isolated from five mouse colonies (HU #1 to HU #6), wildtype and mPepT1 knockout mouse jejunum. Caco-2 cells served as a positive control, and wildtype and mPepT1 knockout mice served as negative controls. HU represents the humanized huPepT1 mice.

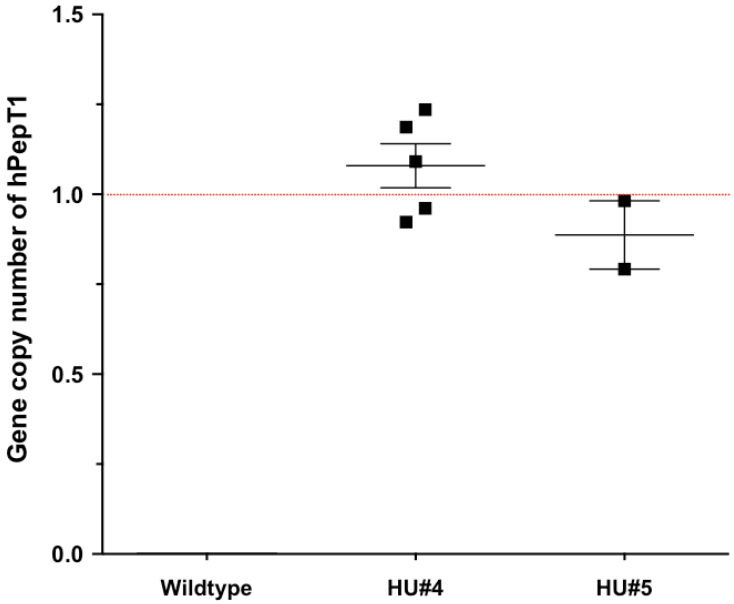

Figure 3.5 Gene copy number of transgenic BAC DNA in humanized huPepT1 mice. Only one copy of BAC integration was detected using real-time PCR. HU represents humanized huPepT1 mice.

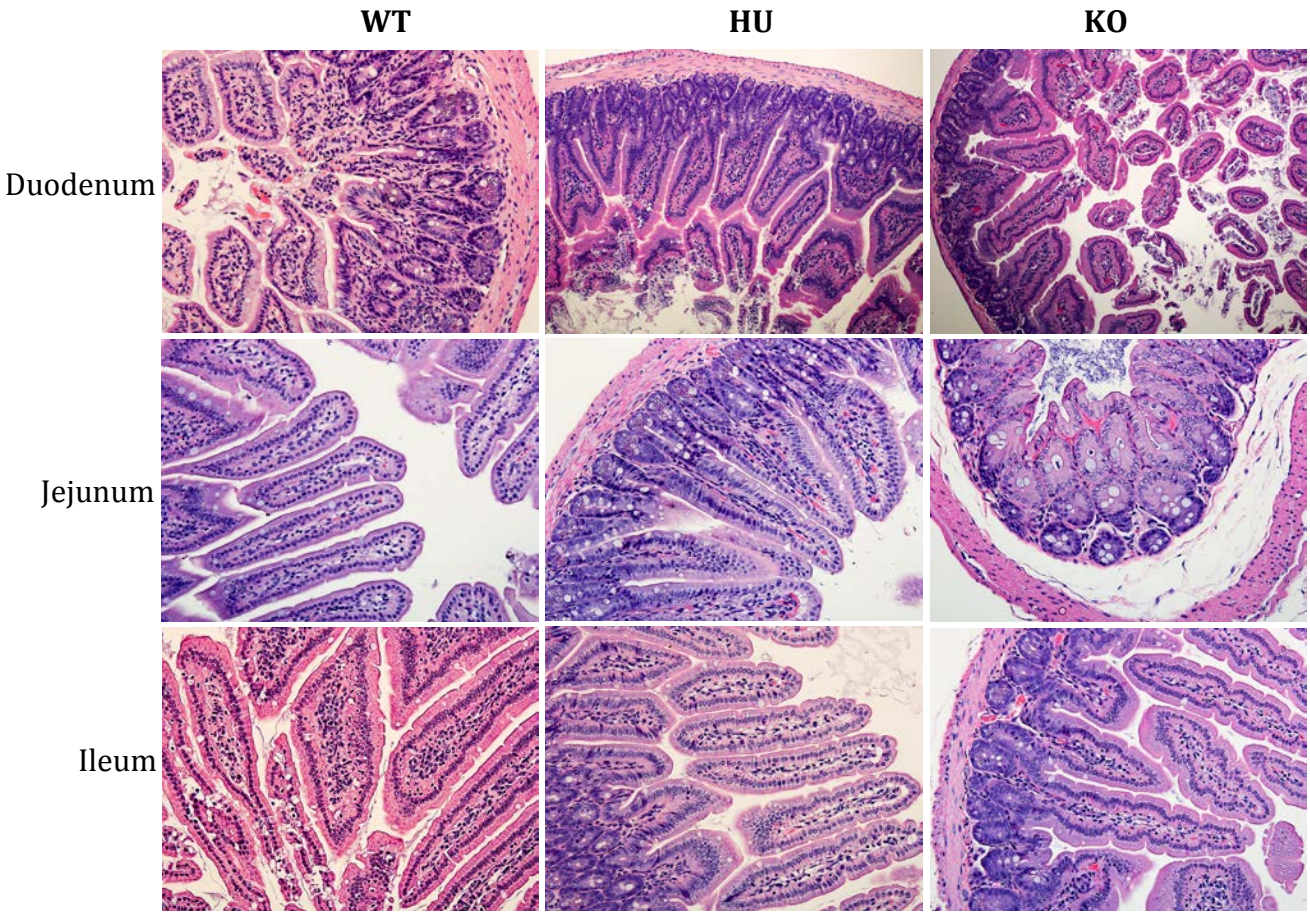

Figure 3.6 H & E staining of the small intestine for wildtype (WT), humanized huPepT1 (HU) and mouse mPepT1 knockout (KO) mice (magnification set at 20x).

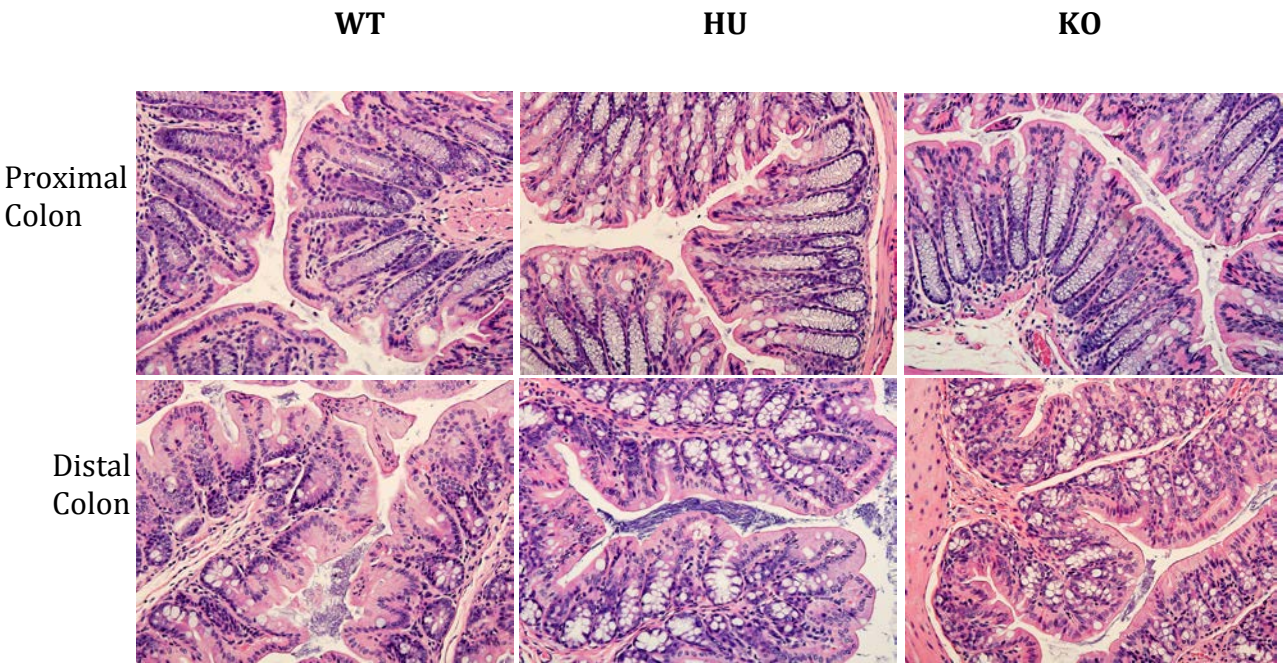

Figure 3.7 H & E staining of the colon for wildtype (WT), humanized huPepT1 (HU) and mouse mPepT1 knockout (KO) mice (magnification set at 20x).

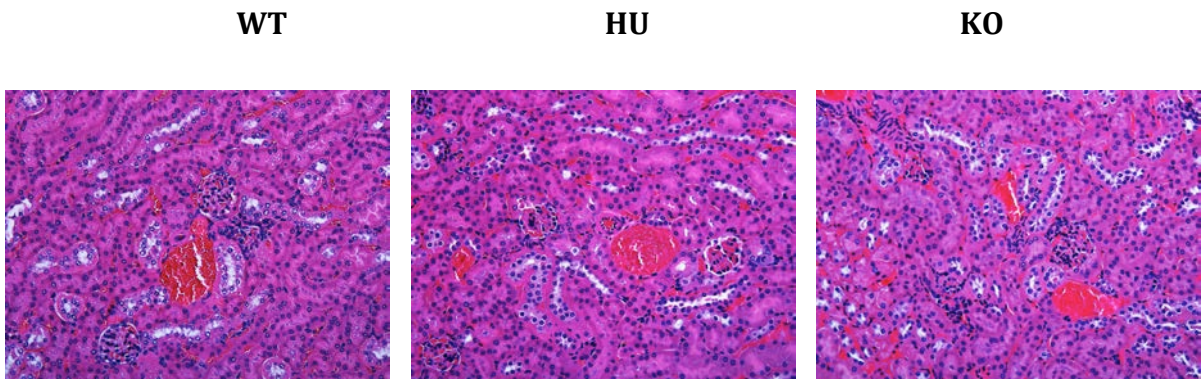

Figure 3.8 H & E staining of the kidney for wildtype (WT), humanized huPepT1 (HU) and mouse mPepT1 knockout (KO) mice (magnification set at 20x).

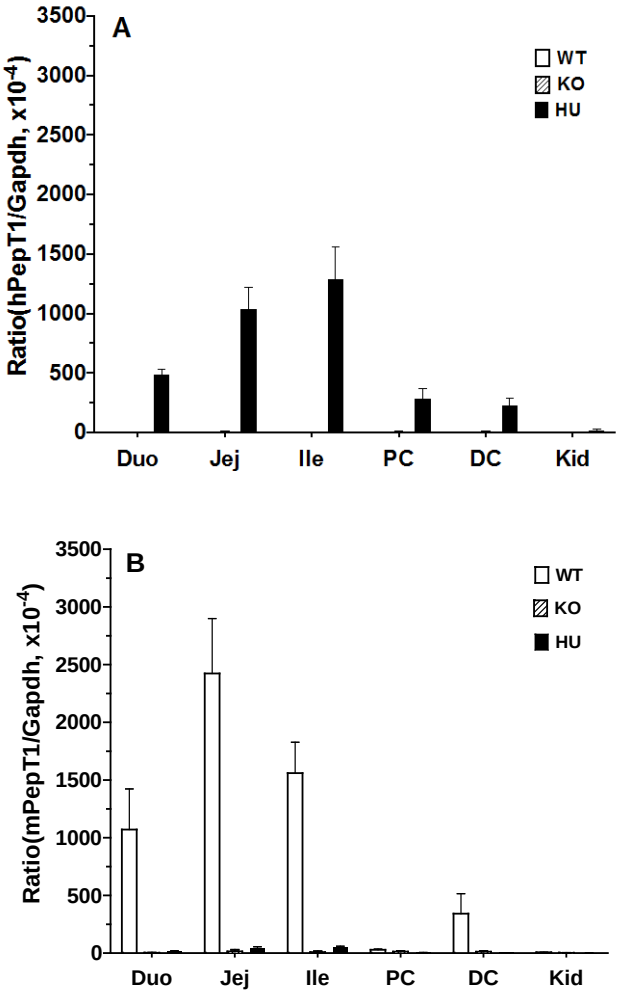

Figure 3.9 Real-time PCR analyses of human hPepT1 (A) and mouse mPepT1 (B) transcripts in the small intestine, colon and kidney of WT, KO and HU mice, where the gene expression levels were normalized by the mouse Gapdh gene. WT represents the wildtype mice, KO the mPepT1 knockout mice, and HU the humanized huPepT1 mice. Duo is the duodenum, Jej the jejunum, Ile the ileum, PC the proximal colon, DC the distal colon, and Kid the kidney. Data were expressed as mean ± SE (n=4-6). Statistical differences were determined for each tissue by ANOVA followed by a Dunnett's post hoc test, where the control group was WT.

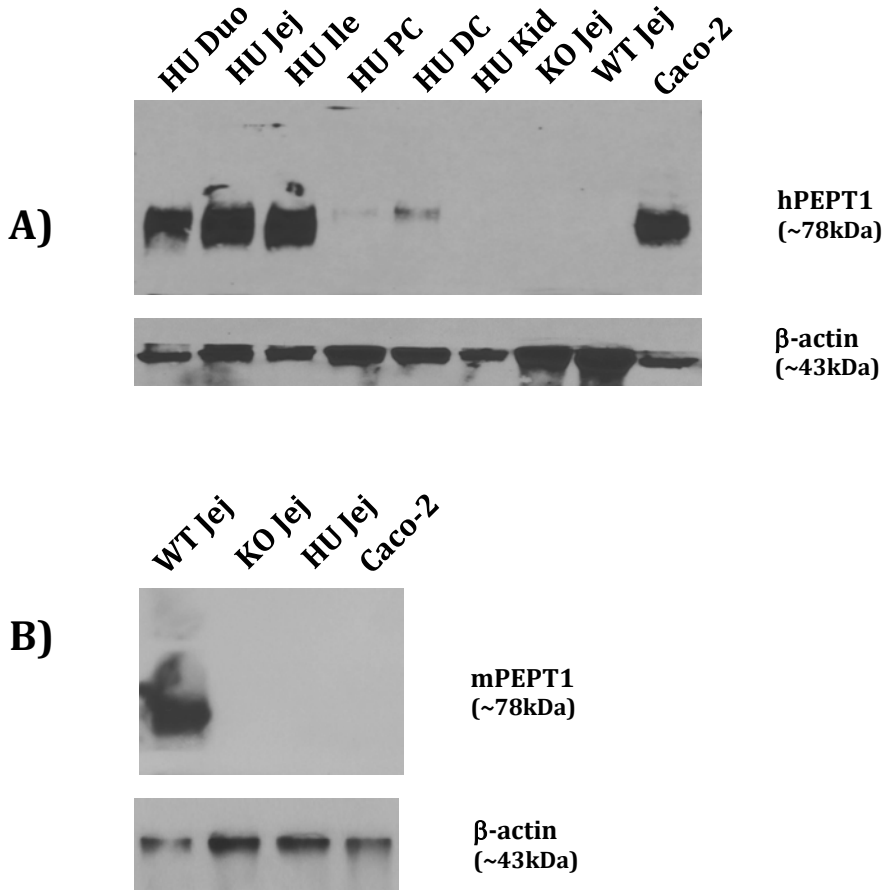

Figure 3.10 Immunoblots of hPepT1 protein in the small intestine, large intestine, and kidney of wildtype (WT), mPepT1 knockout (KO), and humanized huPepT1 (HU) mice (A), and mouse mPepT1 protein in the jejunum of the same genotypes (B). Protein samples were separated by 10% SDS-PAGE, transferred onto PVDF membranes, and incubated for 1.5 hr. with rabbit anti-human hPepT1 antiserum (1:3000) (A) or anti-mouse mPepT1 antiserum (1:5000) (B), and a mouse monoclonal antibody for β-actin (1:1000). The membranes were washed three times with TBST and then incubated for 1 hr with an appropriate secondary antibody of IgG conjugated to HRP (1:3000). Caco-2 cells served as positive and negative controls, respectively, for hPepT1 and mPepT1. Duo represents the duodenum, Jej the jejunum, Ile the ileum, PC the proximal colon, DC the distal colon, and Kid the kidney.

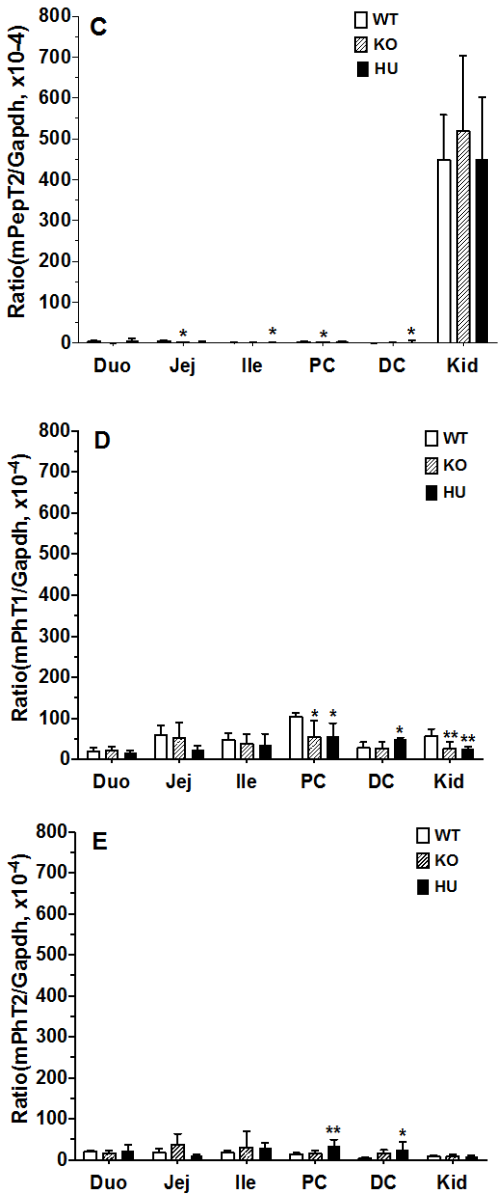

Figure 3.11 Real-time PCR analyses of mouse mPepT2 (C), mouse mPhT1 (D) and mouse mPhT2 (E) transcripts in the small intestine, colon and kidney of WT, KO and HU mice, where the gene expression levels were normalized by the mouse Gapdh gene. WT represents the wildtype mice, KO the mPepT1 knockout mice, and HU the humanized huPepT1 mice. Duo is the duodenum, Jej the jejunum, Ile the ileum, PC the proximal colon, DC the distal colon, and Kid the kidney. Data were expressed as mean ± SE (n=4-6). Statistical differences were determined for each tissue by ANOVA followed by a Dunnett's post hoc test, where the control group was WT. *P < 0.05 and **p < 0.01.

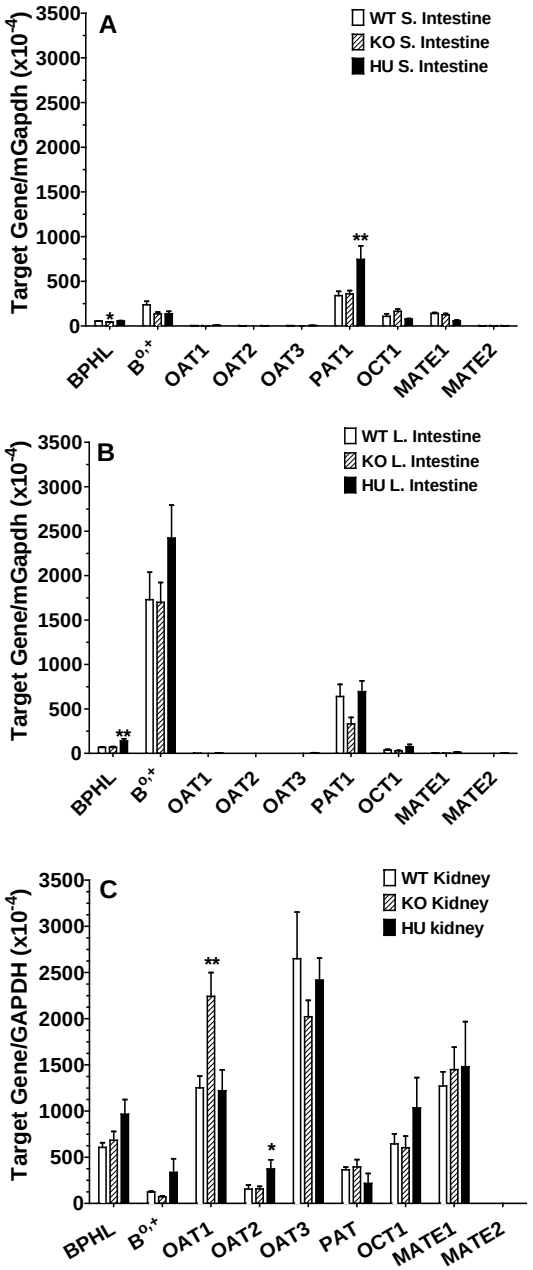

Figure 3.12 Real-time PCR analyses of select non-POT genes (other transporters and enzymes) in the small intestine (A), large intestine (B) and kidney (C), where the gene expression levels were normalized by the mouse Gapdh gene. WT represents the wildtype mice, KO the mPepT1 knockout mice, and HU the humanized huPepT1 mice. Refer to Table 3.2 for gene identification. Data were expressed as mean ± SE (n=4-6). Statistical differences were determined for each gene by ANOVA followed by a Dunnett's post hoc test, where the control group was WT. *P < 0.05 and **p < 0.01.

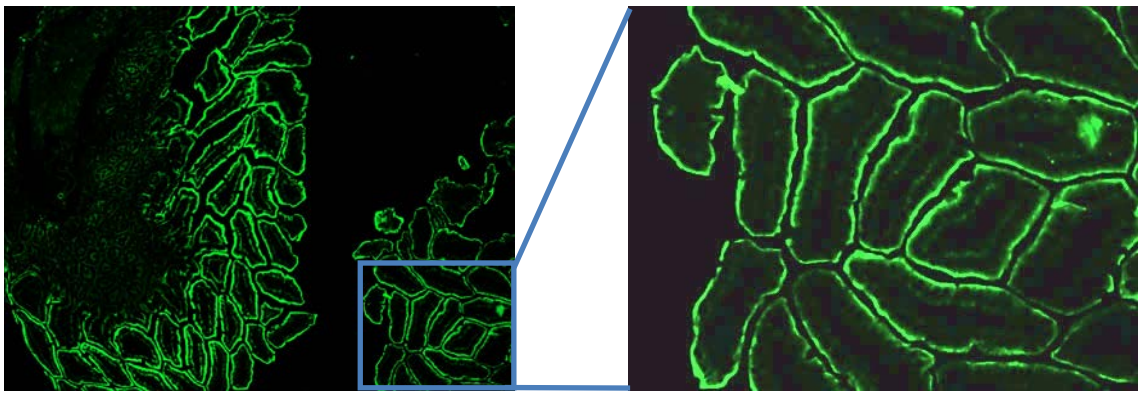

Figure 3.13 Immunofluorescence localization of hPepT1 protein in the jejunum of humanized huPepT1 mice. The hPepT1 protein is clearly observed at the apical side of epithelial cells (highlighted square box was magnified 10x).

REFERENCE

Ayyadurai S, Charania MA, Xiao B, Viennois E and Merlin D (2013) PepT1 expressed in immune cells has an important role in promoting the immune response during experimentally induced colitis. *Lab Invest*. **93:** 888-899.

Buyse M, Berlioz F, Guilmeau S, Tsocas A, Voisin T, Peranzi G, Merlin D, Laburthe M, Lewin MJ, Roze C and Bado A (2001) PepT1-mediated epithelial transport of dipeptides and cephalexin is enhanced by luminal leptin in the small intestine. *J Clin Invest*. **108:** 1483-1494.

Buyse M, Tsocas A, Walker F, Merlin D and Bado A (2002) PepT1-mediated fMLP transport induces intestinal inflammation in vivo. *Am J Physiol Cell Physiol*. **283:** C1795-1800.

Dalmasso G, Charrier-Hisamuddin L, Nguyen HT, Yan Y, Sitaraman S and Merlin D (2008) PepT1-mediated tripeptide KPV uptake reduces intestinal inflammation. *Gastroenterology*. **134:** 166-178.

Dalmasso G, Nguyen HT, Charrier-Hisamuddin L, Yan Y, Laroui H, Demoulin B, Sitaraman SV and Merlin D (2010) PepT1 mediates transport of the proinflammatory bacterial tripeptide L-Ala-{gamma}-D-Glu-meso-DAP in intestinal epithelial cells. *Am J Physiol Gastrointest Liver Physiol*. **299:** G687-696.

Dalmasso G, Nguyen HT, Ingersoll SA, Ayyadurai S, Laroui H, Charania MA, Yan Y, Sitaraman SV and Merlin D (2011) The PepT1-NOD2 signaling pathway aggravates induced colitis in mice. *Gastroenterology*. **141:** 1334-1345.

Devoy A, Bunton-Stasyshyn RK, Tybulewicz VL, Smith AJ and Fisher EM (2012) Genomically humanized mice: technologies and promises. *Nat Rev Genet*. **13:** 14-20.

Fei YJ, Kanai Y, Nussberger S, Ganapathy V, Leibach FH, Romero MF, Singh SK, Boron WF and Hediger MA (1994) Expression cloning of a mammalian proton-coupled oligopeptide transporter. *Nature*. **368:** 563-566.

Fei YJ, Sugawara M, Liu JC, Li HW, Ganapathy V, Ganapathy ME and Leibach FH (2000) cDNA structure, genomic organization, and promoter analysis of the mouse intestinal peptide transporter PEPT1. *Biochim Biophys Acta*. **1492:** 145-154.

Ford D, Howard A and Hirst BH (2003) Expression of the peptide transporter hPepT1 in human colon: a potential route for colonic protein nitrogen and drug absorption. *Histochem Cell Biol*. **119:** 37-43.

Garrigues TM, Martin U, Peris-Ribera JE and Prescott LF (1991) Dose-dependent absorption and elimination of cefadroxil in man. *Eur J Clin Pharmacol*. **41:** 179-183.

Gonzalez FJ and Yu AM (2006) Cytochrome P450 and xenobiotic receptor humanized mice. *Annu Rev Pharmacol Toxicol*. **46:** 41-64.

Gossen JA, de Leeuw WJ and Vijg J (1994) LacZ transgenic mouse models: their application in genetic toxicology. *Mutation research*. **307:** 451-459.

Groneberg DA, Doring F, Eynott PR, Fischer A and Daniel H (2001) Intestinal peptide transport: ex vivo uptake studies and localization of peptide carrier PEPT1. *Am J Physiol Gastrointest Liver Physiol*. **281:** G697-704.

Hu Y, Chen X and Smith DE (2012) Species-dependent uptake of glycylsarcosine but not oseltamivir in Pichia pastoris expressing the rat, mouse, and human intestinal peptide transporter PEPT1. *Drug Metab Dispos*. **40:** 1328-1335.

Hu Y, Smith DE, Ma K, Jappar D, Thomas W and Hillgren KM (2008) Targeted disruption of peptide transporter Pept1 gene in mice significantly reduces dipeptide absorption in intestine. *Mol Pharm*. **5:** 1122-1130.

Hu Y, Xie Y, Keep RF and Smith DE (2014) Divergent developmental expression and function of the proton-coupled oligopeptide transporters PepT2 and PhT1 in regional brain slices of mouse and rat. *J Neurochem*. 10.1111/jnc.12687

Huang Y, Yin X, Zhu C, Wang W, Grierson D, Xu C and Chen K (2013) Standard addition quantitative real-time PCR (SAQPCR): a novel approach for determination of transgene copy number avoiding PCR efficiency estimation. *PloS one*. **8:** e53489.

Ingersoll SA, Ayyadurai S, Charania MA, Laroui H, Yan Y and Merlin D (2012) The role and pathophysiological relevance of membrane transporter PepT1 in intestinal inflammation and inflammatory bowel disease. *Am J Physiol Gastrointest Liver Physiol*. **302:** G484-492.

International Transporter C, Giacomini KM, Huang SM, Tweedie DJ, Benet LZ, Brouwer KL, Chu X, Dahlin A, Evers R, Fischer V, Hillgren KM, Hoffmaster KA, Ishikawa T, Keppler D, Kim RB, Lee CA, Niemi M, Polli JW, Sugiyama Y, Swaan PW, Ware JA, Wright SH, Yee SW, Zamek-Gliszczynski MJ and Zhang L (2010) Membrane transporters in drug development. *Nat Rev Drug Discov*. **9:** 215-236.

Jappar D, Wu SP, Hu Y and Smith DE (2010) Significance and regional dependency of peptide transporter (PEPT) 1 in the intestinal permeability of glycylsarcosine: in situ single-pass perfusion studies in wild-type and Pept1 knockout mice. *Drug Metab Dispos*. **38:** 1740-1746.

Jiang XL, Gonzalez FJ and Yu AM (2011) Drug-metabolizing enzyme, transporter, and nuclear receptor genetically modified mouse models. *Drug Metab Rev*. **43:** 27-40.

Keogh JP (2012) Membrane transporters in drug development. *Adv Pharmacol*. **63:** 1-42.

Konkel DA, Tilghman SM and Leder P (1978) The sequence of the chromosomal mouse beta-globin major gene: homologies in capping, splicing and poly(A) sites. *Cell*. **15:** 1125-1132.

Kovacs-Nolan J, Zhang H, Ibuki M, Nakamori T, Yoshiura K, Turner PV, Matsui T and Mine Y (2012) The PepT1-transportable soy tripeptide VPY reduces intestinal inflammation. *Biochim Biophys Acta*. **1820:** 1753-1763.

Liang R, Fei YJ, Prasad PD, Ramamoorthy S, Han H, Yang-Feng TL, Hediger MA, Ganapathy V and Leibach FH (1995) Human intestinal H+/peptide cotransporter. Cloning, functional expression, and chromosomal localization. *J Biol Chem*. **270:** 6456-6463.

Mancini C, Messana E, Turco E, Brussino A and Brusco A (2011) Gene-targeted embryonic stem cells: real-time PCR assay for estimation of the number of neomycin selection cassettes. *Biol Proced Online*. **13:** 10.

Merlin D, Si-Tahar M, Sitaraman SV, Eastburn K, Williams I, Liu X, Hediger MA and Madara JL (2001) Colonic epithelial hPepT1 expression occurs in inflammatory

bowel disease: transport of bacterial peptides influences expression of MHC class 1 molecules. *Gastroenterology*. **120:** 1666-1679.

Nguyen HT, Dalmasso G, Powell KR, Yan Y, Bhatt S, Kalman D, Sitaraman SV and Merlin D (2009) Pathogenic bacteria induce colonic PepT1 expression: an implication in host defense response. *Gastroenterology*. **137:** 1435-1447 e1431-1432.

Ocheltree SM, Shen H, Hu Y, Keep RF and Smith DE (2005) Role and relevance of peptide transporter 2 (PEPT2) in the kidney and choroid plexus: in vivo studies with glycylsarcosine in wild-type and PEPT2 knockout mice. *J Pharmacol Exp Ther*. **315:** 240-247.

Ogihara H, Saito H, Shin BC, Terado T, Takenoshita S, Nagamachi Y, Inui K and Takata K (1996) Immuno-localization of H+/peptide cotransporter in rat digestive tract. *Biochem Biophys Res Commun*. **220:** 848-852.

Posada MM and Smith DE (2013a) In vivo absorption and disposition of cefadroxil after escalating oral doses in wild-type and PepT1 knockout mice. *Pharm Res*. **30:** 2931-2939.

Posada MM and Smith DE (2013b) Relevance of PepT1 in the intestinal permeability and oral absorption of cefadroxil. *Pharm Res*. **30:** 1017-1025.

Raybon JJ, Pray D, Morgan DG, Zoeckler M, Zheng M, Sinz M and Kim S (2011) Pharmacokinetic-pharmacodynamic modeling of rifampicin-mediated Cyp3a11 induction in steroid and xenobiotic X receptor humanized mice. *The Journal of pharmacology and experimental therapeutics*. **337:** 75-82.

Sanchez-Pico A, Peris-Ribera JE, Toledano C, Torres-Molina F, Casabo VG, Martin-Villodre A and Pla-Delfina JM (1989) Non-linear intestinal absorption kinetics of cefadroxil in the rat. *J Pharm Pharmacol*. **41:** 179-185.

Scheer N, Balimane P, Hayward MD, Buechel S, Kauselmann G and Wolf CR (2012) Generation and characterization of a novel multidrug resistance protein 2 humanized mouse line. *Drug metabolism and disposition: the biological fate of chemicals*. **40:** 2212-2218.

Scheer N and Roland Wolf C (2013) Xenobiotic receptor humanized mice and their utility. *Drug Metab Rev*. **45:** 110-121.

Shen H, Smith DE and Brosius FC, 3rd (2001) Developmental expression of PEPT1 and PEPT2 in rat small intestine, colon, and kidney. *Pediatr Res*. **49:** 789-795.

Shirasaka Y, Suzuki K, Nakanishi T and Tamai I (2011) Differential effect of grapefruit juice on intestinal absorption of statins due to inhibition of organic anion transporting polypeptide and/or P-glycoprotein. *J Pharm Sci*. **100:** 3843-3853.

Smith DE, Clemencon B and Hediger MA (2013) Proton-coupled oligopeptide transporter family SLC15: physiological, pharmacological and pathological implications. *Mol Aspects Med*. **34:** 323-336.

van de Steeg E, Stranecky V, Hartmannova H, Noskova L, Hrebicek M, Wagenaar E, van Esch A, de Waart DR, Oude Elferink RP, Kenworthy KE, Sticova E, al-Edreesi M, Knisely AS, Kmoch S, Jirsa M and Schinkel AH (2012) Complete OATP1B1 and OATP1B3 deficiency causes human Rotor syndrome by interrupting conjugated bilirubin reuptake into the liver. *The Journal of clinical investigation*. **122:** 519-528.

van de Steeg E, van der Kruijssen CM, Wagenaar E, Burggraaff JE, Mesman E, Kenworthy KE and Schinkel AH (2009) Methotrexate pharmacokinetics in transgenic mice with liver-specific expression of human organic anion-transporting polypeptide 1B1 (SLCO1B1). *Drug metabolism and disposition: the biological fate of chemicals*. **37:** 277-281.

van de Steeg E, van Esch A, Wagenaar E, Kenworthy KE and Schinkel AH (2013) Influence of human OATP1B1, OATP1B3, and OATP1A2 on the pharmacokinetics of methotrexate and paclitaxel in humanized transgenic mice. *Clinical cancer research : an official journal of the American Association for Cancer Research*. **19:** 821-832.

Van Keuren ML, Gavrilina GB, Filipiak WE, Zeidler MG and Saunders TL (2009) Generating transgenic mice from bacterial artificial chromosomes: transgenesis efficiency, integration and expression outcomes. *Transgenic Res*. **18:** 769-785.

Walker D, Thwaites DT, Simmons NL, Gilbert HJ and Hirst BH (1998) Substrate upregulation of the human small intestinal peptide transporter, hPepT1. *J Physiol*. **507 (Pt 3):** 697-706.

Wang P, Lu YQ, Wen Y, Yu DY, Ge L, Dong WR, Xiang LX and Shao JZ (2013) IL-16 induces intestinal inflammation via PepT1 upregulation in a pufferfish model: new insights into the molecular mechanism of inflammatory bowel disease. *J Immunol*. **191:** 1413-1427.

Weller S, Blum MR, Doucette M, Burnette T, Cederberg DM, de Miranda P and Smiley ML (1993) Pharmacokinetics of the acyclovir pro-drug valaciclovir after

escalating single- and multiple-dose administration to normal volunteers. *Clin Pharmacol Ther*. **54:** 595-605.

Wuensch T, Schulz S, Ullrich S, Lill N, Stelzl T, Rubio-Aliaga I, Loh G, Chamaillard M, Haller D and Daniel H (2013) The peptide transporter PEPT1 is expressed in distal colon in rodents and humans and contributes to water absorption. *Am J Physiol Gastrointest Liver Physiol*. **305:** G66-73.

Wuensch T, Ullrich S, Schulz S, Chamaillard M, Schaltenberg N, Rath E, Goebel U, Sartor RB, Prager M, Buning C, Bugert P, Witt H, Haller D and Daniel H (2014) Colonic expression of the peptide transporter PEPT1 is downregulated during intestinal inflammation and is not required for NOD2-dependent immune activation. *Inflamm Bowel Dis*. **20:** 671-684.

Xie W, Barwick JL, Downes M, Blumberg B, Simon CM, Nelson MC, Neuschwander-Tetri BA, Brunt EM, Guzelian PS and Evans RM (2000) Humanized xenobiotic response in mice expressing nuclear receptor SXR. *Nature*. **406:** 435-439.

Yang B, Hu Y and Smith DE (2013a) Impact of peptide transporter 1 on the intestinal absorption and pharmacokinetics of valacyclovir after oral dose escalation in wild-type and PepT1 knockout mice. *Drug Metab Dispos*. **41:** 1867-1874.

Yang B and Smith DE (2013b) Significance of peptide transporter 1 in the intestinal permeability of valacyclovir in wild-type and PepT1 knockout mice. *Drug Metab Dispos*. **41:** 608-614.

Zhang Y, Sun J, Sun Y, Wang Y and He Z (2013) Prodrug design targeting intestinal PepT1 for improved oral absorption: design and performance. *Curr Drug Metab*. **14:** 675-687.

Ziegler TR, Fernandez-Estivariz C, Gu LH, Bazargan N, Umeakunne K, Wallace TM, Diaz EE, Rosado KE, Pascal RR, Galloway JR, Wilcox JN and Leader LM (2002) Distribution of the H+/peptide transporter PepT1 in human intestine: up-regulated expression in the colonic mucosa of patients with short-bowel syndrome. *Am J Clin Nutr*. **75:** 922-930.

CHAPTER IV

FUNCTIONAL VALIDATION OF hPEPT1 PROTEIN IN HUMANIZED huPEPT1 MICE USING THE MODEL DIPEPTIDE GLYCYLSARCOSINE

ABSTRACT

Purpose

PepT1, a member of the proton-coupled oligopeptide transporter family, is abundantly expressed in the small intestine and mediates the uptake of protein-digested di-/tri-peptides and peptide-like drugs from the intestinal lumen. However, species differences in PepT1 protein function has been observed in yeast transformants expressing the rat, mouse and human gene. To address such cross-species difference for PepT1, we generated and initially characterized a novel humanized mouse line for hPepT1 using transgenic methodology. In the present study, we evaluated the functional activity of PepT1 in humanized huPepT1, mPepT1 knockout and wildtype mice using the model dipeptide glycylsarcosine (GlySar).

Methods

A humanized mouse line for hPepT1 was successfully generated using a microinjection technique with BAC construction containing the entire human hPepT1 genomic DNA. The transport kinetics of GlySar were evaluated in humanized huPepT1, mPepT1 knockout and wildtype mice by *in situ* single-pass intestinal perfusion studies, and by *in vivo* oral pharmacokinetic studies.

Results

In agreement with previous results regarding the mRNA, protein expression, and tissue distribution of PepT1, *in situ* perfusion studies with GlySar indicated that the small intestinal permeability of dipeptide in humanized huPepT1 mice was ~70% of that observed in wildtype animals. In comparison, the jejunal permeability of GlySar in mPepT1 knockout mice was only ~2.0% of the value observed in wildtype mice. These results were confirmed by *in vivo* studies in which the area under plasma concentration-time curves (AUC) of GlySar were virtually superimposable in humanized and wildtype mice, but ~2-fold lower in mPepT1 knockout mice after oral dosing.

Conclusion

These findings demonstrated that PepT1 had a comparable functional activity in humanized mice as compared to that of mPepT1 knockout and wildtype mice, especially, the transport kinetics of GlySar in colon gave an agreement with colonic occupancy profile of mRNA and protein in humanized mice and wildtype mice, while as of a significant increment of mRNA and protein expression in colon of humanized mice. Such indicated that humanized mice might provide a

value model to investigate the relevant role of hPepT1 protein in the tissue of colon, such as its functional role in colonic inflammatory bowel diseases, and to clarify the species discrepancy of PepT1 in drug development.

INTRODUCTION

The peptide transporter family consists of four mammalian members: PepT1 (SLC15A1), PepT2 (SLC15A2), PhT1 (SLC15A4) and PhT2 (SLC15A3). Among them, PepT1 has received the most attention because of its apical location in the small intestine, and ability to mediate the uptake of nutrients digested from dietary proteins and the intestinal absorption of drugs such as cefadroxil (Posada et al., 2013b) and valacyclovir (Yang et al., 2013b). Currently, PepT1 is being used as a drug target, during the drug discovery and design process, for enhancing the absorption of low-bioavailability drugs (e.g., BCS III and BCS IV categories) (Zhang et al., 2013).

In general, PepT1 can transport dipeptides, tripeptides and peptide-like drugs with low affinity and high capacity. However, PepT1 has shown species differences between rodents and humans in its tissue distribution and functional activity (Garcia-Carbonell et al., 1993, Garrigues et al., 1991, Jappar et al., 2010, Posada et al., 2013a, Wuensch et al., 2013, Yang et al., 2013a). More recently, species differences were observed in the affinity of PepT1 for transporting GlySar in yeast transformants expressing the human, rat and mouse gene (Hu et al., 2012). These findings clearly demonstrated that a species difference existed

between the human, mouse and rat PepT1 transporter, a difference that might affect the absorption and disposition of PepT1 substrates.

In Chapter III, we described the development of a humanized huPepT1 mouse line using transgenic methodology. These humanized mice were initially characterized with respect to the expression levels of PepT1 transcripts and protein, as well as the tissue distribution of PepT1 protein. A cross-species difference was observed between humanized huPepT1 and wildtype mice, as demonstrated by lower mRNA and protein expression levels of hPepT1 in humanized small intestine, but by higher levels of hPepT1 protein in colon (Hu et al., 2014). These findings suggested that physiological and pharmacological differences might occur in the handling of di-/tri-peptides and peptide-like drugs by PepT1-mediated processes. GlySar, a model dipeptide substrate of PepT1 (Hu, et al. 2012, Hu et al., 2008, Jappar et al., 2009, Jappar et al., 2011, Jappar, et al. 2010), was selected to initially characterize the functional activity of PepT1 in humanized mice as compared to wildtype and/or mPepT1 knockout animals.

In the present study, we evaluated the functional activity of PepT1 protein in humanized huPepT1 and wildtype mice with GlySar using *in situ* intestinal perfusion and *in vivo* pharmacokinetic studies after oral administration. Our findings demonstrated that the small intestinal permeability of GlySar was lower in humanized huPepT1 than wildtype mice, but higher in the colon of humanized mice. During the concentration-dependent perfusion studies, the K_m of GlySar in humanized mice was two-fold lower than that in wildtype mice. However, the oral pharmacokinetic studies did not show differences in the systemic exposure of

dipeptide between the two genotypes. Collectively, the findings indicated that the functional activity of PepT1 protein, as judged by oral drug absorption of GlySar, was fully recovered in the humanized huPepT1 mice.

MATERIALS AND METHODS

Chemicals

[^{3}H]GlySar (29.4 Ci/mmol), [^{14}C]GlySar (113 mCi/mmol) and [^{14}C]inulin 5000 (1.1 mCi/g) were purchased from Moravek Biochemicals and Radiochemicals (Brea, CA). Unlabeled GlySar and inulin-5000 were purchased from Sigma-Aldrich (St. Louis, MO). All other chemicals were acquired from standard sources.

Animals

In-house breeding of gender- and weight-matched, 8-10 week, mPepT1$^{+/+}$ (wildtype, WT), mPepT1$^{-/-}$/hPepT1$^{-/-}$ (mPepT1 knockout, KO) and humanized mPepT1$^{-/-}$/hPepT1$^{+/-}$ (humanized huPepT1, HU] mice, on a C57BL/6 background, were used for all experiments unless otherwise noted. The KO and HU mice were identified by genotyping and culled from the same litter. The mice were housed in a temperature-controlled environment with 12-hr light and 12-hr dark cycles, and received a standard diet and water *ad libitum* (Unit for Laboratory Animal Medicine, University of Michigan, Ann Arbor, MI). All mouse studies were

performed in accordance with the Guide for the Care and Use of Laboratory Animals as adopted and promulgated by the U.S. National Institutes of Health (Institute of Laboratory Animal Sources, 1996).

In Situ Single-Pass Intestinal Perfusion Studies

Humanized huPepT1, mPepT1 knockout and wildtype mice were fasted overnight (~12 hrs.) with free access to water and then anesthetized with sodium pentobarbital (40-60mg/kg ip). Perfusion studies of jejunum or other regional segments were carried out according to methods described previously (Adachi et al., 2003, Jappar, et al. 2010). In brief, after sterilizing the abdominal area with 70% ethanol, and keeping the mice on top of a heating pad to maintain body temperature, the intestines were exposed by a mid-line incision of the abdomen. A 4-cm segment of duodenum, 8-cm segment of proximal jejunum (i.e. ~2 cm distal to the ligament of Treitz), 6-cm segment of ileum (i.e. ~1 cm proximal to the cecum), and 4-cm segment of colon (i.e. ~0.5 cm distal to the cecum) was isolated and incisions then made at both the proximal and distal ends. The segments were rinsed with 0.9% isotonic saline solution and a glass cannula (2.0 mm outer diameter) inserted at each end of the intestinal segment, and secured in place with silk sutures. The isolated intestinal segment(s) were covered with saline-wetted gauze and parafilm to prevent dehydration. After cannulation, the animals were transferred to a temperature-controlled chamber, at 31^{o}C, to maintain body temperature during the entire perfusion procedure. The cannulas were then connected to inlet tubing, which was attached to a 10-mL syringe (BD, Franklin Lakes, NJ USA) placed on a perfusion pump (Model 22: Harvard

Apparatus, South Natick, MA), and to outlet tubing which was placed in a collection vial.

The perfusate buffer contained 135 mM NaCl, 5 mM KCl and 10 mM MES/Tris (pH6.5), plus 10 μM of [^{3}H]GlySar (0.5 μCi) and 0.01% (w/v) [^{14}C]inulin-5000 (0.25 μCi) (which served as a nonabsorbable marker to correct for water flux), during the intestinal perfusion studies. The buffer was perfused through the intestinal segments at a flow rate of 0.1 mL/min, and the exiting perfusate was collected every 10 min for 90 min. A 100-μL aliquot of each perfusate collection was added to a vial containing 6.0 mL of scintillation cocktail (Cytosine, Ecolite MP Biochemicals, Solon, OH), and the samples were measured for radioactivity by a dual-channel liquid scintillation counter (Beckman LS 6000 SC, Beckman Coulter Inc., Fullerton, CA). At the end of experimentation, the actual length of intestinal segments was measured.

For the concentration-dependent jejunal perfusion studies, in wildtype and humanized huPepT1 mice, GlySar varied from 0.01-50 mM in perfusate buffer containing 0.5 μCi [^{3}H]GlySar and 0.01% (w/v) [^{14}C]inulin-5000 (0.25 μCi).

In Vivo Oral Pharmacokinetic Studies

Following an overnight fast (~12 hr), humanized huPepT1, mPepT1 knockout and wildtype mice were anesthetized briefly with isoflurane prior to oral administration of [^{14}C]GlySar (5.0 nmol/g, 5.0 μCi/mouse) by gastric lavage in 200 μL of saline. After oral dosing, serial blood samples were collected at 5, 7.5, 15, 30, 45, 60, 90, 120, 180, 240 and 360 min via tail transections. Blood samples (15-20 μL) were harvested into a tube containing 1.0 μL of EDTA-K3

and centrifuged for 3 min at 3000 g to obtain plasma (10 μL). Animals were returned to their cages in between blood sampling where they had free access to water and, 2 hr later, to food. Radioactivity in the plasma samples was measured by a dual-channel liquid scintillation counter (Beckman LS 6000 SC, Beckman Coulter Inc., Fullerton, CA).

Data Analysis

Steady-state loss of drug from perfusate in the intestinal segment was achieved approximately 30 min after the start of perfusion. The effective permeability (P_{eff}) of drug was calculated according to a complete radial mixing (parallel tube) model (Komiya et al., 1980, Kou et al., 1991) as:

$$P_{eff} = \frac{-Q \bullet \ln(C_{out} / C_{in})}{2\pi RL} \quad (1)$$

where Q was the perfusion flow rate (0.1 mL/min), C_{out} the outlet drug concentration after correction for changes in water flux, C_{in} the inlet drug concentration, R the internal radius (0.1 cm for small intestine and 0.2 cm for colon), and L the length of intestinal segment. Water flux across the epithelium was calculated as (Amidon et al., 1988, Johnson et al., 1988):

$$C_{out} = \frac{C_{out,uncorr} \bullet I_{in}}{I_{out}} \quad (2)$$

where $C_{out,uncorr}$ was the original (uncorrected) outlet drug concentration, I_{in} the inulin-5000 inlet concentration, and I_{out} the inulin-5000 outlet concentration.

The intrinsic or wall permeability (P_w) is referenced to intestinal wall concentrations and determined by factoring out the aqueous layer permeability (P_{aq}) using the formula:

$$P_w = \frac{P_{eff}}{1 - P_{eff}/P_{aq}} \tag{3}$$

The boundary layer approach can be used to estimate the aqueous permeability according to:

$$P_{aq} = (A\frac{R}{D}Gz^{1/3})^{-1} \tag{4}$$

$$Gz = \frac{\pi DL}{2Q} \tag{5}$$

where *A* is a unitless constant (see below for calculation), *R* the radius, *D* the diffusion coefficient in water (6.60 x 10^{-4} cm^2/min), and G_z the Graetz number (0.0829). Once the Graetz number was calculated, *A* was estimated as:

A = 2.50 Gz + 1.125 (when Gz ≥ 0.030)

A = 4.50 Gz + 1.065 (when 0.030 > Gz ≥ 0.010)

A = 10.0 Gz + 1.010 (when 0.010 > Gz ≥ 0.004)

Given these relationships, the concentration of drug at the membrane surface (C_w) was calculated as:

$$C_w = C_{in}(1 - \frac{P_{eff}}{P_{aq}}) \tag{6}$$

The intrinsic parameters J_{max} (maximum transport rate) and K_m (Michaelis constant) were determined using the following equation:

$$P_w = \frac{J_{\max}}{K_m + C_w} + P_m \tag{7}$$

where P_m is the passive (nonsaturable) permeability. The carrier permeability (P_c) was calculated as:

$$P_c = \frac{J_{\max}}{K_m} \tag{8}$$

The steady-state flux (J) can also be referenced to intestinal wall concentrations (C_w) and the intrinsic kinetic parameters expressed as:

$$J = \frac{J_{\max} \bullet C_w}{K_m + C_w} + P_m C_w = P_{eff} \bullet C_{in} \tag{9}$$

The apparent kinetic parameters can also be determined by the following:

$$P_{eff} = \frac{J^*_{\max}}{K^*_{\mathrm{m}} + C_{in}} + P^*_m \tag{10}$$

and the flux calculated as:

$$J = \frac{J^*_{\max} \bullet C_{in}}{K^*_{\mathrm{m}} + C_{in}} + P^*_m \bullet C_{in} \tag{11}$$

The concentration-dependent flux (*J*) of GlySar in jejunum was best fit to a single Michaelis-Menten term as:

$$J = P_{eff} \bullet C_{in} = \frac{J^*_{\max} \bullet C_{in}}{K^*_m + C_{in}} = \frac{J_{\max} \bullet C_w}{K_m + C_w} \tag{12}$$

where the parameters J^*_{max} and K^*_m were referenced to inlet drug concentrations (C_{in}), and the parameters J_{max} and K_m were referenced to intestinal wall drug concentrations (C_w), once corrected for the unstirred aqueous layer permeability.

Data were reported as mean ± SE, unless otherwise noted. Statistical differences between two groups were determined using an unpaired t-test. Multiple treatment groups were compared using one-way analysis of variance (ANOVA) followed by either a Tukey's test or Dunnett's test, with wildtype serving as the control group (GraphPad Prism 5.0; GraphPad software, Inc., La Jolla, CA). $P \leq 0.05$ was considered significant. Pharmacokinetics analyses were

carried out using a non-compartmental model (NCA) in Phoenix WinNonlin 6.3 (Certara, St. Louis, MO USA).

RESULTS

In Situ Regional Perfusion Studies of GlySar in Humanized huPepT1 Mice Compared to Wildtype and mPepT1 Knockout Mice

Given the advantage of an intact blood supply, in situ perfusion studies were performed to evaluate the function of PepT1 in regional segments of the small and large intestines for humanized, wildtype and mPepT1 KO mice. As shown in Figure 4.1 and Table 4.1, and in agreement with real-time PCR and immunoblot results, the permeability of GlySar was negligible in mPepT1 KO mice. In comparing PepT1-competent animals, permeability values in the small intestine of humanized mice were about 54-70% of values observed in wildtype mice. In addition, the permeability in colon was 11-fold greater in humanized huPepT1 mice. Thus, it appears that the permeability of GlySar was comparable in the duodenum, jejunum and Ileum of wildtype and humanized mice. However, whereas colonic permeability was < 1% of that in wildtype jejunum, colonic permeability was ~12% of that in humanized jejunum.

Concentration-Dependent Transport Kinetics of GlySar in Humanized and Wildtype mice

To assess if there were species-dependent difference in the PepT1-mediated transport kinetics of GlySar, concentration-dependent perfusion studies were performed in the jejunum of wildtype and humanized huPepT1 mice. As shown in Figure 4.2, the maximal flux J^*_{max} = 3.75 ± 0.11 nmol/cm^2/sec and the Michaelis constant K^*_m = 13.2 ± 1.0 mM for WT mice (r^2 = 0.988). In contrast, the J^*_{max} = 0.50 ± 0.04 nmol/cm^2/sec and the K^*_m = 3.3 ± 0.9 mM for humanized huPepT1 mice (r^2 = 0.838) (Figure 4.2A). As observed, the maximal flux and Michaelis constant of GlySar were substantially lower in humanized huPepT1 mice. Furthermore, when referenced to intestinal wall concentrations, the maximal flux J_{max} = 3.24 ± 0.13 nmol/cm^2/sec and Michaelis constant K_m = 5.5 ± 0.7 mM for WT mice (r^2 = 0.993); the J_{max} = 0.49 ± 0.03 nmol/ cm^2/sec and K_m = 2.7 ± 0.6 mM for humanized huPepT1 mice (r^2 = 0.973) (Figure 4.2B). Thus, the K_m value was also two-fold lower in humanized huPepT1 mice than in wildtype animals. These results demonstrated that a species differences existed in the transport kinetics of intestinal PepT1, and that human hPepT1 is more likely to be saturated than mouse mPepT1.

***In Vivo* Oral Pharmacokinetic Studies of GlySar in Humanized Mice Compared to Wildtype and mPepT1 Knockout Mice**

To assess the *in vivo* functional activity of hPepT1 in humanized mice, pharmacokinetic studies were performed with the model dipeptide GlySar after a single oral dose. As shown in Figure 4.3, plasma concentrations of GlySar

increased rapidly within the absorption phase of wildtype and humanized huPepT1 mice, and then declined over time with virtually superimposable curves. In contrast, mPepT1 knockout mice had substantially reduced plasma concentrations than PepT1-competent mice (Figure 4.3). In fact, the AUC and C_{max} of wildtype and humanized huPepT1 mice were not significantly different, but mPepT1 knockout mice had AUC values that were ~2-fold lower (Table 4.2). Values for mean residence time (MRT) were similar between the three genotypes although a statistically significant difference was observed between wildtype and mPepT1 knockout mice. These findings were consistent with our previous results from *in situ* perfusions of GlySar, where substantial expression of PepT1 in all regions of small intestine accounted for an apparent fully restored hPepT1 function in the oral absorption of GlySar in humanized mice.

DISCUSSION

In Chapter III, a humanized huPepT1 mouse line was successfully established and its biological properties initially defined. Indeed, species differences were observed between wildtype and humanized huPepT1 mice in PepT1 tissue distribution and protein expression levels, consistent with the literature (Jappar, et al. 2010, Merlin et al., 2001, Shen et al., 2001, Wuensch, et al. 2013, Ziegler et al., 2002). However, the functional activity of PepT1 protein in humanized huPepT1 mice needed further evaluation as compared to wildtype mice because: 1) we previously reported a species difference in the affinity of

GlySar for PepT1, in which the K_m values varied over a 5.4-fold range in yeast *Pichia pastoris* expressing the human (0.86 mM), mouse (0.30 mM) and rat (0.16 mM) transformants (Hu, et al. 2012); 2) appropriate mRNA and protein expression does not guarantee that the transporter will maintain correct functional activity; and 3) oral absorption studies were lacking and, as a result, it was important to validate the *in vivo* functionality of hPepT1 in humanized mice as compared to other genotypes.

In this study, we examined the *in situ* intestinal permeability and *in vivo* oral absorption kinetics of GlySar in humanized mice as compared to wildtype animals. Our results clearly showed that: 1) the *in situ* permeability of GlySar in huPepT1 mice was similar to but lower than wildtype animals in small intestine, and greater than wildtype mice in colon; 2) the functional activity of intestinal PepT1 appeared fully restored (compared to mPepT1 knockout mice) as indicated by the nearly identical pharmacokinetics and plasma concentration-time profiles of orally administered GlySar in huPepT1 and wildtype mice; and 3) no difference was observed between wildtype and humanized mice in the *in vivo* pharmacokinetics after a 5 nmol/g oral dose. This dose corresponds to an initial mouse stomach concentration of ~250 μM, which is much lower than the K^*_m values for both genotypes (i.e., 13.2 mM for WT and 3.3 mM for huPepT1 mice).

As compared to wildtype and mPepT1 knockout mice, our humanized huPepT1 mice showed an apparent full restoration of PepT1 functional activity (Figures 4.1-4.3), although humanized huPepT1 mice were maintained as hemizygotes in order to avoid interrupting other endogenous genes. The *in situ*

single-pass perfusion studies showed that the permeability of GlySar in humanized huPepT1 mice was ~71% (duodenum), ~62% (jejunum), and ~54% (ileum) of that in wildtype mice. The absolute values of GlySar permeability in wildtype mouse jejunum were comparable to previous reports (e.g., $2.1x10^{-4}$ cm/sec in this study vs. $1.6x10^{-4}$ cm/sec by Hu et al. 2008; Jappar et al. 2010). Of note, the colonic permeability of GlySar increased by ~11-fold in humanized mice as compared to wildtype and mPepT1 knockout mice. A minor permeability of GlySar in colon was also observed in other mouse studies (Dalmasso et al., 2008, Hu et al., 2008, Jappar, et al. 2010, Nguyen et al., 2009). Only the study by Wuensch et al. (2013) reported a physiological function of PepT1 in the healthy distal colon of mouse, where it contributed to electrolyte and water handling. Taken as a whole, the permeability of GlySar in various intestinal segments was consistent the pattern of PepT1 mRNA and protein expression (Figures 3.6-3.9 in Chapter III). The hPepT1 functional activity in humanized mice also was evaluated further by *in vivo* oral pharmacokinetic studies with GlySar (Figure 4.3). At a dose of 5 nmol/g, the C_{max}, T_{max} and AUC of GlySar was comparable between wildtype and humanized mice, whereas substantial differences were observed between mPepT1 knockout mice and PepT1-competent animals (Table 4.2).

A discrepancy was observed in affinity of GlySar for PepT1 transporter between in yeast expressing system (Hu, et al. 2012) and in mouse model, where the K_m values varied over a 5.4-fold range in yeast *Pichia pastoris* expressing the human (0.86 mM), mouse (0.30 mM) and rat (0.16 mM)

transformants, as while the K_m values in humanized mouse is 2.7 mM and in wildtype mouse 5.5 mM. This opposite of K_m value for PepT1 transporter probably accounts on that yeast *Pichia pastoris* and mouse models belong two different biological systems, which have different post-translational modifications, such as glycosylation and phosphorylation for PepT1 transporters, such results in affinity of GlySar varied.

Overall, the present study demonstrated that the function of PepT1 was fully restored from previously mPepT1 null mice. There is excellent agreement between hPepT1 expression in the intestines, and the *in situ* permeability and *in vivo* oral absorption of the model dipeptide GlySar. These humanized huPepT1 mice should prove a valuable tool in future studies investigating the role, relevance and regulation of Pep T1 in diet and disease, and in the drug discovery process.

Table 4.1 The effective permeability of GlySar in mouse intestinal segments during *in situ* perfusions (pH 6.5)

	WT			KO			HU		
	Mean ($x10^{-4}$cm/s)	**SE**	**N**	**Mean ($x10^{-4}$cm/s)**	**SE**	**N**	**Mean ($x10^{-4}$cm/s)**	**SE**	**N**
Duodenum	1.59	0.060	4	0.0088	0.0030	4	1.12	0.079	4
Jejunum	2.13	0.10	4	0.043	0.017	4	1.33	0.065	6
Ileum	1.20	0.15	4	0.0030	0.0019	4	0.65	0.055	4
Colon	0.015	0.0079	5	0.0012	0.00024	4	0.17	0.028	5

* WT, represents wildtype mice; KO, mPepT1 knockout mice; and HU, humanized huPepT1 mice

Table 4.2 Non-compartmental analysis of the pharmacokinetics of [^{14}C]GlySar following a 5.0 nmol/g oral dose

		WT	KO	HU
C_{max}	(μM)	2.71±0.09 (3)	1.27±0.05 (3)***	2.86±0.09 (3)
T_{max}	(hr)	0.33±0.08 (3)	1.83±0.17 (3)***	0.33±0.08 (3)
$AUC_{0-0.5}$	(hr*μM)	1.12±0.02 (3)	0.34±0.01 (3)***	1.04±0.04 (3)
AUC_{0-1}	(hr*μM)	2.42±0.07 (3)	0.87±0.02 (3)***	2.29±0.07 (3)
AUC_{0-2}	(hr*μM)	4.76±0.12 (3)	2.04±0.04 (3)***	4.61±0.04 (3)
AUC_{0-3}	(hr*μM)	6.75±0.26 (3)	3.27±0.10 (3)***	6.72±0.03 (3)
AUC_{0-4}	(hr*μM)	8.47±0.40 (3)	4.44±0.15 (3)***	8.61±0.11 (3)
AUC_{0-6}	(hr*μM)	11.60±0.59 (3)	6.66±0.25 (3)***	12.11±0.27 (3)
MRT	(hr)	2.68±0.04 (3)	3.07±0.02 (3)***	2.79±0.04 (3)

C_{max}: Highest plasma GlySar concentration observed after oral administration
T_{max}: Time at which the highest GlySar concentration occurs after oral administration
AUC_{0-t}: Area under the plasma concentration-time curve from time 0 to t after dosing
MRT: Mean residence time of a molecule within the body
Data are expressed as mean±SE
******P*<0.001** level against WT as determined by ANOVA/Dunnett's post doc test.
WT, represents wildtype mice; KO, mPepT1 knockout mice; and HU, humanized huPepT1 mice.

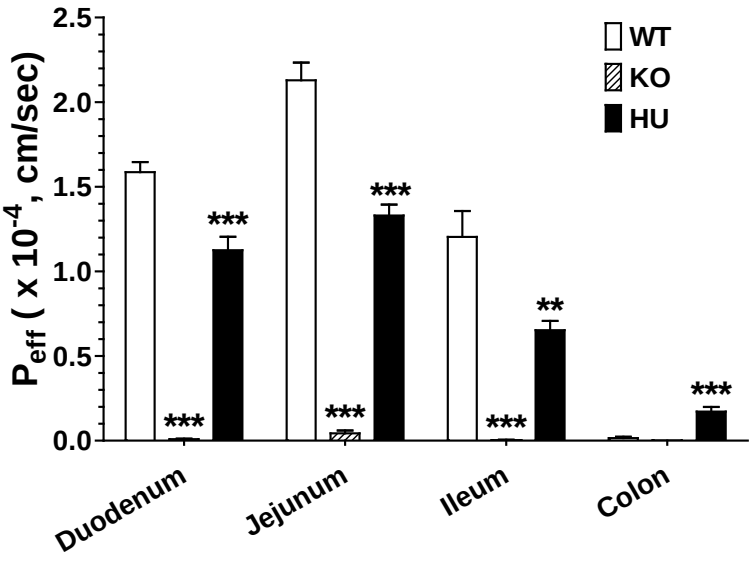

Figure 4.1. *In situ* perfusion studies of 10 μM GlySar in intestinal segments of wildtype (WT), mPepT1 knockout (KO) and humanized huPepT1 (HU) mice. Data are expressed as mean ± SE (n=4-6). ****P*<0.001 as compared to WT.

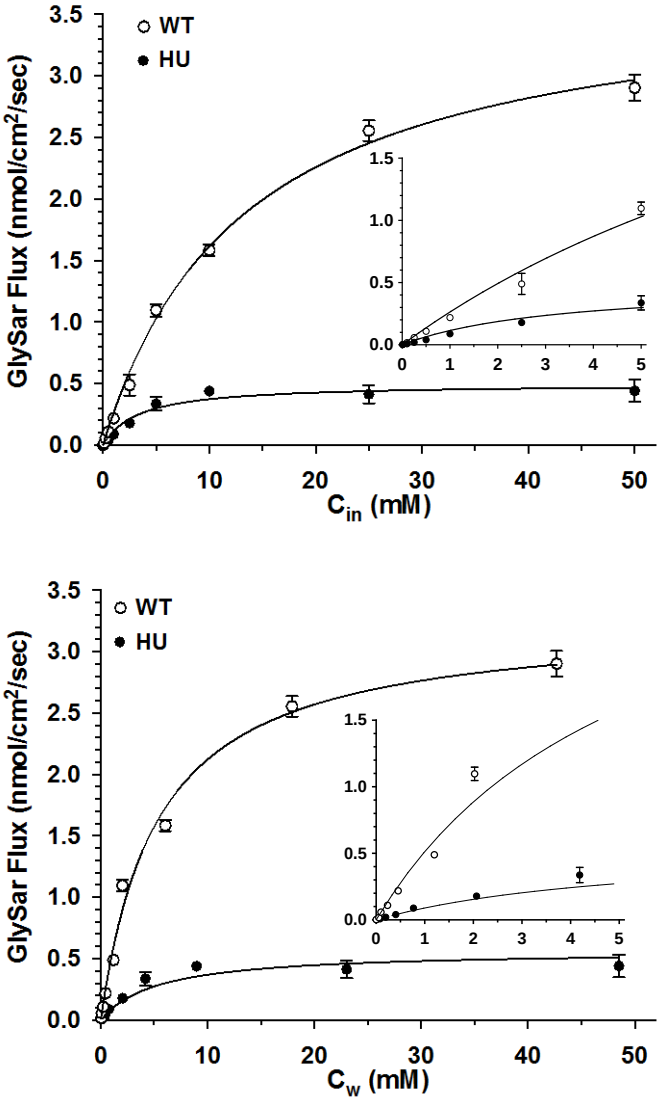

Figure 4.2 Concentration-dependent flux of [^{3}H]GlySar (0.01-50 mM) during jejunal perfusions of wildtype (WT) and humanized huPepT1 (HU) mice. C_{in} is the inlet concentration of GlySar in perfusate in which J^*_{max} = 3.75 ± 0.11 nmol/cm^2/sec and K^*_m = 13.2 ± 1.0 mM for WT mice (r^2 = 0.988); J^*_{max} = 0.50 ± 0.04 nmol/cm^2/sec and K^*_m = 3.3 ± 0.9 mM for HU mice (r^2 = 0.838) (top panel). C_w is the estimated concentration of GlySar at the membrane wall in which J_{max} = 3.24 ± 0.13 nmol/cm^2/sec and K_m = 5.5 ± 0.7 mM for WT mice (r^2 = 0.993); J_{max} = 0.49 ± 0.03 nmol/ cm^2/sec and K_m = 2.7 ± 0.6 mM for HU mice (r^2 = 0.973) (bottom panel). All studies were performed in pH 6.5 buffer. Data are expressed as mean ± SE (n = 4−6).

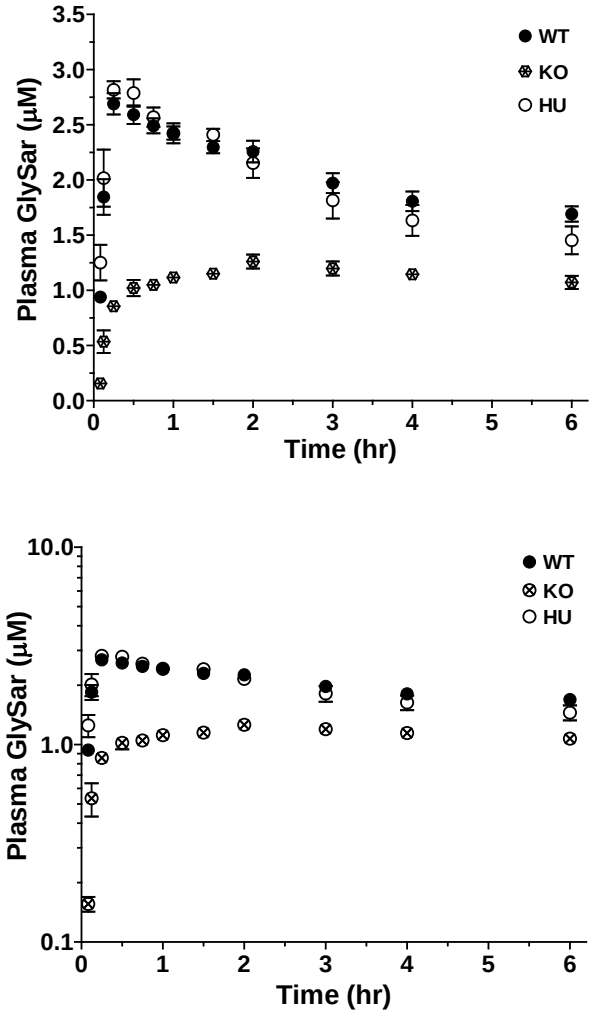

Figure 4.3. *In vivo* pharmacokinetics of 5.0 nmol/g [^{14}C]GlySar after oral gavage in wildtype (WT), mPepT1 knockout (KO) and humanized huPepT1 (HU) mice. Data are expressed as mean ± SE (n=3).

REFERENCE

Adachi Y, Suzuki H and Sugiyama Y (2003) Quantitative evaluation of the function of small intestinal P-glycoprotein: comparative studies between in situ and in vitro. *Pharm Res*. **20:** 1163-1169.

Amidon GL, Sinko PJ and Fleisher D (1988) Estimating human oral fraction dose absorbed: a correlation using rat intestinal membrane permeability for passive and carrier-mediated compounds. *Pharmaceutical research*. **5:** 651-654.

Dalmasso G, Charrier-Hisamuddin L, Nguyen HT, Yan Y, Sitaraman S and Merlin D (2008) PepT1-mediated tripeptide KPV uptake reduces intestinal inflammation. *Gastroenterology*. **134:** 166-178.

Garcia-Carbonell MC, Granero L, Torres-Molina F, Aristorena JC, Chesa-Jimenez J, Pla-Delfina JM and Peris-Ribera JE (1993) Nonlinear pharmacokinetics of cefadroxil in the rat. *Drug Metab Dispos*. **21:** 215-217.

Garrigues TM, Martin U, Peris-Ribera JE and Prescott LF (1991) Dose-dependent absorption and elimination of cefadroxil in man. *Eur J Clin Pharmacol*. **41:** 179-183.

Hu Y, Chen X and Smith DE (2012) Species-dependent uptake of glycylsarcosine but not oseltamivir in Pichia pastoris expressing the rat, mouse, and human intestinal peptide transporter PEPT1. *Drug Metab Dispos*. **40:** 1328-1335.

Hu Y, Smith DE, Ma K, Jappar D, Thomas W and Hillgren KM (2008) Targeted disruption of peptide transporter Pept1 gene in mice significantly reduces dipeptide absorption in intestine. *Mol Pharm*. **5:** 1122-1130.

Hu Y, Xie Y, Wang Y, Chen X and Smith DE (2014) Development and Characterization of a Novel Mouse Line Humanized for the Intestinal Peptide Transporter PEPT1. *Mol Pharm*. 10.1021/mp500497p

Jappar D, Wu SP, Hu Y and Smith DE (2010) Significance and regional dependency of peptide transporter (PEPT) 1 in the intestinal permeability of glycylsarcosine: in situ single-pass perfusion studies in wild-type and Pept1 knockout mice. *Drug Metab Dispos*. **38:** 1740-1746.

Johnson DA and Amidon GL (1988) Determination of intrinsic membrane transport parameters from perfused intestine experiments: a boundary layer approach to estimating the aqueous and unbiased membrane permeabilities. *J Theor Biol*. **131:** 93-106.

Komiya I, Park JY, Kamani A, Ho NFH and Higuchi WI (1980) Quantitative mechanistic studies in simultaneous fluid flow and intestinal absorption using steroids as model solutes. *International Journal of Pharmaceutics*. **4:** 14.

Kou JH, Fleisher D and Amidon GL (1991) Calculation of the aqueous diffusion layer resistance for absorption in a tube: application to intestinal membrane permeability determination. *Pharm Res*. **8:** 298-305.

Merlin D, Si-Tahar M, Sitaraman SV, Eastburn K, Williams I, Liu X, Hediger MA and Madara JL (2001) Colonic epithelial hPepT1 expression occurs in inflammatory bowel disease: transport of bacterial peptides influences expression of MHC class 1 molecules. *Gastroenterology*. **120:** 1666-1679.

Nguyen HT, Dalmasso G, Powell KR, Yan Y, Bhatt S, Kalman D, Sitaraman SV and Merlin D (2009) Pathogenic bacteria induce colonic PepT1 expression: an

implication in host defense response. *Gastroenterology*. **137:** 1435-1447 e1431-1432.

Posada MM and Smith DE (2013a) In vivo absorption and disposition of cefadroxil after escalating oral doses in wild-type and PepT1 knockout mice. *Pharm Res*. **30:** 2931-2939.

Posada MM and Smith DE (2013b) Relevance of PepT1 in the intestinal permeability and oral absorption of cefadroxil. *Pharm Res*. **30:** 1017-1025.

Shen H, Smith DE and Brosius FC, 3rd (2001) Developmental expression of PEPT1 and PEPT2 in rat small intestine, colon, and kidney. *Pediatr Res*. **49:** 789-795.

Wuensch T, Schulz S, Ullrich S, Lill N, Stelzl T, Rubio-Aliaga I, Loh G, Chamaillard M, Haller D and Daniel H (2013) The peptide transporter PEPT1 is expressed in distal colon in rodents and humans and contributes to water absorption. *Am J Physiol Gastrointest Liver Physiol*. **305:** G66-73.

Yang B, Hu Y and Smith DE (2013a) Impact of peptide transporter 1 on the intestinal absorption and pharmacokinetics of valacyclovir after oral dose escalation in wild-type and PepT1 knockout mice. *Drug Metab Dispos*. **41:** 1867-1874.

Yang B and Smith DE (2013b) Significance of peptide transporter 1 in the intestinal permeability of valacyclovir in wild-type and PepT1 knockout mice. *Drug Metab Dispos*. **41:** 608-614.

Zhang Y, Sun J, Sun Y, Wang Y and He Z (2013) Prodrug design targeting intestinal PepT1 for improved oral absorption: design and performance. *Curr Drug Metab*. **14:** 675-687.

Ziegler TR, Fernandez-Estivariz C, Gu LH, Bazargan N, Umeakunne K, Wallace TM, Diaz EE, Rosado KE, Pascal RR, Galloway JR, Wilcox JN and Leader LM (2002) Distribution of the H+/peptide transporter PepT1 in human intestine: up-regulated expression in the colonic mucosa of patients with short-bowel syndrome. *Am J Clin Nutr*. **75:** 922-930.

CHAPTER V

APPLICATION OF HUMANIZED huPEPT1 MOUSE MODEL TO EVALUATE THE ABSORPTION AND DISPOSITION KINETICS OF CEFADROXIL

ABSTRACT

Purpose

Cefadroxil, a first generation β-lactam antibiotic, has high oral bioavailability, good stability in the gastrointestinal tract, and > 90% recovery in urine over 24 hours after oral administration. However, the absorption kinetics of cefadroxil was shown to be saturable with escalating oral doses in humans, a finding that conflicted with other studies in mice. This cross-species discrepancy was attributed to the intestinal transporter PepT1, which is responsible for uptake of cefadroxil from the intestinal lumen. In this study, the *in situ* intestinal permeability and *in vivo* absorption and disposition kinetics of cefadroxil were evaluated in humanized huPepT1 mice as compared to wildtype animals.

Methods

The transport kinetics of cefadroxil was evaluated in humanized huPepT1,

mPepT1 knockout and wildtype mice by *in situ* single-pass intestinal perfusion studies, and by *in vivo* intravenous and oral pharmacokinetic studies in humanized and wildtype mice. Non-compartmental analyses were used to determine the absorption and disposition pharmacokinetic parameters of cefadroxil in mice.

Results

During *in situ* regional perfusion studies, the permeability of cefadroxil was substantial but lower in the duodenum, jejunum and ileum of humanized huPepT1 than in wildtype mice. In contrast, the permeability of cefadroxil was reduced by 95% (or more) in mPepT1 knockout mice as compared to wildtype mice. It was also observed that colonic permeability of cefadroxil in humanized huPepT1 mice was 14-fold higher than in wildtype mice, where permeability was quite low. Specificity studies in wildtype jejunum, using excess concentrations of potential inhibitors, demonstrated that the transport of cefadroxil was highly, if not solely, dependent on the functional activity of PepT1. Moreover, concentration-dependent studies in jejunum indicated that human hPepT1 had a greater affinity for cefadroxil (K_m = 2.7 mM) than did mouse mPepT1 (K_m = 6.0 mM). The disposition kinetics of cefadroxil was evaluated after intravenous bolus doses. The plasma concentration-time profiles of cefadroxil were found to be virtually superimposable between humanized huPpeT1 and wildtype mice at both low and high doses. Pharmacokinetic analyses indicated that the humanized and wildtype mice had similar disposition parameters with no significant differences in CL, V_{ss} and $T_{1/2}$. However, several differences were observed after oral dose escalation

of cefadroxil such that: 1) the plasma concentration-time profiles of cefadroxil were lower in humanized huPepT1 mice than in wildtype animals, 2) the T_{max} and C_{max} values of cefadroxil were 2-fold lower in humanized than in wildtype mice, but no difference was observed in $T_{1/2}$, 3) the partial accumulative AUC or C_{max} vs. Dose relationship of cefadroxil was less than proportional (nonlinear) for humanized mice, but proportional (linear) for wildtype mice, 4) the absorption rate of cefadroxil was slower in humanized mice as compared to wildtype mice, and 5) the $AUC_{0\text{-}120}$ or C_{max} vs. Dose curve was more similar for humanized huPepT1 mice and humans than for wildtype mice and humans.

Conclusion

In this present study, the *in situ* jejunal perfusions revealed a clear species difference between wildtype and humanized huPepT1 mice in the maximal flux and affinity of cefadroxil. Oral dose escalations confirmed that species differences existed *in vivo* in the absorption rate and PepT1-mediated saturable uptake of cefadroxil from the intestinal lumen. Moreover, the AUC or C_{max} vs. Dose relationships were more similar for humanized huPepT1 mice and humans than for wildtype mice and humans. As a result, it appears that humanized huPepT1 mice might provide a valuable animal model in the drug discovery process, as well as to predict the pharmacokinetic profiles of PepT1 substrates in humans.

INTRODUCTION

Cefadroxil, (6R, 7R)-7-[[D-2-amino-2-(4-hydroxyphenyl) acetyl]amino]-3-methyl-8-oxo-5-thia-l-anabicyclo[4.2.0]oct-2-ene-2-carboxylic acid, is a first generation aminocephalosporin with a molecular formula of $C_{16}H_{17}N_3O_5S$ and a molecular weight of 363.39. Because of good patient compliance (Pfeffer et al., 1977), a long-acting effect, high solubility and relatively broad spectrum of anti-bacterial activity, including most gram-positive and negative bacteria (Tanrisever et al., 1986, Yu et al., 1995), cefadroxil is used to treat urinary tract infections (Hausman 1980), skin and soft tissue infections (Ballantyne 1982, Cordero 1976), pharyngitis (Beisel 1980, Randolph 1988) and tonsillitis (Kaminszczik 1986). By binding to trans-peptidase enzymes, penicillin binding proteins (PBPs) (Williamson et al., 1980), cefadroxil can inhibit the cross-linking of peptidoglycan in the synthesis of the bacterial wall, which leads to bacterial autolysis (Goodman et al., 2011).

Compared to cephalexin, cefadroxil has higher serum concentrations after oral administration of an equivalent dose (Buck et al., 1977, Hartstein et al., 1977, Pfeffer, et al. 1977). Cefadroxil also has low plasma protein binding (about 20%) and good oral bioavailability of 90% or more (Garcia-Carbonell et al., 1993, Santella et al., 1982). Cefadroxil is more likely to exhibit saturable secretion by

the kidney and, as a result, has a longer serum half-life (~90 min) than cephalexin (~60 min). Normally, renal excretion is the primary route for the elimination of orally administered cefadroxil, with more than 90% of drug being excreted unchanged in the over 24 hours (Garrigues et al., 1991, Santella, et al. 1982).

As mentioned previously, cefadroxil exhibited a non-proportional increase in area under the plasma concentration-time curve (AUC) with increasing oral doses in humans and rats (Garcia-Carbonell, et al. 1993, Garrigues, et al. 1991, Sanchez-Pico et al., 1989). This finding suggested that membrane transporters might affect dose-dependent changes in the intestinal absorption and systemic disposition of cefadroxil. In particular, influx transporters located in the small intestine may contribute to the high oral bioavailability of cefadroxil (Ries et al., 1994, Wang et al., 1992). Further studies demonstrated that cefadroxil is a substrate of the intestinal peptide transporter PepT1, which is responsibility for the drug's uptake across the apical membrane of small intestine (Ganapathy et al., 1995, Naruhashi et al., 2002, Posada et al., 2013b); in kidney, PepT2 is primarily if not solely responsible for the tubular reabsorption of cefadroxil (Ocheltree et al., 2004); and in brain, PepT2 removes cefadroxil from cerebrospinal fluid (CSF) and into the choroid plexus (Chen et al., 2014, Shen et al., 2005, Shen et al., 2007). Cefadroxil has also been shown to be a substrate of SLC22 family transporters, including SLC22A6 (OAT1), SLC22A7 (OAT2) and SLC22A8 (OAT3), which are localized on the basolateral side of intestinal epithelia cells or renal proximal tubule (Khamdang et al., 2003, Khamdang et al.,

2002, Takeda et al., 2002). More recently, cefadroxil was shown to be transported by rat intestinal ABCC3 (MRP3) and ABCC4 (MRP4) transporters for efflux across the basolateral membrane into the systemic circulation (de Waart et al., 2012), which may partially contribute to its high oral bioavailability.

Our laboratory first evaluated the difference in dipeptide affinity across species by studying the PepT1-mediated uptake of GlySar in yeast cells expressing human, rat and mouse PepT1 cDNA (Hu et al., 2012). Our laboratory also reported the impact of PepT1 ablation on the absorption kinetics after oral dose escalation of cefadroxil (Posada et al., 2013a) and valacyclovir (Yang et al., 2013) in wildtype and mPepT1 knockout mice, and how these results differed from oral pharmacokinetic studies in humans (Garrigues, et al. 1991; Weller et al., 1993). Moreover, species differences in PepT1 transporter permeability was evaluated with GlySar using mouse jejunal perfusion studies in humanized mice as compared to wildtype animals (see Chapter IV and Hu et al., 2014). These findings clearly demonstrated that a species difference exists in the absorption and disposition of drugs by human, mouse and rat PepT1.

In the present study, the permeability of cefadroxil was assessed, for the first time, in humanized huPepT1 and wildtype mice using *in situ* perfusion studies, along with the specificity of PepT1 transporter-mediated transport of drug. Furthermore, the *in vivo* pharmacokinetics of cefadroxil was evaluated by intravenous injection at low (11.01 nmol/g) and high doses (528.40 nmol/g), and after oral dose escalation (11.01, 33.03, 66.06, 132.10, 264.20 and 528.40 nmol/g).

MATERIALS AND METHODS

Chemicals

[^{3}H]cefadroxil (98 mCi/mmol) and [^{14}C]inulin 5000 (1.1 mCi/g) were purchased from Moravek Biochemicals and Radiochemicals (Brea, CA). Unlabeled cefadroxil, inulin, glycylproline (GlyPro), glycylsarcosine (GlySar), glycine, L-histidine, para-aminohippuric acid (PAH), tetraethylammonium (TEA), quinidine, N^{1}-methylnicotinamide (NMN), carnosine, cephalexin, cephalothin, and dimethylamiloride (DMA) were purchased from Sigma-Aldrich (St. Louis, MO). Cytosine Ecolite and hyamine hydroxide were purchased from MP Biochemicals, (Solon, OH). All other chemicals were acquired from standard sources.

Animals

In-house breeding of gender- and weight-matched, 8-10 week, mPepT1$^{+/+}$ (wildtype, WT), mPepT1$^{-/-}$/hPepT1$^{-/-}$ (mPepT1 knockout, KO) and humanized mPepT1$^{-/-}$/hPepT1$^{+/-}$ (humanized hPepT1, HU] mice, on a C57BL/6 background, were used for all experiments unless otherwise noted. The KO and HU mice were identified by genotyping and culled from the same litter. The mice were housed in a temperature-controlled environment with 12 hr light and 12 hr dark cycles, and received a standard diet and water *ad libitum* (Unit for Laboratory Animal Medicine, University of Michigan, Ann Arbor, MI). All mouse studies were

performed in accordance with the Guide for the Care and Use of Laboratory Animals as adopted and promulgated by the U.S. National Institutes of Health (Institute of Laboratory Animal Sources, 1996).

In Situ Single-Pass Intestinal Perfusion Studies

Humanized huPepT1, mPepT1 knockout and wildtype mice were fasted overnight (~12 hr) with free access to water and then anesthetized with sodium pentobarbital (40-60mg/kg ip). Perfusion studies of jejunum or other regional segments were carried out according to methods described previously (Adachi et al., 2003, Jappar et al., 2010). In brief, after sterilizing the abdominal area with 70% ethanol, and keeping the mice on top of a heating pad to maintain body temperature, the intestines were exposed by a mid-line incision of the abdomen. A 4-cm segment of duodenum, 8-cm segment of proximal jejunum (i.e. ~2 cm distal to the ligament of Treitz), 6-cm segment of ileum (i.e. ~1 cm proximal to the cecum), and 4-cm segment of colon (i.e. ~0.5 cm distal to the cecum) was isolated and incisions then made at both the proximal and distal ends. The segments were rinsed with 0.9% isotonic saline solution and a glass cannula (2.0 mm outer diameter) inserted at each end of the intestinal segment, and secured in place with silk sutures. The isolated intestinal segment(s) were covered with saline-wetted gauze and parafilm to prevent dehydration. After cannulation, the animals were transferred to a temperature-controlled chamber, at 31^{o}C, to maintain body temperature during the entire perfusion procedure. The cannulas were then connected to inlet tubing, which was attached to a 10-mL syringe (BD,

Franklin Lakes, NJ USA) placed on a perfusion pump (Model 22: Harvard Apparatus, South Natick, MA), and to outlet tubing, which was placed in a collection vial.

The perfusate buffer contained 135 mM NaCl, 5 mM KCl and 10 mM MES/Tris (pH6.5) plus 10 μM of [^{3}H]cefadroxil (0.5 μCi) and 0.01% (w/v) [^{14}C]-inulin (0.25 μCi) (which served as a nonabsorbable marker to correct for water flux) during the intestinal perfusion studies. The buffer was perfused through the intestinal segments at a flow rate of 0.1 mL/min, and the exiting perfusate was collected every 10 min for 90 min. A 100-μL aliquot of each perfusate collection was added to a vial containing 6.0 mL of scintillation cocktail (Cytosine, Ecolite MP Biochemicals, Solon, OH), and the samples were measured for radioactivity by a dual-channel liquid scintillation counter (Beckman LS 6000 SC, Beckman Coulter Inc., Fullerton, CA). At the end of experimentation, the actual length of intestinal segments was measured.

For the inhibition studies in jejunum, 10 mM of potential inhibitors were added to the perfusate, except for DMA (0.1 mM). For the concentration-dependent studies in jejunum, cefadroxil varied from 0.01-25 mM in perfusate buffer containing [^{3}H]cefadroxil (0.5 μCi) and 0.01% (w/v) [^{14}C]inulin (0.25 μCi).

In Vivo Intravenous Pharmacokinetic Studies

Humanized huPepT1, mPepT1 knockout and wildtype mice were anesthetized with (40-60 mg/kg ip) sodium pentobarbital before intravenous bolus injection of [^{3}H]cefadroxil (11.01 and 528.40 nmol/g body weight, 5.0 μCi/each) in 100 μL of saline. After dosing, serial blood samples were collected

at 1, 2.5, 5, 10, 20, 30, 45, 60, 90 and 120 min via tail transections. Blood samples (15-20 μL) were harvested into a tube containing 1.0 μL of EDTA-K3 and centrifuged for 3 min x 3000 g to obtain the plasma (10 μL). A 30-μL aliquot of 30% H_2O_2 was then added, followed by 6.0 mL of Cytosine scintillation cocktail and 20 μL of 0.5 M acetic acid. Animals were returned to their cages in between blood samplings, where they had free access to water and food. Radioactivity in the plasma samples was measured by a dual-channel liquid scintillation counter (Beckman LS 6000 SC, Beckman Coulter Inc., Fullerton, CA).

For the biodistribution studies, 0.2 μCi of [^{14}C]inulin in 100 μL of saline was injected intravenously 2.0 min prior to 120 min, the time at which tissue samples was harvested. The tissues, including a blood sample, were weighed and 300 μL of hyamine hydroxide was then added and incubated at 37^{o}C until the entire tissue was dissolved. After the samples cooled down to room temperature, 30 μL of 30% H_2O_2 was added, followed by 6.0 mL of Cytosine scintillation cocktail and 20 μL of 0.5 M acetic acid. Radioactivity in these samples was measured by a dual-channel liquid scintillation counter (Beckman LS 6000 SC, Beckman Coulter Inc., Fullerton, CA). The cefadroxil tissue-to-plasma concentration ratios were also calculated at 120 min.

In Vivo Oral Pharmacokinetic Studies

Following an overnight fast (~12 hr), humanized huPepT1, mPepT1 knockout and wildtype mice were anesthetized briefly with isoflurane prior to oral administration of [^{3}H]cefadroxil (11.01, 33.03, 66.06, 132.10, 264.20, 528.40 nmol/g, 10 μCi/each) by gastric lavage (oral) in 200 μL of saline. After oral

dosing, serial blood samples were collected at 2.5, 5, 10, 20, 30, 45, 60, 90 and 120 min via tail transections. Animals were returned to their cages in between blood sampling where they had free access to water and, 2 hr later, to food. Blood samples (15-20 μL) were harvested into a tube containing 1.0 μL of EDTA-K3 and centrifuged for 3 min x 3000 g to obtain plasma (10 μL). A 30-μL aliquot of 30% H_2O_2 was then added, followed by 6.0 mL of Cytosine scintillation cocktail and 20 μL of 0.5 M acetic acid. Radioactivity in the plasma samples was measured by a dual-channel liquid scintillation counter (Beckman LS 6000 SC, Beckman Coulter Inc., Fullerton, CA).

Urinary Recovery of Cefadroxil

Following an overnight fast, humanized huPepT1 and wildtype mice were briefly anesthetized with isoflurane, and then administered 200 μL [^{3}H]cefadroxil (5.0 μCi) by oral gavage at doses of 11.01 nmol/g and 528.40 nmol/g. A 100-μL aliquot of [^{14}C]inulin-5000 (0.5 μCi) was also administered by tail vein injection to evaluate the accuracy of urine collections. Each animal was placed in a metabolic cage containing a diuresis adapter (Nalge Nunc International, Naperville, IL), and the urine and feces collected 24 hours after dosing. After the feces were removed, the metabolic cage was washed with water three times and then added to the urine collection. A 100-μL aliquot of the diluted fecal and urine samples were added into scintillation vials containing 6 mL of Cytoscint cocktail, and the radioactivity measured by a dual-channel liquid scintillation counter (Beckman LS 6000 SC, Beckman Coulter Inc., Fullerton, CA).

Data Analysis

Steady-state loss of drug from perfusate in the intestinal segment was achieved approximately 30 min after the start of perfusion. The effective permeability (P_{eff}) of drug was calculated according to a complete radial mixing (parallel tube) model (Komiya et al., 1980, Kou et al., 1991) as:

$$P_{eff} = \frac{-Q \bullet \ln(C_{out} / C_{in})}{2\pi RL} \quad (1)$$

where Q was the perfusion flow rate (0.1 mL/min), C_{out} the outlet drug concentration after correction for changes in water flux, C_{in} the inlet drug concentration, R the internal radius (0.1 cm for small intestine and 0.2 cm for colon), and L the length of intestinal segment. Water flux across the epithelium was calculated as (Amidon et al., 1988, Johnson et al., 1988):

$$C_{out} = \frac{C_{out,uncorr} \bullet I_{in}}{I_{out}} \quad (2)$$

where $C_{out,uncorr}$ was the original (uncorrected) outlet drug concentration, I_{in} the inulin-5000 inlet concentration, and I_{out} the inulin-5000 outlet concentration.

The intrinsic or wall permeability (P_w) is referenced to intestinal wall concentrations and determined by factoring out the aqueous layer permeability (P_{aq}) using the formula:

$$P_w = \frac{P_{eff}}{1 - P_{eff} / P_{aq}} \quad (3)$$

The boundary layer approach can be used to estimate the aqueous permeability according to:

$$P_{aq} = (A\frac{R}{D}Gz^{1/3})^{-1} \quad (4)$$

$$Gz = \frac{\pi DL}{2Q} \tag{5}$$

where *A* is a unitless constant (see below for calculation), *R* the radius, *D* the diffusion coefficient in water (3.82 x 10^{-4} cm^2/min), and G_z the Graetz number (0.0829). Once the Graetz number was calculated, *A* was estimated as:

A = 2.50 Gz + 1.125 (when Gz ≥ 0.030)

A = 4.50 Gz + 1.065 (when 0.030 > Gz ≥ 0.010)

A = 10.0 Gz + 1.010 (when 0.010 > Gz ≥ 0.004)

Given these relationships, the concentration of drug at the membrane surface (C_w) was calculated as:

$$C_w = C_{in}(1 - \frac{P_{eff}}{P_{aq}}) \tag{6}$$

The intrinsic parameters J_{max} (maximum transport rate) and K_m (Michaelis constant) were determined using the following equation:

$$P_w = \frac{J_{\max}}{K_m + C_w} + P_m \tag{7}$$

where P_m is the passive (nonsaturable) permeability. The carrier permeability (P_c) was calculated as:

$$P_c = \frac{J_{\max}}{K_m} \tag{8}$$

The steady-state flux (J) can also be referenced to intestinal wall concentrations (C_w) and the intrinsic kinetic parameters expressed as:

$$J = \frac{J_{\max} \bullet C_w}{K_m + C_w} + P_m C_w = P_{eff} \bullet C_{in} \tag{9}$$

The apparent kinetic parameters can also be determined by the following:

$$P_{eff} = \frac{J^*_{\max}}{K^*_m + C_{in}} + P^*_m \tag{10}$$

and the flux calculated as:

$$J = \frac{J^*_{\max} \bullet C_{in}}{K^*_m + C_{in}} + P^*_m \bullet C_{in} \tag{11}$$

The concentration-dependent flux (J) of cefadroxil in jejunum was best fit to a single Michaelis-Menten term as:

$$J = P_{eff} \bullet C_{in} = \frac{J^*_{\max} \bullet C_{in}}{K^*_m + C_{in}} = \frac{J_{\max} \bullet C_w}{K_m + C_w} \tag{12}$$

where the parameters J^*_{max} and K^*_m were referenced to inlet drug concentrations (C_{in}), and the parameters J_{max} and K_m were referenced to intestinal wall drug concentrations (C_w), once corrected for the unstirred aqueous layer permeability.

The body surface area (BSA) of mice was calculated by:

$$BSA_{mice} = \left(\frac{Body\ Weight_{mice}(kg)}{Body\ Weight_{humans}(kg)}\right)^{0.75} * BSA_{humans}$$

where the body weight of humans was 70 kg, the BSA_{humans} was 1.8 m^2.

Data were reported as mean ± SE, unless otherwise noted. Statistical differences between two groups were determined using an unpaired t-test. Multiple treatment groups were compared using one-way analysis of variance (ANOVA) followed by either a Tukey's test or Dunnett's test, with wildtype serving as the control group (GraphPad Prism 5.0; GraphPad software, Inc., La Jolla, CA). $P \leq 0.05$ was considered significant. Pharmacokinetics analyses were carried out using a non-compartmental model (NCA) in Phoenix WinNonlin 6.3 (Certara, St. Louis, MO USA).

RESULTS

Concentration-Dependent *In Situ* Transport Kinetics of Cefadroxil in Jejunum of Humanized huPepT1 and Wildtype Mice

The J_{max} and K_m of GlySar for the PepT1 transporter were previously shown to be much lower in humanized mice than in wildtype animals during *in situ* jejunal perfusions (Figure 4.2, Chapter IV). Therefore, we believed that the transport kinetics of cefadroxil would also be significantly lower in humanized huPepT1 mice than in wildtype mice during these single-pass perfusion studies. As shown in Figure 5.1, both genotypes demonstrated a saturable transport of cefadroxil. When referenced to cefadroxil inlet concentrations (C_{in}), the maximal flux J^*_{max}=0.380 nmol/cm^2/sec for wildtype vs. 0.057 nmol/cm^2/sec for humanized mice, and the Michaelis constant K^*_m =6.01 mM for wildtype vs. 2.69 mM for humanized mice (Figure 5.1A). When referenced to cefadroxil wall concentrations (C_w), the maximal flux J_{max}=0.392 nmol/cm^2/sec for wildtype vs. 0.056 nmol/cm^2/sec for humanized mice, and the Michaelis constant K_m=4.80 mM for wildtype vs. 2.37 mM for humanized mice (Figure 5.1B). Thus, the affinity of cefadroxil for PepT1 in humanized mice was higher (i.e., lower K_m) than that of wildtype mice.

In Situ Transport Kinetics of Cefadroxil in Regional Intestinal Segments of Humanized huPepT1 and Wildtype Mice

Given a K_m for cefadroxil on the order of 2.4-6.0 mM, subsequent studies were performed at 10 μM cefadroxil to maintain conditions of transport linearity. Based on the GlySar results (Chapter IV), we hypothesized that the permeability of cefadroxil would be significantly lower in all regions of small intestine, and significantly higher in the colon, of humanized huPepT1 mice as compared to wildtype animals during the intestinal perfusions. As shown in Figure 5.2, the permeability of cefadroxil was considerable in duodenum, jejunum and ileum of wildtype and humanized mice, although it was 50-60% lower in humanized mice. In contrast, the permeability of cefadroxil in mPepT1 knockout mice was minimal, with a residual permeability of 5% or less as compared to wildtype animals. Still, the permeability of cefadroxil in the colon of humanized mice was measurable and 14-fold higher than that of wildtype mice.

Substrate Specificity of hPepT1 in Humanized Mouse Jejunum by *In Situ* Perfusion Studies

In the presence of excess concentrations of potential inhibitors, the permeability of cefadroxil was reduced 90% by GlyPro, 80% by GlyGlyHis and about 60% by carnosine or cephalexin during jejunal perfusion studies in humanized huPepT1 mice (Figure 5.3). In contrast, amino acid inhibitors (glycine and L-histidine), OAT inhibitors (probenecid and PAH), OCT inhibitors (TEA, quinidine and NMN), and cephalosporins lacking a α-amino group (cephalothin) had no effect on the jejunal permeability of cefadroxil in humanized huPepT1

mice. However, DMA, an inhibitor of the sodium-proton exchanger, was able to reduce the permeability of cefadroxil by 50% as compared to the control group.

In Vivo Pharmacokinetic Studies Following Intravenous Bolus Doses of Cefadroxil

Humanized huPepT1 mice were evaluated following single intravenous doses of [^{3}H]cefadroxil at 11.01 nmol/g and 528.40 nmol/g (5 μCi). As shown in Figure 5.4, the plasma concentration-time profiles of cefadroxil were virtually superimposable between genotypes for each dose. Non-compartmental analyses indicated that both wildtype and humanized mice had similar pharmacokinetic parameters, including CL, V_{ss} and $T_{1/2}$ (Table 5.1). In fact, no significant differences in pharmacokinetics were observed between humanized huPepT1 mice and wildtype animals for either dose. Furthermore, two-way ANOVA showed no significant differences with respect to dose or genotype. As shown in Figure 5.5, no significant differences were found between humanized huPepT1 and wildtype mice in any of the tissues studied.

In Vivo Pharmacokinetic Studies Following Oral Dose Escalation Dose of Cefadroxil

The *in vivo* functional activity of PepT1 was evaluated in humanized and wildtype mice after increasing oral doses of cefadroxil. Mouse dose were scaled from human doses (250-2000 mg for adults) by body surface area, and produced similar concentrations of cefadroxil in the stomach as well as systemic circulation. As shown in Figure 5.6, the plasma concentrations of cefadroxil were

much lower in humanized mice than in wildtype animals for all doses (11.01, 33.03, 66.06, 132.10, 264.20, 528.40 nmol/g). According to non-compartmental analyses (Table 5.2), area under the plasma concentration-time curve (AUC) and peak plasma concentrations (C_{max}) of cefadroxil were about 2-fold lower in humanized mice than in wildtype mice, and the time to reach peak concentrations (T_{max}) about 2-fold longer in humanized mice. However, the terminal half-life ($T_{1/2}$) was not significantly different between humanized and wildtype mice, which agreed with the results following single intravenous doses.

Bioavailability of Cefadroxil in Humanized and Wildtype Mice

Mass balance studies of [^{3}H]cefadroxil were performed in wildtype and humanized huPepT1 mice using a metabolic cage studies. As shown in Table 5.7, the bioavailability (F) of radiolabelled cefadroxil was 83.8 % and 82.4% in wildtype mice, and 82.1% and 81.7% in humanized huPepT1 mice, respectively, after the 11.01 nmol/g and 528.40 nmol/g oral doses of drug. However, the bioavailability (F) of cefadroxil, calculated from plasma data, was 82.6% and 105.0% for wildtype mice, but only 47.1% and 52.7% for humanized huPepT1 mice, after these same oral doses of 11.01 nmol/g and 528.40 nmol/g (Table 5.8).

Evaluation of Partial AUC versus Time or Dose for Comparison of Cefadroxil Absorption Kinetics between Humanized and Wildtype Mice

The rate of drug absorption was evaluated by comparing the partial AUC-time curves of cefadroxil from 5 to 30 min. As shown in Figure 5.7 and Table 5.3, the slopes of cefadroxil for all 6 oral doses were about 2-fold steeper in wildtype

mice than in humanized mice, indicating a greater absorption rate of cefadroxil in these animals. Because of the higher affinity of cefadroxil for human over mouse PepT1, as determined by *in situ* perfusion studies, the oral absorption of cefadroxil was more likely to be saturated in humanized mice than in wildtype animals. As shown in Figure 5.8 and Table 5.4, a nonlinear relationship was observed for the partial cumulative AUC vs. dose profiles of cefadroxil in humanized huPepT1 but not wildtype mice during oral dose escalation studies. In fact, values of $AUC_{0\text{-}120}$ vs. Dose (body surface area-normalized) for cefadroxil were strikingly similar between the humanized huPepT1 mice and human values obtained from the literature (Garrigues et al, 1991) (Figure 5.9 and Table 5.5). A similar relationship for cefadroxil's C_{max} was also observed in Figure 5.10 and Table 5.6, where the C_{max} vs. Dose (body surface area-normalized) curves were linear for wildtype, but nonlinear and strikingly close for humanized huPepT1 mice and human values obtained from the literature (Garrigues et al, 1991). Taken as a whole, it appears that humanized huPepT1 mice are a good model to predict the oral absorption and disposition of cefadroxil in humans.

DISCUSSION

In the present study, the effective permeability of cefadroxil during *in situ* single-pass intestinal perfusions, and pharmacokinetics of cefadroxil following intravenous and oral dosing were examined in humanized huPepT1 and wildtype mice. From these experiments, we made the following observations:

1) the *in situ* permeability pattern of cefadroxil in small intestine was comparable, but smaller, in huPepT1 mice as compared wildtype mice. However, the colonic permeability of cefadroxil was measurable and higher in humanized huPepT1 animals.

2) a species difference was found in the *in situ* PepT1-mediated kinetics of cefadroxil in jejunum, in which the J_{max} and K_m of drug were significantly lower in humanized huPepT1 mice as compared to wildtype animals.

3) inhibition studies showed that cefadroxil uptake from the intestinal lumen depended primarily upon PepT1 functional activity, which was influenced by the proton gradient.

4) After intravenous dosing of cefadroxil (11.01 and 528.40 nmol/g), the plasma concentration-time profiles were virtually superimposable between humanized hPepT1 and wildtype mice. No significant differences were observed between genotypes in the disposition parameters (e.g., CL and V_{ss}) of cefadroxil, or pattern of tissue distribution.

5) after oral dose escalation of cefadroxil (11.01, 33.03, 66.06, 132.10, 264.20 and 528.40 nmol/g), non-compartmental analyses demonstrated that the C_{max}, T_{max} and AUC of drug were lower in humanized huPepT1 mice (Hemizygotes) than that in wildtype animals. Moreover, the partial AUC-Dose and C_{max}-Dose profiles of cefadroxil indicated a nonlinear relationship for humanized huPepT1 mice but not for wildtype mice.

6) the slope of partial AUC-Time curves indicated that the rate and extent of absorption for cefadroxil were significantly lower in humanized huPepT1 mice than in wildtype animals.

7) the C_{max}-Dose and AUC_{120}-Dose profiles of cefadroxil were similar between human subjects and humanized huPepT1, as compared to human subjects and wildtype mice, indicating that the humanized huPepT1 mouse model might be preferred for translating the intestinal absorption and systemic exposure of orally administered drugs to humans.

The interpretation of our observations depends upon the faithful expression and functional activity of PepT1 in the small and large intestines, and the initial stomach concentrations of cefadroxil after the escalating oral doses. PepT1 is considered a high-capacity, low-affinity transporter with K_m values ranging from 0.2 to 10 mM (Brandsch et al., 2008, Rubio-Aliaga et al., 2002, Rubio-Aliaga et al., 2008). During our *in situ* jejunal perfusion studies, the affinity of cefadroxil was two-fold higher in humanized mice (K_m=2.7 mM) than in wildtype animals (K_m=6.0 mM). These values are similar to the K_m of 2-4 mM during jejunal perfusions in wildtype mice (Posada, et al. 2013b), and to the Km of 5.9 mM (Sinko et al., 1988) and 6.6 mM (Sanchez-Pico, et al. 1989) during small intestinal perfusions of cefadroxil in rat.

The cefadroxil permeability of $0.80x10^{-4}$ cm/s, as reported by Posada et al (2013b), was similar to our permeability estimate of $0.62x10^{-4}$ cm/s in wildtype mice, but larger than the $0.17x10^{-4}$ cm/s estimate in humanized mice during *in situ* jejunal perfusions. The intestinal permeability of cefadroxil in humans,

however, is currently not available. Still, the permeability of cephalexin (another PepT1 substrate) was $1.56x10^{-4}$ cm/s in human jejunum (Cao et al., 2006, Lennernas 2007, Zakeri-Milani et al., 2007). Even though both compounds are from the same class of orally administered aminocephalosporin drugs, they do have different chemical structures that could impart different affinities between species and, as a result, have different permeability in the small intestine. Different substrate affinities for a particular transporter, along with different expression patterns of transporters (and enzymes), can account for differences in drug absorption and bioavailability between rodents and humans (Cao, et al. 2006).

During our *in situ* perfusion studies, the permeability of cefadroxil was two-fold larger in the small intestine (duodenal, jejunal and ileal segments) of wildtype vs. humanized mice, but lower in the colon of wildtype vs. humanized huPepT1 animals (Figure 5.2). These results are in agreement with the protein expression pattern of PepT1 in the small and large intestines of these two genotypes. Similar differences in intestinal permeability were reported previously by our group for GlySar in humanized huPepT1 and wildtype mice (Hu et al., 2014) and for cefadroxil in wildtype and mPepT1 knockout mice during *in situ* perfusion studies (Posada, et al. 2013b). Given these species differences, it was hypothesized that the *in vivo* oral absorption and systemic availability of cefadroxil would differ between humanized huPepT1 and wildtype mice.

Our laboratory has previously performed a number of substrate specificity studies for PepT1, using a wide range of potential inhibitors, during *in situ*

perfusion studies (Jappar, et al. 2010, Ma et al., 2011, Posada, et al. 2013b). Cefadroxil can be transported by both SLC and ABC family members. Using excess concentrations of potential inhibitors, the jejunal permeability of cefadroxil was significantly reduced by GlyPro, GlyGlyHis, carnosine and cephalexin, indicating that the uptake of cefadroxil from intestinal lumen was mainly mediated by PepT1 transporters. This observation was supported by a study demonstrating that PepT1 protein accounted for about 50% of all relevant transporters in human small intestine (Drozdzik et al., 2014), and that ABCC3 protein, which is responsible for cellular efflux of cefadroxil across the basolateral membrane, accounted for only 7% of all relevant transporters in this region. Even though PhT1, another POT transporter, was reported in chicken intestine (Zwarycz et al., 2013) and mouse intestine (Hu et al., 2008), it has an intracellular localization in which its function is unrelated to the uptake of cefadroxil from the intestinal lumen (Nakamura et al., 2014, Sasawatari et al., 2011). The lack of a PhT1 effect was confirmed in our studies such that the jejunal permeability of cefadroxil was unchanged when perfused with high concentrations of L-histidine (Figure 5.3).

Studies have shown that the impact of pH is limited during *in situ* perfusion studies of cefadroxil when the buffer was changed from 5.0 to 7.4 (Jappar, et al. 2010). This finding probably reflects the fact that the acidic microclimate layer, formed by mucus and sodium/proton exchange at the brush border membrane, is highly resistant to changes by bulk fluid pH in the intestine (Hogerle et al., 1983, Lucas 1983, McKie et al., 1988). Therefore, DMA (dimethyl-amiloride), an

inhibitor of the sodium/proton exchanger (NHE), was used to diminish exchange of Na^+ and H^+ across the brush border membrane within this thin layer. As a result, the permeability of cefadroxil was reduced by 50% in humanized mouse jejunum during co-perfusion with DMA. To rule out other potential transporters, the jejunal permeability of cefadroxil was evaluated by co-perfusing the drug with high concentrations (10 mM) of known OAT (i.e., probenecid and PAH) and OCT transport inhibitors (TEA, quinidine and NMN), as well as the non-aminocephalosporin drug cephalothin. In doing so, no significant difference was observed in the permeability of cefadroxil (Figure 5.3), thereby, ruling out the importance of transporters other than PepT1 in its intestinal uptake. The negligible permeability of cefadroxil in all segments of the small intestine of mPepT1 knockout mice also demonstrated that other transporters have little to no influence on the uptake of cefadroxil from intestinal lumen (Figure 5.2).

After oral administration of cefadroxil, less than proportional increases in AUC and C_{max} were observed in humans (Garrigues, et al. 1991) and rats (Garcia-Carbonell, et al. 1993, Sanchez-Pico, et al. 1989, Wang, et al. 1992) with increasing doses of drug. In contrast, linear oral absorption kinetics were observed in wildtype mice under similar dosing conditions (Posada, et al. 2013a). We also observed a dose-proportional increase of AUC and C_{max} in our oral wildtype mouse studies; however, in our humanized mice a less than proportional increase of AUC and C_{max} was observed after oral escalation dose. Potential reasons for this inter-species discrepancy in the oral pharmacokinetics of cefadroxil might include: 1) a saturable PepT1-mediated intestinal absorption of

drug in humans (or humanized huPepT1 mice) but not in mice, and 2) a saturable OAT-mediated secretion and/or PepT2-mediated reabsorption in the renal tubules of one species and not the other. Regarding the second point, a previous study by our group reported the concentration-dependent saturation of renal tubular secretion by OATs and renal tubular reabsorption by PepT2 for cefadroxil following a range of intravenous doses (Shen, et al. 2007). However, in the present study, the plasma concentration-time profiles of cefadroxil were virtually superimposable in humanized huPepT1 and wildtype mice after either low (11.01 nmol/g) or high (528.40 nmol/g) intravenous doses of drug (Figure 5.4). Thus, no differences were observed in the disposition parameters of cefadroxil between both genotypes and as a function of dose (Table 5.2). Although one cannot totally rule out dose-dependent alterations in the renal tubular secretion and reabsorption of cefadroxil, since equal and opposite changes would result in an “apparent” linear relationship between AUC and dose, this outcome is unlikely. Moreover, the lack of significant changes in transcript levels of PepT2, Oat1/3 and others in kidney (Figure 3.3, Chapter III), and the lack of significant differences between wildtype and humanized huPepT1 mice in cefadroxil tissue distribution (Figure 5.4), would argue against dispositional changes occurring with intravenous dose. Therefore, we concluded that the non-linear relationship between AUC or C_{max} with cefadroxil dose in humanized mice was not caused by changes in disposition, but by saturable intestinal absorption of hPepT1 after oral escalation dose.

A saturable intestinal absorption rate was also considered for cefadroxil by evaluating the partial AUC vs. time profiles of drug after oral dose escalation. In this regard, the plasma concentrations of cefadroxil were about two-fold higher in wildtype than humanized hPepT1 mice during the first 30 min of oral dosing, and the time to reach peak concentration (T_{max}) about two-fold lower in wildtype animals. This would suggest that wildtype mice absorbed drug as twice the rate as compared to humanized huPepT1 mice. Further analysis confirmed this suggestion, where the slopes of partial cumulative AUC vs. time (over 5-30 min) in wildtype mice were double of that in humanized huPepT1 mice (Table 5.3), a method which was proposed as a good way of determining absorption rate, as compared to other methods such as C_{max} and T_{max} (Chen 1992, Chen et al., 2001, Yang, et al. 2013). The ratio of slopes (HU/WT) may also suggest a saturable PepT1 absorption rate since these values were reduced somewhat with increasing dose (i.e., from 0.55 to 0.37).

For the oral escalation dose studies, cefadroxil doses (11.01 to 528.40 nmol/g) were chosen in mice (20 g) so that their initial stomach concentrations would mimic that observed after clinical oral doses of 250 to 2000 mg in humans (70 kg). Thus, given a stomach fluid volume of 0.4 ml for mice (McConnell et al., 2008) and 250 ml for humans (Rowland et al., 2009), the initial stomach concentrations of cefadroxil were similar between species, ranging from 0.55-26.4 mM in mice and from 2.8-22.1 mM in humans. These estimated stomach concentrations were higher than the K_m values of cefadroxil as estimated during the *in situ* jejunal perfusions of wildtype (i.e., 6.0 mM) and humanized huPepT1

mice (i.e., 2.7 mM) (Figure 5.1). However, given the lower K_m value, it is more likely for the humanized mice to show saturable PepT1 intestinal absorption of cefadroxil in vivo than wildtype animals. This contention was confirmed in Figure 5.8, where the AUC from 0-30, 0-60, 0-90 and 0-120 min increased linearly with increasing dose in wildtype mice, a result consistent with our previous reports for cefadroxil (Posada, et al. 2013a) and valacyclovir (Yang, et al. 2013). In contrast, the AUC values (from 0-30, 0-60, 0-90 and 0-120 min) in humanized huPepT1 mice increased less than proportionately with increasing dose, a result consistent with the systemic profiles of cefadroxil after oral dosing in humans (Garrigues, et al. 1991) and rats (Garcia-Carbonell, et al. 1993, Sanchez-Pico, et al. 1989). A similar finding was also observed in comparing the C_{max} vs. oral dose relationship in wildtype and humanized huPepT1 mice (Figure 5.9).

Possible reasons to explain the dose-proportional increase of AUC or C_{max} in wildtype mice might include the following: 1) as cefadroxil travels down from proximal to distal regions of small intestine, the concentration of drug remains below its K_m value, and 2) since AUC=F•Dose/CL, perhaps there are changes in cefadroxil F (bioavailability) and CL (clearance) that are of the same magnitude and direction, thereby, masking dose-dependent changes in AUC. The latter explanation is unlikely, though, since bioavailability did not change as a function of dose. This claim was based on subsequent 24-hr mass balance studies of orally administered cefadroxil, as shown in Table 5.7. In this regard, the bioavailability of cefadroxil in wildtype mice was 83.8% after an 11.01 nmol/g oral dose and 82.1% after a 528.40 nmol/g oral dose. However, a discrepancy in

bioavailability was observed between genotypes when plasma data calculations were compared with mass balance calculations for this parameter (see Tables 5.7 and 5.8). For example, at the 11.01 nmol/g dose, the bioavailability of cefadroxil in humanized huPepT1 mice was only 47.1% when based on plasma data but 82.1% when calculated from mass balance studies. This discrepancy might reflect the fact that different animals were used to determine plasma AUC following the oral and intravenous doses of drug (i.e., not a cross-over design). It is also possible, but unlikely, that substantial cefadroxil still remains in the body after oral dosing in the humanized, but not wildtype, mice such that the extrapolated AUC (i.e., post 2-hr collection) does not account for this effect in calculating the bioavailability parameter.

In concluding, the *in situ* jejunal studies revealed a clear species difference between wildtype and humanized huPepT1 mice in the maximal flux and affinity of cefadroxil. The oral dose escalation studies confirmed that species differences existed *in vivo* in the absorption rate and PepT1-mediated saturable uptake of cefadroxil from the intestinal lumen. Moreover, the AUC or C_{max} vs. Dose relationships were more similar for humanized huPepT1 mice and humans than for wildtype mice and humans. As a result, it appears that humanized huPepT1 mice might provide a valuable animal model in the drug discovery process, as well as to predict the pharmacokinetic profiles of PepT1 substrates in humans.

Table 5.1 Non-compartmental pharmacokinetics of cefadroxil after intravenous bolus dosing in wildtype and humanized huPepT1 mice[a]

Parameters	11.01 nmol/g IV		528.40 nmol/g IV	
	WT	**HU**	**WT**	**HU**
CL (mL/hr)	21.57 ± 1.04	21.63 ± 0.84	25.48 ± 2.63	23.99 ± 1.81
$T_{1/2}$ (min)	51.66 ± 3.41	56.15 ± 1.25	44.13 ± 12.65	72.37 ± 26.80
V_{ss} (mL)	11.99 ± 1.25	11.90 ± 0.70	17.25 ± 5.26	13.37 ± 2.30
MRT (min)	19.55 ± 0.77	18.46 ± 1.30	19.12 ± 0.40	16.91 ± 0.57
$AUC_{0\text{-}120}$ (μM•min)	569 ± 31	564 ± 21	23614 ± 2638	23826 ± 2219
$AUC_{0\text{-}\infty}$ (μM•min)	616 ± 30	613 ± 23	25482 ± 2926	26744 ± 2086
% Extrapolation	7.6	8.0	7.3	10.9

[a] CL: Total clearance of cefadroxil from plasma

$T_{1/2}$: Elimination half-life

V_{ss}: Volume of distribution under steady state conditions based on drug concentration in plasma

$AUC_{0\text{-}t}$: Area under the plasma concentration-time curve from time 0 to t after dosing

MRT: Mean residence time of a molecule within the body

Data are expressed as mean ± SE (n=3-5). No significant differences were observed between wildtype (WT) and humanized huPepT1 (HU) mice in the disposition parameters and as a function of dose, as evaluated by two-way ANOVA (except for differences in AUC between the low and high doses; $p<0.001$).

Table 5.2 Non-compartmental analysis of disposition parameters of [^{3}H]cefadroxil following oral dose escalation in wildtype and humanized mice[a]

Dose (nmol/g)	C_{max} (μM)		T_{max} (min)		$T_{1/2}$ (min)	
	WT	**HU**	**WT**	**HU**	**WT**	**HU**
11.01	14.20±1.12	6.86±1.00***	9.28±1.89	20.71±4.42***	32.13±8.68	32.45±4.03
33.03	36.99±1.34	17.76±3.59***	13.33±2.11	27.5±4.03***	36.31±5.25	38.45±6.56
66.06	96.26±4.27	41.33±7.71***	7.50±1.18	30.00±5.00***	28.00±1.08	33.62±3.07
132.10	185.38±4.40	84.40±11.84***	9.17±0.83	21.67±1.67***	26.06±1.29	28.94±1.10
264.20	382.04±15.93	173.78±15.40***	10.00±0.00	18.33±1.67***	23.98±1.94	27.19±2.36
528.40	636.77±34.59	263.47±34.90***	13.33±2.11	24.28±2.02***	29.82±3.12	31.49±2.71

Dose (nmol/g)	AUC_{0-120} (μM•min)		$AUC_{0-\infty}$ (μM•min)		Extrapolation %	
	WT	**huPepT1**	**WT**	**huPepT1**	**WT**	**huPepT1**
11.01	473±28	263±20***	509±31	289±15***	7.6	9.8
33.03	1605±86	793±116***	1785±133	887±110***	11.2	11.8
66.06	2823±299	2223±197***	2979±337	2468±185***	5.5	11.0
132.10	6067±235	3948±244***	6365±252	4270±248***	4.9	7.1
264.20	12149±841	7921±518***	12616±905	8415±526***	3.8	6.2
528.40	25336±1342	12718±1329***	26749±1414	14101±1425***	5.6	10.8

[a]Data are expressed as mean ± SE (n=6-7). *** P<0.001, as evaluated by unpaired t-test between wildtype (WT) and humanized huPept1 (HU) mice.

Table 5.3 Slopes of partial cumulative area under the plasma concentration-time curve (AUC) of [^{3}H]cefadroxil vs. time (5-30 min) after oral dose escalation in wildtype and humanized huPepT1 mice[a]

Dose (nmol/g)	From 5 min to 30 min						Ratio HU/WT
	Slope		R^2		Dose Normalized Slope		
	WT	HU	WT	HU	WT	HU	
11.01	10.39 ± 0.73	5.27 ±0.76	0.88	0.65	10.39 ± 0.73	5.27 ±0.76***	0.51
33.03	30.53 ± 1.18	16.69 ± 2.42	0.97	0.73	10.17 ± 0.39	5.56 ± 0.81***	0.55
66.06	62.34 ± 4.11	33.08 ± 5.19	0.91	0.65	10.39 ± 0.68	5.51 ± 0.87***	0.53
132.10	138.4 ± 6.28	69.33 ± 7.06	0.96	0.81	11.53 ± 0.52	5.77 ± 0.59***	0.50
264.20	290.0 ± 11.39	140.9 ± 10.16	0.97	0.90	12.08 ± 0.47	5.87 ± 0.42***	0.49
528.40	544.6 ± 18.71	200.8 ± 23.16	0.97	0.74	11.35 ± 0.39	4.18 ± 0.48***	0.37

[a]Data are expressed as mean ± SE (n=6-7). *** P<0.001, as evaluated by unpaired t-test between wildtype (WT) and humanized huPepT1 (HU) mice (hemizygotes).

Table 5.4 Regression parameters of partial cumulative area under the plasma concentration-time curve (AUC) of [^{3}H]cefadroxil vs. dose after oral dose escalation in wildtype and humanized huPepT1 mice[a]

	WT		HU		
Partial AUC	**Linear**		**Nonlinear**		
(min*μM)	**Slope**	**R^2**	**AUC_{max} (μM•min)**	**K_m (nmol/g)**	**R^2**
AUC_{0-30}	27.53±0.65	0.98	12313±4775	724.9±431.4	0.78
AUC_{0-60}	40.92±1.20	0.97	28688±11397	1023±568	0.86
AUC_{0-90}	45.69±1.44	0.97	35898±13610	1082±565	0.89
AUC_{0-120}	47.95±1.39	0.97	40789±15263	1156±587	0.90

[a]AUC_{0-t}: Area under plasma cefadroxil concentration-time profile from time 0 to time t after administration

Data are expressed as mean ± SE (n=6-7), where WT is wildtype and HU is humanized.

Nonlinear regression equation: $AUC = \frac{AUC_{max} * Dose}{K_m + Dose}$

Table 5.5 Regression parameters of area under the plasma concentration-time curve from 0-120 min (AUC_{0-120}) of [^{3}H]cefadroxil vs. dose after oral dose escalation in wildtype and humanized huPepT1 mice, and in human subjects[a]

WT		**HU**			**Humans**		
Linear		**Nonlinear**			**Nonlinear**		
Slope (min*m^2/L)	**R^2**	**AUC_{max} (min*μM)**	**K_m (μmol/m^2)**	**R^2**	**AUC_{max} (min*μM)**	**K_m (μmol/m^2)**	**R^2**
24.78±0.72	0.971	40794±15267	5838±2965	0.899	38494±8410	6177±1910	0.989

[a]Data are expressed as mean ± SE (n=6-7), where WT is wildtype and HU is humanized mice.

Nonlinear regression equation: $AUC = \frac{AUC_{max} * Dose}{K_m + Dose}$

Table 5.6 Regression parameters of C_{max} of [^{3}H]cefadroxil vs. dose after oral dose escalation in wildtype and humanized huPepT1 mice, and in human subjects[a]

WT		**HU**			**Humans**		
Linear		**Nonlinear**			**Nonlinear**		
Slope (m^2/L)	**R^2**	**C_{max} (μM)**	**K_m (μmol/m^2)**	**R^2**	**C_{max} (μM)**	**K_m (μmol/m^2)**	**R^2**
0.59 ± 0.013	0.998	554±187	4002±2030	0.843	322±42	3762±818	0.962

[a]Data are expressed as mean ± SE (n=6-7), where WT is wildtype and HU is humanized mice.

Nonlinear regression equation: $C = \frac{C_{max} * Dose}{K_m + Dose}$

Table 5.7 Bioavailability of cefadroxil, as assessed by mass balance, in wildtype and humanized huPepT1 mice after oral doses[a]

	[^{3}H]Cefadroxil Oral Dose – 11.01 nmol/g						[^{3}H]Cefadroxil Oral Dose – 528.40 nmol/g					
	WT			HU			WT			HU		
	Urine	Feces	F	Urine	Feces	F	Urine	Feces	BA	Urine	Feces	F
%Cef	81.6	8.3	83.8	78.2	12.2	82.1	76.3	6.6	82.4	75.6	9.4	81.7
%Inu	97.4	3.7	101.1	95.2	3.5	98.5	92.6	4.0	96.6	92.5	2.9	95.4

[a]Data are expressed as the mean of n=4 animals for each treatment group. Mass balance studies were performed in wildtype (WT) and humanized (HU) mice in which the urine and feces were collected for 24 hours after dosing. The bioavailability (F) of cefadroxil was calculated as: %Cef recovered in the urine divided by %Inu recovered in the urine; the bioavailability (F) of inulin was calculated as: %Inu recovered in the urine plus feces, where inulin was given as a [^{14}C]-labeled intravenous bolus injection at the same time as the oral dosing of cefadroxil. Cef represents cefadroxil and Inu represents inulin.

Table 5.8 Bioavailability of cefadroxil, as assessed by plasma, in wildtype and humanized huPepT1 mice after oral doses[a]

	11.01 nmol/g of cefadroxil		528.40 nmol/g of cefadroxil	
	WT	**HU**	**WT**	**HU**
AUC_{oral}(min*μM)	509	289	26749	14101
AUC_{iv}(min*μM)	616	613	25482	26744
F (%)	82.6	47.1	105.0	52.7

[a]Data are expressed as mean (n=3-5), for wildtype (WT) and humanized (HU) mice. The %bioavailability (F) of cefadroxil was calculated as: AUC_{oral} (min*μM) divided by AUC_{iv}(min*μM) in which AUC was the area under the plasma concentration-time profile from time zero to infinity.

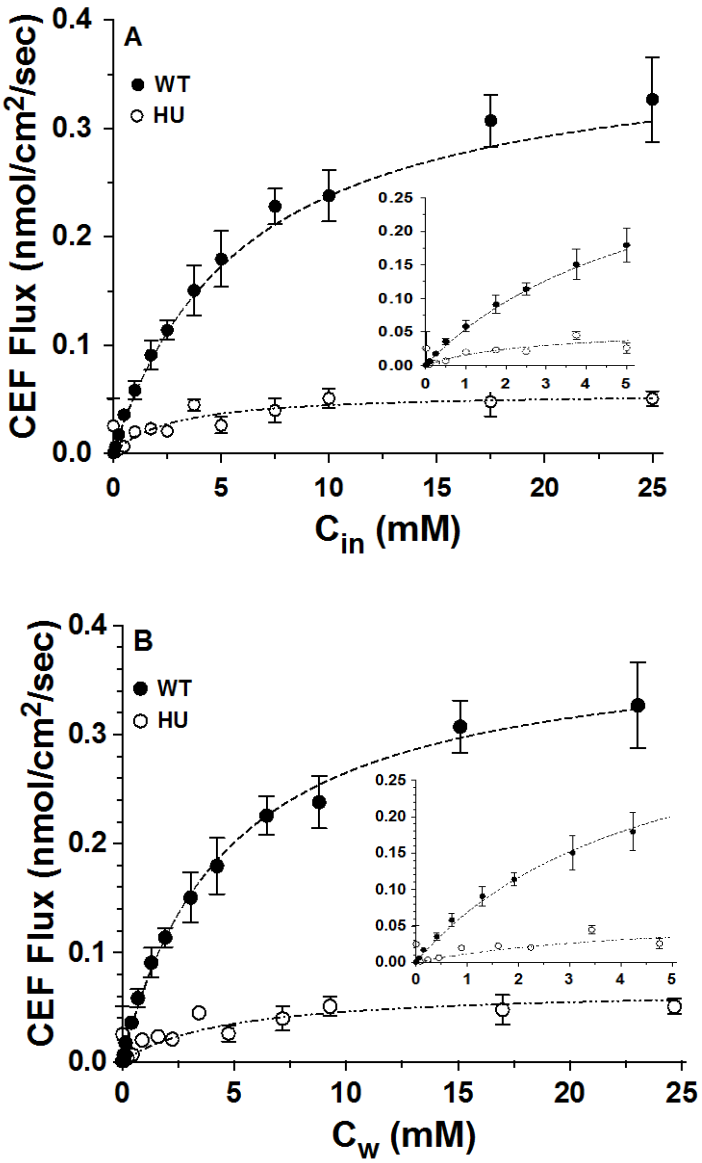

Figure 5.1 Concentration-dependent flux of [^{3}H]cefadroxil (0.01 to 25.0 mM) during jejunal perfusion studies in wildtype (WT) and humanized huPepT1 (HU) mice (n=4). C_{in} is the inlet concentration of drug, where J^*_{max}=0.380±0.001 nmol/cm^2/sec and K^*_m=6.01±0.46 mM for WT (r^2=0.982); J^*_{max}=0.057±0.006 nmol/cm^2/sec and K^*_m=2.69±0.928 mM for HU mice (r^2=0.658) (A). C_w is the estimated concentration of drug at the membrane wall where J_{max} =0.392±0.010 nmol/cm^2/sec and K_m=4.80±1.0 mM for WT (r^2=0.996); J_{max}=0.0557±0.009 nmol/cm^2/sec and K_m=2.37±1.21 mM for HU (r^2=0.728) (B).

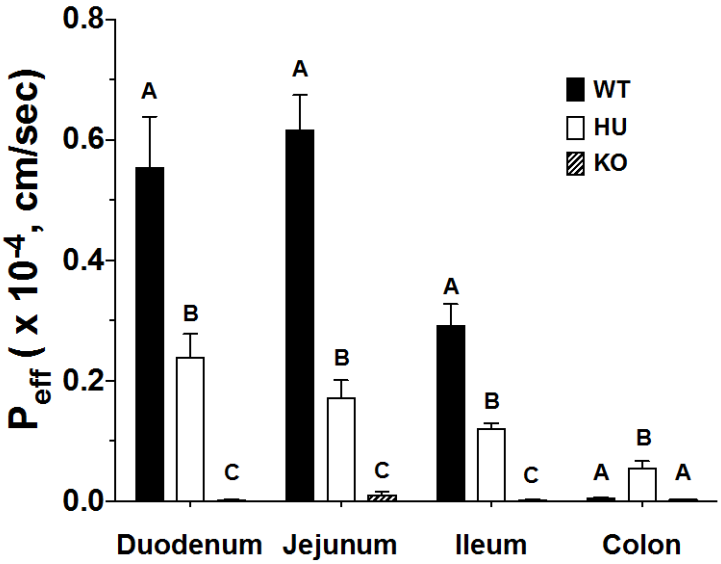

Figure 5.2 Effective permeability of 10 μM [^{3}H]cefadroxil in different regions of small and large intestines in wildtype (WT), humanized huPepT1 (HU) and mPepT1 knockout (KO) mice (n=4). Different letters represent significant differences between the treatment groups, as evaluated by ANOVA/Tukey's test.

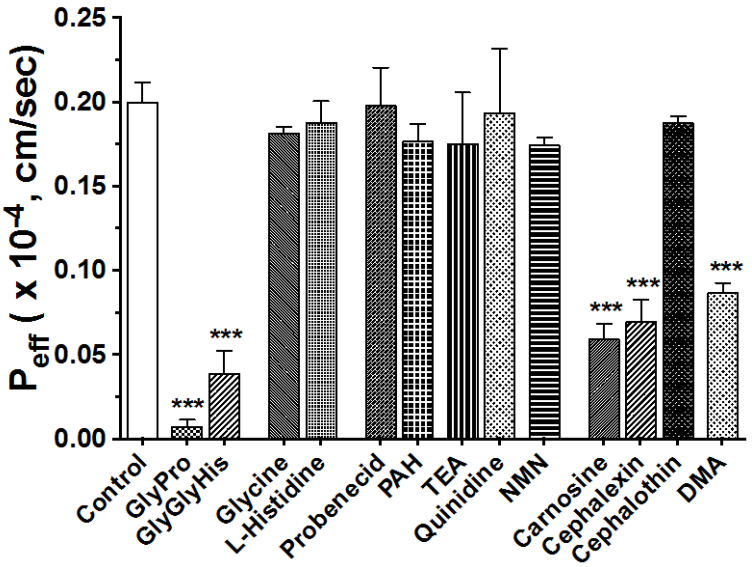

Figure 5.3 Specificity studies on the jejunal permeability of 10 μM [^{3}H]cefadroxil, +/- 10 mM of potential inhibitors (0.1 mM for DMA) in humanized huPept1 mice (n=3). ***P<0.001, as evaluated by ANOVA/Dunnett's test in which HU without inhibitor was set as the control group. PAH, p-aminohippuric acid, TEA, tetraethylammonium; NMN, N^1-methylnicotinamide; DMA, dimethy-lamiloride.

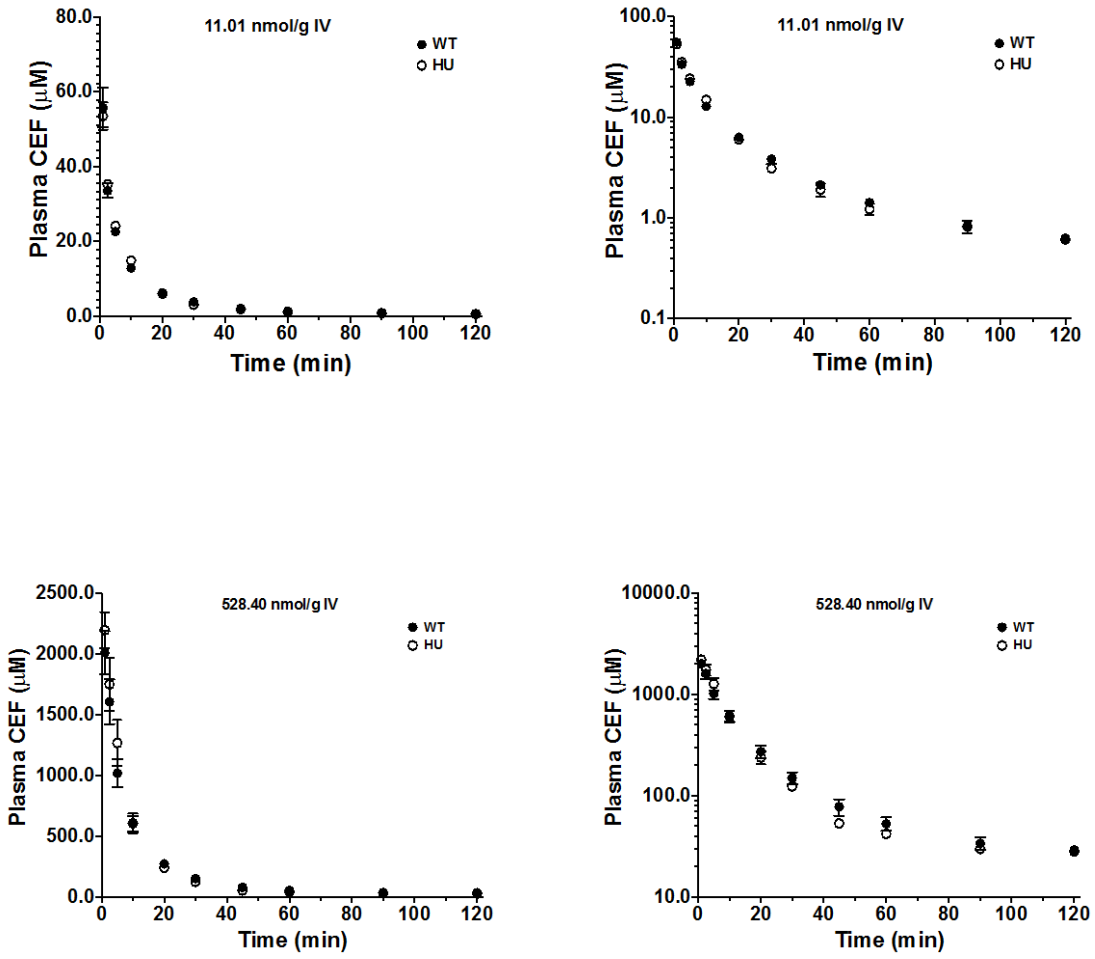

Figure 5.4 Plasma concentration-time profiles of [^{3}H]cefadroxil in wildtype (WT) and humanized huPepT1 (HU) mice following intravenous bolus injections (n=4-5) in which the y-axis is displayed on a linear scale (left panel) and on a logarithmic scale (right panel).

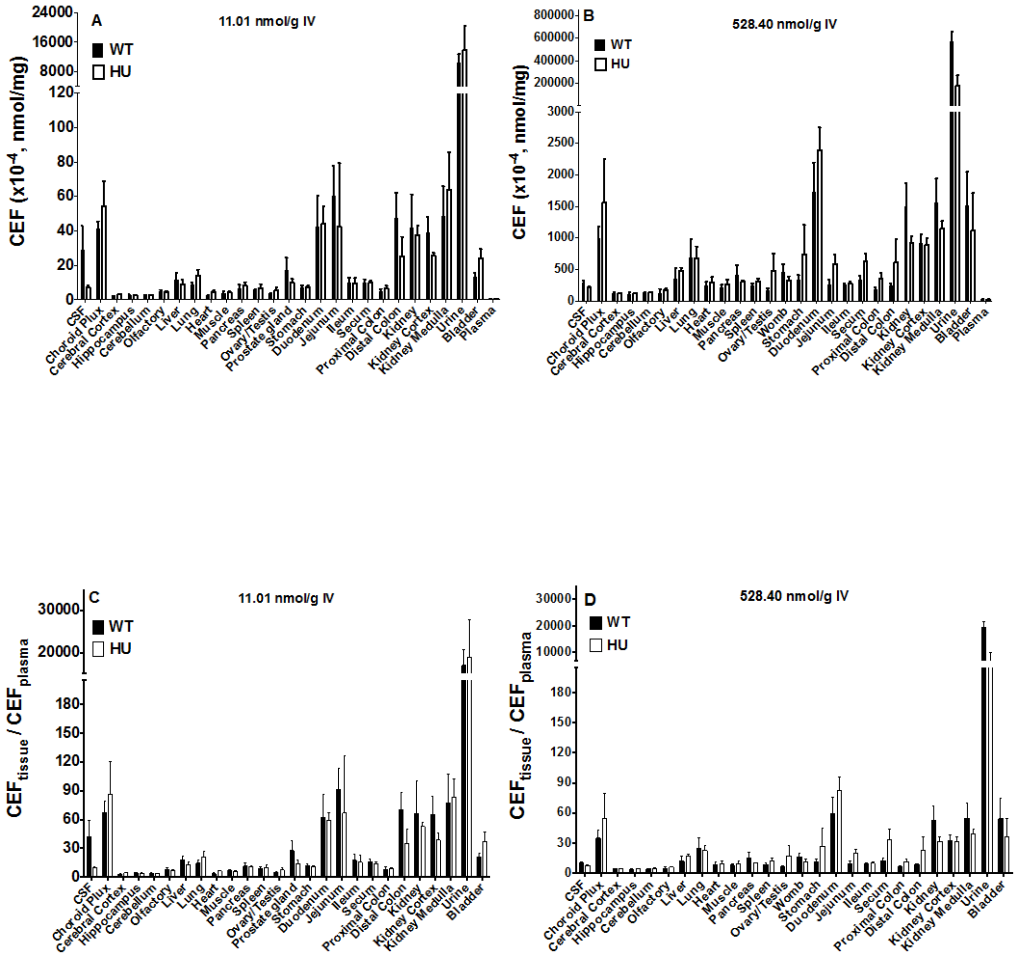

Figure 5.5 Tissue distribution and plasma-normalized tissue distribution profiles of [^{3}H]cefadroxil in wildtype (WT) and humanized huPepT1 (HU) mice following intravenous bolus dosing. Tissues were collected 120 min after dosing (n=4-5). No significant differences were observed between the two genotypes, as evaluated by unpaired t-test.

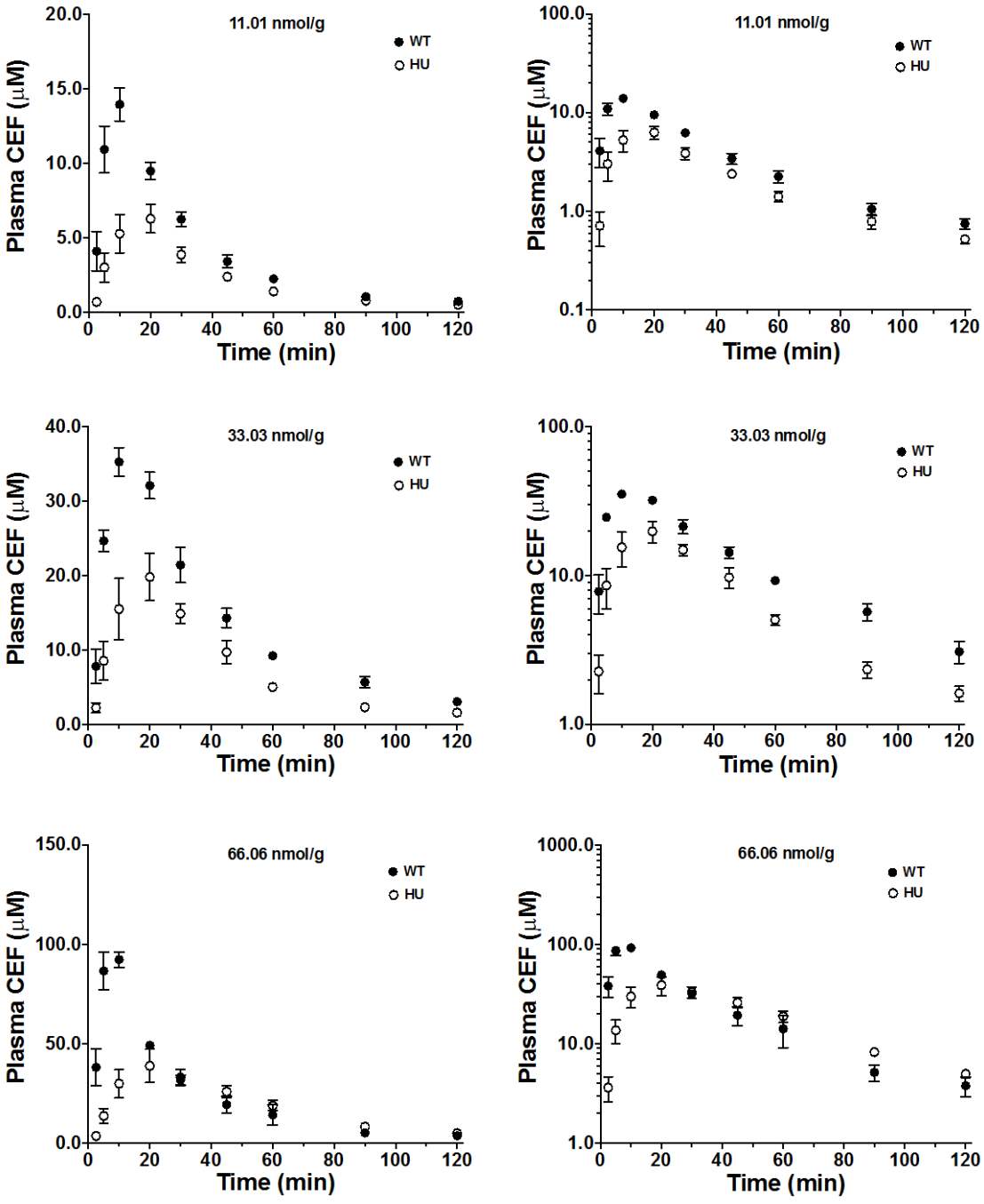

Figure 5.6 Plasma concentration-time profiles of [^{3}H]cefadroxil in wildtype (WT) and humanized huPepT1 (HU) mice following oral dose escalation (n=6-7) in which the y-axis is displayed on a linear scale (left panel) and on a logarithmic scale (right panel).

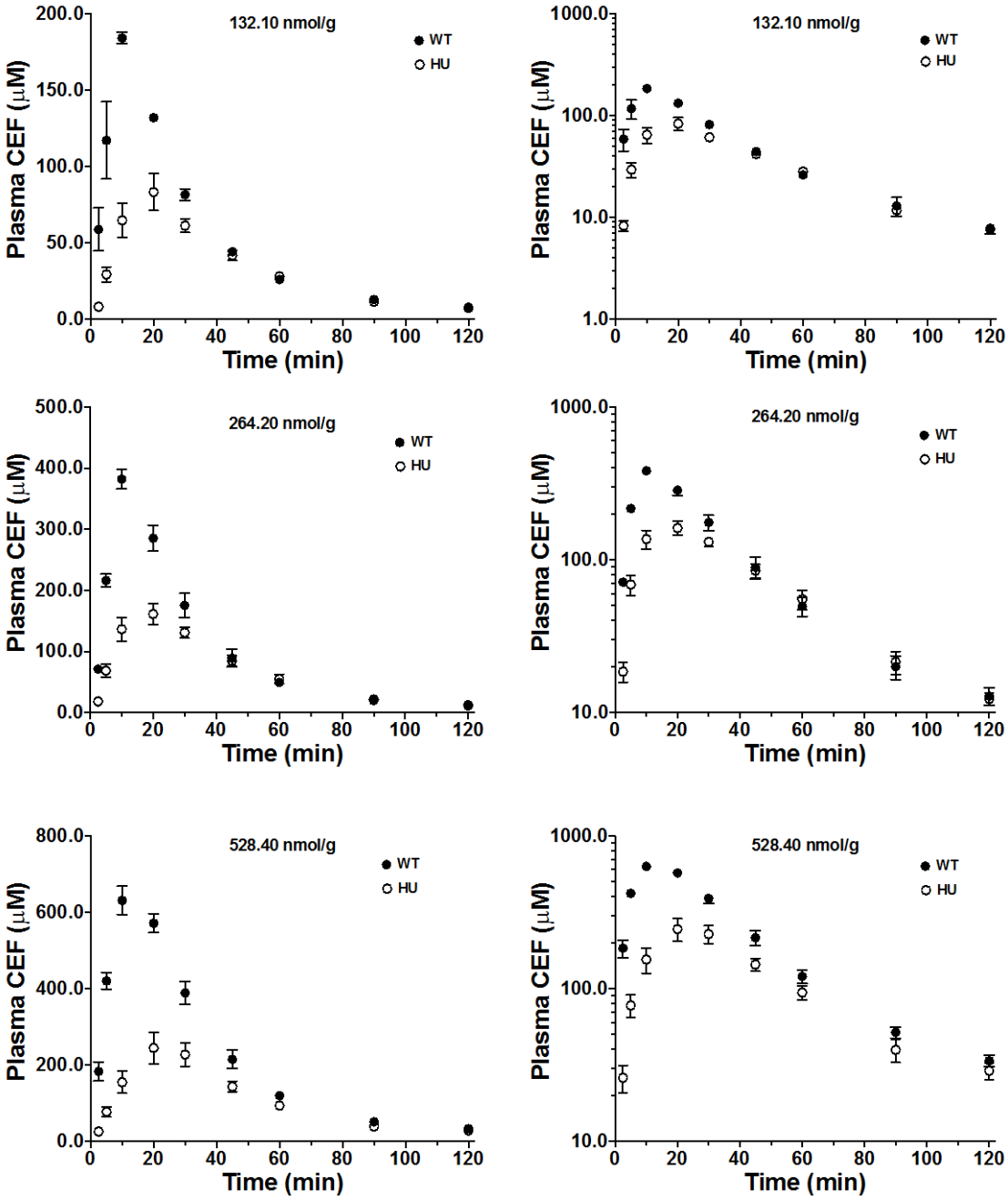

Figure 5.6 Continued (see previous page for description)

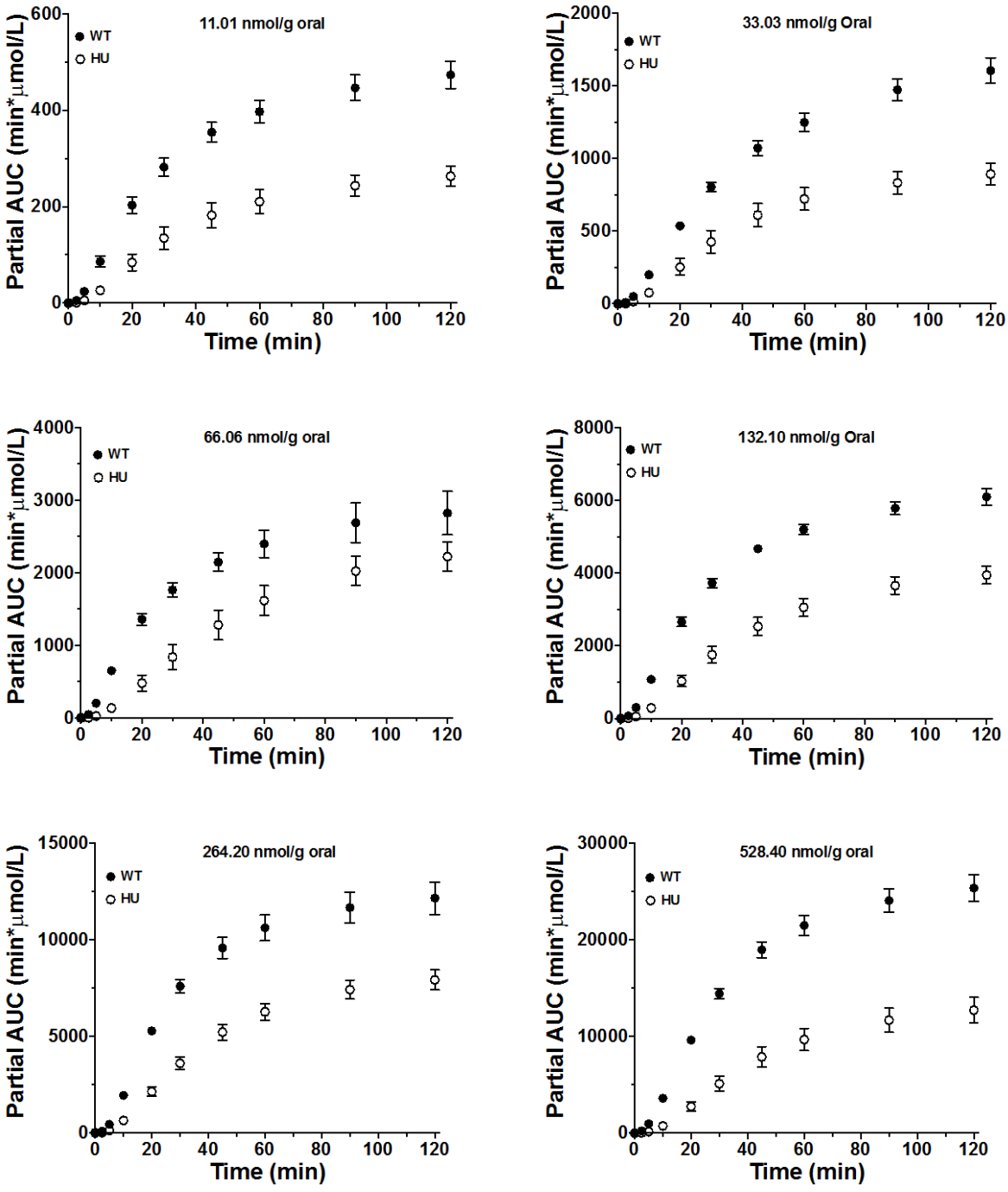

Figure 5.7 Partial cumulative area under the plasma concentration-time curve (AUC) of [^{3}H]cefadroxil as a function of time in wildtype (WT) and humanized huPepT1 (HU) mice. Data are expressed as mean ± SE (n=6-7).

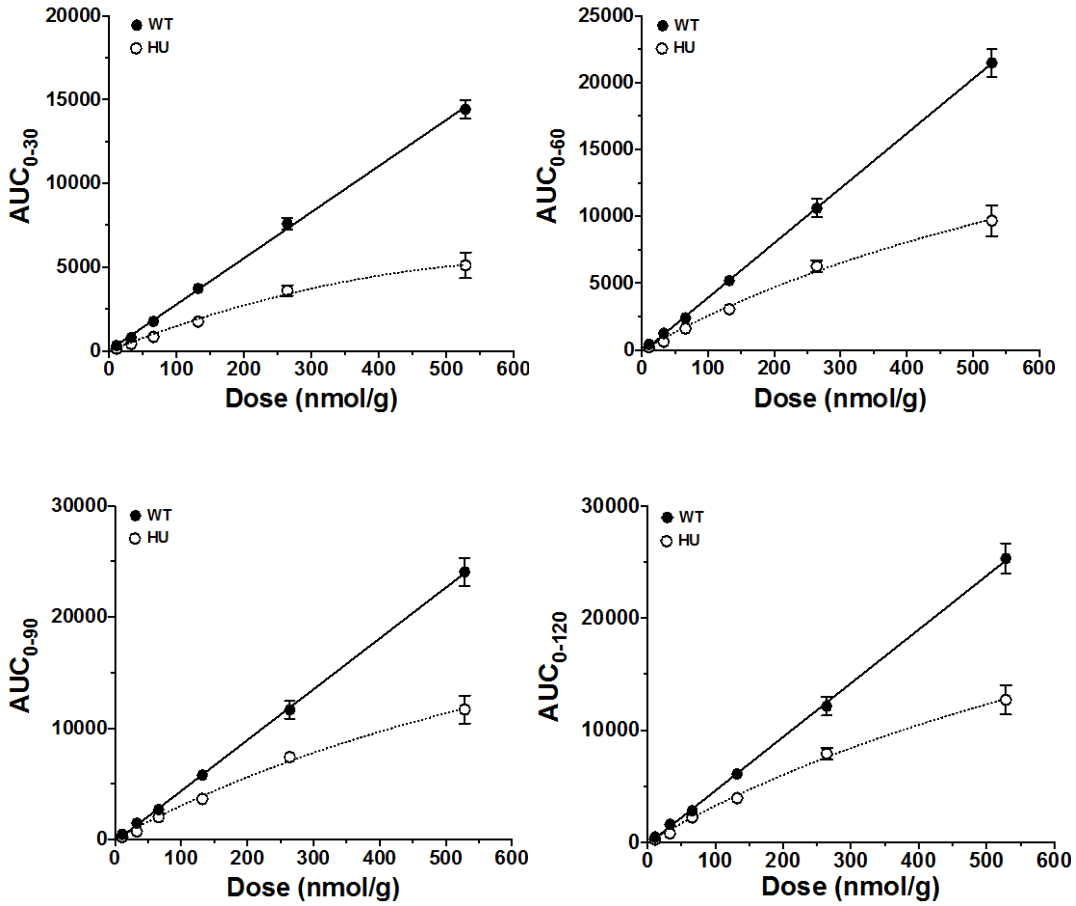

Figure 5.8 Partial cumulative area under the plasma concentration-time curve (AUC) of [^{3}H]cefadroxil vs. dose in wildtype (WT) and humanized huPepT1 (HU) mice following oral dose escalation. A proportional increase of AUC vs. dose was observed in WT mice, whereas this relationship was nonlinear in HU mice. Data are expressed as mean ± SE (n=6-7).

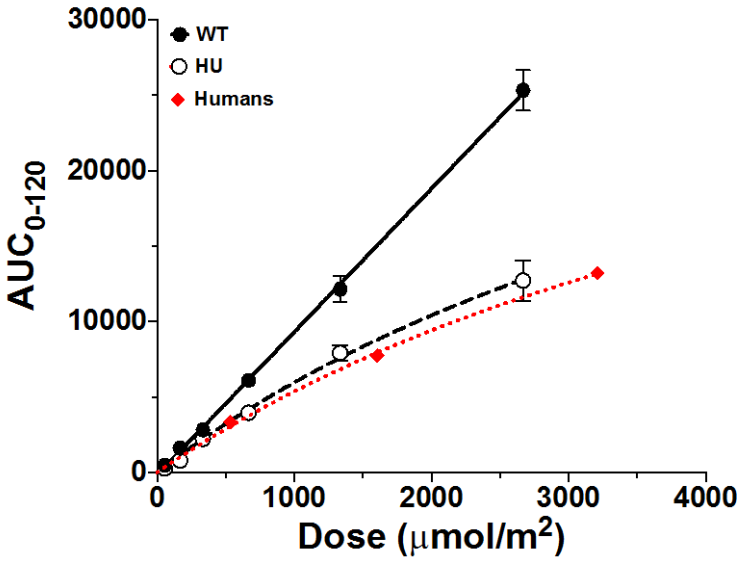

Figure 5.9 Area under the plasma concentration-time curve from 0-120 min (AUC_{0-120}) of [^{3}H]cefadroxil vs. Dose in wildtype (WT), humanized huPepT1 (HU) and clinical data (Humans, n=3) obtained from Garrigues et al.(Garrigues, et al. 1991)

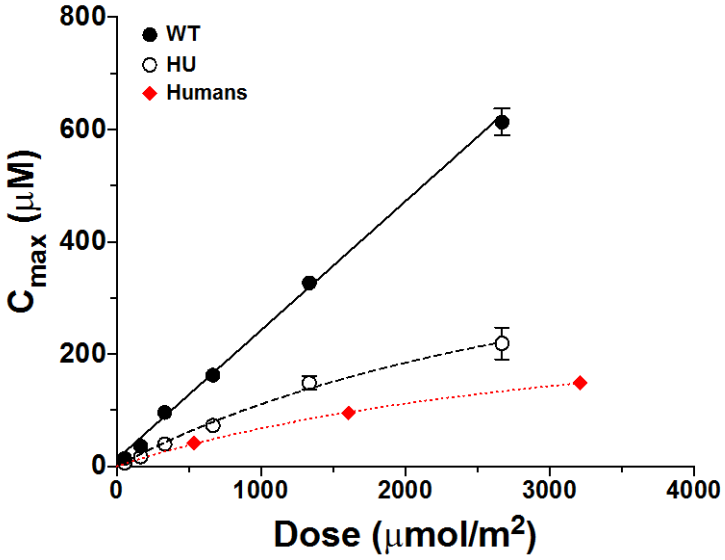

Figure 5.10 C_{max} vs. Dose of [^{3}H]cefadroxil in wildtype (WT) mice, humanized huPepT1 (HU) mice, and clinical data (Humans, n=3) obtained from Garrigues et al. (Garrigues, et al. 1991)

REFERENCE

Adachi Y, Suzuki H and Sugiyama Y (2003) Quantitative evaluation of the function of small intestinal P-glycoprotein: comparative studies between in situ and in vitro. *Pharm Res*. **20:** 1163-1169.

Amidon GL, Sinko PJ and Fleisher D (1988) Estimating human oral fraction dose absorbed: a correlation using rat intestinal membrane permeability for passive and carrier-mediated compounds. *Pharmaceutical research*. **5:** 651-654.

Ballantyne F (1982) Cefadroxil in the treatment of skin and soft tissue infections. *The Journal of antimicrobial chemotherapy*. **10 Suppl B:** 143-147.

Beisel L (1980) Efficacy and safety of cefadroxil in bacterial pharyngitis. *The Journal of international medical research*. **8:** 87-93.

Brandsch M, Knutter I and Bosse-Doenecke E (2008) Pharmaceutical and pharmacological importance of peptide transporters. *The Journal of pharmacy and pharmacology*. **60:** 543-585.

Buck RE and Price KE (1977) Cefadroxil, a new broad-spectrum cephalosporin. *Antimicrobial agents and chemotherapy*. **11:** 324-330.

Cao X, Gibbs ST, Fang L, Miller HA, Landowski CP, Shin HC, Lennernas H, Zhong Y, Amidon GL, Yu LX and Sun D (2006) Why is it challenging to predict intestinal drug absorption and oral bioavailability in human using rat model. *Pharmaceutical research*. **23:** 1675-1686.

Chen ML (1992) An alternative approach for assessment of rate of absorption in bioequivalence studies. *Pharmaceutical research*. **9:** 1380-1385.

Chen ML, Lesko L and Williams RL (2001) Measures of exposure versus measures of rate and extent of absorption. *Clin Pharmacokinet*. **40:** 565-572.

Chen X, Loryan I, Payan M, Keep RF, Smith DE and Hammarlund-Udenaes M (2014) Effect of transporter inhibition on the distribution of cefadroxil in rat brain. *Fluids Barriers CNS*. **11:** 25.

Cordero A (1976) Treatment of skin and soft tissue infections with cefadroxil, a new oral cephalosporin. *The Journal of international medical research*. **4:** 176-178.

de Waart DR, van de Wetering K, Kunne C, Duijst S, Paulusma CC and Oude Elferink RP (2012) Oral availability of cefadroxil depends on ABCC3 and ABCC4. *Drug metabolism and disposition: the biological fate of chemicals*. **40:** 515-521.

Drozdzik M, Groer C, Penski J, Lapczuk J, Ostrowski M, Lai Y, Prasad B, Unadkat JD, Siegmund W and Oswald S (2014) Protein abundance of clinically relevant multidrug transporters along the entire length of the human intestine. *Molecular pharmaceutics*. **11:** 3547-3555.

Ganapathy ME, Brandsch M, Prasad PD, Ganapathy V and Leibach FH (1995) Differential recognition of beta -lactam antibiotics by intestinal and renal peptide transporters, PEPT 1 and PEPT 2. *The Journal of biological chemistry*. **270:** 25672-25677.

Garcia-Carbonell MC, Granero L, Torres-Molina F, Aristorena JC, Chesa-Jimenez J, Pla-Delfina JM and Peris-Ribera JE (1993) Nonlinear pharmacokinetics of cefadroxil in the rat. *Drug Metab Dispos*. **21:** 215-217.

Garrigues TM, Martin U, Peris-Ribera JE and Prescott LF (1991) Dose-dependent absorption and elimination of cefadroxil in man. *Eur J Clin Pharmacol*. **41:** 179-183.

Goodman LS, Brunton LL, Blumenthal DK, Murri N and Hilal-Dandan R (2011) Goodman & Gilman's The pharmacological basis of therapeutics *McGraw-Hill Medical* New York 9780071624428

Hartstein AI, Patrick KE, Jones SR, Miller MJ and Bryant RE (1977) Comparison of pharmacological and antimicrobial properties of cefadroxil and cephalexin. *Antimicrobial agents and chemotherapy*. **12:** 93-97.

Hausman MS (1980) Treatment of urinary tract infections with cefadroxil, a new cephalosporin. *The Journal of international medical research*. **8:** 21-28.

Hogerle ML and Winne D (1983) Drug absorption by the rat jejunum perfused in situ. Dissociation from the pH-partition theory and role of microclimate-pH and unstirred layer. *Naunyn-Schmiedeberg's archives of pharmacology*. **322:** 249-255.

Hu Y, Chen X and Smith DE (2012) Species-dependent uptake of glycylsarcosine but not oseltamivir in Pichia pastoris expressing the rat, mouse, and human intestinal peptide transporter PEPT1. *Drug Metab Dispos*. **40:** 1328-1335.

Hu Y, Smith DE, Ma K, Jappar D, Thomas W and Hillgren KM (2008) Targeted disruption of peptide transporter Pept1 gene in mice significantly reduces dipeptide absorption in intestine. *Mol Pharm*. **5:** 1122-1130.

Hu Y, Xie Y, Wang Y, Chen X and Smith DE (2014) Development and characterization of a novel mouse line humanized for the intestinal peptide transporter PEPT1. *Mol Pharm*. **11:** 3737-3746.

Jappar D, Wu SP, Hu Y and Smith DE (2010) Significance and regional dependency of peptide transporter (PEPT) 1 in the intestinal permeability of glycylsarcosine: in situ single-pass perfusion studies in wild-type and Pept1 knockout mice. *Drug Metab Dispos*. **38:** 1740-1746.

Johnson DA and Amidon GL (1988) Determination of intrinsic membrane transport parameters from perfused intestine experiments: a boundary layer approach to estimating the aqueous and unbiased membrane permeabilities. *J Theor Biol*. **131:** 93-106.

Kaminszczik I (1986) Treatment of acute and chronic sinusitis with cefadroxil. *Drugs*. **32 Suppl 3:** 33-38.

Khamdang S, Takeda M, Babu E, Noshiro R, Onozato ML, Tojo A, Enomoto A, Huang XL, Narikawa S, Anzai N, Piyachaturawat P and Endou H (2003) Interaction of human and rat organic anion transporter 2 with various cephalosporin antibiotics. *European journal of pharmacology*. **465:** 1-7.

Khamdang S, Takeda M, Noshiro R, Narikawa S, Enomoto A, Anzai N, Piyachaturawat P and Endou H (2002) Interactions of human organic anion transporters and human organic cation transporters with nonsteroidal anti-inflammatory drugs. *The Journal of pharmacology and experimental therapeutics*. **303:** 534-539.

Komiya I, Park JY, Kamani A, Ho NFH and Higuchi WI (1980) Quantitative mechanistic studies in simultaneous fluid flow and intestinal absorption using steroids as model solutes. *International Journal of Pharmaceutics*. **4:** 14.

Kou JH, Fleisher D and Amidon GL (1991) Calculation of the aqueous diffusion layer resistance for absorption in a tube: application to intestinal membrane permeability determination. *Pharm Res*. **8:** 298-305.

Lennernas H (2007) Animal data: the contributions of the Ussing Chamber and perfusion systems to predicting human oral drug delivery in vivo. *Adv Drug Deliv Rev*. **59:** 1103-1120.

Lucas M (1983) Determination of acid surface pH in vivo in rat proximal jejunum. *Gut*. **24:** 734-739.

Ma K, Hu Y and Smith DE (2011) Peptide transporter 1 is responsible for intestinal uptake of the dipeptide glycylsarcosine: studies in everted jejunal rings from wild-type and Pept1 null mice. *J Pharm Sci*. **100:** 767-774.

McConnell EL, Basit AW and Murdan S (2008) Measurements of rat and mouse gastrointestinal pH, fluid and lymphoid tissue, and implications for in-vivo experiments. *The Journal of pharmacy and pharmacology*. **60:** 63-70.

McKie AT, Kusel M, McEwan GT and Lucas ML (1988) The effect of heat-stable Escherichia coli enterotoxin, theophylline and forskolin on cyclic nucleotide levels and mucosal surface (acid microclimate) pH in rat proximal jejunum in vivo. *Biochimica et biophysica acta*. **971:** 325-331.

Nakamura N, Lill JR, Phung Q, Jiang Z, Bakalarski C, de Maziere A, Klumperman J, Schlatter M, Delamarre L and Mellman I (2014) Endosomes are specialized platforms for bacterial sensing and NOD2 signalling. *Nature*. **509:** 240-244.

Naruhashi K, Sai Y, Tamai I, Suzuki N and Tsuji A (2002) PepT1 mRNA expression is induced by starvation and its level correlates with absorptive transport of cefadroxil longitudinally in the rat intestine. *Pharmaceutical research*. **19:** 1417-1423.

Ocheltree SM, Shen H, Hu Y, Xiang J, Keep RF and Smith DE (2004) Mechanisms of cefadroxil uptake in the choroid plexus: studies in wild-type and PEPT2 knockout mice. *The Journal of pharmacology and experimental therapeutics*. **308:** 462-467.

Pfeffer M, Jackson A, Ximenes J and de Menezes JP (1977) Comparative human oral clinical pharmacology of cefadroxil, cephalexin, and cephradine. *Antimicrob Agents Chemother*. **11:** 331-338.

Posada MM and Smith DE (2013a) In vivo absorption and disposition of cefadroxil after escalating oral doses in wild-type and PepT1 knockout mice. *Pharm Res*. **30:** 2931-2939.

Posada MM and Smith DE (2013b) Relevance of PepT1 in the intestinal permeability and oral absorption of cefadroxil. *Pharmaceutical research*. **30:** 1017-1025.

Randolph MF (1988) Clinical comparison of once-daily cefadroxil and thrice-daily cefaclor in the treatment of streptococcal pharyngitis. *Chemotherapy*. **34:** 512-518.

Ries M, Wenzel U and Daniel H (1994) Transport of cefadroxil in rat kidney brush-border membranes is mediated by two electrogenic H+-coupled systems. *J Pharmacol Exp Ther*. **271:** 1327-1333.

Rowland M and Tozer TN (2009) Clinical pharmacokinetics and pharmacodynamics: concepts and applications *Lippincott William & Wilkins* Philadelphia 9780781750097

0781750091

Rubio-Aliaga I and Daniel H (2002) Mammalian peptide transporters as targets for drug delivery. *Trends in pharmacological sciences*. **23:** 434-440.

Rubio-Aliaga I and Daniel H (2008) Peptide transporters and their roles in physiological processes and drug disposition. *Xenobiotica; the fate of foreign compounds in biological systems*. **38:** 1022-1042.

Sanchez-Pico A, Peris-Ribera JE, Toledano C, Torres-Molina F, Casabo VG, Martin-Villodre A and Pla-Delfina JM (1989) Non-linear intestinal absorption kinetics of cefadroxil in the rat. *J Pharm Pharmacol*. **41:** 179-185.

Santella PJ and Henness D (1982) A review of the bioavailability of cefadroxil. *The Journal of antimicrobial chemotherapy*. **10 Suppl B:** 17-25.

Sasawatari S, Okamura T, Kasumi E, Tanaka-Furuyama K, Yanobu-Takanashi R, Shirasawa S, Kato N and Toyama-Sorimachi N (2011) The solute carrier family 15A4 regulates TLR9 and NOD1 functions in the innate immune system and promotes colitis in mice. *Gastroenterology*. **140:** 1513-1525.

Shen H, Keep RF, Hu Y and Smith DE (2005) PEPT2 (Slc15a2)-mediated unidirectional transport of cefadroxil from cerebrospinal fluid into choroid plexus. *The Journal of pharmacology and experimental therapeutics*. **315:** 1101-1108.

Shen H, Ocheltree SM, Hu Y, Keep RF and Smith DE (2007) Impact of genetic knockout of PEPT2 on cefadroxil pharmacokinetics, renal tubular reabsorption, and brain penetration in mice. *Drug metabolism and disposition: the biological fate of chemicals*. **35:** 1209-1216.

Sinko PJ and Amidon GL (1988) Characterization of the oral absorption of beta-lactam antibiotics. I. Cephalosporins: determination of intrinsic membrane absorption parameters in the rat intestine in situ. *Pharmaceutical research*. **5:** 645-650.

Takeda M, Babu E, Narikawa S and Endou H (2002) Interaction of human organic anion transporters with various cephalosporin antibiotics. *European journal of pharmacology*. **438:** 137-142.

Tanrisever B and Santella PJ (1986) Cefadroxil. A review of its antibacterial, pharmacokinetic and therapeutic properties in comparison with cephalexin and cephradine. *Drugs*. **32 Suppl 3:** 1-16.

Wang HP, Bair CH and Huang JD (1992) Uptake of cefadroxil derivatives in rat intestinal brush-border membrane vesicles. *J Pharm Pharmacol*. **44:** 1027-1029.

Williamson R, Hakenbeck R and Tomasz A (1980) In vivo interaction of beta-lactam antibiotics with the penicillin-binding proteins of Streptococcus pneumoniae. *Antimicrobial agents and chemotherapy*. **18:** 629-637.

Yang B, Hu Y and Smith DE (2013) Impact of peptide transporter 1 on the intestinal absorption and pharmacokinetics of valacyclovir after oral dose escalation in wild-type and PepT1 knockout mice. *Drug Metab Dispos*. **41:** 1867-1874.

Yu GV and Novicki DC (1995) Cefadroxil in skin and skin-structure foot infections: a retrospective review. *Adv Ther*. **12:** 1-10.

Zakeri-Milani P, Valizadeh H, Tajerzadeh H, Azarmi Y, Islambolchilar Z, Barzegar S and Barzegar-Jalali M (2007) Predicting human intestinal permeability using single-pass intestinal perfusion in rat. *J Pharm Pharm Sci*. **10:** 368-379.

Zwarycz B and Wong EA (2013) Expression of the peptide transporters PepT1, PepT2, and PHT1 in the embryonic and posthatch chick. *Poultry science*. **92:** 1314-1321.

APPENDICES

Appendix A: Individual data from Chapter III

Table A.3.3 mRNA transcripts of hPepT1 in funder of humanized huPepT1 mice

Mouse	Mean value	SEM	N
Caco-2	565.3489	16.1015	2
HU#1	3.992029	0.2168624	2
HU#3	29.41921	3.315452	2
HU#4	1530.387	403.6676	2
HU#5	7.692222	1.770403	2
HU#6	64.327	10.28008	2
Wildtype	0.05577244	0.0007595922	2
mPepT1 KO	0.07403623	0.02631376	2

Table A.3.4 Gene copy number of BAC DNA in huPepT1 mice

Mouse	wildtype	HU#4	HU#5
1	0.00000303	1.090869	0.791723
2	0.0000654	0.960634	0.982002
3	0.0000498	0.922837	
4	0.000044	1.235112	
5	0.0000569	1.186792	

Table A.3.6 Real-time PCR analysis of PepT1 gene in WT, KO and huPepT1

hPepT1 in huPepT1						
Tissue	#1	#2	#3	#4	#5	#6
Duo	430.81	494.39	493.43	445.42	552.41	514.89
Jej	916.01	1133.30	715.35	1170.58	1086.30	1196.34
Ile	1053.68	1115.71	1301.21	1045.89	1703.89	1500.04
PC	257.52	187.04	226.62	297.31	390.35	368.98
DC	230.80	121.98	207.02	263.66	293.40	267.39
Kid	4.76	4.48	4.75	42.89	14.13	14.31

hPepT1 in Wildtype						
Tissue	#1	#2	#3	#4	#5	#6
Duo	3.44	1.99	1.77	1.70	2.95	4.03
Jej	2.52	2.29	2.07	2.43	3.58	3.11
Ile	1.13	2.19	4.79	2.58	1.94	2.69
PC	0.53	0.39	0.28	0.30	0.48	0.62
DC	0.28	0.48	0.77	0.43	0.48	0.89
Kid	0.42	0.26	0.51	0.32	0.20	0.07

hPepT1 in mPepT1 KO						
Tissue	#1	#2	#3	#4	#5	#6
Duo	0.57	0.78	1.49	0.48	0.54	5.53
Jej	7.84	0.25	2.74	2.74	1.77	3.01
Ile	0.84	5.11	3.16	0.34	0.34	0.33
PC	7.91	1.09	1.30	6.73	0.69	3.93
DC	0.87	1.70	7.73	0.61	0.43	9.84
Kid	1.26	0.80	0.40	0.85	0.45	0.60

mPepT1 in huPepT1						
Tissue	#1	#2	#3	#4	#5	#6
Duo	13.47	13.95	15.21	21.55	18.05	21.53
Jej	34.67	55.63	26.00	54.43	38.36	50.17
Ile	49.57	53.61	38.66	54.45	42.91	64.08
PC	1.56	1.62	1.19	4.98	5.25	5.17
DC	2.41	2.42	2.25	3.72	3.07	3.68
Kid	1.37	1.04	1.02	1.64	0.43	1.94

mPepT1 in Wildtype						
Tissue	#1	#2	#3	#4	#5	#6
Duo	1353.81	898.34	1027.85	709.77	805.54	1626.68
Jej	2580.85	2094.82	2958.01	2967.34	2008.34	1929.59
Ile	1594.45	1244.70	1904.47	1798.29	1273.88	1542.56
PC	27.41	31.68	34.52	16.44	27.08	34.13
DC	169.66	286.96	514.92	274.60	206.72	596.76
Kid	6.26	7.60	7.10	7.44	5.69	4.89

hPepT1 in mPepT1 KO						
Tissue	#1	#2	#3	#4	#5	#6
Duo	4.62	0.79	1.02	0.52	0.56	3.48
Jej	5.88	22.56	39.80	10.79	4.41	3.72
Ile	6.50	19.20	18.50	4.00	2.49	0.85
PC	12.63	14.80	1.33	17.70	14.23	14.79
DC	12.34	14.80	17.52	18.21	5.09	5.43
Kid	2.38	0.98	1.00	2.85	0.96	0.43

Table A.3.7 Real-time PCR analysis of POT gene in WT, KO and huPepT1

PepT2 in huPepT1						
Tissue	#1	#2	#3	#4	#5	#6
Duo	0.91	0.79	1.09	14.82	7.74	9.97
Jej	4.10	4.94	4.09	0.56	0.58	0.56
Ile	1.12	0.94	0.95	2.34	2.66	2.96
PC	6.22	3.81	4.18	2.33	4.58	2.88
DC	5.00	6.66	5.43	0.82	0.75	0.55
Kid	575.76	376.19	231.73	655.44	394.62	471.86

mPePT2 in Wildtype						
Tissue	#1	#2	#3	#4	#5	#6
Duo	5.90	1.37	0.93	4.88	4.44	4.58
Jej	3.09	8.12	1.93	2.64	3.34	4.45
Ile	0.52	0.23	0.79	1.67	0.61	0.36
PC	2.13	2.68	0.88	2.81	4.47	4.19
DC	0.28	0.46	0.48	0.00	0.38	0.64
Kid	446.84	531.57	544.36	520.48	259.25	383.85

mPepT2 in mPepT1 KO						
Tissue	#1	#2	#3	#4	#5	#6
Duo	0.68	0.03	0.33	0.16	0.32	0.17
Jej	1.67	1.12	0.95	0.39	1.03	0.44
Ile	0.26	0.49	1.59	0.09	0.08	0.18
PC	2.71	0.20	0.14	0.73	0.21	0.44
DC	0.03	1.93	0.06	0.05	0.03	0.90
Kid	302.04	664.96	545.39	434.00	376.84	790.39

mPhT1 in huPepT1						
Tissue	#1	#2	#3	#4	#5	#6
Duo	11.95	13.45	10.27	23.91	20.80	19.97
Jej	24.99	22.08	21.79	15.23	17.24	43.14
Ile	54.77	52.66	67.90	29.10	11.42	0.39
PC	110.13	46.36	62.22	31.77	68.61	18.28
DC	47.75	49.44	42.59	52.35	54.14	46.16
Kid	34.53	25.22	28.97	20.36	21.29	22.62

mPhT1 in Wildtype						
Tissue	#1	#2	#3	#4	#5	#6
Duo	17.96	19.57	33.22	10.38	26.36	10.37
Jej	96.68	54.37	37.11	78.21	33.14	52.18
Ile	16.33	43.46	55.22	51.06	60.24	56.63
PC	108.26	115.55	99.35	96.60	86.39	110.84
DC	42.30	28.53	0.00	26.88	30.96	38.11
Kid	49.25	75.64	65.13	72.75	46.10	30.71

mPhT1 in mPepT1 KO						
Tissue	#1	#2	#3	#4	#5	#6
Duo	14.21	33.87	17.86	22.49	6.71	30.68
Jej	31.82	25.47	96.05	30.88	28.67	103.05
Ile	63.61	66.41	42.45	26.51	10.84	16.14
PC	125.98	23.51	10.50	65.72	49.34	49.79
DC	36.66	56.33	10.25	18.72	19.30	16.81
Kid	39.38	40.71	8.15	43.30	16.96	9.69

mPhT2 in huPepT1						
Tissue	#1	#2	#3	#4	#5	#6
Duo	12.37	8.72	8.31	47.28	25.09	30.15
Jej	11.71	11.08	9.32	12.68	8.12	11.57
Ile	42.86	42.74	31.12	21.46	22.20	18.67
PC	24.48	16.33	21.22	39.47	59.94	38.90
DC	8.17	10.80	7.00	47.15	46.99	25.32
Kid	6.66	5.54	5.35	12.49	11.89	7.50

mPhT2 in Wildtype						
Tissue	#1	#2	#3	#4	#5	#6
Duo	21.12	21.47	20.68	16.47	16.27	22.93
Jej	25.20	17.94	16.02	33.77	5.74	11.86
Ile	10.07	25.07	16.94	19.33	14.13	18.38
PC	19.17	13.98	16.03	10.97	8.26	12.81
DC	3.78	6.32	4.14	3.72	4.28	4.35
Kid	5.80	7.58	7.83	12.07	6.66	9.06

mPhT2 in mPepT1 KO						
Tissue	#1	#2	#3	#4	#5	#6
Duo	12.00	19.26	21.06	3.71	18.59	20.35
Jej	53.92	12.82	23.41	14.08	39.46	80.43
Ile	18.03	38.91	106.70	5.13	6.38	5.99
PC	25.35	18.48	19.06	14.06	3.54	9.28
DC	22.37	7.21	5.23	19.03	12.32	26.29
Kid	4.96	5.25	6.13	15.32	4.61	13.33

Table A.3.8 Real-time PCR analysis of relevant gene in WT, KO and HU

Genes in huPepT1 small intestine						
gene	#1	#2	#3	#4	#5	#6
BPHL	47.02	55.28	69.78	46.82		
$B^{0,+}$	124.53	121.43	214.82	82.68		
OAT1	0.94	0.84	14.43	12.37		
OAT2	0.04	0.04	2.72	2.63		
OAT3	0.19	0.10	8.74	8.47		
PAT1	92.14	63.13	79.33	71.08		
OCT1	50.88	41.79	85.40	51.70		
MATE1	0.08	0.07	2.52	2.09		
MATE2	47.02	55.28	69.78	46.82		

Genes in wildtype small intestine						
gene	#1	#2	#3	#4	#5	#6
BPHL	55.63	61.72	50.83	52.63	54.86	47.10
$B^{0,+}$	216.42	214.93	213.44	164.02	429.86	180.73
OAT1	1.93	2.04	5.85	2.51	3.62	0.97
OAT2	0.44	0.53	3.70	0.99	0.99	0.39
OAT3	0.76	1.14	5.13	2.01	4.25	0.64
PAT1	96.18	180.73	0.00	117.60	184.53	68.96
OCT1	99.58	134.15	123.44	148.85	157.34	172.17
MATE1	1.02	0.92	4.52	1.98	3.97	0.79
MATE2	55.63	61.72	50.83	52.63	54.86	47.10

Genes in mPepT1 KO small intestine						
gene	#1	#2	#3	#4	#5	#6
BPHL	51.19	34.96	39.61	46.78	37.73	46.45
$B^{0,+}$	174.58	52.26	129.58	136.02	114.38	200.54
OAT1	1.38	1.55	2.05	0.88	1.89	2.04
OAT2	0.23	0.23	0.31	0.15	0.27	0.19
OAT3	0.92	0.89	1.01	0.29	1.12	1.02
PAT1	84.90	136.02	153.03	250.33	136.02	222.51
OCT1	73.40	98.20	147.82	158.43	115.18	157.34
MATE1	0.83	1.48	1.34	0.62	0.98	1.15
MATE2	51.19	34.96	39.61	46.78	37.73	46.45
Gene in huPepT1 Large Intestine						
gene	#1	#2	#3	#4	#5	#6
BPHL	194.17	153.86	135.81	75.34		

$B^{0,+}$	2762.03	2701.44	2906.79	1320.72		
OAT1	0.56	0.77	3.60	3.40		
OAT2	0.36	0.07	0.58	0.60		
OAT3	0.53	0.32	8.55	8.25		
PAT1	97.07	135.28	27.81	38.59		
OCT1	22.00	18.16	4.91	4.59		
MATE1	0.30	0.03	2.61	2.04		
MATE2	194.17	153.86	135.81	75.34		

Genes in WT Large Intestine						
gene	#1	#2	#3	#4	#5	#6
BPHL	89.74	65.24	81.44	66.61	43.95	54.11
$B^{0,+}$	2300.47	1549.63	2973.02	1008.30	1174.40	1367.87
OAT1	1.19	1.43	1.14	1.37	0.62	0.97
OAT2	0.24	0.24	0.16	0.15	0.06	0.13
OAT3	1.12	0.59	0.44	0.46	0.04	0.17
PAT1	37.73	76.52	47.10	19.67	14.70	21.82
OCT1	0.64	1.03	0.77	3.80	0.24	0.81
MATE1	0.40	0.58	0.14	0.22	0.04	0.05
MATE2	89.74	65.24	81.44	66.61	43.95	54.11
Genes in mPepT1 KO Large Intestine						
gene	#1	#2	#3	#4	#5	#6
BPHL	78.13	77.59	90.37	37.21	75.99	44.56
$B^{0,+}$	1743.43	2268.80	2332.58	915.05	1615.44	1321.27
OAT1	0.78	1.23	1.14	0.55	0.65	0.72
OAT2	0.14	0.17	0.14	0.04	0.13	0.02
OAT3	0.15	1.49	0.37	0.11	0.18	0.14

PAT1	36.70	29.20	47.43	16.77	29.20	9.97
OCT1	2.13	1.41	0.79	0.67	2.51	0.88
MATE1	0.25	0.66	0.24	0.07	0.04	0.02
MATE2	78.13	77.59	90.37	37.21	75.99	44.56

Genes in huPepT1 Kidney						
gene	#1	#2	#3	#4	#5	#6
BPHL	831.35	719.83	1432.00	879.85		
$B^{0,+}$	164.68	88.24	751.18	336.86		
OAT1	929.18	803.59	1806.66	1340.09		
OAT2	260.03	159.42	592.64	479.84		
OAT3	2853.10	2630.30	2438.39	1750.82		
PAT1	501.92	584.52	1930.30	1118.47		
OCT1	644.58	649.87	2513.55	2112.47		
MATE1	831.35	719.83	1432.00	879.85		
MATE2	164.68	88.24	751.18	336.86		
Genes in wildtype Kidney						
gene	#1	#2	#3	#4	#5	#6
BPHL	717.94	774.82	633.72	486.98	467.14	555.53
$B^{0,+}$	138.88	128.69	143.78	137.92	84.31	102.37
OAT1	1182.57	1029.49	1339.72	953.91	1166.29	1830.11
OAT2	328.04	129.58	72.39	37.73	236.83	124.30
OAT3	2891.72	3142.53	4292.83	3208.56	1111.05	1250.00
PAT1	1051.12	733.02	708.05	651.54	451.23	268.30
OCT1	2030.63	1036.65	1158.24	1150.23	1199.08	1051.12
MATE1	0.71	0.09	0.35	0.48	0.31	0.10
MATE2	717.94	774.82	633.72	486.98	467.14	555.53

Genes in mPepT1 KO Kidney						
gene	#1	#2	#3	#4	#5	#6
BPHL	1073.21	807.72	529.22	642.57	651.54	1073.21
$B^{0,+}$	48.09	89.12	32.40	78.67	93.55	48.09
OAT1	2431.64	2348.81	3035.49	2222.11	2316.47	2431.64
OAT2	127.80	105.25	89.74	166.31	275.84	127.80
OAT3	1649.38	1707.55	2517.39	1894.65	1731.39	1649.38
PAT1	780.21	764.15	1051.12	339.60	387.41	780.21
OCT1	1907.82	1842.84	2087.72	973.96	1294.08	1907.82
MATE1	0.17	0.11	0.14	0.01	0.23	0.17
MATE2	1073.21	807.72	529.22	642.57	651.54	1073.21

Appendix B: Individual data from Chapter IV

Table B.4.1 *In Situ* Perfusion studies with GlySar in intestinal segments

Permeability in huPepT1 (10^{-4}, cm/sec)						
Tissue	#1	#2	#3	#4	#5	#6
Duo	1.209	1.305	1.016	0.969		
Jej	1.487	1.478	1.314	1.351	1.052	1.299
Ile	0.602	0.728	0.523	0.757		
Colon	0.188	0.113	0.120	0.266	0.170	

Permeability in Wildtype (10^{-4}, cm/sec)						
Tissue	#1	#2	#3	#4	#5	#6
Duo	1.512	1.557	1.512	1.763		
Jej	2.283	2.261	1.827	2.144		
Ile	1.630	1.224	0.968	0.994		
Colon	0.008	0.005	0.003	0.046	0.015	

Permeability in mPepT1 KO (10^{-4}, cm/sec)						
Tissue	#1	#2	#3	#4	#5	#6
Duo	0.0100	0.0170	0.0042	0.0042		
Jej	0.0144	0.0616	0.0811	0.0155		
Ile	0.0012	0.0010	0.0012	0.0087		
Colon	0.0008	0.0011	0.0009	0.0018		

Table B.4.2 Concentration-dependent flux of GlySar by *in situ* jejunal Perfusion studies in huPepT1 and Wildtype mice

Flux of GlySar in huPEPT1 Jejunum (nmol/cm^2/sec)						
Conc. (mM, Cin)	#1	#2	#3	#4	#5	#6
0.010	0.00149	0.00148	0.00131	0.00135	0.00105	0.00130
0.100	0.00900	0.00740	0.00851	0.00632		
0.250	0.03220	0.01680	0.00729	0.02223		
0.500	0.04360	0.05300	0.02177	0.04080		
1.000	0.06240	0.10800	0.09685	0.08607		
2.500	0.15640	0.16760	0.24178	0.14849		
5.000	0.43440	0.43420	0.26197	0.21715		
10.000	0.35960	0.44220	0.50230	0.45306		
25.000	0.32340	0.25640	0.51148	0.56380		

Flux of GlySar in Wildtype Jejunum (nmol/cm^2/sec)						
Concentration (mM, Cin)	#1	#2	#3	#4	#5	#6
0.010	0.00228	0.00226	0.00183	0.00214		
0.100	0.01820	0.01840	0.02090	0.01130		
0.250	0.07120	0.06340	0.05720	0.04030		
0.500	0.12660	0.11580	0.13218	0.06072		
1.000	0.22920	0.18740	0.23420	0.22230		
2.500	0.54300	0.70520	0.36100	0.34690		
5.000	1.10380	1.15360	1.17630	0.95370		
10.000	1.68710	1.63220	1.47870	1.54200		
25.000	2.43900	2.62960	2.39560	2.75710		

Table B.4.3 Plasma concentration of GlySar after oral administration (μM)

	huPepT1			**Wildtype**			**mPepT1 KO**		
Time(hour)	#1	#2	#3	#1	#2	#3	#1	#2	#3
0.08	1.392	1.432	0.929	0.965	0.904	0.947	0.153	0.134	0.181
0.13	2.204	2.340	1.505	2.151	1.780	1.605	0.580	0.339	0.684
0.25	2.820	2.680	2.950	2.881	2.577	2.609	0.832	0.808	0.927
0.50	2.947	2.545	2.870	2.682	2.424	2.666	0.993	1.160	0.909
0.75	2.732	2.433	2.541	2.623	2.405	2.441	1.010	1.114	1.022
1.00	2.600	2.306	2.360	2.487	2.306	2.482	1.054	1.191	1.104
1.50	2.452	2.475	2.302	2.192	2.321	2.377	1.159	1.176	1.115
2.00	2.317	2.252	1.889	2.066	2.394	2.311	1.133	1.321	1.327
3.00	2.113	1.787	1.544	1.968	2.128	1.816	1.082	1.303	1.207
4.00	1.755	1.790	1.355	1.791	1.967	1.660	1.108	1.237	1.089
6.00	1.528	1.624	1.206	1.648	1.827	1.599	0.986	1.187	1.041

Appendix C: Individual data from Chapter V

Table C.5.1 Concentration dependent flux of cefadroxil in jejunal perfusions (nmol/cm^2/sec)

	huPepT1				**Wildtype**			
Conc. (mM, C_{in})	#1	#2	#3	#4	#1	#2	#3	#4
0.010	0.10116	0.00021	0.00023	0.00014	0.00066	0.00052	0.00052	0.00076
0.100	0.00126	0.00103	0.00192	0.00137	0.00605	0.00596	0.00695	0.00616
0.250	0.00144	0.00131	0.00697	0.00504	0.01476	0.02145	0.01929	0.01464
0.500	0.00587	0.00721	0.00735	0.00599	0.03573	0.02826	0.04949	0.03001
1.000	0.02341	0.01904	0.01445	0.02310	0.05942	0.04297	0.04927	0.08165
1.750	0.01524	0.03328	0.02317	0.02028	0.12942	0.07031	0.09029	0.07369
2.500	0.01584	0.02809	0.01830	0.02071	0.11955	0.12015	0.08802	0.12839
3.750	0.04411	0.05078	0.05502	0.02954	0.11331	0.13552	0.21789	0.13559
5.000	0.03115	0.00751	0.04362	0.02182	0.15881	0.12823	0.24983	0.18129
7.500	0.01223	0.04102	0.03822	0.06740	0.20729	0.22210	0.27674	0.20685
10.000	0.04894	0.04433	0.07574	0.03469	0.17313	0.24420	0.24660	0.28832
17.500	0.01223	0.04102	0.06726	0.07080	0.29207	0.26860	0.29124	0.37721
25.000	0.03146	0.06318	0.05079	0.05749	0.29071	0.25861	0.32014	0.43816

Table C.5.2 Effective permeability of cefadroxil in intestinal perfusions ($x10^{-4}$,cm/sec)

	huPepT1				**Wildtype**				**mPepT1 KO**			
	#1	#2	#3	#4	#1	#2	#3	#4	#1	#2	#3	#4
Duodenum	0.148	0.338	0.216	0.251	0.447	0.622	0.759	0.385	0.004	0.001	0.002	0.002
Jejunum	0.101	0.208	0.233	0.141	0.658	0.518	0.523	0.762	0.005	0.028	0.001	0.008
Ileum	0.118	0.096	0.141	0.126	0.196	0.320	0.369	0.278	0.002	0.001	0.002	0.004
Colon	0.067	0.079	0.027	0.046	0.000	0.007	0.009	0.001	0.001	0.003	0.005	0.002

Table C.5.3 Substrate specificity of cefadroxil in jejunal perfusions ($x10^{-4}$,cm/sec)

	Control	**GlyPro**	**GlyGlyHis**	**Glycine**	**L-Histidine**	**Probenecid**	**Quinidine**
#1	0.204664	0.002628807	0.04567644	0.1860432	0.1908105	0.1730913	0.191484
#2	0.176511	0.003623258	0.05791553	0.1737148	0.2080944	0.2430571	0.128626
#3	0.217475	0.01525932	0.0122279	0.183770	0.164126	0.1767742	0.260177
	NMN	**Cephalexin**	**Cephalothin**	**Carnosine**	**TEA**	**PAH**	**DMA**
#1	0.1810611	0.05597154	0.1865378	0.04168647	0.1568414	0.157590	0.07851509
#2	0.1647314	0.09567235	0.1799209	0.07425112	0.2349168	0.192994	0.08304737
#3	0.1761521	0.05596873	0.1951328	0.0608801	0.1333012	0.178770	0.09818064

Table C.5.4 Plasma concentration of cefadroxil after IV single dose (μM)

	IV single dose at 11.01 nmol/g BW									
	huPepT1					**Wildtype**				
Time (min)	#1	#2	#3	#4	#5	#1	#2	#3	#4	#5
1.0	55.50	61.43	64.90	81.27	48.26	57.75	101.87	62.39	52.24	
2.5	120.72	128.23	133.58	157.33	104.31	122.12	175.94	130.47	113.59	
5.0	199.98	202.15	209.07	234.96	169.54	193.23	236.44	207.72	185.70	
10.0	300.79	297.52	307.02	344.30	254.41	276.39	321.64	309.19	270.89	
20.0	397.15	408.73	414.05	459.58	347.80	360.65	424.60	422.93	353.61	
30.0	435.10	463.07	465.31	500.39	392.02	401.46	484.11	481.67	398.05	
45.0	460.84	505.48	513.49	531.25	433.10	436.44	536.58	533.48	438.31	
60.0	476.35	534.85	544.68	547.58	458.35	459.05	563.31	565.49	463.72	
90.0	497.80	576.76	580.98	569.03	490.69	487.10	593.67	606.08	501.01	
120.0	513.64	605.14	606.72	585.20	512.14	506.57	611.82	632.48	525.76	

	IV single dose at 528.40 nmol/g BW									
	huPepT1					**Wildtype**				
Time (min)	#1	#2	#3	#4	#5	#1	#2	#3	#4	#5
1.0	2139.75	2473.47	1970.97			1757.08	2350.22	1914.96		
2.5	1426.19	2160.88	1659.34			1347.07	1962.90	1504.01		
5.0	897.66	1380.95	1519.09			995.24	1228.59	827.24		
10.0	456.73	731.85	625.90			622.28	702.65	481.90		
20.0	169.79	265.95	279.88			259.04	346.35	209.66		
30.0	101.01	133.77	136.36			133.32	189.87	126.75		
45.0	46.35	57.01	56.63			59.11	106.20	67.87		
60.0	38.28	41.26	46.64			44.10	69.02	45.58		
90.0	28.39	30.79	30.50			26.99	43.37	31.08		
120.0	27.91	26.95	29.33			27.89	32.04	27.33		

Table C.5.6 Plasma concentration of cefadroxil after oral escalation doses (μM)

	Cefadroxil Oral Dose at 11.01 nmol/g BW													
	huPepT1							**Wildtype**						
Time (min)	#1	#2	#3	#4	#5	#6	#7	#1	#2	#3	#4	#5	#6	#7
2.5	0.28	0.63	1.30	2.12	0.23	0.21	0.24	7.29	5.16	9.97	0.62	2.59	0.65	2.49
5.0	0.59	1.91	5.93	7.46	2.13	1.61	1.50	15.93	11.9	15.26	7.28	11.61	4.24	10.3
10.0	0.76	3.24	10.95	8.43	5.29	3.93	4.35	18.58	15.99	13.49	10.08	14.94	10.76	13.8
20.0	1.00	7.68	8.29	8.33	6.53	5.60	6.58	12.33	8.74	7.23	9.38	9.83	9.8	9.06
30.0	1.14	5.55	4.69	3.94	4.34	3.45	3.99	7.28	7.41	4.49	6	4.64	7.85	6.11
45.0	2.31	1.98	1.87	1.85	2.57	2.91	3.29	4.68	2.64	1.8	3.84	2.82	4.98	3.16
60.0	1.69	0.91	0.90	0.98	1.84	1.74	1.83	3.47	1.4	1.35	2.42	2.53	2.95	1.66
90.0	1.23	0.41	0.48	0.52	0.71	1.00	1.18	1.08	0.7	0.64	1.31	0.87	1.73	1.03
120.0	0.79	0.44	0.46	0.44	0.40	0.54	0.60	0.96	0.57	0.65	0.73	0.53	1.21	0.59

	Cefadroxil Oral Dose at 33.03 nmol/g BW													
	huPepT1							**Wildtype**						
Time (min)	#1	#2	#3	#4	#5	#6	#7	#1	#2	#3	#4	#5	#6	#7
2.5	2.78	2.89	0.74	4.15	0.79			10.82	17.78	6.31	3.28	5.41	3.36	
5.0	9.09	11.59	2.59	16.48	3.14			26.90	29.54	22.78	23.23	25.78	19.69	
10.0	21.11	20.22	4.74	24.82	6.63			39.00	41.83	34.85	29.69	35.63	30.53	
20.0	23.84	23.24	13.53	27.48	10.99			27.55	36.26	27.46	37.97	30.62	32.66	
30.0	12.76	15.87	16.70	18.18	11.02			12.87	24.99	17.18	28.06	19.92	25.59	
45.0	5.72	8.26	15.02	10.74	8.88			10.97	14.44	12.70	20.26	13.63	13.88	
60.0	3.50	5.22	5.17	5.41	5.94			7.65	9.28	8.46	10.44	9.48	10.22	
90.0	2.12	3.09	1.67	1.88	2.95			3.76	7.06	7.11	7.86	4.75	3.73	
120.0	1.80	2.18	1.40	1.06	1.67			2.51	2.74	2.24	5.27	3.83	1.92	

	Cefadroxil Oral Dose at 66.06 nmol/g BW													
	huPepT1							**Wildtype**						
Time (min)	#1	#2	#3	#4	#5	#6	#7	#1	#2	#3	#4	#5	#6	#7
2.5	1.99	6.44	7.21	2.24	1.76	2.13		71.48	47.77	45.21	11.05	16.05	37.55	
5.0	5.72	26.49	23.59	10.52	6.90	8.770001		100.82	95.76	109.07	64.63	50.55	99.09	
10.0	8.32	51.47	50.39	25.65	18.22	25.74		102.98	91.21	103.44	92.06	78.63	85.73	
20.0	14.27	64.22	62.95	30.12	23.50	38.30		52.49	46.55	54.88	45.95	54.90	40.54	
30.0	16.42	46.72	39.40	36.07	28.31	31.33		34.22	27.86	41.32	30.40	33.47	23.38	
45.0	14.85	23.88	21.54	36.50	29.57	29.41		14.35	23.77	38.22	11.90	17.03	11.01	
60.0	13.79	13.18	12.58	23.92	25.39	24.24		8.02	13.10	39.07	7.02	11.58	6.34	
90.0	8.08	7.09	6.43	6.97	10.42	10.66		4.24	5.87	9.53	3.32	5.06	2.95	
120.0	5.32	4.26	4.08	4.00	5.26	7.09		3.65	5.02	7.33	1.76	2.66	2.31	

	Cefadroxil Oral Dose at 132.10 nmol/g BW													
	huPepT1							**Wildtype**						
Time (min)	#1	#2	#3	#4	#5	#6	#7	#1	#2	#3	#4	#5	#6	#7
2.5	6.94	11.25	5.69	6.39	8.89	10.64		107.44	42.15	97.75	29.39	41.25	35.22	
5.0	16.18	41.15	27.63	19.17	46.19	26.55		198.72	153.06	164.46	59.75	60.83	65.99	
10.0	36.42	97.45	95.62	37.44	71.05	51.11		191.32	190.62	181.12	188.82	186.24	166.79	
20.0	50.24	106.08	125.04	59.97	95.80	62.88		140.33	126.58	132.28	132.99	120.80	138.96	
30.0	41.24	57.85	70.19	66.36	69.97	62.52		74.11	65.31	86.80	87.80	88.94	86.49	
45.0	33.34	33.60	37.31	46.86	52.36	48.39		46.49	33.24	51.31	44.39	46.66	43.72	
60.0	28.81	21.04	23.42	28.00	32.00	35.66		28.68	23.51	23.42	23.66	32.50	25.22	
90.0	11.53	8.39	11.13	12.44	13.36	13.64		25.08	9.44	16.74	10.72	7.44	8.55	
120.0	6.65	7.35	9.03	9.30	7.28	6.31		9.71	8.11	8.34	5.33	5.06	10.50	

	Cefadroxil Oral Dose at 264.20 nmol/g BW													
	huPepT1							**Wildtype**						
Time (min)	#1	#2	#3	#4	#5	#6	#7	#1	#2	#3	#4	#5	#6	#7
2.5	15.34	11.89	11.21	23.48	21.36	28.01		66.67	89.70	74.51	61.73	57.97	77.12	
5.0	55.18	39.05	47.28	95.59	74.93	100.49		191.82	228.34	260.22	193.07	213.82	210.69	
10.0	172.81	68.31	107.63	158.17	116.33	195.71		320.04	363.47	408.42	366.06	414.50	419.74	
20.0	221.16	116.24	144.01	187.00	178.59	122.16		210.02	329.09	242.13	317.16	273.55	340.82	
30.0	156.58	107.96	101.47	147.69	139.57	132.87		141.77	262.12	122.41	180.71	181.11	165.00	
45.0	72.66	80.08	58.93	81.20	96.44	119.98		59.13	143.47	48.62	86.85	116.16	80.95	
60.0	41.77	75.19	36.40	35.78	67.26	74.49		54.58	73.14	21.87	46.25	59.38	42.48	
90.0	20.35	23.39	12.07	10.30	31.72	30.72		21.12	36.14	11.74	16.59	19.72	14.59	
120.0	13.35	12.90	13.14	6.83	15.00	12.24		15.16	20.35	11.32	10.94	9.75	9.41	

	Cefadroxil Oral Dose at 528.40 nmol/g BW													
	huPepT1							**Wildtype**						
Time (min)	#1	#2	#3	#4	#5	#6	#7	#1	#2	#3	#4	#5	#6	#7
2.5	16.11	53.02	34.63	26.13	10.81	18.53	23.41	292.35	192.34	176.41	110.70	177.36	152.43	
5.0	28.88	123.39	112.02	99.77	53.67	56.57	69.76	438.53	427.63	449.07	361.31	492.51	353.00	
10.0	48.16	269.09	179.98	227.67	120.26	89.93	151.51	743.71	556.41	714.83	521.72	670.00	579.34	
20.0	65.97	344.38	208.34	356.91	295.77	142.41	300.85	479.36	579.20	647.22	533.52	625.30	563.91	
30.0	93.27	266.16	143.42	303.31	240.58	236.37	309.29	305.65	337.99	515.51	409.96	377.53	387.88	
45.0	92.28	135.86	99.72	192.75	170.43	168.79	146.96	148.99	136.80	282.16	229.97	252.52	241.05	
60.0	75.11	64.68	61.52	104.58	113.53	112.88	127.18	108.27	64.45	143.83	130.35	136.87	137.14	
90.0	27.07	25.54	21.03	38.73	36.33	62.96	66.85	48.51	39.20	71.07	50.31	54.86	46.68	
120.0	24.20	21.91	17.63	24.31	31.58	41.08	41.93	26.13	24.96	40.02	31.05	39.10	40.88	

Appendix D: Species-dependent uptake of glycylsarcosine but not oseltamivir in *Pichia Pastoris* expressing rat, mouse, and human intestinal peptide transporter PEPT1

1521-009X/12/4007-1328–1335$25.00
DRUG METABOLISM AND DISPOSITION
Vol. 40, No. 7
44263/3776489
DMD 40:1328–1335, 2012

DRUG METABOLISM & DISPOSITION

Species-Dependent Uptake of Glycylsarcosine but Not Oseltamivir in *Pichia pastoris* Expressing the Rat, Mouse, and Human Intestinal Peptide Transporter PEPT1

Yongjun Hu, Xiaomei Chen, and David E. Smith

Department of Pharmaceutical Sciences, College of Pharmacy, University of Michigan, Ann Arbor, Michigan

Received February 9, 2012; accepted April 9, 2012

ABSTRACT:

The purpose of this study was to determine whether glycylsarcosine (a model dipeptide) and oseltamivir (an antiviral prodrug) exhibited a species-dependent uptake in yeast *Pichia pastoris* expressing the rat, mouse, and human homologs of PEPT1. Experiments were performed with [^{3}H]glycylsarcosine (GlySar) in yeast *P. pastoris* expressing human, mouse, and rat peptide transporter 1 (PEPT1), in which uptake was examined as a function of time, concentration, potential inhibitors, and the dose-response inhibition of GlySar by oseltamivir. Studies with [^{14}C]oseltamivir were also performed under identical experimental conditions. We found that GlySar exhibited saturable uptake in all three species, with K_m values for human (0.86 mM) > mouse (0.30 mM) > rat (0.16 mM). GlySar uptake in the yeast transformants was specific for peptides (glycylproline) and peptide-like drugs (cefadroxil, cephradine, and valacyclovir), but was unaffected by glycine, L-histidine, cefazolin, cephalothin, cephapirin, acyclovir, 4-acetamido-4′-isothiocyanostilbene-2,2′-disulfonic acid, tetraethylammonium, and elacridar. Although oseltamivir caused a dose-dependent inhibition of GlySar uptake [IC_{50} values for human (27.4 mM) > rat (18.3 mM) > mouse (10.7 mM)], the clinical relevance of this interaction would be very low in humans. Of importance, oseltamivir was not a substrate for the intestinal PEPT1 transporter in yeast expressing the three mammalian species tested. Instead, the prodrug exhibited nonspecific binding to the yeast vector and PEPT1 transformants. Finally, the mouse appeared to be a better animal model than the rat for exploring the intestinal absorption and pharmacokinetics of peptides and peptide-like drugs in human.

Introduction

Oseltamivir phosphate (Tamiflu), an ethyl ester prodrug of the active metabolite Ro 64-0802 (oseltamivir carboxylate), is used for the treatment and prophylaxis of influenza A or B in adults and children ≥1 year of age (Moscona, 2005; Davies 2010). The prodrug is well absorbed (75–80%) from the gastrointestinal tract and is efficiently converted by human liver carboxylesterase 1 to Ro 64-0802 (Shi et al., 2006). This drug moiety acts as a potent neuraminidase inhibitor, thereby preventing the release of virions from infected host cells and viral replication. Oseltamivir has dose-proportional absorption and a linear pharmacokinetic profile with respect to the active metabolite. Ro 64-0802 accumulates less than 2-fold after oral dosing of oseltamivir over a dose range of 50 to 500 mg twice daily. The pharmacokinetics of both oseltamivir and oseltamivir carboxylate are seemingly uncomplicated because of low protein binding (i.e., 42% for prodrug and 3% for active metabolite), a lack of cytochrome P450 interactions, and no other metabolic species being formed (He et al., 1999; Dutkowski et al., 2003). Renal clearance of both compounds exceeds their filtration clearance because of active tubular secretion via the organic anionic pathway (Hill et al., 2002). However, this mechanism has low potential for drug-drug interactions given the weak affinity of Ro 64-0802 for human OAT1 (K_i of 45.1 mM).

Oseltamivir has a good safety record in which the most common side effects are transient nausea, vomiting, and abdominal pain, which occur in approximately 5 to 10% of the patient population (Moscona, 2005). More recently, however, there have been postmarketing reports (mostly from Japan) of neuropsychiatric side effects in younger patients taking oseltamivir, in some cases resulting in fatal outcomes (http://www.gene.com/gene/products/information/tamiflu/pdf/pi.pdf). This finding has led to a number of studies evaluating the mechanism by which oseltamivir and oseltamivir carboxylate are transported across capillary endothelial cells forming the blood-brain barrier (Morimoto et al., 2008; Ose et al., 2008, 2009). It was demonstrated that oseltamivir and its active metabolite were actively effluxed by luminally expressed P-glycoprotein (Pgp) and multidrug resistance-associated protein 4, respectively, thereby limiting their penetration in brain. The mechanism by which prodrug and active metabolite could enter the brain was uncertain but, at least for Ro 64-0802, may be related to the expression of organic anion transporter 3 on both luminal and abluminal membranes of capillary endothelia. Moreover,

This work was supported by the National Institutes of Health National Institute of General Medical Sciences [Grant R01-GM035498] (to D.E.S.).

D.E.S. was a consultant for Roche (Basel, Switzerland).

Article, publication date, and citation information can be found at http://dmd.aspetjournals.org.

http://dx.doi.org/10.1124/dmd.111.044263.

ABBREVIATIONS: Pgp, P-glycoprotein; PEPT1, peptide transporter 1; PEG, polyethylene glycol; GlySar, glycylsarcosine; PCR, polymerase chain reaction; PPB, potassium phosphate buffer, pH 6.5; YNB, yeast nitrogen base; GlyPro, glyclyproline; SITS, 4-acetamido-4′-isothiocyanostilbene-2,2′-disulfonic acid; TEA, tetraethylammonium; h, human; m, mouse; r, rat; AUC, area under the plasma concentration-time curve.

Appendix E: Divergent developmental expression and function of the proton-coupled oligopeptide transporters PepT2 and PhT1 in regional brain slices of mouse and rat.

Journal of Neurochemistry JNC

JOURNAL OF NEUROCHEMISTRY | 2014 | 129 | 955–965 doi: 10.1111/jnc.12687

ORIGINAL ARTICLE

Divergent developmental expression and function of the proton-coupled oligopeptide transporters PepT2 and PhT1 in regional brain slices of mouse and rat

Yongjun Hu,* Yehua Xie,* Richard F. Keep† and David E. Smith*

**Department of Pharmaceutical Sciences, College of Pharmacy, University of Michigan, Ann Arbor, MI, USA*

†*Departments of Neurosurgery and Physiology, Medical School, University of Michigan, Ann Arbor, MI, USA*

Abstract

This study evaluated the developmental gene and protein expression of proton-coupled oligopeptide transporters (POTs: peptide transporter, PepT1 and PepT2; peptide-histidine transporter, PhT1 and PhT2) in different regions of rodent brain, and the age-dependent uptake of a POT substrate, glycylsarcosine (GlySar), in brain slices. Slices were obtained from cerebral cortex, cerebellum and hippocampus of wildtype and PepT2 null mice, and from rats at different ages. Gene and protein expression were determined by real-time PCR and immunoblot analyses. Brain slice uptakes of radiolabeled glycylsarcosine were determined in the absence and presence of excess unlabeled glycylsarcosine or L-histidine, the latter being an inhibitor of PhT1/2 but not PepT1/2. As PepT2 and PhT1 transcripts were abundantly expressed in all three regions of mouse brain, little to no expression was observed for PepT1 and PhT2. PhT1 protein was present in brain regions of adult but not neonatal mice and expression levels increased with age in rats. Glycylsarcosine uptake, inhibition and transporter dominance did not show regional brain or species differences. However, there were clear age-related differences in functional activity, with PepT2 dominating in neonatal mice and rats, and PhT1 dominating in adult rodents. These developmental changes may markedly impact the neural activity of both endogenous and exogenous (drug) peptides/mimetics.

Keywords: brain, development, expression, function, PepT2, PhT1.

J. Neurochem. (2014) **129**, 955 965.

The activity of small peptides and peptide-like drugs in brain is tightly regulated by mechanisms controlling their concentration in the interstitial fluid. Mechanisms may include the synthesis and release of peptides/mimetics from brain parenchyma, entry and/or efflux via the blood-brain and blood-cerebrospinal fluid barriers, degradation by membrane-bound or intracellular enzymes and uptake into glial and neuronal cells (Keep and Smith 2013). A number of studies have investigated the role of specific oligopeptide transporters in regulating peptide/mimetic transport in the brain and, in particular, at the apical interface of the blood-CSF barrier (i.e., CSF-facing side of the choroid plexus) (Smith *et al.* 2004). However, few studies have evaluated whether or not differences exist in the transporter-mediated disposition of peptides/mimetics in various regions of the brain (Smith *et al.* 2011).

The proton-coupled oligopeptide transporter (POT) family is phylogenetically conserved and its members serve as integral membrane proteins in the cellular uptake of di/tripeptides and some pharmacologically active drugs (Wang *et al.* 2010; Smith *et al.* 2013). This family consists of four mammalian carriers, of which three are expressed in brain. PepT2 (SLC15A2), a low-capacity high-affinity carrier, is

Received November 18, 2013; revised manuscript received January 26, 2014; accepted February 13, 2014.

Address correspondence and reprint requests to Dr. David E. Smith, Department of Pharmaceutical Sciences, University of Michigan, 4742C Medical Sciences II, 1150 W. Medical Center Drive, Ann Arbor, MI 48109-5633, USA. E-mail: smithb@umich.edu

Abbreviations used: 5-ALA, 5-aminolevulinic acid; COS7, monkey kidney fibroblast-like cell line; GlySar, glycylsarcosine; HEK293T, human embryonic kidney cell line; NOD1, nucleotide-binding oligomerization domain-containing protein 1; PhT(s), peptide-histidine transporter(s); POT(s), proton-coupled oligopeptide transporter(s); RAW264.7, murine macrophage-like cell line; Slc, solute carrier family; TLR9, toll-like receptor 9.

Appendix F: Development and characterization of a novel mouse line humanized for the intestinal peptide transporter PEPT1

molecular pharmaceutics

Article

pubs.acs.org/molecularpharmaceutics

Development and Characterization of a Novel Mouse Line Humanized for the Intestinal Peptide Transporter *PEPT1*

Yongjun Hu,[†] Yehua Xie,[†] Yuqing Wang,[‡] Xiaomei Chen,[†] and David E. Smith*[,†]

[†]Department of Pharmaceutical Sciences, College of Pharmacy, University of Michigan, Ann Arbor, Michigan 48109, United States
[‡]College of Pharmaceutical Sciences, Zhejiang University, Hangzhou 310058, P. R. China

ABSTRACT: The proton-coupled oligopeptide transporter PEPT1 (SLC15A1) is abundantly expressed in the small intestine, but not colon, of mammals and found to mediate the uptake of di/tripeptides and peptide-like drugs from the intestinal lumen. However, species differences have been observed in both the expression (and localization) of PEPT1 and its substrate affinity. With this in mind, the objectives of this study were to develop a humanized *PEPT1* mouse model (*huPEPT1*) and to characterize hPEPT1 expression and functional activity in the intestines. Thus, after generating *huPEPT1* mice in animals previously nulled for mouse *Pept1*, phenotypic, PCR, and immunoblot analyses were performed, along with *in situ* single-pass intestinal perfusion and *in vivo* oral pharmacokinetic studies with a model dipeptide, glycylsarcosine (GlySar). Overall, the *huPEPT1* mice had normal survival rates, fertility, litter size, gender distribution, and body weight. There was no obvious behavioral or pathological phenotype. The mRNA and protein profiles indicated that *huPEPT1* mice had substantial PEPT1 expression in all regions of the small intestine (i.e., duodenum, jejunum, and ileum) along with low but measurable expression in both proximal and distal segments of the colon. In agreement with PEPT1 expression, the *in situ* permeability of GlySar in *huPEPT1* mice was similar to but lower than wildtype animals in small intestine, and greater than wildtype mice in colon. However, a species difference existed in the *in situ* transport kinetics of jejunal PEPT1, in which the maximal flux and Michaelis constant of GlySar were reduced 7-fold and 2- to 4-fold, respectively, in *huPEPT1* compared to wildtype mice. Still, the *in vivo* function of intestinal PEPT1 appeared fully restored (compared to *Pept1* knockout mice) as indicated by the nearly identical pharmacokinetics and plasma concentration−time profiles following a 5.0 nmol/g oral dose of GlySar to *huPEPT1* and wildtype mice. This study reports, for the first time, the development and characterization of mice humanized for *PEPT1*. This novel transgenic *huPEPT1* mouse model should prove useful in examining the role, relevance, and regulation of PEPT1 in diet and disease, and in the drug discovery process.

KEYWORDS: *PEPT1, humanized mice, mRNA and protein expression, glycylsarcosine, in situ intestinal perfusions, in vivo oral pharmacokinetics*

INTRODUCTION

Mammalian PEPT1 (SLC15A1), along with PEPT2 (SLC15A2), PHT1 (SLC15A4) and PHT2 (SLC15A3), belong to the solute carrier group of membrane transport proteins (i.e., SLC15) that mediate the cellular uptake of di- and tripeptides in addition to several peptidomimetic drugs. Following discovery of rabbit Pept1,[1] the human and mouse orthologues were cloned (85% amino acid identity)[2,3] in which they contained 708 and 709 amino acid residues, respectively. These Pept1 transporters have 12 transmembrane domains, C- and N-termini facing the cytoplasm, and Tyr12, His57, Tyr64, Trp294, Phe297, and Glu595 residues located within highly conserved transmembrane domains (H1, H2, H5, H7, and H10).[4]

In contrast to PEPT2, a high-affinity low-capacity transporter primarily responsible for the reabsorption of peptides/mimetics in kidney,[5] PEPT1 is a low-affinity high-capacity transporter that is important in the absorption of digested peptides (mostly di- and tripeptides) from dietary protein in the small intestine. PEPT1 is also crucial for the intestinal uptake and absorption of therapeutic drugs such as the β-lactam antibiotic cefadroxil[6] and the antiviral nucleoside prodrug valacyclovir.[7] Previous studies using polymerase chain reaction (PCR) and immunoblot analyses have demonstrated that in rodents and humans PEPT1 is abundantly expressed in the apical membrane of enterocytes in duodenal, jejunal, and ileal regions.[8−11] The expression of PEPT1 in colon is controversial and perhaps species dependent. Nevertheless, under normal conditions, PEPT1 is unlikely to have much impact on the absorption of peptides/mimetics from this region.

Species differences in PEPT1 expression and functional activity have been reported in mouse and human colonic tissue.[11,12] Moreover, our laboratory demonstrated *in vivo* that both cefadroxil[6] and valacyclovir[7] exhibited dose-proportional absorption in wildtype and *Pept1* knockout mice after oral dose escalation. The "apparent" dose linearity observed in these mouse studies is contrary to the nonlinear intestinal absorption kinetics reported in rats and humans for cefadroxil[13,14] and in humans for valacyclovir.[15] Interspecies differences in transporter-mediated activity are difficult to sort out given that

Received: July 22, 2014
Revised: August 15, 2014
Accepted: August 22, 2014
Published: August 22, 2014

Appendix G: Impact of peptide transporter 1 on the intestinal absorption and pharmacokinetics of valacyclovir after oral dose escalation in wild-type and PepT1 knockout mice

1521-009X/41/10/1867–1874$25.00
DRUG METABOLISM AND DISPOSITION
http://dx.doi.org/10.1124/dmd.113.052597
Drug Metab Dispos 41:1867–1874, October 2013

DRUG METABOLISM & DISPOSITION

Impact of Peptide Transporter 1 on the Intestinal Absorption and Pharmacokinetics of Valacyclovir after Oral Dose Escalation in Wild-Type and *PepT1* Knockout Mice

Bei Yang, Yongjun Hu, and David E. Smith

Department of Pharmaceutical Sciences, College of Pharmacy, University of Michigan, Ann Arbor, Michigan

Received April 26, 2013; accepted August 7, 2013

ABSTRACT

The primary objective of this study was to determine the in vivo absorption properties of valacyclovir, including the potential for saturable proton-coupled oligopeptide transporter 1 (PepT1)-mediated intestinal uptake, after escalating oral doses of prodrug within the clinical dose range. A secondary aim was to characterize the role of PepT1 on the tissue distribution of its active metabolite, acyclovir. [^{3}H]Valacyclovir was administered to wild-type (WT) and *PepT1* knockout (KO) mice by oral gavage at doses of 10, 25, 50, and 100 nmol/g. Serial blood samples were collected over 180 minutes, and tissue distribution studies were performed 20 minutes after a 25-nmol/g oral dose of valacyclovir. We found that the C_{max} and area under the curve $(AUC)_{0-180}$ of acyclovir were 4- to 6-fold and 2- to 3-fold lower, respectively, in KO mice for all four oral doses of valacyclovir. The time to peak concentration of acyclovir was 3- to 10-fold longer in KO compared with WT mice. There was dose proportionality in the C_{max} and AUC_{0-180} of acyclovir in WT and KO mice over the valacyclovir oral dose range of 10–100 nmol/g (i.e., linear absorption kinetics). No differences were observed in the peripheral tissue distribution of acyclovir once these tissues were adjusted for differences in perfusing drug concentrations in the systemic circulation. In contrast, some differences were observed between genotypes in the concentrations of acyclovir in the distal intestine. Collectively, the findings demonstrate a critical role of intestinal PepT1 in improving the rate and extent of oral absorption for valacyclovir. Moreover, this study provides definitive evidence for the rational development of a PepT1-targeted prodrug strategy.

Introduction

Proton-coupled oligopeptide transporter 1 (PepT1, solute carrier 15A1), a member of the proton-coupled oligopeptide transporter family, is a highly conserved influx transporter that is expressed in several mammalian species, including human, rat, and mouse (Brandsch et al., 2008; Rubio-Aliaga and Daniel, 2008; Smith et al., 2013). The mammalian PepT1, comprising 707–710 amino acid residues, depending on species, has 12 transmembrane domains with both the N and C termini facing the cytosolic side. PepT1 couples the influx of substrate with a proton in which the inwardly-directed proton gradient and negative membrane potential are driving forces for the uphill movement of substrate. As a high-capacity, low-affinity influx transporter, PepT1 is located principally on the brush-border membrane of epithelial cells in the small intestine and functions as the active uptake carrier of dipeptides and tripeptides generated by the digestion of dietary proteins. Since approximately 80% of digested proteins are absorbed in the form of dipeptides or tripeptides, as opposed to free amino acids, PepT1 plays an essential physiologic role in protein assimilation (Ganapathy et al., 2006).

The pharmacological relevance of PepT1 lies mainly in its ability to transport a wide spectrum of drugs from some important therapeutic classes (Brandsch et al., 2008; Rubio-Aliaga and Daniel, 2008; Tsume et al., 2008). For example, many β-lactam antibiotics (e.g., oral cephalosporin and penicillin drugs) and some angiotensin-converting enzyme inhibitors (e.g., captopril and enalapril) are known substrates of PepT1. Moreover, a number of amino acids or dipeptide-conjugated prodrugs (e.g., midodrine, valacyclovir, valganciclovir, and 5′-L-phenylalanyl-L-glycyl-floxuridine) undergo PepT1-mediated transport. Prodrugs of this type are commonly referred to as PepT1-targeted prodrugs, an area of research that is under intense investigation as a promising strategy to improve the oral availability of polar, hydrophilic compounds (Varma et al., 2010).

Valacyclovir is widely viewed as the model of PepT1-targeted prodrugs. Valacyclovir, an L-valyl ester prodrug of the potent antiviral agent acyclovir, is used for the treatment and prophylaxis of herpes, varicella zoster, and cytomegalovirus infection. In humans, the systemic availability of acyclovir, after oral administration of valacyclovir, is nearly 55%, as opposed to only 10% to 20% after oral dosing of acyclovir (Soul-Lawton et al., 1995). However, the uptake and pharmacokinetic properties of valacyclovir have shown some inconsistent or even controversial findings. On the one hand, numerous cell culture studies demonstrated the PepT1-mediated uptake of valacyclovir into cells constitutively expressing or transfected with PepT1 (Balimane et al., 1998; Ganapathy et al., 1998; Han et al., 1998; Guo et al., 1999; Balimane and Sinko, 2000). On the other hand, valacyclovir was also found to interact with other transporters such as human organic anion transporter 3 (Takeda et al., 2002), human peptide histidine transporter 1 (Bhardwaj et al., 2006), rat organic cation transporters (Sinko and Balimane, 1998), a human peptide

This work was supported by the National Institutes of Health National Institute of General Medical Sciences [Grant R01-GM035498] (to D.E.S.).
dx.doi.org/10.1124/dmd.113.052597.

ABBREVIATIONS: AUC, area under the curve; GI, gastrointestinal; HPLC, high-performance liquid chromatography; KO, *PepT1* knockout mice; PepT1, proton-coupled oligopeptide transporter 1; WT, wild-type mice.

Appendix H: Corticosterone mediates stress-related increased intestinal permeability in a region-specific manner

Neurogastroenterology & Motility

Neurogastroenterol Motil (2013) **25**, e127–e139 doi: 10.1111/nmo.12066

Corticosterone mediates stress-related increased intestinal permeability in a region-specific manner

G. ZHENG,* S.-P. WU,† Y. HU,† D. E. SMITH,† J. W. WILEY* & S. HONG*

*Department of Internal Medicine, University of Michigan, Ann Arbor, MI, USA
†Department of Pharmaceutical Sciences, University of Michigan, Ann Arbor, MI, USA

Abstract

Background *Chronic psychological stress (CPS) is associated with increased intestinal epithelial permeability and visceral hyperalgesia. It is unknown whether corticosterone (CORT) plays a role in mediating alterations of epithelial permeability in response to CPS.* ***Methods*** *Male rats were subjected to 1-h water avoidance (WA) stress or subcutaneous CORT injection daily for 10 consecutive days in the presence or absence of corticoid receptor antagonist RU-486. The visceromotor response (VMR) to colorectal distension (CRD) was measured. The in situ single-pass intestinal perfusion was used to measure intestinal permeability in jejunum and colon simultaneously.* ***Key Results*** *We observed significant decreases in the levels of glucocorticoid receptor (GR) and tight junction proteins in the colon, but not the jejunum in stressed rats. These changes were largely reproduced by serial CORT injections in control rats and were significantly reversed by RU-486. Stressed and CORT-injected rats demonstrated a threefold increase in permeability for PEG-400 (MW) in colon, but not jejunum and significant increase in VMR to CRD, which was significantly reversed by RU-486. In addition, no differences in permeability to PEG-4000 and PEG-35 000 were detected between control and WA groups.* ***Conclusions & Inferences*** *Our findings indicate that CPS was associated with region-specific decrease in epithelial tight junction protein levels in the colon, increased colon epithelial permeability to low molecular weight macromolecules which were largely reproduced by CORT treatment in control rats and prevented by RU-486. These observations implicate a novel, region-specific role for CORT as a mediator of CPS-induced increased permeability to macromolecules across the colon epithelium.*

Keywords *chronic stress, corticosterone, epithelial permeability, region specificity, tight junction proteins.*

Abbreviations: CPS, Chronic psychological stress; CORT, corticosterone; CRF, corticotropin releasing factor; GR, glucocorticoid receptor; HPA, hypothalamic-pituitary-adrenal; IBS, Irritable Bowel Syndrome; PEG, polyethylene glycol; WA, water avoidance; ZO-1, zona occludens-1.

Address for Correspondence
Shuangsong Hong, Department of Internal Medicine, University of Michigan, 1150 W. Medical Center Dr., MSRB III, Room 9315, Ann Arbor, MI 48109, USA.
Tel: 1 734-615-6621; fax: 1 734-763-2535,
e-mail: hongss@med.umich.edu
Received: 3 July 2012
Accepted for publication: 15 November 2012

INTRODUCTION

The intestinal epithelial barrier regulates transport and host defense mechanisms at the mucosal interface with the outside environment to maintain gut homeostasis. Increased gut permeability and defects in intestinal barrier function are associated with several functional gastrointestinal disorders such as irritable bowel syndrome (IBS).[1] Studies using urine excretion showed increased intestinal permeability to ^{50}Cr-EDTA and low molecule polyethylene glycol (PEG-400) in patients with IBS.[2,3] More recently, Rao *et al.*[4] reported that both small bowel and colon permeability were increased in IBS patients with diarrhea by measuring saccharides lactulose and mannitol secretion in urine collections. Another study using intestinal biopsies in Ussing chambers demonstrated that colonic paracellular permeability to sulfonic acid was significantly increased in IBS patients regardless of IBS subtype.[5]

Chronic psychological stress (CPS) activates the hypothalamic-pituitary-adrenal (HPA) axis that affects various physiologic functions of the gastrointestinal tract including visceral sensitivity, gut permeability,

Appendix I: Functional and Molecular Expression of the Proton-Coupled Oligopeptide Transporters in Spleen and Macrophages from Mouse and Human

molecular pharmaceutics

Article

pubs.acs.org/molecularpharmaceutics

Functional and Molecular Expression of the Proton-Coupled Oligopeptide Transporters in Spleen and Macrophages from Mouse and Human

Dongli Sun,[†] Yuqing Wang,[†] Fuqing Tan,[‡] Danbo Fang,[‡] Yongjun Hu,[§] David E. Smith,[§] and Huidi Jiang*[,†]

[†]College of Pharmaceutical Sciences, Zhejiang University, Hangzhou, Zhejiang, P. R. China

[‡]First Affiliated Hospital, College of Medicine, Zhejiang University, Hangzhou, Zhejiang, P. R. China

[§]Department of Pharmaceutical Sciences, College of Pharmacy, University of Michigan, Ann Arbor, Michigan, United States

ABSTRACT: The aim of this study was to determine the expression and function of proton-coupled oligopeptide transporters (POTs) in spleen and macrophages and their contribution to innate immune response induced by bacterial peptidomimetics γ-iE-DAP and MDP. Quantitative real-time PCR (qRT-PCR) and Western blot results revealed the mRNA and protein expression of PepT2, PhT1, and PhT2, but not PepT1, in the spleen of mice and humans. In comparison to lymphocytes of the spleen, macrophages had higher transcript levels of PepT2 and PhT2. The cellular uptake of Ala-Lys-AMCA in mouse splenic macrophages was pH-dependent with maximum uptake at pH 6.0, and the kinetic parameters were K_m = 75.5 ± 14.3 μM and V_{max} = 25.4 ± 2.1 pmol/min per mg protein. The uptake of Ala-Lys-AMCA by mouse splenic macrophages was not inhibited by histidine but was significantly inhibited by glycyl-sarcosine (GlySar) and carnosine ($P < 0.01$), and by bacterial peptidomimetics γ-iE-DAP and MDP, ligands of nucleotide-binding oligomerization domain (NOD)-containing proteins. Carnosine and GlySar, but not histidine, attenuated the inflammatory response induced by γ-iE-DAP and MDP in mouse splenic macrophages. Functional expression of POTs was also demonstrated in THP-1 cells, and dipeptides reduced the immune response induced by γ-iE-DAP. In conclusion, our findings are novel by providing important information on the molecular and functional expression of POTs in the spleen. Moreover, it appears that the PepT2-mediated uptake of γ-iE-DAP and MDP in macrophages further contributes to the innate immune response.

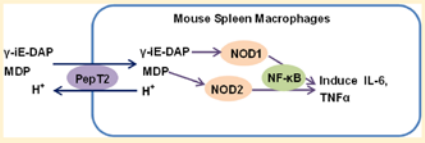

KEYWORDS: *POTs, PepT2, spleen, expression, function, NOD*

1. INTRODUCTION

Proton-coupled oligopeptide transporters (POTs) are electrogenic membrane transporters that mediate the cellular uptake of di/tripeptides and many peptidomimetics utilizing an inwardly directed proton gradient and negative membrane potential.[1−3] In mammals, the POT family has four members which are encoded by SLC15 genes, including PepT1 (SLC15A1), PepT2 (SLC15A2), PhT1 (SLC15A4), and PhT2 (SLC15A3). All of these members are predicted to contain 12 transmembrane domains, with the N- and C-termini in the cytosol. PepT1 and PepT2 have high amino acid identity, around 50%, and have broad substrate specificity in which they mediate the cellular uptake of small peptides and peptide-like drugs such as cefadroxil, valacyclovir, and others. PhT1 and PhT2, in contrast, mediate the transport of histidine in addition to di/tripeptides. With respect to tissue distribution, PepT1 is abundantly expressed in the small intestine[4] and PepT2 in the kidney,[5] brain,[6,7] and lung.[8] PhT1 is highly expressed in the brain and eye,[9] whereas PhT2 is found mainly in the lung, spleen, and thymus.[10]

PepT1 has been shown to mediate the transport of bacterially produced peptidomimetics, such as fMet-Leu-Phe, Tri-DAP, and MDP, in intestinal epithelial cells and Caco-2/BBE cell cultures.[11,12] Tri-DAP and MDP can be recognized by nucleotide-binding oligomerization domain-containing 1 (NOD1) and 2 (NOD2) which are intracellular NOD-like receptors (NLRs).[13] Intracellular accumulation of γ-iE-DAP (a constituent form of Tri-DAP) or MDP recognized by NLRs can activate NF-κB and then induce the production of proinflammatory cytokines, such as IL-6 and TNFα, which are part of NOD signaling pathways.[13] However, whether all POT family members are relevant in the transport of γ-iE-DAP or MDP has not yet reached consensus. In fact, Marina-García et al.[14] carried out studies regarding the internalization of MDP in bone-derived mouse macrophages and ruled out the involvement of PepT1.

The spleen is a unique lymphoid organ that combines innate and adaptive immune system responses and contains B and T cells, macrophages, dendritic cells, and others.[15] Anatomical features of the spleen, combined with its highly adaptive

Received: December 10, 2012
Revised: February 7, 2013
Accepted: February 26, 2013
Published: February 26, 2013

Appendix J: Expression and regulation of the proton-coupled oligopeptide transporter PhT2 by LPS in macrophages and mouse spleen

molecular pharmaceutics

Article

pubs.acs.org/molecularpharmaceutics

Expression and Regulation of the Proton-Coupled Oligopeptide Transporter PhT2 by LPS in Macrophages and Mouse Spleen

Yuqing Wang,[†] Dongli Sun,[†,‡] Feifeng Song,[†] Yongjun Hu,[§] David E. Smith,[§] and Huidi Jiang*[,†]

[†]Laboratory of Pharmaceutical Analysis and Drug Metabolism, Zhejiang Province Key Laboratory of Anti-Cancer Drug Research, College of Pharmaceutical Sciences, Zhejiang University, Hangzhou, Zhejiang 310058, P. R. China

[‡]Women's Hospital School of Medicine, Zhejiang University, Hangzhou, Zhejiang 310006, P. R. China

[§]Department of Pharmaceutical Sciences, College of Pharmacy, University of Michigan, Ann Arbor, Michigan 48109, United States

ABSTRACT: Membrane transporter PhT2 (SLC15A3), which belongs to the proton-coupled oligopeptide transporter family, mediates the transport of di/tripeptides and histidine utilizing an inwardly directed proton gradient and negative membrane potential. The aim of this study was to elucidate the molecular expression of PhT2 in macrophages and mouse tissues and to explore the regulation of PhT2 by lipopolysaccharide (LPS). The results showed relatively high expression of PhT2 in J774A.1 and THP-1 macrophage cells, mouse spleen, and lung. Using an LPS-induced inflammatory cell model, we found that hPhT2 mRNA expression was up-regulated in THP-1 cells and that the up-regulation was suppressed by pyrrolidine dithiocarbamate, a specific inhibitor of NF-κB. Similar results were observed in mouse spleen during LPS-induced acute inflammation. Using dual-labeling immunofluorescence and confocal laser scanning microscopy, we confirmed that mPhT2 was colocalizing with lysosome-associated membrane protein 1 in transfected HEK293 cells. These results suggested that PhT2, a lysosomal membrane transporter, was up-regulated by LPS via the NF-κB signaling pathway.

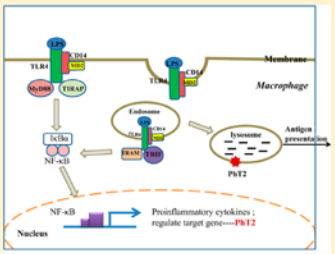

KEYWORDS: *PhT2, macrophage, LPS, NF-κB, lysosome*

1. INTRODUCTION

The proton-coupled oligopeptide transporter (POT) family mediates the cellular uptake of di/tripeptides and many peptidomimetics utilizing an inwardly directed proton gradient and negative membrane potential.[1−3] The family consists of 4 mammalian members, PepT1 (SLC15A1), PepT2 (SLC15A2), PhT1 (SLC15A4), and PhT2 (SLC15A3). All these members are predicted to contain 12 transmembrane domains with both the N- and C-termini facing the cytosol.[1,4] The majority of POT isoform characterization studies have focused on PepT1 and PepT2, which have been widely demonstrated to actively mediate the influx of numerous peptide-based therapeutic agents. They also have been shown to mediate the transport of bacterially produced peptidomimetics, like L-Ala-γ-D-Glu-*meso*-diaminopimelic acid and muramyl dipeptide,[5,6] which may initiate nucleotide-binding oligomerization domain (NOD)-like receptor signaling pathways to induce the production of pro-inflammatory cytokines.[7] In contrast, there is scant information on PhT1 and PhT2, which transport histidine in addition to di/tripeptide substrates and drugs.[8]

Recent studies suggest that PhT1 is associated with diabetes,[9] inflammatory bowel disease,[10] and systemic lupus erythematosus[11] and promotes colitis through Toll-like receptor 9 and NOD1-dependent innate immune responses.[12] The physiological role and pharmacologic relevance of PhT2, however, has remained largely unknown. PhT2 is predominately expressed in the spleen, thymus, and lung of rat, and its subcellular localization was identified in the lysosomes of HEK293T and BHK transfected cells.[13] As the transport activity of PhT2 is pH-dependent, it is assumed to transport histidine and oligopeptide fragments, produced from digested proteins in the lysosomes, (pH ≈ 5.0) to the cytosol (pH ≈ 7.2). Therefore, it is conceivable that PhT2 may play an important role in the protein catabolic pathway where it can maintain intracellular balance.

Macrophages are key players in the immune response in which they stand sentinel against invading pathogens in the cell. Their role is to phagocytize, or engulf and then digest, cellular debris and pathogens. They also have an important role to help regulate host defense and secrete inflammatory cytokines.[14] Studies by our group in macrophages isolated from mouse and human spleen,[5] and that of others in macrophages generated from blood monocytes,[15] demonstrated that PhT2 was highly expressed in these macrophage preparations. Therefore, we hypothesized that the physiological role of PhT2 in macrophages was to mediate the transport of protein digestion products out from lysosomes and that the functional expression

Received: January 7, 2014
Revised: April 13, 2014
Accepted: April 23, 2014
Published: April 23, 2014

dx.doi.org/10.1021/mp500014r | *Mol. Pharmaceutics* 2014, 11, 1880−1888

Appendix K: Abbreviations

ABC transporters:	ATP-binding cassette transporters
AUC:	Area Under Plasma Concentration-Time
BAC:	Bacterial Artificial Chromosome;
BSA:	Body Surface Area
hPepT1:	human source peptide transporter 1;
Gapdh:	Glyceraldehyde 3-phosphate dehydrogenase;
GlySar:	Glycylsarcosine;
IBD:	Inflammatory Bowel Diseases;
mPepT1:	mouse source peptide transporter 1;
NHE:	sodium proton exchanger
PepT2:	peptide transporter 2, also called SLC15a2;
PhT1:	peptide/histidine transporter 1, also called SLC15a4;
PhT2:	peptide/histidine transporter 2, also called LSC15a3;
OAT:	Organic Anion Transporter;
OCT:	Organic Cation Transporter;
PBS:	Phosphate Buffered Saline;
PCR:	Polymerase Circle Reaction;
PK/PD:	Pharmacokinetics/Pharmacodynamics;
POT:	Proton-Coupled Oligopeptide Transporter;
PPB:	Potassium Phosphate Buffer pH 6.5;
SLC transporters:	Solute Carrier Transporters